FOSSIL ENERGY

DOE/PC/91008-4
(DE98000453)

IMPROVED METHODS FOR WATER SHUTOFF

Annual Report
October 1, 1996 to September 30, 1997

By
Randall S. Seright

November 1997

Performed Under Contract No. DE-AC22-94PC91008
Subcontract Number G4S60330

New Mexico Petroleum Recovery Research Center
New Mexico Institute of Mining and Technology
Socorro, New Mexico

National Petroleum Technology Office
U. S. DEPARTMENT OF ENERGY
Tulsa, Oklahoma

DISCLAIMER

This report was prepared as an account of work sponsored by an agency of the United States Government. Neither the United States Government nor any agency thereof, nor any of their employees, makes any warranty, expressed or implied, or assumes any legal liability or responsibility for the accuracy, completeness, or usefulness of any information, apparatus, product, or process disclosed, or represents that its use would not infringe privately owned rights. Reference herein to any specific commercial product, process, or service by trade name, trademark, manufacturer, or otherwise does not necessarily constitute or imply its endorsement, recommendation, or favoring by the United States Government or any agency thereof. The views and opinions of authors expressed herein do not necessarily state or reflect those of the United States Government.

This report has been reproduced directly from the best available copy.

Available to DOE and DOE contractors from the Office of Scientific and Technical Information, P.O. Box 62, Oak Ridge, TN 37831; prices available from (615) 576-8401.

Available to the public from the National Technical Information Service, U.S. Department of Commerce, 5285 Port Royal Rd., Springfield VA 22161

DOE/PC/91008-4
Distribution Category UC-122

Improved Methods For Water Shutoff

Annual Report
October 1, 1996 to September 30. 1997

By
Randall S. Seright

November 1997

Work Performed Under Contract No. DE-AC22-94PC91008
Subcontract Number G4S60330

Prepared for
BDM-Oklahoma/
U.S. Department of Energy
Assistant Secretary for Fossil Energy

Jerry Casteel, Project Manager
National Petroleum Technology Office
P.O. Box 3628
Tulsa, OK 74101

Prepared by:
New Mexico Petroleum Recovery Research Center
New Mexico Institute of Mining and Technology
Socorro, New Mexico 87801

ABSTRACT

In the United States, more than 20 billion barrels of water are produced each year during oilfield operations. There is a tremendous economic incentive to reduce water production if that can be accomplished without significantly sacrificing hydrocarbon production. For each 1% reduction in water production, the cost-savings to the oil industry could be between $50,000,000 and $100,000,000 per year. Reduced water production would result directly in improved oil recovery (IOR) efficiency in addition to reduced oil-production costs. A substantial positive environmental impact could also be realized if significant reductions are achieved in the amount of water produced during oilfield operations.

In an earlier project, we identified fractures (either naturally or artificially induced) as a major factor that causes excess water production and reduced oil recovery efficiency, especially during waterfloods and IOR projects. We also found fractures to be a channeling and water-production problem that has a high potential for successful treatment by gels and certain other chemical blocking agents. By analogy, these blocking materials also have a high potential for treating narrow channels behind pipe and small casing leaks. We also determined that the ability of blocking agents to reduce permeability to water much more than that to oil is critical to the success of these blocking treatments in production wells if zones are not protected during placement of the blocking agent.

This research project has three objectives. The first objective is to identify chemical blocking agents that will (a) during placement, flow readily through fractures without penetrating significantly into porous rock and without "screening out" or developing excessive pressure gradients and (b) at a predictable and controllable time, become immobile and resist breakdown upon exposure to moderate to high pressure gradients. The second objective is to identify schemes that optimize placement of the above blocking agents. The third objective is to explain why gels and other chemical blocking agents reduce permeability to one phase (e.g., water) more than that of another phase (e.g., oil or gas). We also want to identify conditions that maximize this phenomenon. This project consists of three tasks, each of which addresses one of the above objectives.

This report describes work performed during the second period of the project. Results from the first period of the project can be found in Ref. 1. In Chapter 2, we examine the validity of using water/oil ratio plots to distinguish between coning and channeling water production mechanisms. In Chapter 3, we develop a method to size gelant treatments in hydraulically fractured production wells. In Chapter 4, we identify characteristics of naturally fractured reservoirs where gel treatments have the greatest potential. In Chapter 5, we report experimental results from studies of gel properties in fractures. Finally, in Chapter 6, we investigate the mechanism responsible for gels reducing the permeability to water more than that to oil. This project will continue through September, 1998. The project is supported financially by BDM-Oklahoma, the U.S. Department of Energy, and a consortium of 17 oil and service companies. The most recent project review was held April 29-30 in Socorro, NM. The review was attended by 28 people representing 16 different organizations.

TABLE OF CONTENTS

ABSTRACT iii
TABLE OF FIGURES vi
LIST OF TABLES ix
ACKNOWLEDGMENTS x
EXECUTIVE SUMMARY xi
1. INTRODUCTION 1
Objectives 1
Report Content 1
2. USING WATER/OIL RATIOS TO DIAGNOSE EXCESSIVE WATER PRODUCTION MECHANISMS 2
Why Determine Excessive Water Production Mechanisms? 2
WOR Diagnostic Plots 2
Problem Statement 5
Channeling Model 6
Water Coning 10
Channeling Simulation Results 12
Coning Simulation Results 23
Discussion 28
Conclusions 31
3. SIZING GELANT TREATMENTS IN HYDRAULICALLY FRACTURED PRODUCTION WELLS 33
Fracture Volume Versus Leakoff Volume 33
Leakoff Distance Versus Length Along a Fracture 35
Use of Viscous Gelants 36
Productivity Losses and WOR Improvement 37
Determining CL_f Values 44
Limitations 47
Method for Sizing Gelant Treatments in Hydraulically Fractured Production Wells 47
Conclusions 48
4. THE POTENTIAL OF GEL TREATMENTS FOR REDUCING CHANNELING THROUGH NATURALLY FRACTURED RESERVOIRS 50
Representation of a Naturally Fractured Reservoir 50
Tracer Transit Times In a Single Fracture 52
Transit Times In a Fracture System 53
Sweep Efficiency 56
Gelant Front Profiles 61
Effect of Plugging the Most Direct Fracture 63
Injection and Production Rates 64
Diagonally Oriented Fractures 66
Uneven Fracture Spacing 70
Future Work 75
Conclusions 75

5. GEL PROPERTIES IN FRACTURES 76
Gel Extrusion Through Fractures 76
Water Flow After Gel Placement 87
Interpreting the Rheological Behavior of Gels in Fractures 89
Schemes To Optimize Gel Placement In Fractures 91
Effect of Length on Gel Propagation Through Tubes 93
Conclusions 96
6. DISPROPORTIONATE PERMEABILITY REDUCTION 97
Introduction 97
Oil-Water Experiments in a 2-ft Berea Core 98
Constant-Pressure Experiments 99
Effect of Capillary Forces and Gel Elasticity on Disproportionate Permeability Reduction 101
Segregated Oil and Water Pathways 104
Conclusions 108

NOMENCLATURE 109
REFERENCES 111

APPENDIX A: Data and Figure Supplement for Chapter 2 117
APPENDIX B: Derivation Supplement to Chapter 3 151
Derivation of Eq. 13 151
Derivations of Eqs. 14, 15, 16, and 17 152
Derivations of Eqs. 18 and 19 155
APPENDIX C: Fortran Program for Finding Pressures, Flow Rates, and Front Positions During a Unit-Mobility Displacement in a Simple Naturally Fractured Reservoir. Dispersion Not Included 156
APPENDIX D: Fortran Program for Finding Pressures, Flow Rates, and Front Positions During a Unit-Mobility Displacement in a Simple Naturally Fractured Reservoir. Dispersion Included at the Rear but not the Front of the Tracer Bank. 165
APPENDIX E: Fortran Program for Finding Pressures, Flow Rates, and Front Positions During Displacement in a Simple Naturally Fractured Reservoir. Dispersion Included at Both the Front and Rear of the Tracer Bank. 192
APPENDIX F: Derivation of Eq. 55 in Chapter 5 223
APPENDIX G: Data Supplement for Chapter 6 227
APPENDIX H: Technology Transfer 241

TABLE OF FIGURES

Fig. 1. Water coning and channeling WOR comparison. After Chan (1995).[7] 3
Fig. 2. Multi-layer channeling WOR and WOR derivatives. After Chan (1995).[7] 3
Fig. 3. Bottom-water coning WOR and WOR derivatives. After Chan (1995).[7] 4
Fig. 4. Bottom-water coning with later time channeling behavior. After Chan (1995).[7] 4
Fig. 5. Channeling model grid dimensions. 7
Fig. 6. Channeling model with crossflow between adjacent layers. 7
Fig. 7. Channeling model with no crossflow between adjacent layers. 8
Fig. 8. General overview of the channeling model dimensions. 8
Fig. 9. Relative permeability curves for the channeling model. 9
Fig. 10. 2D radial model used to simulate water coning in an oil reservoir. 11
Fig. 11. Multi-layer channeling base case 13
Fig. 12. WOR and WOR' behavior for the no-crossflow case (Case 1) shown in Fig. 11 13
Fig. 13. WOR and WOR' for the k_v/k_h=0.1 case (Case 2) shown in Fig. 11 14
Fig. 14. WOR and WOR' behavior for the vertical-equilibrium case (Case 3) shown in Fig. 11. 14
Fig. 15. Viscous crossflow versus gravity drainage 15
Fig. 16. Schematic top views of the 2D (upper) and 3D (lower) linear flow models. 16
Fig. 17. 2D versus 3D linear flow for equal drainage areas and different gridblock sizes. 17
Fig. 18. 2D versus 3D linear flow for different drainage areas and equal gridblock sizes. 17
Fig. 19. 3D radial flow model, [13×13×3(5)] gridblocks. 18
Fig. 20. 2D linear flow versus 3D radial flow for varying degree of vertical communication. 19
Fig. 21. Case 4 WOR behavior for varying degrees of crossflow. 20
Fig. 22. WOR and WOR' curves for the no-crossflow case shown in Fig. 21 20
Fig. 23. WOR and WOR' behavior for the k_v=0.1k_h case shown in Fig. 21. 21
Fig. 24. WOR and WOR' curves for the vertical equilibrium case shown in Fig. 21 21
Fig. 25. WOR and WOR' behavior for the coning base case. 24
Fig. 26. Comparison of different boundary conditions. 25
Fig. 27. Effect of varying the drainage area for coning case. 26
Fig. 28. Effect of different degree of vertical communication for coning case. 26
Fig. 29. Effect of using different capillary pressure curves (defined in Fig. A.57). 27
Fig. 30. Effect of using different water relative permeability curves for the base case. 28
Fig. 31. Field case example 30
Fig. 32. Comparison; simulation model results versus analytical model results. 31
Fig. 33. Gelant volume versus front position when the leakoff flux is independent of distance along the fracture. 34
Fig. 34. Leakoff flux versus distance along the fracture. 35
Fig. 35. Gelant volume versus front position when the leakoff flux depends on distance along the fracture. 36
Fig. 36. Effect of gelant resistance factor on C values. 37
Fig. 37. Productivity retained when gel extends over the entire fracture face. r_e=500 ft. 38
Fig. 38. Productivity retained when gel covers part of the fracture area. L_p=1 ft, r_e=500 ft. 39
Fig. 39. Productivity retained when gel covers part of the fracture area. L_p=10 ft, r_e=500 ft. 39
Fig. 40. A gel treatment in a vertical fracture that cuts through oil and water zones. 40
Fig. 41. Sensitivity of Example 1 to gelant volume. F_{rrw}=100, F_{rro}=10. 42

Fig. 42. Sensitivity of Example 1 to gelant volume. F_{rrw}=1,000, F_{rro}=100. 43
Fig. 43. Productivity increase from hydraulic fracturing (from Refs. 29 and 30). 44
Fig. 44. Models of naturally fractured reservoirs 51
Fig. 45. Plan view of an injector-producer pair in a simple naturally fractured reservoir. 51
Fig. 46. Transit times through a single 1,000-ft-long fracture. 54
Fig. 47. Results of interwell tracer tests conducted before and after a gel treatment (taken from Ref. 41). Injection rate = 250 BWPD. Production rate = 550 BWPD. 54
Fig. 48. Injector-producer tracer transit times in naturally fractured systems relative to that for a single direct fracture (unit-mobility displacement, fixed pressure drop, continuous injection, no dispersion). 55
Fig. 49. Injector-producer tracer transit times in naturally fractured systems relative to that for a single direct fracture (unit-mobility displacement, fixed pressure drop, 10% fracture-volume tracer bank, with dispersion at the rear of the tracer bank). 55
Fig. 50. Severity of channeling through the most direct x-direction fracture. 57
Fig. 51. Flow rate in the second most direct fracture relative to that in the most direct fracture. .58
Fig. 52. Flow rate in the least direct fracture relative to that in the most direct fracture. 59
Fig. 53. Flow rate in the midway fractures relative to that in the most direct fracture. 59
Fig. 54. Maximum produced tracer concentration when injecting a tracer bank. (Results determined using the program in Appendix D.) 60
Fig. 55. Produced tracer concentrations when injecting a tracer bank with n=11. (Results determined using the program in Appendix E.) 61
Fig. 56. Front profiles at gelant breakthrough in the producer when all fractures have the same conductivity. (Unit-mobility displacement.) 62
Fig. 57. Gelant front profiles versus R when n=11. (Unit-mobility displacement.) 62
Fig. 58. Gelant front profiles versus R when n=101. (Unit-mobility displacement.) 63
Fig. 59. Effect of plugging the most direct fracture. 64
Fig. 60. Injectivity in a naturally fractured system relative to that for a single fracture that directly connects an injector-producer pair. $R \geq 1$. 65
Fig. 61. Injectivity in a naturally fractured system relative to that for a single fracture that directly connects an injector-producer pair. $R \leq 1$. 65
Fig. 62. Fractures oriented diagonally relative to the wells. 67
Fig. 63. Relative injection rates for diagonally oriented fractures. 67
Fig. 64. Intermediate fracture orientations relative to the injector-producer pair. 68
Fig. 65. Relative injection rates for intermediate fracture orientations. $R \geq 1$ 68
Fig. 66. Relative injection rates for intermediate fracture orientations. $R \leq 1$ 69
Fig. 67. Tracer curves when injector and producer were located at (1,1) and (11,2), respectively. 69
Fig. 68. Gelant front profiles when fracture spacing for y-direction fractures is greater than that for x-direction fractures. Number of y-direction fractures is fixed at 11. R=1. 71
Fig. 69. Gelant front profiles when fracture spacing for x-direction fractures is greater than that for y-direction fractures. Number of x-direction fractures is fixed at 21. R=1. 71
Fig. 70. Effect of plugging the most direct fracture when fracture spacing for y-direction fractures is greater than for x-direction fractures. Number of y-direction fractures is fixed at 11 73

Fig. 71. Effect of plugging the most direct fracture when fracture spacing for x-direction fractures is greater than for y-direction fractures. Number of x-direction fractures is fixed at 21 73
Fig. 72. Relative injection rates when fracture spacing for y-direction fractures is greater than that for x-direction fractures. Number of y-direction fractures is fixed at 11. 74
Fig. 73. Relative injection rates when fracture spacing for x-direction fractures is greater than that for y-direction fractures. Number of x-direction fractures is fixed at 21. 74
Fig. 74. Chromium and HPAM effluent concentrations during gel injection into Core 15. 77
Fig. 75. Pressure gradients during gel injection into Core 15. 78
Fig. 76. Chromium and HPAM concentrations for gel in the fracture of Core 15 (relative to the concentrations of the injected gel) versus distance along the fracture (122-cm total length). 78
Fig. 77. After applying a constant pressure drop of 35 psi across a 4-ft-long core (Core 16), gel flow effectively stopped after 10 days or less than 4 fracture volumes of gel injection. 79
Fig. 78. Chromium and HPAM effluent concentrations during gel injection into Core 16. 80
Fig. 79. Chromium and HPAM effluent concentrations during gel injection into Core 18. 81
Fig. 80. Chromium and HPAM effluent concentrations during gel injection into Core 20. 82
Fig. 81. Chromium and HPAM effluent concentrations during gel injection into Core 22. 82
Fig. 82. Pressure gradient versus fracture conductivity for a fixed volumetric injection rate. 84
Fig. 83. Chromium and HPAM effluent concentrations during gel injection into Core 19. 85
Fig. 84. Chromium and HPAM concentrations for gel in the fracture of Core 19. 85
Fig. 85. Chromium and HPAM effluent concentrations during gel injection into Core 21. 85
Fig. 86. Chromium and HPAM effluent concentrations during gel injection into Core 23. 86
Fig. 87. Chromium and HPAM concentrations for gel in the fracture of Core 23. 86
Fig. 88. Chromium and HPAM effluent concentrations during gel injection into Core 24. 86
Fig. 89. Chromium and HPAM concentrations for gel in the fracture of Core 24. 87
Fig. 90. Core conductivity during brine injection after gel placement 88
versus fracture conductivity before gel placement 88
Fig. 91. Chromium and HPAM concentrations produced from Cores 23 and 24 88
(relative to the original values) during brine injection after gel placement. 88
Fig. 92. Correlating behavior in short tubes (3 to 15 ft) and short fractures (0.5 to 4 ft). 89
Fig. 93. Use of the Bingham model to predict the thickness of the lubricating layer based on Fig. 92, Eq. 54, and Eq. 55. 90
Fig. 94. Idealized locations for gels in fractures. 91
Fig. 95. Extrusion of a 24-hr-old Cr(III)-acetate-HPAM gel through a 100-ft-long, 0.03-inch-ID tube at 35,000 ft/d. 41°C. 93
Fig. 96. Schematic of the core-tube experiment. 95
Fig. 97. Long Berea core 98
Fig. 98. Balance between capillary forces and gel elasticity when forcing oil or water through an aqueous gel 102
Fig. 99. Pressure spike during oil injection immediately after shut-in (SSH-154, 155). 104
Fig. 100. Segregated oil and water pathways 104

LIST OF TABLES

Table 1. Properties of Long Fractured Cores 77
Table 2. Effect of Fracture Conductivity on Gel Propagation 83
Table 3. Schemes to Optimize Gel Placement in Fractures 92
Table 4. Extrusion of 24-hr-old Cr(III)-Acetate-HPAM Gels Through Tubes 95
Table 5. Summary of Permeabilities for a 2-ft Berea Core (SSH-156) Before Gel 98
Table 6. Summary of F_{rrw} and F_{rro} for a 2-ft Berea Core (SSH-156) After Gel 99
Table 7. Summary of F_{rrw} and F_{rro} for a Constant-Pressure Experiment (SSH-138) 100
Table 8. Summary of F_{rrw} and F_{rro} for a Constant-Pressure Experiment (SSH-137) 100
Table 9. Effect of Pressure Drawdown on Disproportionate Permeability Reduction 101
Table 10. F_{rrw} and F_{rro} Values For a Water-Based Gel (SSH-122, 129, 135, 151) 106
Table 11. F_{rrw} and F_{rro} Values For a Water-Based Gel (SSH-122, 160) 107
Table 12. F_{rrw} and F_{rro} Values For a Water-Based Gel (SSH-122, 152, 164) 107

ACKNOWLEDGMENTS

Financial support for this work is gratefully acknowledged from the United States Department of Energy, BDM-Oklahoma, ARCO, British Petroleum, Chevron, Chinese Petroleum Corporation, Conoco, Eniricerche, Exxon, Halliburton, Marathon, Norsk Hydro, Phillips Petroleum, Saga, Schlumberger-Dowell, Shell, Statoil, Texaco, and Unocal. I greatly appreciate the efforts of those individuals who contributed to this project. The work in Chapter 2 was performed and written by Mailin Seldal as part of her M.S. degree in Petroleum Engineering. She also aided during the work described in Chapter 3, along with Dr. Jenn-Tai Liang. Professor Robert L. Lee wrote the simulators for the work described in Chapter 4. Richard Schrader performed the experimental work described in Chapter 5. Dr. Jenn-Tai Liang played the major role in the work described in Chapter 6. Dr. Jill Buckley and Jostein Kolnes (of Stavanger College) participated in helpful discussions during this work. John Hagstrom performed most of the experiments described in Chapter 6. I especially appreciate the thorough review of the manuscript by Julie Ruff.

EXECUTIVE SUMMARY

This report describes work performed during the second period of the project, "Improved Methods for Water Shutoff." This project has three general objectives. The first objective is to identify chemical blocking agents that will (a) during placement, flow readily through fractures without penetrating significantly into porous rock and without "screening out" or developing excessive pressure gradients and (b) at a predictable and controllable time, become immobile and resist breakdown upon exposure to moderate to high pressure gradients. The second objective is to identify schemes that optimize placement of the above blocking agents. The third objective is to explain why gels and other chemical blocking agents reduce permeability to one phase (e.g., water) more than that of another phase (e.g., oil or gas). We also want to identify conditions that maximize this phenomenon.

Water/Oil Ratio Diagnostic Plots. Water/oil ratio (WOR) diagnostic plots have been proposed as a method to diagnose excessive water production mechanisms. This method is said to be capable of distinguishing whether a production well is experiencing premature water breakthrough caused by water coning or channeling through high-permeability layers. According to this method, gradually increasing WOR curves with negative derivative slopes are unique for coning problems, and rapidly increasing WOR curves with positive derivative slopes are indicative of a channeling problem. To investigate whether diagnostic plots can be applied generally or if they have limitations, reservoir models were built for water coning and channeling, respectively, and a sensitivity analysis was performed using numerical simulation. Reservoir and fluid parameters were varied, and their effect on WOR and WOR derivative behavior were studied for both coning and channeling production problems. The results from this study demonstrate that multi-layer channeling problems can easily be mistaken as bottomwater coning, and vice versa, if WOR diagnostic plots are used alone to identify an excessive water production mechanism. Hence, WOR diagnostic plots can easily be misinterpreted and should therefore not be used by themselves to diagnose the specific cause of a water production problem.

Sizing Gelant Treatments in Hydraulically Fractured Production Wells. Often, when production wells are stimulated by hydraulic fracturing, the fracture unintentionally extends through shale barriers into water zones, causing substantially increased water production. Gelant treatments have frequently been applied in an attempt to correct this problem. However, the design of the gelant volumes for these applications has been strictly empirical, and consequently, the success rates for these treatments have been erratic. We develop a sound engineering basis for sizing gelant treatments. We present a simple 11-step procedure for sizing gelant treatments in hydraulically fractured production wells. We incorporated this procedure in user-friendly graphical-user-interface software.

The Potential Of Gel Treatments For Reducing Channeling Through Naturally Fractured Reservoirs. We investigated the applicability of gel treatments in naturally fractured reservoirs—in particular, when channeling occurs between injector-producer pairs. In a naturally fractured reservoir, we define an R-value as the conductivity of fractures that are aligned with direct flow between an injector-producer pair divided by the conductivity of fractures that are not

aligned with direct flow between wells. We also define an n-value as the number of fractures between an injector-producer pair, where these fractures are not aligned with the direct flow direction. The n-value is a measure of fracture spacing.

During simulation studies, we found that gel treatments in naturally fractured reservoirs have the greatest potential when R-values are high (greater than 10). Produced tracer concentrations from interwell tracer studies can be useful in identifying reservoirs with high R-values. We propose that the potential for a gel treatment becomes greater as the produced tracer concentration increases above 30% of the injected value. When produced tracer concentrations are low, gel treatments are unlikely to be effective. The potential of gel treatments is insensitive to fracture spacing for fractures that are not aligned with the direct flow direction. For fractures that are aligned with the direct flow direction, the potential of gel treatments decreases with increased fracture spacing.

Our simulation studies also revealed that tracer transit times are not sensitive to R- or n-values. Consequently, tracer transit times can be very useful when estimating the permeability or conductivity of the most direct fracture.

Gel Properties in Fractures. We performed many experiments where one-day-old Cr(III)-acetate-HPAM gels were extruded through 2.7- to 4-ft-long fractures. We found that in fractures with conductivities between 1 and 242 darcy-ft (effective average widths between 0.006 and 0.04 inches), the gel was concentrated (or dehydrated) by a factor typically between 20 and 40 during the extrusion process. This dehydration effect delayed propagation of the gel through fractures by factors ranging from 20 to 40. The gel dehydration effect became less pronounced as the fracture width increased. However, a fracture width around 0.4 inches was required to completely eliminate the effect.

For a given fracture conductivity and width, a minimum pressure gradient (i.e., a yield stress) appears to be required to extrude gel through the fracture. For fractures with conductivities ($k_f w_f$, in darcy-ft) between 1 and 1,000,000 darcy-ft (widths between 0.006 and 0.6 inches), the required pressure gradient can be estimated using the relation: $dp/dl=280(k_f w_f)^{-0.58}$ (where dp/dl is in psi/ft). To extrude this gel with a pressure gradient of only 1 psi/ft (a typical pressure gradient in a reservoir), the fracture width should be at least 0.1 inches.

During brine injection after gel placement, we saw no evidence of significant gel washout for fractures with widths up to 0.4 inches. For fractures with widths greater than 0.1 inches, the gel did not completely heal the fracture (i.e., reduce its flow capacity to near zero). However, the fracture conductivities were reduced substantially.

We also found that extrusion of gels through long tubes cannot adequately imitate the behavior of gels during extrusion through long fractures.

Disproportionate Permeability Reduction. The ability of blocking agents to reduce the permeability to water much more than to oil is critical to the success of water-shutoff treatments in production wells if hydrocarbon-productive zones cannot be protected during placement.

Results from the literature and our own experimental work have shown that many polymers and gels exhibit this disproportionate permeability reduction. In our previous studies, we extensively examined several possible mechanisms for this disproportionate permeability reduction. Although we still do not have a plausible explanation for this phenomenon, many interesting leads have been generated during the course of the study. Our previous studies ruled out gravity and lubrication effects as possible mechanisms. Also, gel shrinking and swelling are unlikely to be responsible for this phenomenon. Our experimental results indicate that wettability may play a role; however its effect is unclear.

Based on a micromodel study by Dawe and Zhang, we speculated that a balance between capillary forces and gel elasticity might contribute to disproportionate permeability reduction. However, results from our studies indicate that this mechanism is valid only in micromodels and small glass tubes, not in porous rock.

Based on results from core experiments using an oil-based gel, we proposed that disproportionate permeability reduction might be caused by oil and water following segregated pathways on a microscopic scale. We speculated that if this theory is valid, simultaneous injection of oil and an aqueous gelant during placement should enhance disproportionate permeability reduction. However, we found that the injection of oil with an aqueous gelant using gelant/oil volume ratios of 50/50, 30/70, and 95/5 did not enhance the disproportionate permeability reduction. These findings do not support the segregated-oil-and-water-pathway theory. We suspect that the capillary redistribution of fluids closed the open oil channels during the shut-in period. One possible way to prevent the capillary redistribution of fluids from closing the oil channels is to maintain the oil flow during the gelation period. Results from oil-water experiments suggest that with the proper gelant/oil volume ratio, continuous oil injection during the gelation period could enhance the disproportionate permeability reduction. Additional experiments are underway to understand this interesting phenomenon.

We also performed an oil-water experiment in a 2-ft Berea core. Results from this experiment showed that the disproportionate permeability reduction did not vary with core length. Also, flow behavior of water and oil after gel treatment in the 2-ft Berea core was consistent with our observations in 6-in Berea cores.

To study the effect of pressure drawdown on disproportionate permeability reduction, we performed three sets of constant-pressure oil-water experiments using different pressure gradients during residual-resistance-factor measurements. For each pressure gradient, we performed two similar oil-water experiments; one with oil injected immediately after shut-in to measure F_{rro} and the other with brine injected immediately after shut-in to measure F_{rrw}. Results from these experiments showed that the disproportionate permeability reduction decreased with increasing pressure drawdown between 90 and 180 psi/ft. Additional work is underway to determine if this phenomenon can be exploited in field applications.

1. INTRODUCTION

In the United States, more than 20 billion barrels of water are produced each year during oilfield operations. Today, the cost of water disposal is typically between $0.25 and $0.50 per bbl for pipeline transport and $1.50 per bbl for trucked water. Therefore, there is a tremendous economic incentive to reduce water production if that can be accomplished without significantly sacrificing hydrocarbon production. For each 1% reduction in water production, the cost-savings to the oil industry could be between $50,000,000 and $100,000,000 per year. Reduced water production would result directly in improved oil recovery (IOR) efficiency in addition to reduced oil-production costs. A substantial positive environmental impact could also be realized if significant reductions are achieved in the amount of water produced during oilfield operations.

In an earlier project, we identified fractures (either naturally or artificially induced) as a major factor that causes excess water production and reduced oil recovery efficiency, especially during waterfloods and IOR projects. We also found fractures to be a channeling and water-production problem that has a high potential for successful treatment by gels and certain other chemical blocking agents. By analogy, these blocking materials also have a high potential for treating narrow channels behind pipe and small casing leaks. We also determined that the ability of blocking agents to reduce permeability to water much more than that to oil is critical to the success of these blocking treatments in production wells if zones are not isolated during placement of the blocking agent.

Objectives

This project has three general objectives. The first objective is to identify chemical blocking agents that will (a) during placement, flow readily through fractures without penetrating significantly into porous rock and without "screening out" or developing excessive pressure gradients and (b) at a predictable and controllable time, become immobile and resist breakdown upon exposure to moderate to high pressure gradients. The second objective is to identify schemes that optimize placement of the above blocking agents. The third objective is to explain why gels and other chemical blocking agents reduce permeability to one phase (e.g., water) more than that of another phase (e.g., oil or gas). We also want to identify conditions that maximize this phenomenon.

Report Content

This report describes work performed during the second year of the project. Results from the first period of the project can be found in Ref. 1. In Chapter 2, we examine the validity of using water/oil ratio plots to distinguish between coning and channeling water production mechanisms. In Chapter 3, we develop a method to size gelant treatments in hydraulically fractured production wells. In Chapter 4, we identify characteristics of naturally fractured reservoirs where gel treatments have the greatest potential. In Chapter 5, we report experimental results from studies of gel properties in fractures. Finally, in Chapter 6, we investigate the mechanism responsible for gels reducing the permeability to water more than that to oil.

2. USING WATER/OIL RATIOS TO DIAGNOSE EXCESSIVE WATER PRODUCTION MECHANISMS

Why Determine Excessive Water Production Mechanisms?

Water production from hydrocarbon reservoirs is increasing worldwide, as more reservoirs are depleted. Water handling and disposal costs often shorten the economic life of a well.[1] Disposal of produced water is also an environmental concern, especially offshore.

Two important causes of excessive water production are coning and channeling.[2] Water coning occurs when the water/oil contact (WOC) locally rises toward the completed interval in a well that partially penetrates the pay zone. Water channeling is common when high-permeability layers or fractures allow early water breakthrough during waterflooding.

Gel treatments have been applied to many wells to reduce water cut.[3-5] In these treatments, a gel is often formed through the reaction between a polymer solution and a crosslinking agent, creating a semi-solid material that is capable of blocking fluid flow in the reservoir.

Although many successful gel applications have been reported in the literature, the overall success rate has been low.[6] To improve the success rate of future gel treatments, the source and nature of the excess water production should be identified. Several methods can be useful in this process, including simple injectivity and productivity calculations, interwell tracer studies,[6] reservoir simulation, pressure transient analysis, and various logs. This chapter considers the use of plots of water/oil ratio versus time to diagnose excessive water production mechanisms.

WOR Diagnostic Plots

Water/oil ratio (WOR) and gas/oil ratio (GOR) diagnostic plots[7,8] have been proposed as an easy, fast, and inexpensive method to identify excessive water and gas production mechanisms. According to this method, a log-log plot of WOR or GOR versus time will show different behavior for the varying mechanisms. Log-log plots of WOR and GOR time derivatives versus time are said to be capable of differentiating whether a production well is experiencing water or gas coning, channeling due to high-permeability layers, or near-wellbore channeling.[7,8] If these diagnostic plots can be used to determine the mechanism for excessive water production, they will be useful for identifying wells where gel treatments may be effective for water shutoff.

According to Chan,[7,8] Figs. 1 through 4 illustrate how the diagnostic plots are supposed to differentiate among the various water production mechanisms. Fig. 1 shows a comparison of WOR diagnostic plots for coning and channeling. The WOR behavior for both coning and channeling is divided into three periods; the first period extends from production start to water breakthrough, where the WOR is constant for both mechanisms. When water production begins, Chan claims that the behavior becomes very different for coning and channeling. This event denotes the beginning of the second time period.

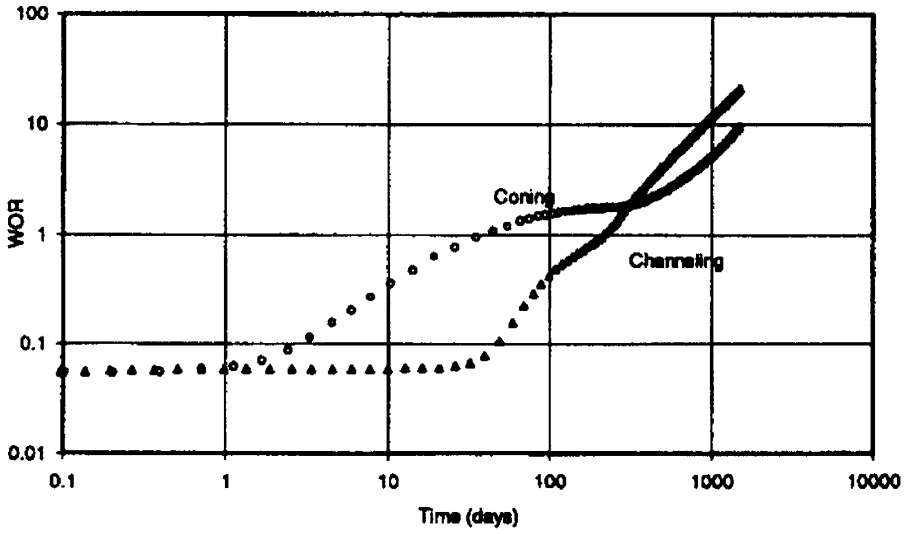

Fig. 1. Water coning and channeling WOR comparison. After Chan (1995).[7]

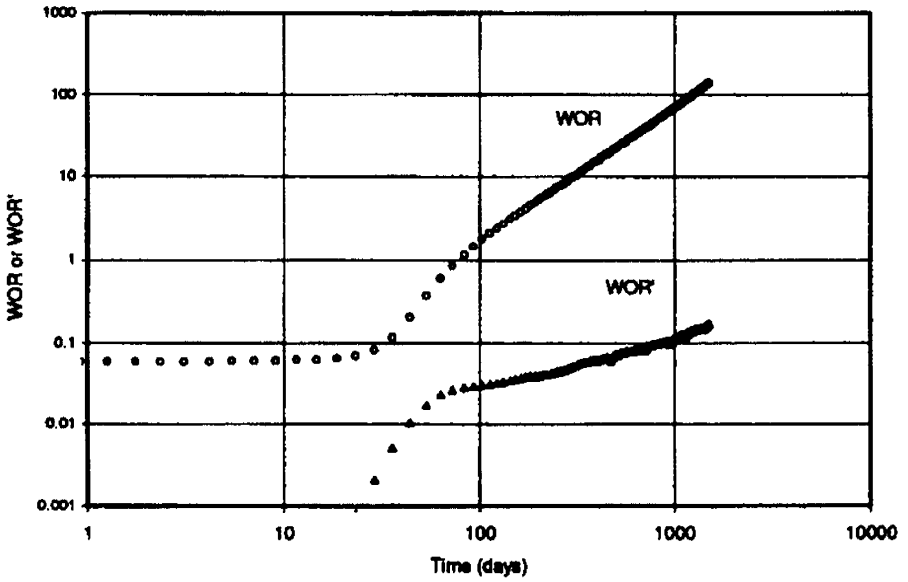

Fig. 2. Multi-layer channeling WOR and WOR derivatives. After Chan (1995).[7]

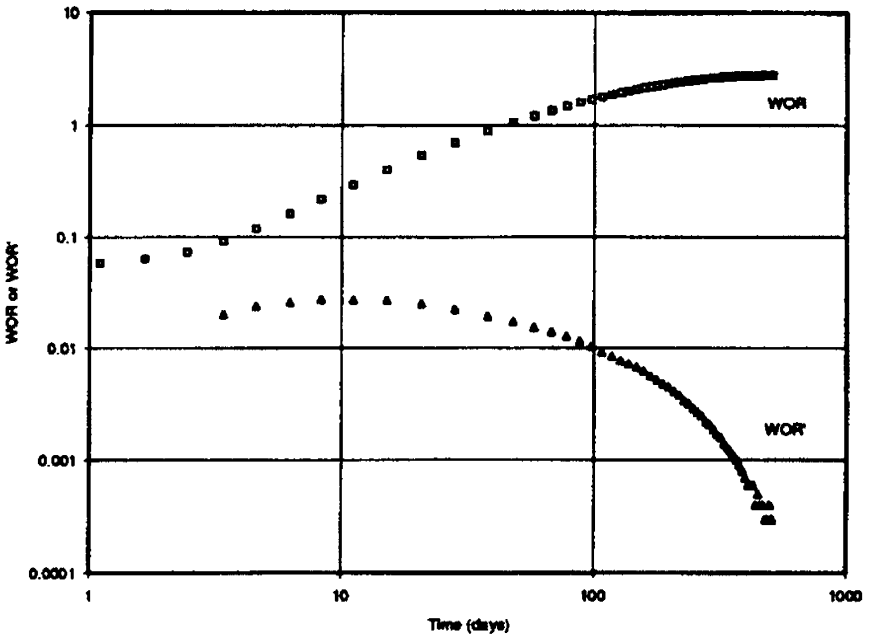

Fig. 3. Bottom-water coning WOR and WOR derivatives. After Chan (1995).[7]

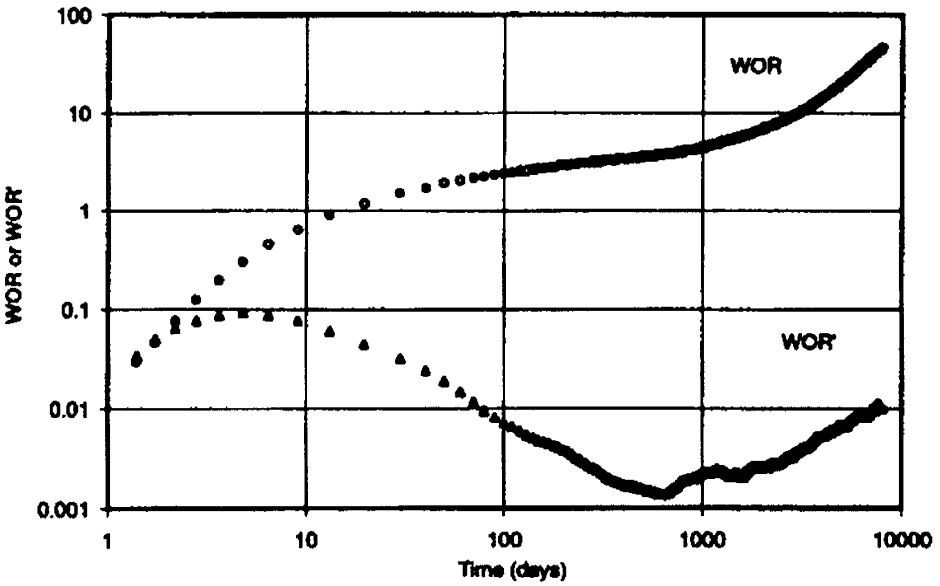

Fig. 4. Bottom-water coning with later time channeling behavior. After Chan (1995).[7]

For coning, the departure time is often short (depending on several variables), and corresponds to the time when the underlying water has been drawn up to the bottom of the perforations. According to Chan, the rate of WOR increase after water breakthrough is relatively slow and gradually approaches a constant value. This occurrence is called the transition period.

For channeling, the departure time corresponds to water breakthrough for the most water-conductive layer in a multi-layer formation, and usually occurs later than for coning. Chan claims that the WOR increases relatively quickly for the channeling case, but it could slow down and enter a transition period, which is said to correspond to production depletion of the first layer. Thereafter, the WOR resumes the same rate as before the transition period. This second departure point corresponds to water breakthrough for the layer with the second highest water conductivity. According to Chan, the transition period between each layer breakthrough may only occur if the permeability contrast between adjacent layers is greater than four.

After the transition period(s), Chan describes the WOR increase to be quite rapid for both mechanisms, which indicates the beginning of the third period. The channeling WOR resumes its initial rate of increase, since all layers have been depleted. The rapid WOR increase for the coning case is explained by the well producing mainly bottom water, causing the cone to become a high-conductivity water channel where the water moves laterally towards the well. Chan, therefore, classifies this behavior as channeling.[7]

Log-log plots of WOR and WOR time derivatives (WOR') versus time for the different excessive water production mechanisms are shown in Figs. 2 through 4. Chan proposed that the WOR derivatives can distinguish between coning and channeling.[7,8] Channeling WOR' curves should show an almost constant positive slope (Fig. 2), as opposed to coning WOR' curves, which should show a changing negative slope (Fig. 3). A negative slope turning positive when "channeling" occurs (Fig. 4) characterizes a combination of the two mechanisms, which Chan classifies as coning with late channeling behavior.

Recently, the use of Chan's WOR diagnostic plots has received significant interest in the oil and gas industry.[9] Therefore, a need exists to determine the validity of using these plots as a diagnostic method.

Problem Statement

The purpose of this study is to determine whether the WOR diagnostic plots can be used to distinguish between water coning and multi-layer channeling, and if so, whether the method can be applied generally or if there are limitations.

To meet this objective, reservoir models were built for water coning and channeling, respectively, and a sensitivity analysis was performed using numerical simulation. Reservoir and fluid parameters were varied, and their effects on WOR and WOR' behavior were studied for both coning and channeling production problems.

The reservoir simulator SABRE, developed by Holditch & Associates, Inc., was used for this study. SABRE is a three-dimensional reservoir simulator developed to model the performance of petroleum reservoirs under different depletion or enhanced recovery scenarios. It can simulate complex three-dimensional, three-phase black oil and volatile oil systems as well as simple single-phase, one-dimensional problems. The simulator can model reservoirs using rectangular or radial coordinate systems, in addition to full-field studies or single well investigations.

In this work, we examine how different reservoir parameters affect the WOR and WOR' behavior for coning and channeling. For channeling, we varied the degree of vertical communication and permeability contrast among layers, pressure gradient in the reservoir, saturation distribution, and relative permeability curves. For coning, we studied the effects of different vertical-to-horizontal permeability ratios, well spacing, capillary pressure curves, and relative permeability curves.

Channeling Model

The channeling case was modeled using a two-dimensional (2D) cross-sectional grid (Fig. 5). The wells were placed in a direct line-drive pattern with a 40-acre drainage area, which gave a distance of approximately 933 ft between a producer and an injector. The model was divided into 42 gridblocks of varying sizes in the x-direction. A producer was placed in gridblock 1 and an injector in gridblock 42, and the pressure drop between the wells was 1,000 psi (pressure gradient of 1.07 psi/ft). The grid was refined in the vicinity of the wells. One 30-ft gridblock constituted the y-direction. For the crossflow base cases, three producing layers were used in the z-direction (Fig. 6). To generate corresponding no-crossflow cases, an impermeable layer was placed between each pair of producing layers, giving five gridblocks in the z-direction (Fig. 7). An overview of the model dimensions is shown in Fig. 8.

Different permeabilities were assigned to each layer, which were arranged in order of descending permeability. Changing the vertical-to-horizontal permeability ratio can vary the degree of crossflow. Actual reservoirs range from those having zero crossflow (no vertical communication between layers) to those having unrestricted crossflow between strata.[10] The degree of crossflow can be evaluated by the closeness to vertical equilibrium. Vertical equilibrium, which implies the maximum degree of crossflow possible,[11,12] means that the horizontal pressure gradients are equal at all vertical positions at a given longitudinal position along the reservoir. Vertical equilibrium is associated with large values of the G-shape scaling group:

$$G_{shape} = \frac{k_v}{k_h}\left[\frac{\Delta X}{\Delta Z}\right]^2 \qquad (1)$$

where k_v/k_h is the vertical-to-horizontal permeability ratio, ΔX is the total length, and ΔZ is the height of the system. The G_{shape} factor is approximately 110 for the base case if k_v/k_h equals 1.

Three different cases were considered: vertical-to-horizontal permeability ratios of 0 (no crossflow), 0.1, and 1 (vertical equilibrium).

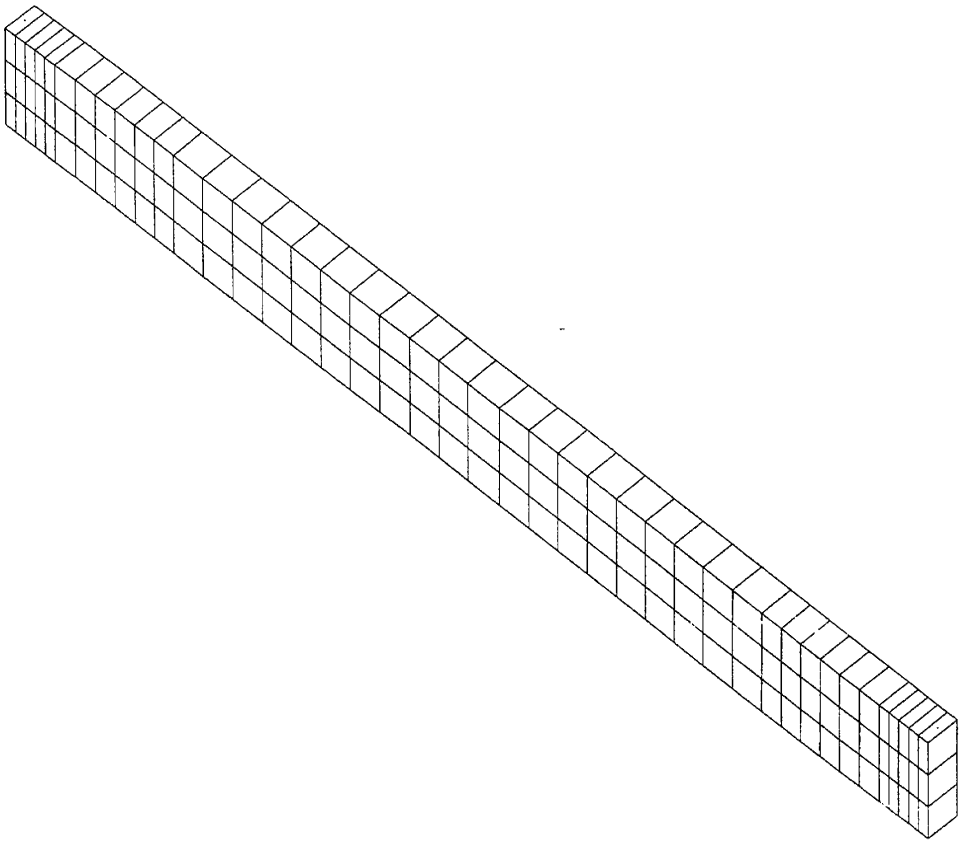

Fig. 5. Channeling model grid dimensions.

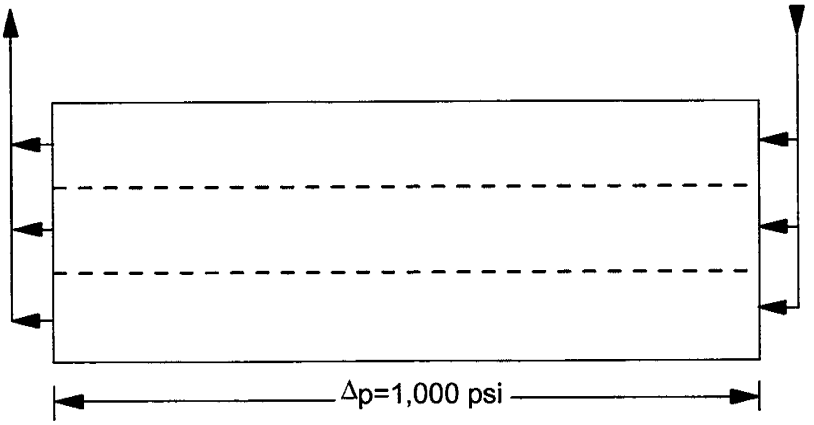

Fig. 6. Channeling model with crossflow between adjacent layers.

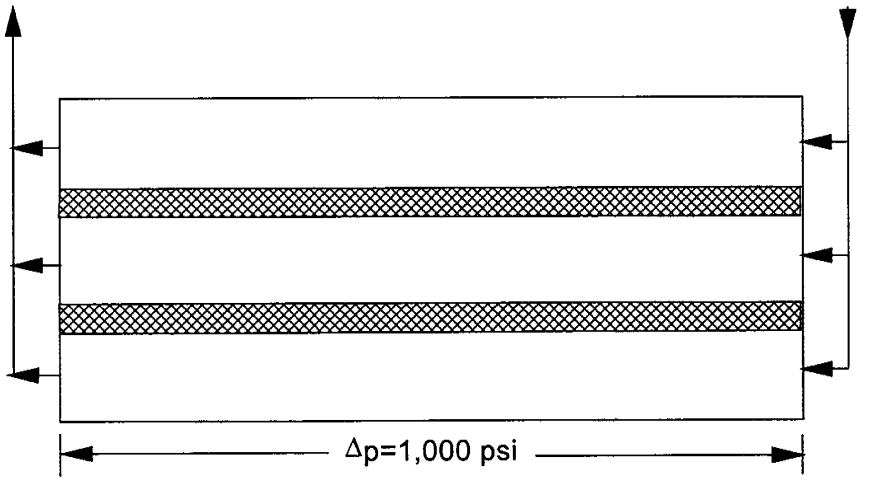

Fig. 7. Channeling model with no crossflow between adjacent layers.

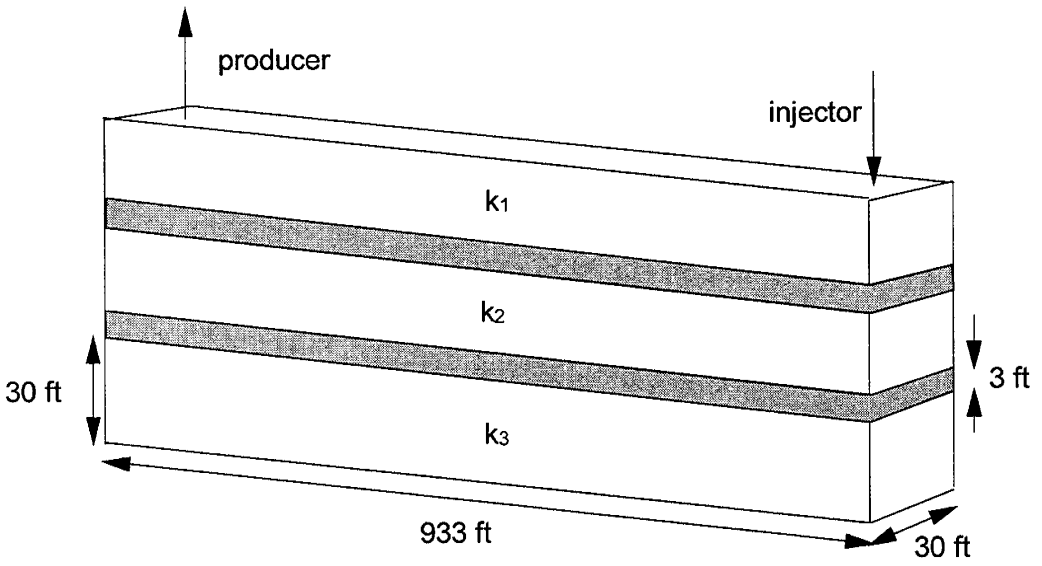

Fig. 8. General overview of the channeling model dimensions.

The water and oil relative permeabilities (Fig. 9) were assumed to be functions of water saturation only and were calculated using the Corey equations:[13]

$$k_{rw} = k_{rw}^{0}\left(\frac{S_w - S_{wr}}{1 - S_{wr} - S_{or}}\right)^{n_w} \tag{2}$$

$$k_{ro} = k_{ro}^{0}\left(\frac{1-S_w-S_{or}}{1-S_{wr}-S_{or}}\right)^{n_o} \tag{3}$$

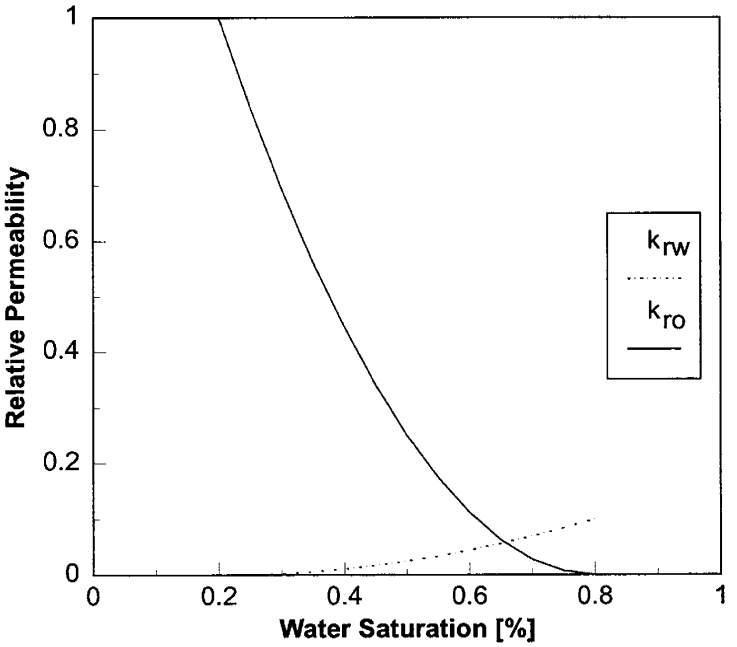

Fig. 9. Relative permeability curves for the channeling model.

A producer and injector pair with a corresponding well constant was assigned to each producing layer. The well constant is closely related to the productivity index of the well, and is defined by the basic flow equation describing the flow between a well and the cell in which it is completed.[14]

$$q_p = \frac{0.00708khk_{rp}\left(p_{well}-p_{cell}\right)}{B_p\mu_p \ln\left(r_o / r_{wa}\right)} = WC\left(\frac{k_{rp}}{B_p\mu_p}\right)\left(p_{well}-p_{cell}\right) \tag{4}$$

This relation gives the following equation for the well constant:

$$WC = \frac{0.00708kh}{\ln\left(r_o / r_{wa}\right)} \tag{5}$$

The equivalent well-block radius is calculated using Peaceman's solution for non-square gridblocks.[15] If the well-block permeability is isotropic and the well is located in the center of the gridblock, the equivalent well-block radius (where the actual flowing pressure equals the numerically calculated well-block pressure) is given by

$$r_o = 0.14\left(\Delta x^2 + \Delta y^2\right)^{1/2} \tag{6}$$

Eq. 6 is valid for any aspect ratio, $\Delta y/\Delta x$. Skin factors (assumed to be 0 for these cases) can be taken into account by using an apparent wellbore radius of

$$r_{wa} = r_w e^{-s} \tag{7}$$

The top of the upper reservoir layer was located 5,000 ft below the surface. The vertical depth to the oil/water contact was 10,000 ft. This study considered only two-phase flow of oil and water (gas is not included in the simulation).

Eq. 8 shows that the endpoint mobility ratio is 0.25. Hence, this is a favorable displacement process where the oil is more mobile than water.

$$M = \frac{k_{rw}^0 \cdot \mu_o}{k_{ro}^0 \cdot \mu_w} = \frac{0.1 \cdot 1.1}{1 \cdot 0.44} = 0.25 \tag{8}$$

Additional reservoir and fluid data are listed in Table A.1 of Appendix A.

Water Coning

Coning Mechanism. During pressure drawdown at high rates, the water table can deform into a cone-shape. The cone rises to a height where the dynamic force is balanced by the hydrostatic head of the elevated water column. Water coning occurs when the dynamic pressure gradients associated with oil production exceed the hydrostatic pressure gradient of water.[16] At this point, the cone becomes unstable, and the water flows up toward the well. The formation of an unstable cone defines the critical oil rate, or maximum water-free oil production rate. For a vertical well with a three-dimensional (3D) coning problem, the critical rate can be calculated using Eq. 9.[17]

$$q_c = \frac{\pi k \quad g(\rho_w - \rho_o)(h_e^2 - h_w^2)}{\mu_o \ln(r_e / r_w)} \tag{9}$$

A distinction can be made between "classical" coning, where the only available energy is fluid and rock expansion, and water-drive coning, where the oil zone is underlain by an active water drive system.[18] Bottom-water drive can be modeled by water injection into the water zone, or by using a very high value of porosity in one of the aquifer cells located at the boundary.

Coning Model. A 2D (r,z) radial model with a drainage area of 160 acres was built to simulate an oil reservoir with a water coning problem (Fig. 10). The r-direction consists of 11 gridblocks, whose size increases with radius from the production well. Sixteen gridblocks were used in the z-direction. The ten upper gridblocks represent the oil zone (each 10 ft thick), and the six lower gridblocks represent the water zone (each 30 ft thick).

Different vertical gridblock sizes were tested for the oil zone. Five 20-ft blocks gave similar WOR behavior as the 10-ft case, but larger gridblocks made it more difficult to predict how the

cone develops vertically. Refining the vertical gridblocks to 5 ft in the vicinity of the well resulted in identical WOR behavior as for the 10-ft case, but instabilities were observed due to large saturation changes in one gridblock over a timestep. Smaller timestep sizes, which resulted in fairly long runtimes, were not able to eliminate the instabilities; the oil zone was therefore modeled using 10×10 ft vertical gridblocks.

The top of the reservoir was located at 5,000 ft below the surface; hence, the vertical depth to the oil/water contact was 5,100 ft. Water-drive coning was simulated by assigning block (11, 16) a very high porosity value, which makes the reservoir close to infinite-acting. The vertical-to-horizontal permeability ratio was 0.1 in both the oil and water zone. A producer was placed in the center of the model and perforated through Layers 1 and 2, which corresponds to the upper 20% of the oil zone. The well produced at a total fluid rate of 5,000 STB/D.

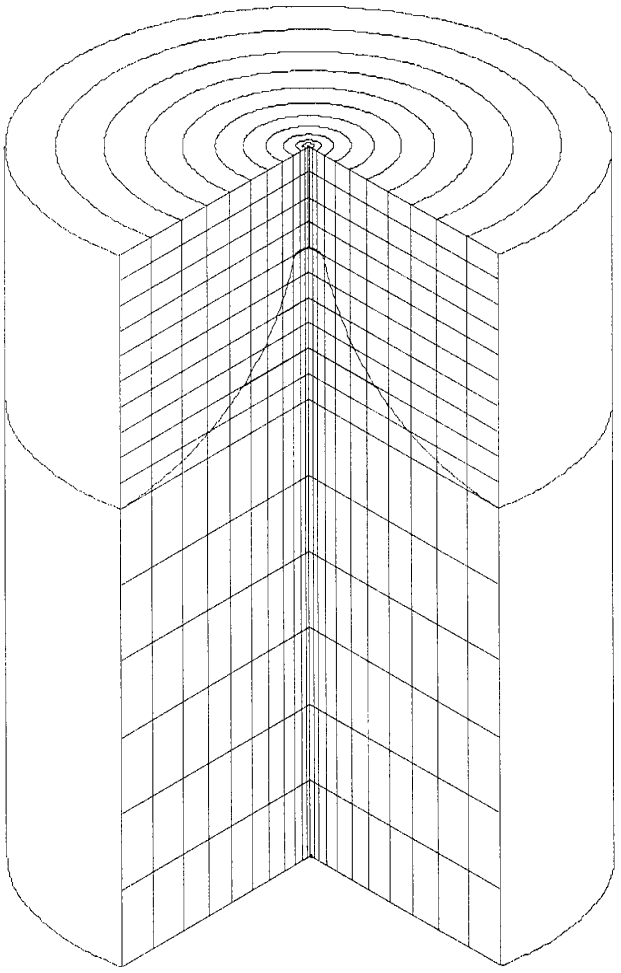

Fig. 10. 2D radial model used to simulate water coning in an oil reservoir.

Eq. 10 gives the well constant for a radial model,

$$WC = \frac{0.00708kh}{\ln(r_1 / r_w) + s} \tag{10}$$

where r_1 is the distance from the center of the wellbore to the center of the first gridblock and r_w is the actual wellbore radius. The skin factor is assumed to be zero for these simulations.

The coning model reservoir and fluid data are similar to those of the oil-water coning problem described by MacDonald and Coats[19] and are listed in Tables A.2 and A.3 of Appendix A.

Channeling Simulation Results

The main point of the following analysis is that channeling behavior can show positive, negative, and/or zero-slope plots of WOR derivative versus time. Later, we show that the same is true of coning behavior. Depending on reservoir conditions and fluid properties, it seems likely that virtually any WOR behavior observed during coning could also be observed during channeling, and vice versa. Thus, without some prior knowledge of (1) reservoir conditions and fluid properties, and (2) the likely cause of excess water production, WOR plots, by themselves, will not provide a priori determination of the problem mechanism.

Two-Dimension Linear Model. Layer permeabilities of 200, 100, and 50 md were used for the base case. Figs. 11 through 14 show the diagnostic plots for the base case, i.e. WOR and WOR time derivatives plotted versus time in a log-log plot. Different degrees of crossflow are shown, with vertical-to-horizontal permeability ratios of 0, 0.1, and 1. (These cases will hereafter be referred to as Cases 1, 2, and 3, respectively).

The WOR behavior for the three cases with varying degree of crossflow is shown in Fig. 11. The earliest sudden increase in WOR represents water breakthrough in the production well. For all cases, water in the most-permeable layer breaks through first, since all other factors are equal. Case 1 (k_v/k_h=0) shows a pronounced increase in the WOR for each layer breakthrough. The WOR then levels out until the next layer breaks through. This effect is also seen for Case 2 (k_v/k_h=0.1), but Layers 2 and 3 break through earlier than for Case 1, due to some crossflow of water from high- to low-permeability layers. For Case 3 (k_v/k_h=1), the breakthrough of Layers 2 and 3 are indiscernible since they occur immediately after Layer 1 breaks through. This is due to the unrestricted crossflow of water from high- to low-permeability layers.

If crossflow can occur between layers in a reservoir, a favorable mobility ratio (the displaced phase being more mobile than the displacing phase) will cause the displacing fluids to penetrate into low-permeability layers to a greater extent than if crossflow is not possible, thus improving the vertical sweep efficiency.[11,12] The direction of crossflow is from the high-to-low velocity layers at the trailing water front and in the opposite direction at the leading front, thus causing the leading and trailing fronts to be reversed and advanced, respectively, over their no-crossflow positions. These observations are consistent with the results from this study.

Fig. 11 also shows that the higher the degree of crossflow, the later the water breakthrough, which also is explained by the process described above. After all layers start producing water, the WOR increases gradually with a constant rate that is very similar for all cases. The time period simulated was 20 years for all cases.

The WOR and WOR' behaviors for Case 1 (k_v/k_h=0) are shown in Fig. 12. Each layer breakthrough is characterized by peaks in the WOR derivative, caused by rapid increases in the WOR over short periods of time. After each layer breakthrough, the WOR curve levels out and the derivative curve shows a negative slope until the next layer breaks through. The constant rate WOR increase after the last layer breakthrough results in a nearly flat derivative curve.

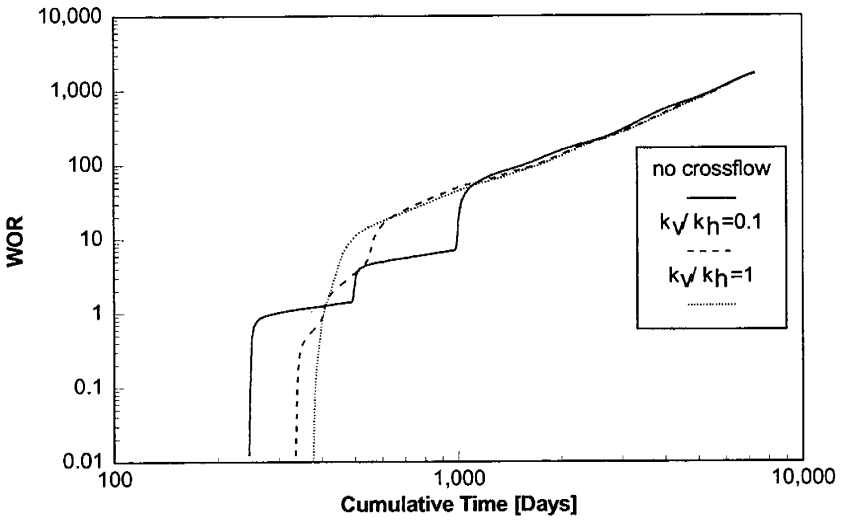

Fig. 11. Multi-layer channeling base case.
WOR behavior is shown for varying degree of crossflow.

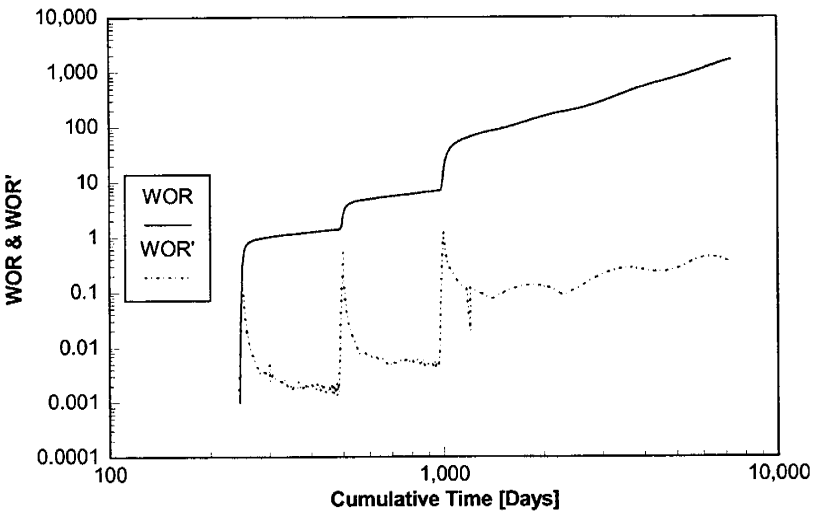

Fig. 12. WOR and WOR' behavior for the no-crossflow case (Case 1) shown in Fig. 11.

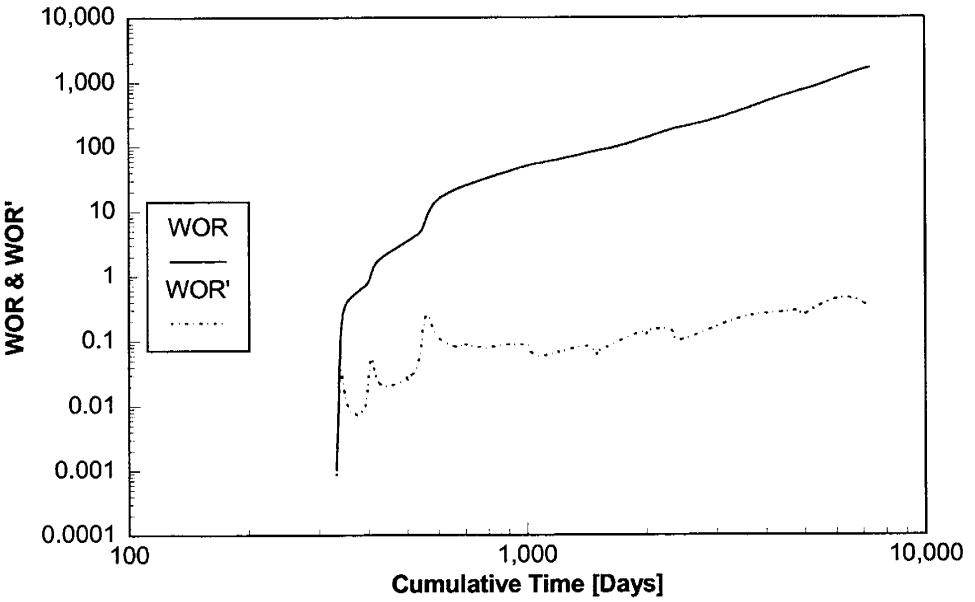

Fig. 13. WOR and WOR' for the k_v/k_h=0.1 case (Case 2) shown in Fig. 11.

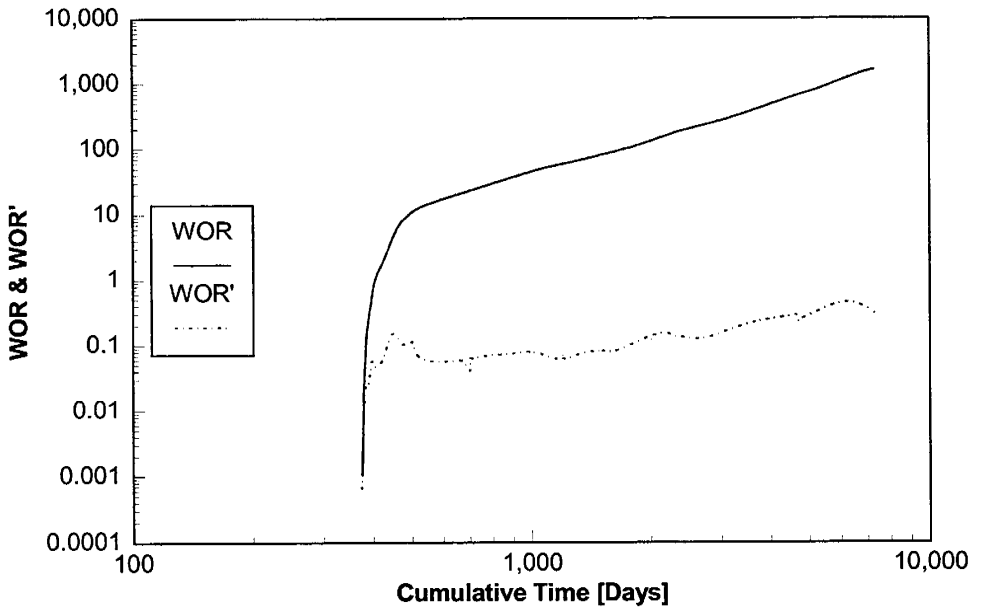

Fig. 14. WOR and WOR' behavior for the vertical-equilibrium case (Case 3) shown in Fig. 11.

Fig. 13 shows the WOR and WOR' curves for Case 2 (k_v/k_h=0.1). The peaks in the WOR derivative curve were not as distinctive as for Case 1, neither were the negative slopes due to the earlier breakthroughs of each layer. The WOR derivative curve remained flat after the last layer broke through. The same behavior was observed for Case 3 (k_v/k_h=1), shown in Fig. 14. Since all layers broke through between 370 and 450 days, the WOR derivative peaks were small or negligible.

To determine whether some of the crossflow was caused by gravity drainage, or water running under the oil, Cases 2 and 3 were run with the layers arranged in order of increasing permeability (the high-permeability layer on the bottom). The density difference between water and oil was approximately 13 lb/ft^3. Fig. 15 shows that when the high-permeability layer (Layer 1) was placed at the bottom and some crossflow occurred, the most permeable layer broke through about 10-20 days earlier than for the base case (Layer 1 at the top). Also, the two less-permeable layers broke through a little later. However, the overall behavior was very similar for each of the crossflow cases, independent of how the layers are arranged. This result suggests that even if gravity drainage affects the layer breakthrough times to some extent, viscous forces dominate the crossflow between layers for these cases. We performed several simulations using lower pressure gradients to investigate cases where gravity dominates the flow pattern during the displacement (see Figs. A.21-A.23 in Appendix A). As expected, these figures show that when crossflow is possible and gravity dominates over viscous forces, the ordering of the low- and high-permeability layers has a substantial effect on the WOR versus time curves. Additional diagnostic plots for multi-layer channeling cases are shown in Appendix A (Figs. A.1 to A.23).

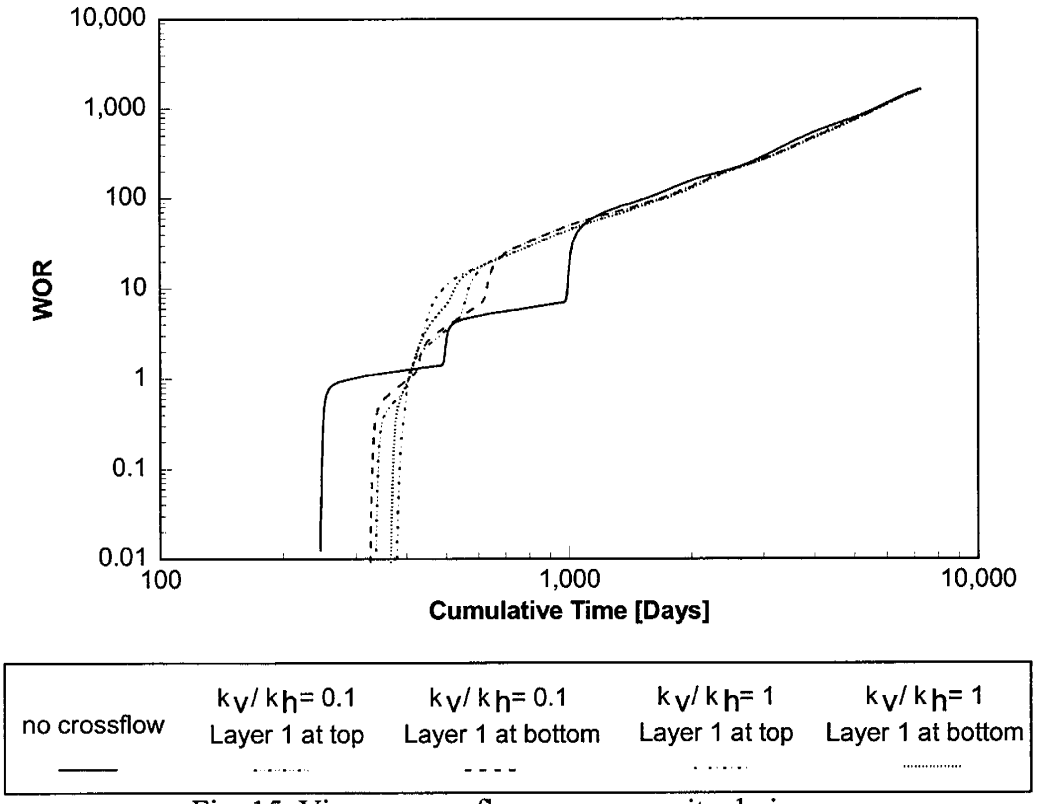

Fig. 15. Viscous crossflow versus gravity drainage.

Three-Dimension Linear Model. The two-dimensional multi-layer channeling results discussed in the previous section are also valid for three-dimensional linear flow. Running the base cases using more than one gridblock in the y-direction can show this fact. The base case model was modified for this purpose by dividing the 30-ft gridblock in the y-direction into three blocks, each 10 ft long (bottom of Fig. 16). Three injectors and three producers were placed in x-gridblocks 1 and 42, respectively. The short distance between each of the injectors causes the flow from the wells to interfere rapidly, thus creating a linear waterfront throughout the reservoir. The drainage area is the same for both models. Fig. 17 shows a comparison between 2D and 3D linear flow for different degrees of vertical communication between layers.

If all other parameters are kept the same and the flow is linear, the results will be very similar for larger drainage areas since the amounts of injected water and produced oil increase by the same factor. This finding is shown in Fig. 18, where the gridblock size in the y-direction for the 3D model was increased to 30 ft (by a factor of 3). Hence, the drainage area is three times larger than for the 2D case and the gridblock sizes are equal.

For a given degree of vertical communication between layers, Figs. 17 and 18 show virtually the same behavior for the 2D and 3D linear models.

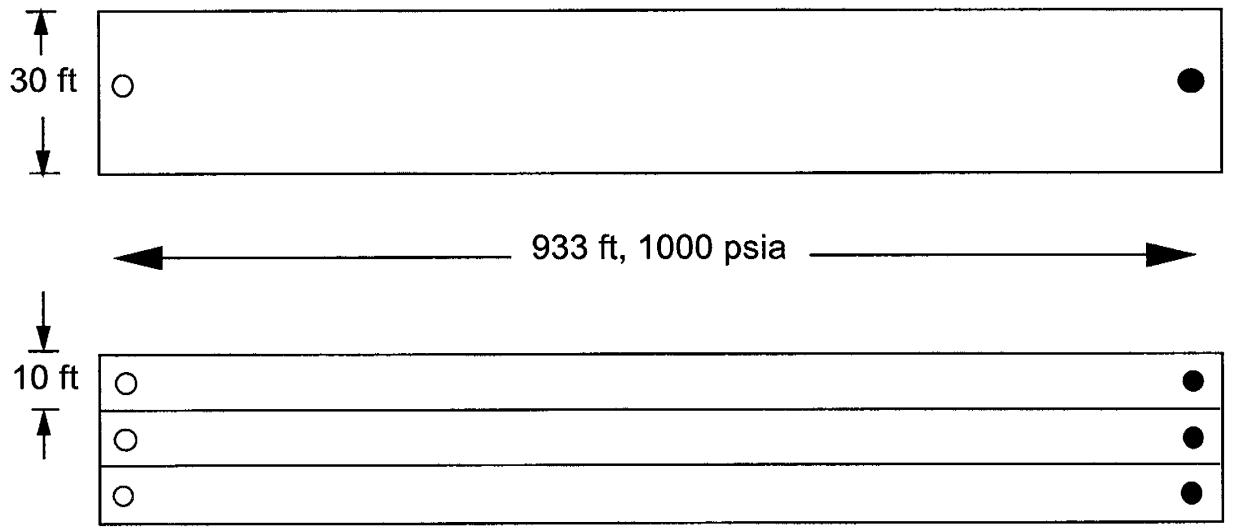

Fig. 16. Schematic top views of the 2D (upper) and 3D (lower) linear flow models. The open circles represent producers and the solid circles represent injectors. Note that the gridblock dimensions in the z-direction are not shown.

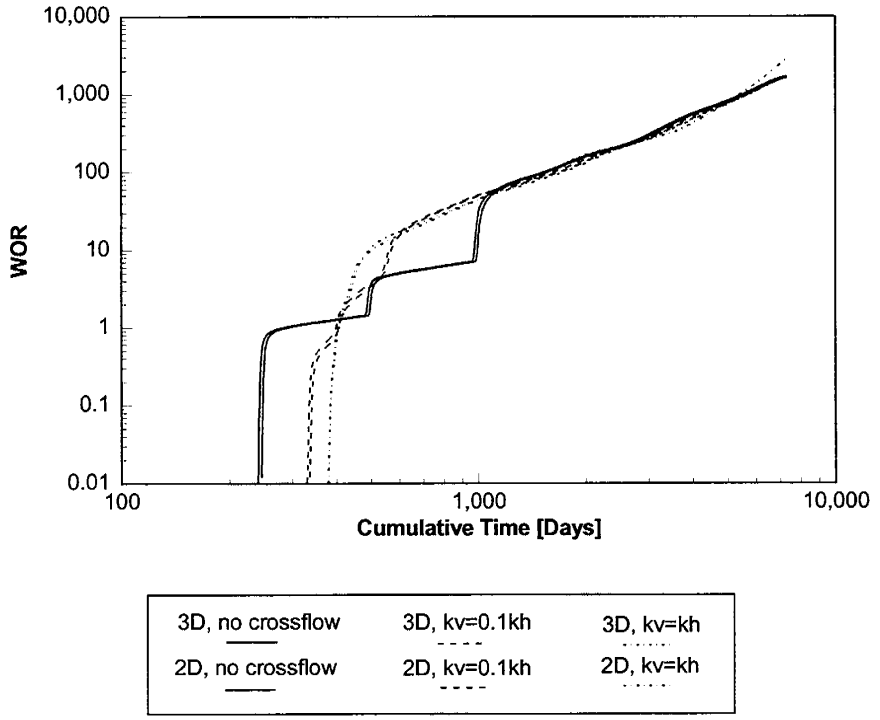

Fig. 17. 2D versus 3D linear flow for equal drainage areas and different gridblock sizes.

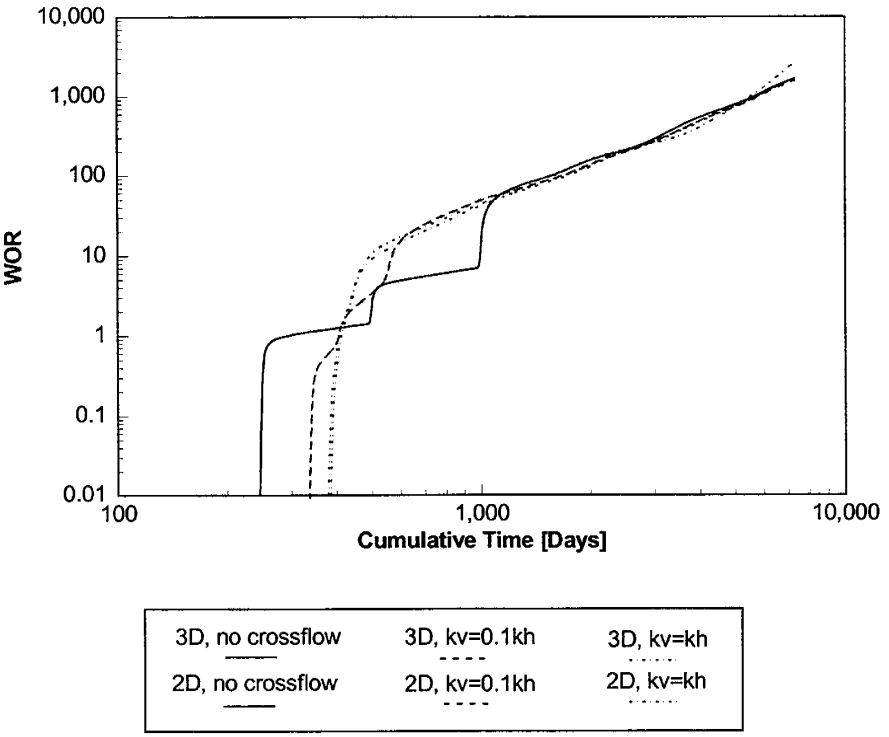

Fig. 18. 2D versus 3D linear flow for different drainage areas and equal gridblock sizes.

Three-Dimension Radial Model. A 3D areal model was built to investigate the response that the diagnostic plots show for radial flow. Different grid dimensions were evaluated: 11×11×3(5), 13×13×3(5), and 21×21×3(5) gridblocks. The first model gave earlier water breakthrough than the two others and the last model gave very long run times, especially for no-crossflow cases. Therefore, the 13×13×3(5) gridblock model was used for this study (Fig. 19).

The wells are assumed to be placed in a 40-acre five-spot pattern, so that the distance between an injector and a producer is 933 ft. One-fourth of the drainage area was modeled, so each layer height was multiplied by four to get the correct original oil in place (OOIP). All other parameters were identical to those of the linear cases.

Fig. 20 compares the radial and the 2D linear flow models for varying degrees of vertical communication. The WOR behavior (and therefore also the WOR derivative behavior) was very similar for the two models, except that much later water breakthrough occurred for all layers for the radial cases.

Multi-layer channeling diagnostic plots for a given degree of crossflow were very similar for two- and three-dimensional linear and radial models. Therefore, the base case 2D cross-sectional model will be used to predict WOR and WOR derivative behavior for all multi-layer channeling cases in the remainder of this chapter.

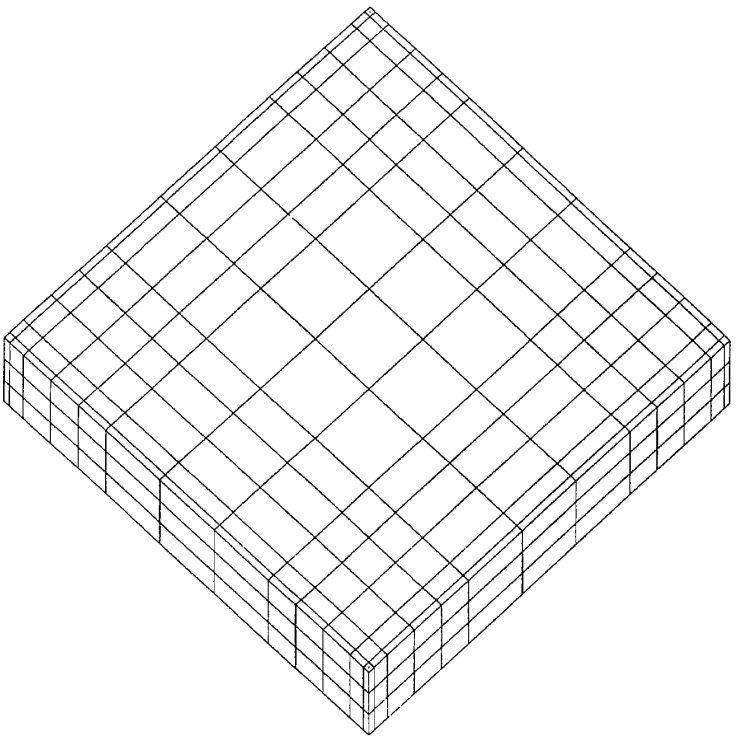

Fig. 19. 3D radial flow model, [13×13×3(5)] gridblocks.

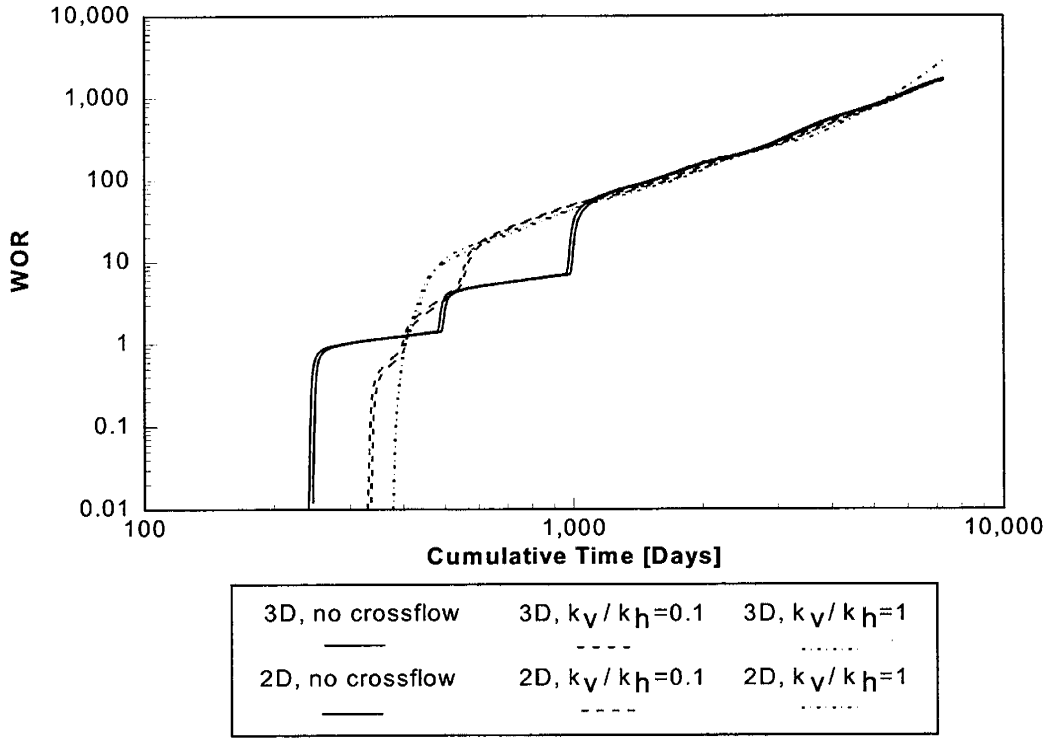

Fig. 20. 2D linear flow versus 3D radial flow for varying degree of vertical communication.

WOR Derivative Behavior. The base-case diagnostic plots (Figs. 11-14) demonstrate that a negative WOR' can be observed for multi-layer channeling, and the effect is particularly distinctive for the no-crossflow case (Fig. 12). Thorough examination of Figs. A.1 through A.20 in Appendix A reveals that this effect becomes more evident as the layer permeability contrast increases.

Early water breakthrough is often caused by water channeling through a layer of much higher permeability than the rest of the formation. To simulate this case, the layer permeabilities of the base case were changed to 500, 25, and 20 md (hereafter referred to as Case 4), which give a permeability contrast of 20 between the two most permeable layers.

Figs. 21 through 24 show the diagnostic plots for Case 4. The no-crossflow derivative curve clearly has a negative slope for approximately 2,000 days, until Layer 2 starts producing water (Fig. 22). The two crossflow cases show a negative derivative trend for between 100 and 300 days. After all layers break through, the slope is close to zero (Figs. 23 and 24).

These results clearly contradict Chan's claim that diagnostic plots with a negative derivative trend diagnose the excessive water production mechanism as bottom-water coning.

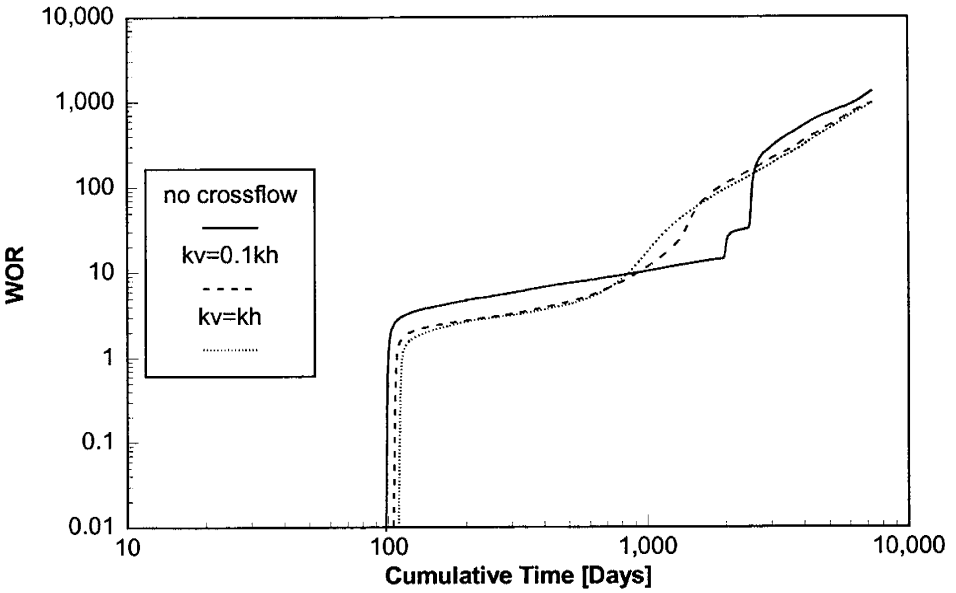

Fig. 21. Case 4 WOR behavior for varying degrees of crossflow. The permeability contrast between Layers 1 and 2 is 20.

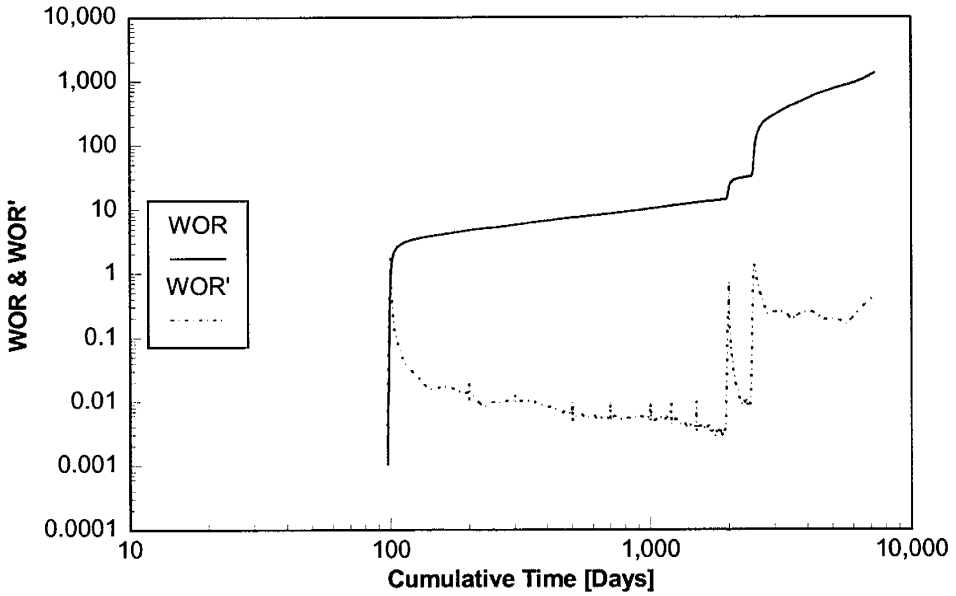

Fig. 22. WOR and WOR' curves for the no-crossflow case shown in Fig. 21.

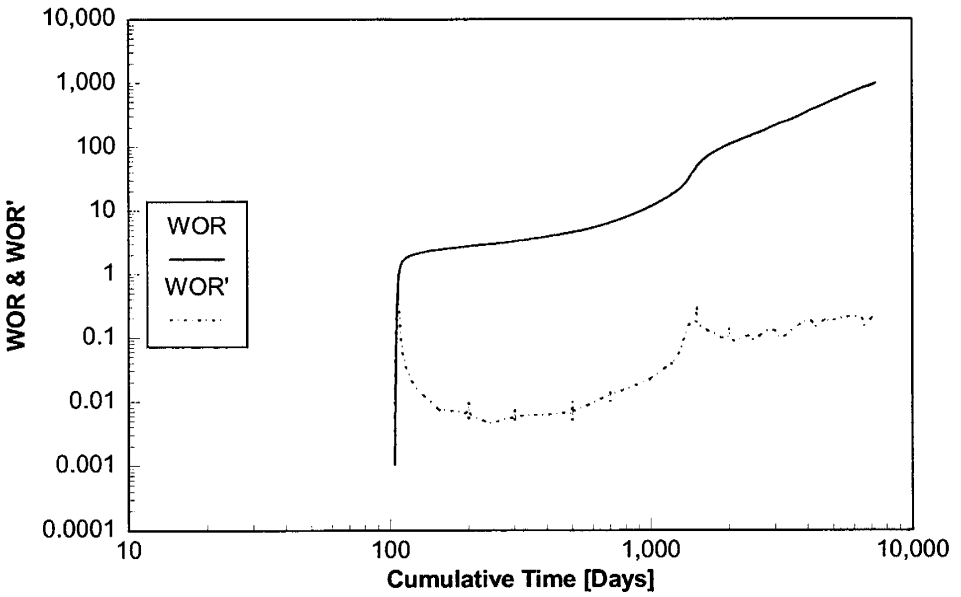

Fig. 23. WOR and WOR' behavior for the $k_v=0.1k_h$ case shown in Fig. 21.

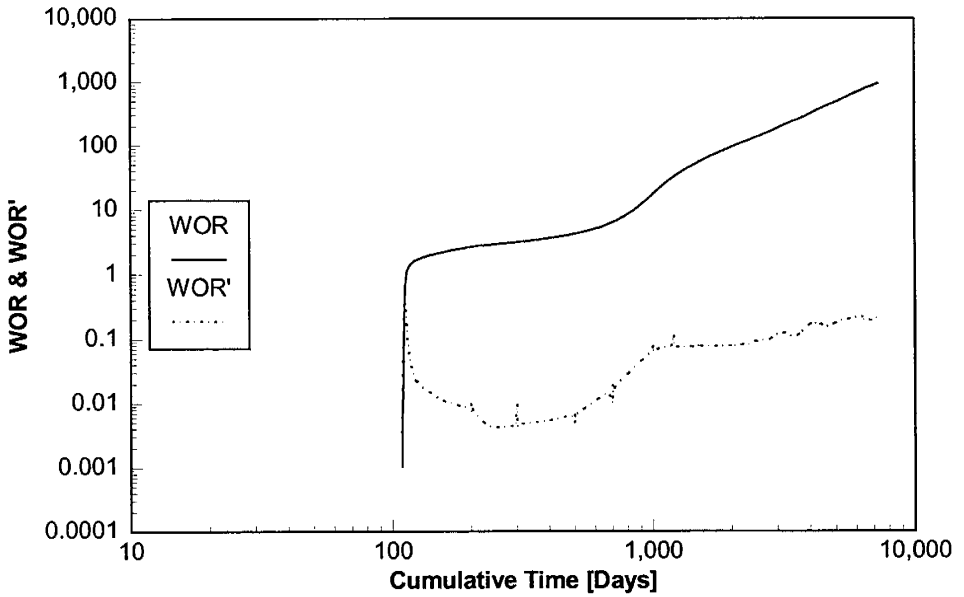

Fig. 24. WOR and WOR' curves for the vertical equilibrium case shown in Fig. 21.

Sensitivity Study. The WOR will have a constant value before water breakthrough if the initial water saturation in the reservoir is larger than the irreducible water saturation. If the values are equal, the WOR will be zero until the most water-conductive layer breaks through. This is shown in Figs. A.24 to A.26 (Appendix A), where the effect of changing the base-case initial water saturation was studied. As expected, the plots reveal that the higher the initial water saturation, the larger the constant WOR value before water breakthrough, and also the earlier the water breakthrough for all layers. This result occurs for all degrees of vertical communication studied. Higher initial water saturation also results in a smoother and more gradual WOR increase for each layer breakthrough.

According to Chan[7,8], the time length of the initial period (from start of production to water breakthrough) depends on the water-drive mechanism. Hence, Chan suggests that the first sharp increase in WOR should occur at an earlier time for coning than for channeling, if the cases are simulated using the same set of reservoir and fluid data.

As shown earlier, for the channeling cases, the onset of a rapid WOR increase varies with saturation distribution and degree of vertical communication among layers. Other factors that affect the water breakthrough are layer permeability contrast, pressure differential between injector and producer, well spacing, and relative permeability curves. Figs. A.27 to A.29 demonstrate that higher permeability of the most permeable layer causes earlier breakthrough.

The pressure gradient in the reservoir was changed by varying the injector pressure and keeping the producer pressure and the distance between the wells constant (Figs. A.30-A.32), and by changing the well spacing and keeping the pressure differential constant (Figs. A.33-A.35). As expected, earlier water breakthrough occurred when the pressure gradient increases. The fracture gradient of the reservoir was assumed to be 0.75 psi/ft, a fairly conservative estimate. This assumption gave a fracturing pressure of about 3,830 psia at 5,090 ft, so the highest injector pressure of 3,500 psia was less than this value.

Increasing the endpoint relative permeability to water also causes earlier water breakthrough and higher WOR at a given time (Figs. A.36-A.38), as more water is moving at a given saturation. The base-case oil relative permeability curve and the water exponent (slope of the water relative permeability curve) were not changed. Figs. A.39 through A.41 show the effect of changing the endpoint permeability to oil for the base case.

Figs. A.42 through A.44 show the effect of varying the oil exponent in Eq. 3, hence the curvature of the oil relative permeability curve. An oil exponent of 1 corresponds to a straight curve, and the curvature increases with increasing exponent. Hence, the oil relative permeability becomes smaller at a given saturation, causing the oil to move at a lower rate as the exponent increases. This situation causes later water breakthrough for larger oil exponents. The transition periods between each of the layer breakthroughs are notable for the cases with $k_v/k_h=0$ and $k_v/k_h=0.1$, even if the permeability contrast between adjacent layers is only two. The last transition period is very pronounced for all degrees of vertical communication, provided that the oil relative permeability curve has some curvature. Cases with straight oil relative permeability curves show

very rapid WOR increase and no transition period (when all layers have experienced break through), which resembles the behavior observed by Chan.

The slope of the water relative permeability curve is only important at low water saturations, since the base-case endpoint relative permeability value is so low. This fact causes the relative permeability values to be almost identical at high water saturations, independent of water exponent value. This result, in turn, gives very similar WOR behavior. Higher water exponents provide a lower relative permeability to water at a given saturation, especially at low water saturations, thus making the water move slower and causing later water breakthrough. This result is shown in Figs. A.45 to A.47.

Chan claims[7,8] that the transition periods of the channeling case are indiscernible if the layer permeability contrast is less than 4. The permeability contrast of the upper and lower layer is exactly 4 for the base case, so the layer permeabilities were changed to 300, 250, and 200 md, which give a maximum permeability contrast of 1.5. No other variables were changed. Figs. A.42 to A.44 reveal that the curvature of the oil relative permeability curve affects the magnitude of the transition period after all layers break through. The oil exponent was therefore varied for the new set of layer permeabilities. The results are shown in Figs. A.48 to A.50. The last transition period (when all layers have broken through) is still notable for all cases where the oil exponent is larger than 1, and transition periods between each of the layer breakthroughs are seen for no-crossflow cases.

The results from the sensitivity study show that several parameters affect the WOR (and thereby the WOR') behavior for multi-layer channeling. The oil exponent value dictates the slope of the WOR curve after all layers have broken through. An oil exponent value close to 1 makes the WOR increase rapidly (and will give a positive derivative slope), in contrast to a higher value, which gives a more gradual WOR increase (and may give a negative derivative slope). Chan suggests that a positive derivative slope always indicates a channeling problem.

For these cases, the water exponent value does not affect the WOR behavior much. A high permeability contrast between adjacent layers promotes longer periods of constant WOR increase and thereby zero and negative derivative slopes, which Chan claims is indicative of a coning problem. Varying the endpoint relative permeability values for oil and water and varying the pressure gradient in the reservoir mainly affect the breakthrough time, where the WOR starts increasing rapidly. The overall WOR behavior is similar for these cases. However, crossflow cases with lower endpoint relative permeability to oil show a smoother and more s-shaped WOR curve. The same effect can be observed for initial water saturations higher than the irreducible water saturation. According to Chan's diagnostic plots, this behavior is typical for coning.

Coning Simulation Results

Base Case. The diagnostic plot for the water coning base case (simulated over 10,000 days) is shown in Fig. 25. Breakthrough occurred at 30 days. After this point, the WOR increased up to approximately 200 days, where it increased more gradually with a fairly constant slope until it reached 10,000 days. The overall derivative trend was constant (zero slope), which contradicts

the results obtained by Chan, according to whom a coning case should always show a partial negative slope.

For Chan's coning model, bottom-water influx was simulated by constant pressure water injection at the edge and only into the lower water layer. For this study, the reservoir was made close to infinite-acting by giving the outer radial gridblock of the lower water layer a very high porosity. To make sure that the differing results obtained from these two studies were not caused by different boundary conditions, a new model was made by adding an extra 2-ft radial gridblock to the base case coning model. The size of gridblock 11 was reduced by 2 ft to keep the drainage area the same. A well was placed in this outer gridblock, injecting water into the lower water layer at a constant pressure of 3,000 psia. The porosity of the outer and lower radial gridblock was reduced to 20%. A comparison of the two cases is presented in Fig. 26. The curves show a very similar WOR behavior, and they are indistinguishable after 2,000 days. This result suggests that both methods can be applied to represent a bottom-water drive mechanism. For this study, however, the "infinite-acting" case was chosen for all of the simulations.

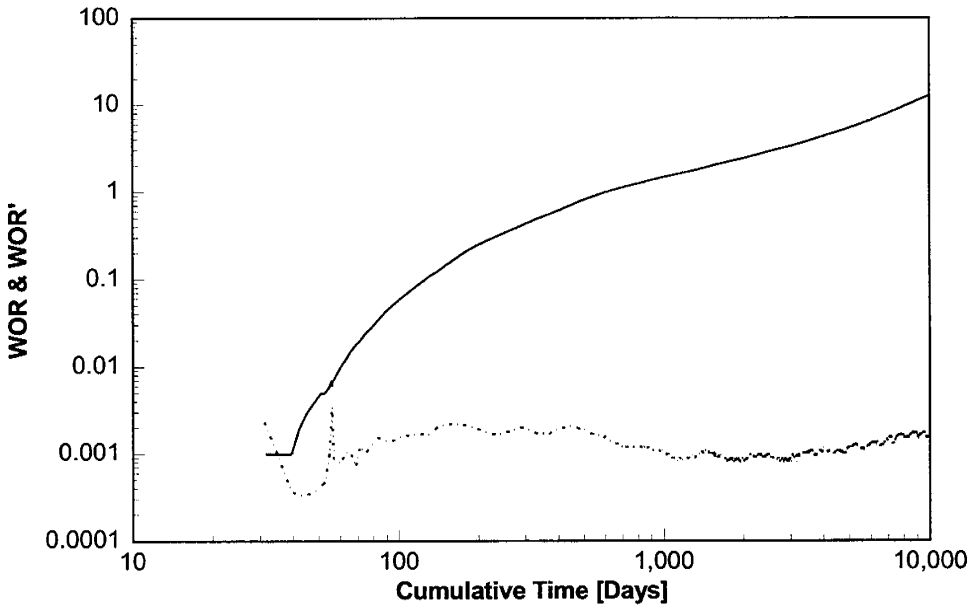

Fig. 25. WOR and WOR' behavior for the coning base case.
160-acre drainage area and $k_v=0.1k_h$.

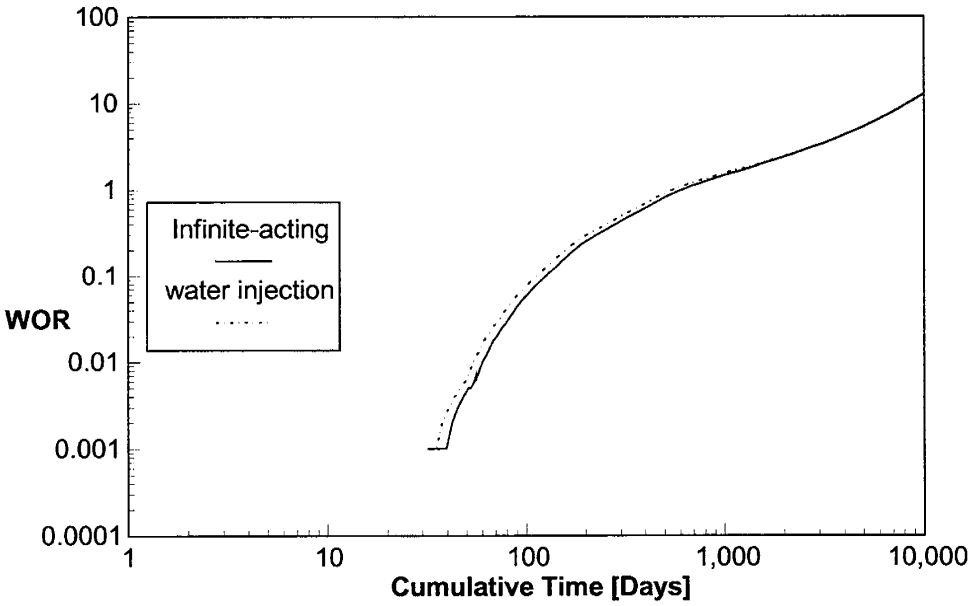

Fig. 26. Comparison of different boundary conditions.
Constant pressure water injection at the edge into lower water layer versus making the reservoir "infinite-acting" by assigning a very high porosity to lower and outer radial gridblock.

Sensitivity Study. Fig. 27 shows the effect of running the base case for different drainage areas (vertical-to- horizontal permeability ratio equals 0.1 for all cases). The water production becomes more severe as the drainage area decreases; thus, the WOR curves grow steeper. This is caused by the cone growing faster to cover the perforations and also expanding faster laterally for smaller drainage areas. All cases break through at approximately the same time. The WOR increase is fairly rapid for the 20- and 40-acre drainage areas, so their WOR curves show a positive derivative slope. Confirming this behavior, Figs. A.51 to A.53 (Appendix A) show the diagnostic plots for the smaller drainage areas. The 80-acre drainage area case shows a gentle, positive derivative slope throughout the simulated period.

Fig. 28 shows the effect of running the base case (160-acre drainage area) for different vertical-to-horizontal permeability ratios. As expected, a lower degree of vertical communication gives later breakthrough times than for the base case. Diagnostic plots corresponding to Fig. 28 are shown in Figs. A.54 to A.56. The $k_v=0.05k_h$ case shows a near-zero slope throughout the simulated period. Both cases with a high degree of crossflow ($k_v=0.5k_h$ and $k_v=k_h$) exhibit a negative slope that levels out to a constant value after 1,000 days.

Fig. 29 shows how different capillary pressure curves (from Fig. A.57) affect the coning WOR behavior. The solid curve represents the base case. The corresponding capillary pressure curve has a fairly low endpoint value of 4 psi that drops rapidly to a low value that remains close to constant for the given saturation range. For the middle curve (Case 1, defined in Fig. A.57), the endpoint capillary pressure for the base case has increased to 10 psi. The third capillary pressure curve (Case 2, defined in Fig. A.57) also has an endpoint value of 10 psi, but it shows higher values for a given saturation than the other two curves.

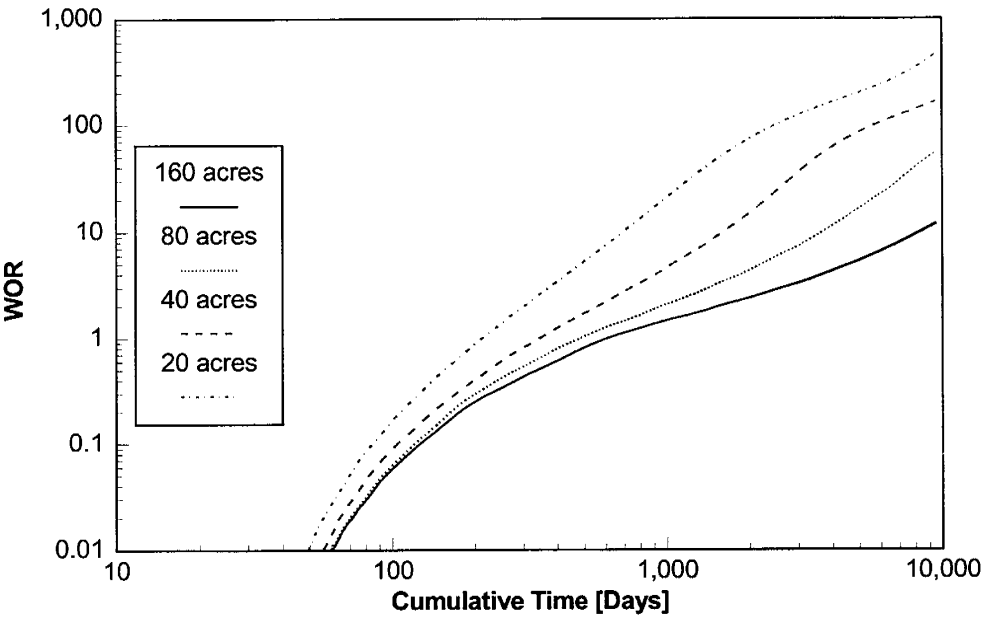

Fig. 27. Effect of varying the drainage area for coning case.
The solid line represents the base case.

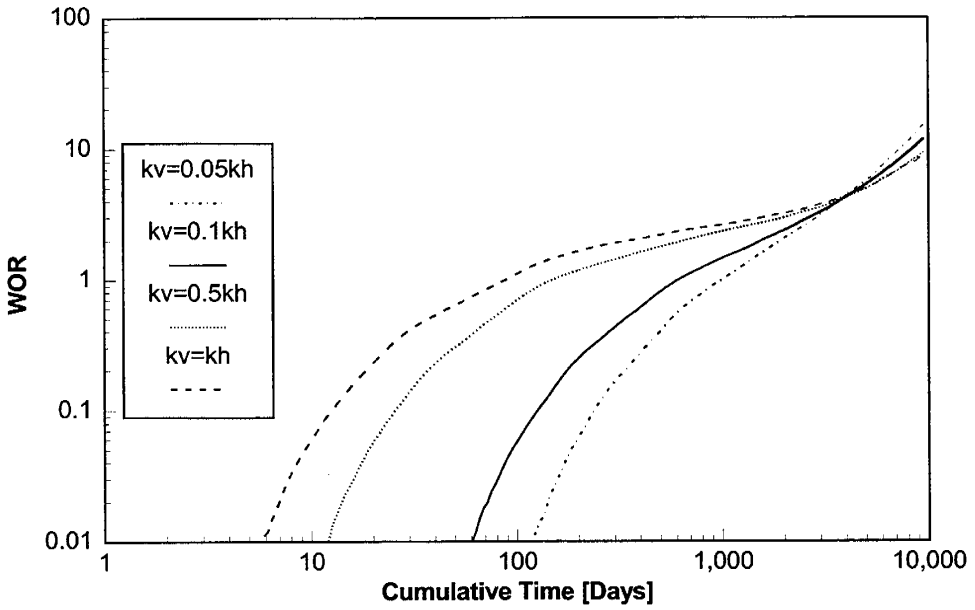

Fig. 28. Effect of different degree of vertical communication for coning case.

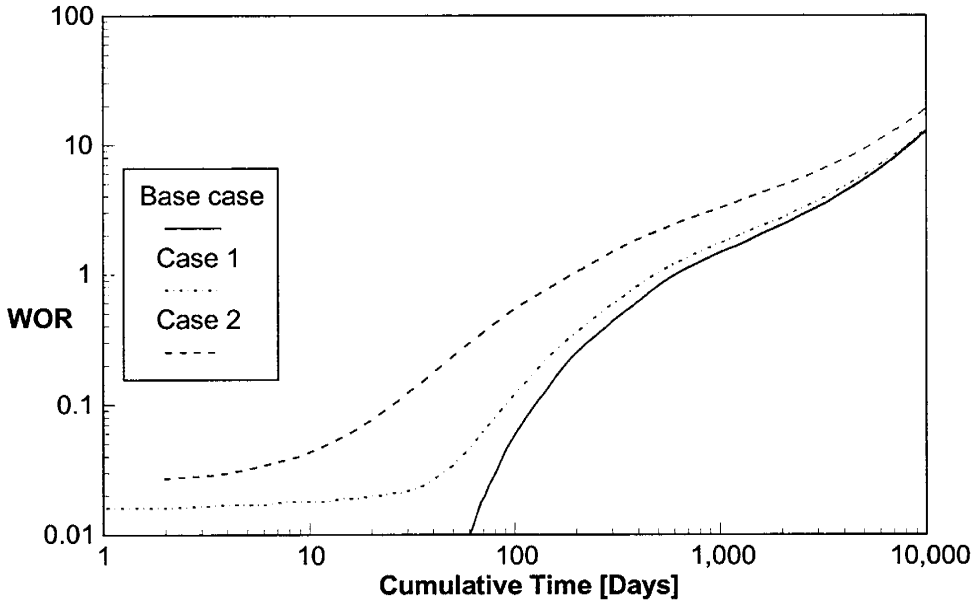

Fig. 29. Effect of using different capillary pressure curves (defined in Fig. A.57). The relative permeability curves were not changed.

The capillary pressure curve may cause a transition zone of increased water saturation in the oil zone, where the initial water saturation increases with closeness to the WOC. If the capillary pressure curve has relatively high values for all saturations, the thickness of the transition zone may approach (and also exceed) the pay zone thickness. Saturation plots reveal that Layers 6-10 of the oil zone has an initial water saturation that is higher than the irreducible water saturation for Case 2. For the base case, Layer 10 alone has an increased water saturation. Higher initial water saturation causes earlier water breakthrough and higher WOR values at a given time. Compared to the base case, the initial WOR increases for Cases 1 and 2 are less abrupt (Fig. 29). This behavior results in negative derivative slopes between 100 and 1,000 days, as shown in the diagnostic plots for Cases 1 and 2 (Figs. A.58-A.59).

Fig. 30 demonstrates how different water relative permeability curves (shown in Fig. A.60), affect the WOR behavior. The oil relative permeability curve was the same for all cases. Figs. A.61 and A.62 show the corresponding derivative curves. The low endpoint value of 0.1 results in a constant positive derivative slope (Fig. A.61), and the high endpoint value of 0.95 results in a changing negative derivative slope (Fig. A.62).

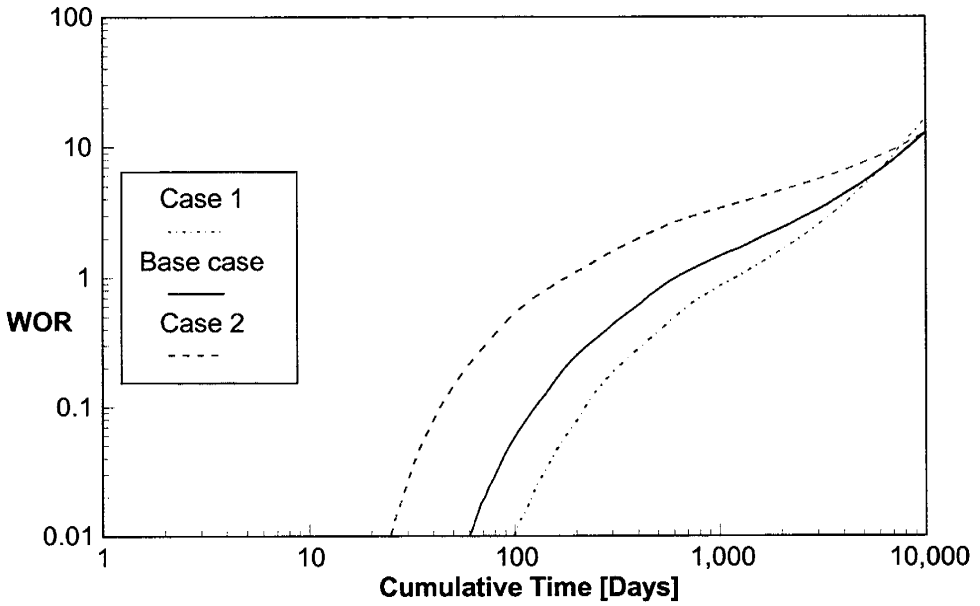

Fig. 30. Effect of using different water relative permeability curves for the base case. The oil relative permeability curve was not changed.

The results from this sensitivity study demonstrate that positive, zero, and negative WOR derivative slopes and also combinations of these can be observed for water coning problems. High values of vertical-to-horizontal permeability ratio, endpoint capillary pressure, or endpoint relative permeability to water give partial negative WOR' slopes. Small drainage areas, small values of vertical-to-horizontal permeability ratio, or low endpoint relative permeability to water, on the other hand, tend to give positive WOR' slopes. Chan, however, suggests that all coning problems will be characterized by partial negative derivative slopes.

Discussion

WOR Diagnostic Plots. Earlier, we demonstrated that the WOR and WOR derivative behavior for a multi-layer channeling case depends mainly on variables such as the degree of vertical communication and permeability contrast among layers, saturation distribution, and relative permeability curves. Varying these parameters makes it possible to create a wide variety of WOR (and WOR') responses, as shown in this chapter and Appendix A.

If mobile water is present in the reservoir, a high degree of crossflow among layers will result in smooth, s-shaped WOR curves that, according to Chan's diagnostic-plot method, should indicate a coning problem. Large oil-exponent values (or high curvature of the oil relative permeability curves) will make the WOR curve flatten out for a long period of time, as opposed to oil exponents close to 1 (straight relative permeability curves), which will make the WOR increase rapidly after all layers break through.

The WOR' will always be partially negative for no crossflow channeling cases, and may also be negative for crossflow cases provided the permeability contrast between two adjacent layers is large enough (greater than 10). Using Chan's WOR diagnostic plots, a negative derivative slope supposedly identifies the water production problem as coning.

Coning WOR and WOR derivative behavior depends mainly on the vertical-to-horizontal permeability ratio, well spacing, capillary pressure, and relative permeability curves. Large drainage areas and high vertical-to-horizontal permeability ratio values give the predicted diagnostic plot response, hence a gradual WOR increase that approaches a constant value, after which it increases rapidly. The transition period becomes more difficult to discern as the drainage area decreases; thus, the WOR increases quickly after breakthrough, giving a positive derivative slope. The same effect can be observed by decreasing the vertical-to-horizontal permeability ratio. Low capillary pressure values and low endpoint permeability to water promote a positive derivative slope. According to the diagnostic plot method, a rapid WOR increase with a corresponding positive derivative slope is a certain indication of a multi-layer channeling problem.

These results clearly show that WOR diagnostic plots are not general, since channeling cases can produce negative derivative slopes under different circumstances, just as coning cases can show positive derivative slopes. Another reason why this method cannot be valid for all cases is that the WOR and its derivative are plotted versus time, not versus dimensionless time. Dimensionless groups are commonly used to generalize problems or plots, e.g., type curves in well testing.

Diagnostic plots are supposed to show the same behavior whether the undesired produced phase is gas or water. Fig. 31 shows field data from a Prudhoe Bay oil well with a gas production problem.[8] The excessive gas production mechanism was diagnosed as coning with late-time channeling behavior, using the diagnostic plot method. However, the derivative data are so scattered that no conclusion can be drawn with respect to slope directions. Hence, WOR/GOR diagnostic plots may easily be misinterpreted.

Limitations of Simulation Study. All coning and channeling cases were simulated using favorable mobility ratios of 0.98 and 0.25, respectively. The results from this study might differ some for unfavorable mobility ratios (greater than 1), where there is a tendency for the displacing phase to channel or finger through the displaced phase.[21]

For cases with no crossflow and unfavorable mobility ratios, one would expect earlier water breakthrough and a more rapid WOR increase, as high oil saturations will remain in regions bypassed by the water.[22] In the case of crossflow, the flow directions are reversed compared to a favorable mobility ratio; hence, the direction of crossflow is from low to high velocity layers at the trailing water front and in the opposite direction at the leading front. Thus, leading and trailing fronts become farther apart compared to their no-crossflow positions.[12] The crossflowing fluid is an oil-water mixture at both fronts, as opposed to a case with favorable mobility ratio, where the crossflowing fluid is either all oil (leading front) or all water (trailing front). Compared

to the no-crossflow displacement for mobility ratios larger than one, the mixing fluid is shown to improve the vertical sweep efficiency even if the water front positions are farther apart.

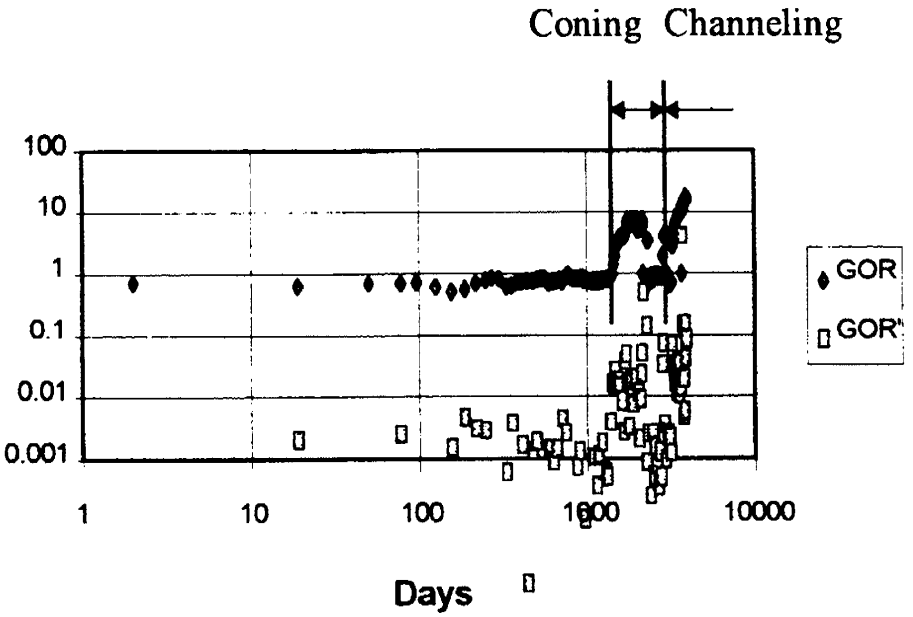

Fig. 31. Field case example.
GOR diagnostic plot showing a gas cone turning into channeling. After Chan (1996).[8]

Dipping reservoirs have not been considered for this study, which would be an interesting sensitivity case both for coning and channeling, especially if the reservoir layers are dipping into the water zone or if water is being injected updip. Depending on the mobility ratio and also on whether viscous forces or gravity forces dominate, cusping or a more stable displacement of water towards the well can be observed.

An unstable displacement in the form of cusping happens if the well is produced at high rates for an edgewater drive mechanism (or water is injected updip at high rates), causing the viscous force to prevail over the gravity force. This results in a tongue of water under-running the oil due to the density difference between the two phases, which leads to premature water breakthrough. This may only happen for unfavorable mobility ratios. In cases where the mobility ratio is less than or equal to 1, the displacement will be unconditionally stable.[23]

Validation of No-Crossflow Channeling Model. An analytical model based on fractional flow theory and material balance calculations was used to validate the no-crossflow channeling model. The input data were identical to those of the base case.

Fig. 32 compares the results from the simulation study and the analytical model. The overall match is very good, although all layers of the analytical model show earlier breakthrough than the corresponding layers of the simulation model. This result may be caused by the wells being

placed in the center of a (10×30×30) ft^3 gridblock. Thus, there is a 160-bbl pore volume behind the injector that must be filled before the water starts flowing towards the producer, causing a delay in breakthrough times.

It is impractical to solve cases with crossflow among layers analytically; therefore those are difficult to validate. However, the crossflow cases for this study were modeled by eliminating the impermeable layer that is placed between each pair of producing layers for the no-crossflow cases, and changing the vertical-to-horizontal permeability ratio. When comparing curves for corresponding cases, the behavior of the crossflow cases relative to the no-crossflow cases was what one might expect intuitively. This observation suggests also that the crossflow models are correct.

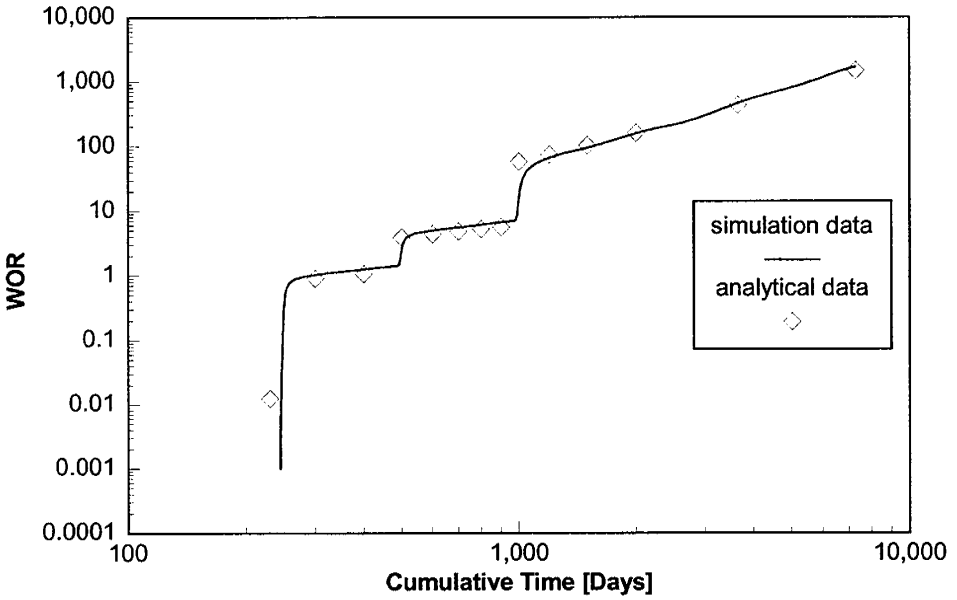

Fig. 32. Comparison; simulation model results versus analytical model results.

Conclusions

The following conclusions were drawn from this study:

1. Multi-layer channeling WOR and WOR' behavior is dictated by the degree of vertical communication and permeability contrast among layers, saturation distribution, pressure gradient in the reservoir, and relative permeability curves.
2. No-crossflow channeling cases always show partial negative derivative slope; crossflow cases show negative slope for large permeability contrasts. Oil relative permeability curves with a high degree of curvature tend to level out the WOR curve, thus increasing the probability of seeing negative WOR' slopes. According to Chan's diagnostic-plot method, gradually increasing WOR curves with negative derivative slopes are unique for coning problems.

3. Bottom-water coning WOR and WOR' behavior is governed by vertical-to-horizontal permeability ratio, well spacing, relative permeability, and capillary pressure curves.

4. Coning cases with low vertical-to-horizontal permeability ratios and small drainage areas can give rapid WOR increase and positive derivative slopes. Chan's diagnostic-plot method will identify this behavior as channeling through high-permeability layers.

5. This study demonstrates that multi-layer channeling problems can easily be mistaken as bottom-water coning, and vice versa, if WOR diagnostic plots are used alone to identify an excessive water production mechanism.

6. WOR diagnostic plots can easily be misinterpreted and should therefore not be used by themselves to diagnose the specific cause of a water production problem.

3. SIZING GELANT TREATMENTS IN HYDRAULICALLY FRACTURED PRODUCTION WELLS

A large number of gel treatments have been applied in production wells with the objective of reducing water production without sacrificing hydrocarbon production.[6] The most successful treatments occurred when the excess water production was caused either by flow behind pipe or by channeling or "coning" through fractures.[3,6,24] For gel treatments in fractured production wells, the design of the gelant volumes has been strictly empirical. A survey of field activity revealed that the vast majority of gel treatments were very small—less than 1,000 bbl/well.[6] The sizing of gelant treatments varies somewhat from vendor to vendor. For some vendors, the gelant volume is initially planned as 1/2 to 1 day's production volume. Other vendors plan for a certain number of barrels of gelant per foot of net pay. Still others plan to inject gelant to reach a certain radius from the wellbore. The latter plan seems ironic since most treated wells are thought to be fractured, where the flow geometry is described better as linear rather than radial.[6]

Substantial improvements are needed in the design methods used for sizing gel treatments. We strongly suspect that the most effective design procedures will vary with the type of problem being treated. In particular, different design procedures should be used for (1) flow-behind-pipe problems, (2) unfractured wells where crossflow cannot occur, (3) unfractured wells where crossflow can occur, (4) hydraulically fractured wells, and (5) naturally fractured reservoirs. The focus in this paper is on sizing gelant treatments in hydraulically fractured production wells. First, the volume of gelant that leaks off into the porous rock is shown to be usually substantially greater than the fracture volume. Second, conditions are quantified when leakoff occurs at a rate that is independent of length along the fracture. Third, we quantify oil and water productivity losses and improvement in the water/oil ratio after a gel treatment. Next, parameters are discussed that are necessary to design a gel treatment, and the most expedient methods to obtain that information are identified. Finally, we present a simple 11-step procedure for sizing gelant treatments in hydraulically fractured production wells. This procedure has been incorporated in a software package.

Fracture Volume Versus Leakoff Volume

When a gelant is injected, what fraction of the gelant volume locates in the fracture versus in the porous rock? Usually, the volume associated with a given fracture is quite small unless the fracture is exceptionally wide. To illustrate this point, consider a vertical two-wing fracture with height, h_f, effective width, w_f, porosity, ϕ_f, and half-length, L_f. The total fracture volume, V_f, in both wings of the fracture is given by Eq. 11.

$$V_f = 2h_f L_f w_f \phi_f \tag{11}$$

For gelant that leaks off evenly from the fracture faces, Eq. 12 describes the relation between gelant volume in the matrix, V_m, leakoff distance, L_p, and matrix porosity, ϕ_m, for two wings of a fracture that cut through a single zone of height, h_f.

$$V_m = 4h_f L_p L_f \phi_m \tag{12}$$

Dividing Eq. 12 by Eq. 11 reveals that the ratio, V_m/V_f, equals $(2L_p\phi_m)/(w_f\phi_f)$. If L_p=1ft, w_f=0.1 in., ϕ_f=1, and ϕ_m=0.2, then the gelant leakoff volume is 48 times greater than the volume in the fracture. Thus, in a typical gel treatment, unless the fractures are unusually wide, the gelant volume in the matrix will be substantially greater than that in the fracture.

Consider the propagation of a gelant front in a fracture as a function of volume of gelant injected. To simplify this problem, assume that fluid leaks off from the fracture faces at a flux that is independent of distance along the fracture. Also, assume that the gelant has the same viscosity and mobility as the water that originally occupies the fracture. (We will relax both of these assumptions in later sections.) Then, Eq. 13 describes the relation between the gelant front in the fracture, L, and the volume of gelant injected, V. Eq. 13 is derived in Appendix B (Eq. B5).

$$V / V_f = -\ln(1 - L / L_f) \tag{13}$$

Using Eq. 13, Fig. 33 plots the fracture volumes of gelant injected (V/V_f) versus the position of the gelant front relative to the total fracture length (L/L_f). The plot is fairly linear for L/L_f values between 0 and 0.6. At higher values, the plot curves sharply upward. Fig. 33 shows that injection of 1, 2, 3, and 4 fracture volumes leads to L/L_f values of 0.63, 0.87, 0.95, and 0.98, respectively. Interestingly, much more than 1 fracture volume of gelant must be injected to fill the fracture. In fact, Eq. 13 predicts that the gelant front will never reach the end of the fracture. However, for practical purposes, the fracture is effectively filled after injecting 3 or 4 fracture volumes. This volume is very small for most gel treatments.

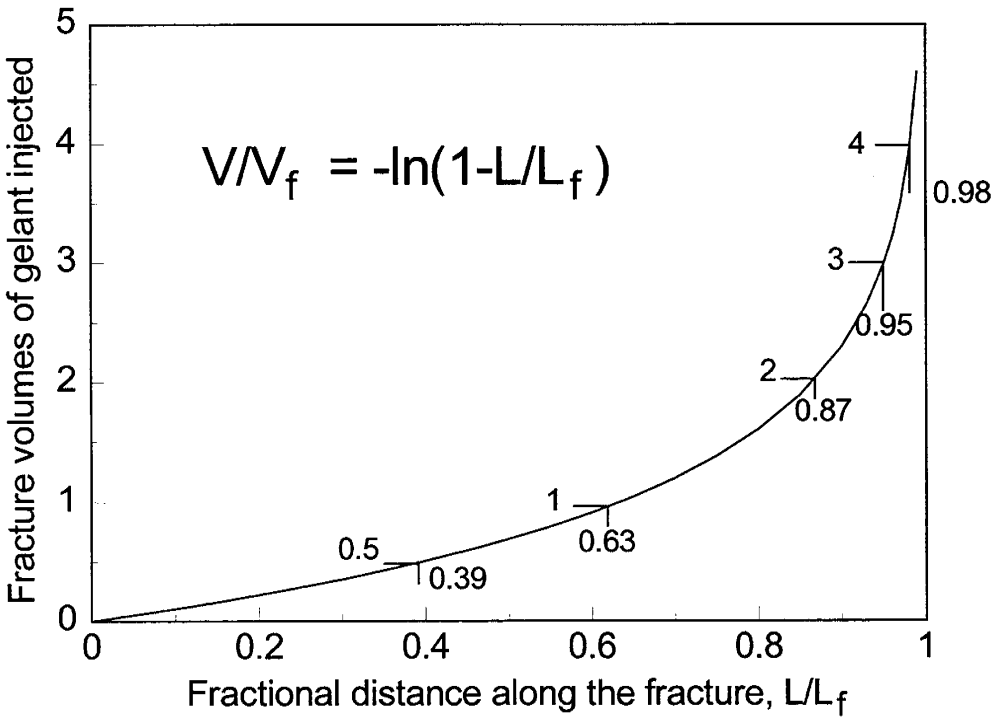

Fig. 33. Gelant volume versus front position when the leakoff flux is independent of distance along the fracture.

Leakoff Distance Versus Length Along a Fracture

An important assumption made in deriving Eq. 13 was that the leakoff flux, u, was independent of distance along the fracture. When is this assumption valid, and what does the leakoff profile really look like along a fracture? This question is addressed by Eq. 14, which is derived in Appendix B (Eq. B33).

$$u = -\frac{q_0 C[e^{CL} + e^{2CL_f} e^{-CL}]}{2h_f(1-e^{2CL_f})} \tag{14}$$

In Eq. 14, q_o is the total volumetric injection rate, and C is a constant given by Eq. 15.

$$C = \sqrt{2k_m / (k_f w_f r_e)} \tag{15}$$

In Eq. 15, k_m is the permeability of the porous rock, and r_e is the external drainage radius of the well. Eq. 16 (from Eq. B.35 in Appendix B) expresses Eq. 14 in a slightly different form.

$$\frac{u}{u_0} = \frac{e^{CL} + e^{2CL_f} e^{-CL}}{1+e^{2CL_f}} \tag{16}$$

Here, u_o is the leakoff flux at the wellbore (i.e., at L=0).

Fig. 34 plots u/u_o versus L/L_f for several values of the parameter, CL_f. Note that the leakoff flux is basically independent of distance along the fracture when CL_f is 0.3 or less. However, for CL_f values above 3, the leakoff flux is quite sensitive to distance along the fracture. Therefore, CL_f is an important parameter for gel treatments in hydraulically fractured wells.

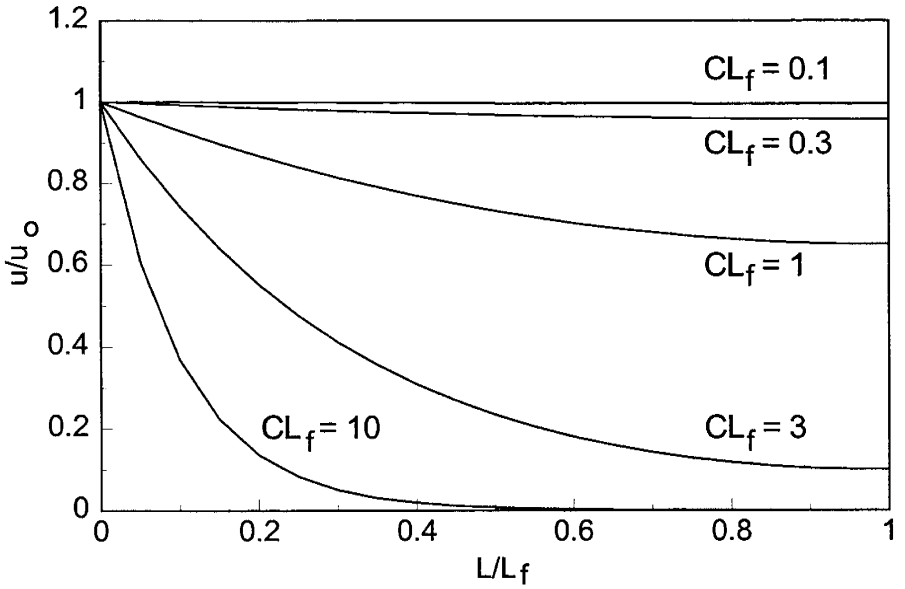

Fig. 34. Leakoff flux versus distance along the fracture.

Using Eq. 16, Eq. 17 was derived (Eq. B46 in Appendix B).

$$\frac{V}{V_f} = \left[\frac{e^{-CL_f} - e^{CL_f}}{2CL_f}\right] \ln\left[\left(\frac{e^{CL_f} - e^{CL}}{e^{CL_f} + e^{CL}}\right)\left(\frac{e^{CL_f} + 1}{e^{CL_f} - 1}\right)\right] \tag{17}$$

Eq. 17 was used to produce Fig. 35. This figure, which is analogous to Fig. 33, plots V/V_f versus L/L_f for various values of CL_f. For CL_f values below 1, the plots are virtually the same as the curve in Fig. 33. However, significant deviations are seen when CL_f is greater than 1. Again, this result indicates that CL_f is an important parameter for gel treatments in hydraulically fractured wells.

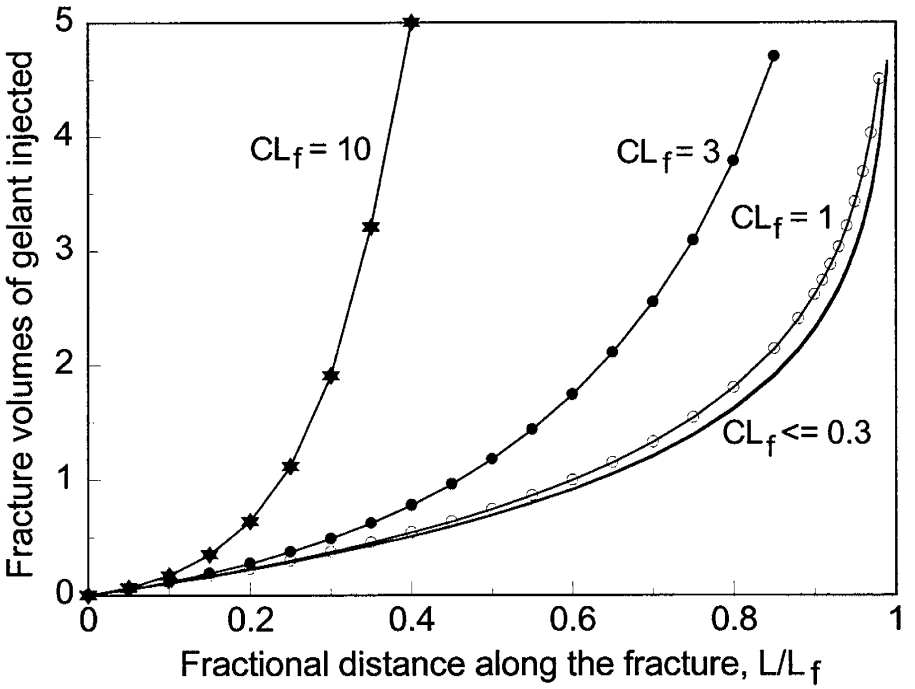

Fig. 35. Gelant volume versus front position when the leakoff flux depends on distance along the fracture.

Use of Viscous Gelants

In the above figures and equations, we assumed that the gelant had the same viscosity and mobility as that of the fluid that was displaced from the fracture and porous rock. How will the above results change if the gelant is more viscous than the reservoir fluids? Appendix B (Eqs. B47-B51) demonstrates that increased gelant viscosity (or resistance factor, F_r) affects the propagation of a gelant front by increasing C. In Eq. 18 (from Eq. B50 in Appendix B), C′ is defined for viscous gelants.

$$C' = \sqrt{\frac{2F_r k_m}{k_f w_f [(r_e - L_p) + F_r L_p]}} \tag{18}$$

In Eq. 18, L_p is the distance of gelant leakoff from the fracture face. Dividing Eq. 18 by Eq. 15 yields Eq. 19.

$$\frac{C'}{C} = \sqrt{\frac{F_r r_e}{(r_e - L_p) + F_r L_p}} \tag{19}$$

Eq. 19 was used to produce Fig. 36, which plots C'/C versus gelant resistance factor for L_p values ranging from 0.1 to 10 ft (r_e=500 ft). Fig. 36 shows that increasing the gelant resistance factor from 1 to 10 increases C'/C by a factor of 3. Also, Fig. 36 shows that the leakoff distance has a relatively minor effect unless gelant resistance factors are large.

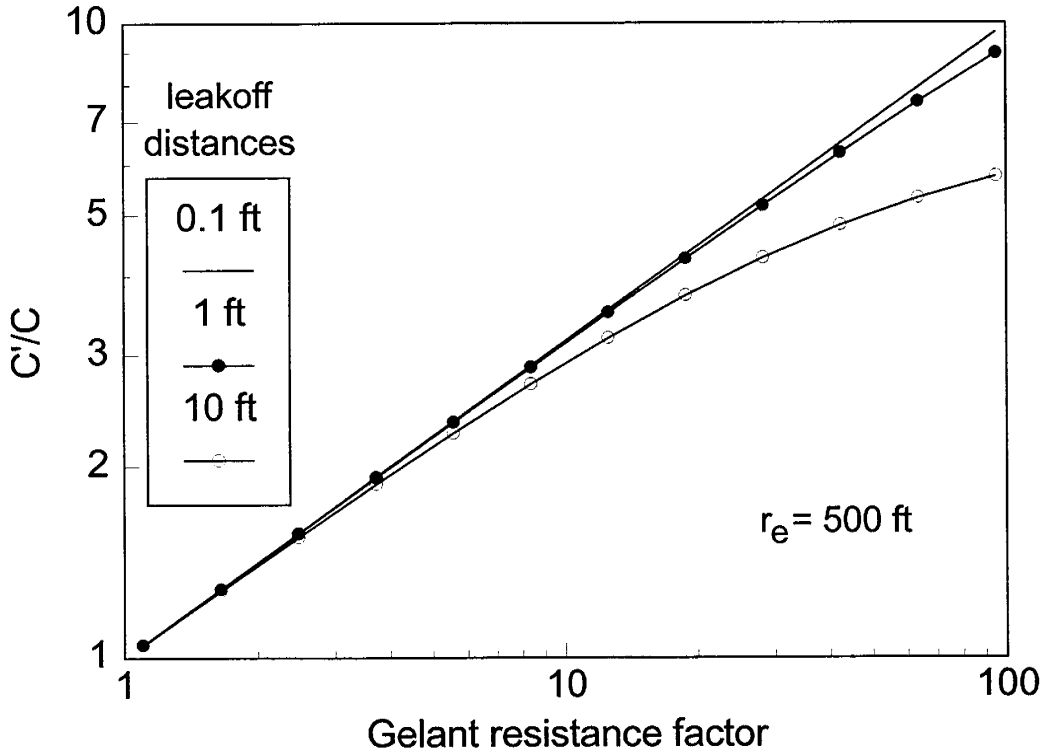

Fig. 36. Effect of gelant resistance factor on C values.

Productivity Losses and WOR Improvement

What reductions in oil and water productivity can be expected after a gel treatment? Consider the case where the gel has penetrated a distance, L_p, from the fracture face into the porous rock for the entire length of the fracture. Eq. 20 (taken from Ref. 25) estimates the productivity after a gel treatment (J_a) relative to that before the gel treatment (J_b) for a gel that reduces permeability by a factor, F_{rr}, (i.e., the residual resistance factor) in the gel-contacted part of the rock.

$$\frac{J_a}{J_b} = \frac{1}{1+(L_p / r_e)(F_{rr}-1)} \tag{20}$$

Based on Eq. 20, Fig. 37 plots J_a/J_b (the fraction of original productivity retained) versus the residual resistance factor for leakoff distances ranging from 0.1 to 30 ft. (In Fig. 37, r_e=500 ft. Also, we assumed that the well productivity was affected by gel in the porous rock much more than by gel in the fracture— i.e., the gel does not significantly restrict flow in the fracture.)

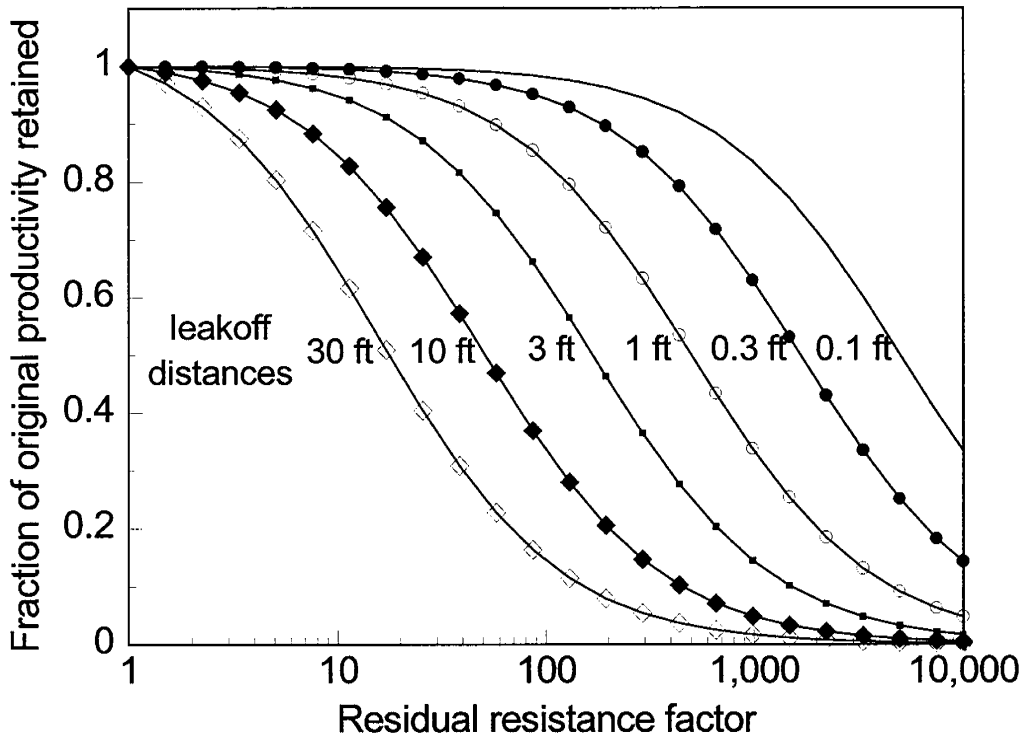

Fig. 37. Productivity retained when gel extends over the entire fracture face. r_e=500 ft.

As mentioned above, Eq. 20 and Fig. 37 assume that the gel leakoff distance is the same along the entire length of the fracture. What if the gel leakoff distance is uniform but only to some distance, L, along the fracture? In that case, J_a/J_b is given by Eq. 21.

$$\frac{J_a}{J_b} = \frac{1+(L_p / r_e)(F_{rr}-1)[1-(L / L_f)]}{1+(L_p / r_e)(F_{rr}-1)} \tag{21}$$

Figs. 38 and 39 were generated using Eq. 21, assuming leakoff distances of 1 ft and 10 ft, respectively. Figs. 37 through 39 reveal that productivity losses from a well are influenced in important ways by all three variables—residual resistance factor, leakoff distance, and distance of gel propagation along the fracture.

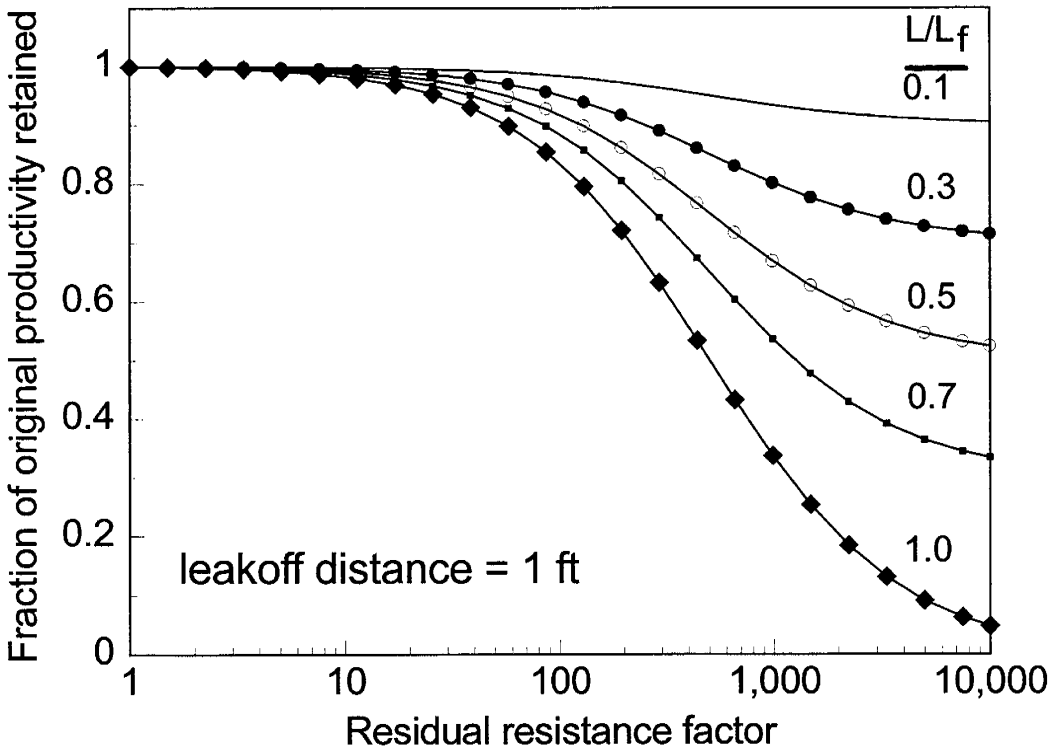

Fig. 38. Productivity retained when gel covers part of the fracture area. L_p=1 ft, r_e=500 ft.

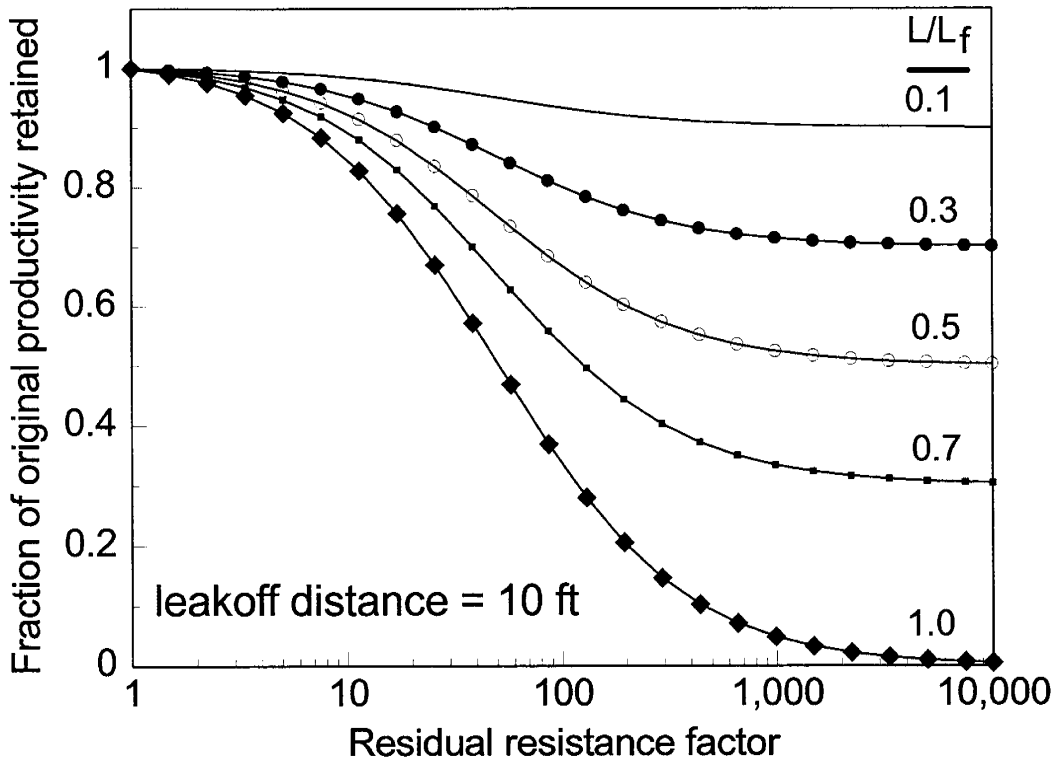

Fig. 39. Productivity retained when gel covers part of the fracture area. L_p=10 ft, r_e=500 ft.

Figures like Figs. 37 through 39 can be very useful when designing a gel treatment for a fractured production well.[2,25-27] Two examples will be given to illustrate this point.

Example 1—Gel Extends Over the Entire Fracture Face. First, consider the case illustrated by Fig. 40. A hydraulically fractured production well produces 10 times as much water as oil. The fracture cuts through one oil zone and one water zone. An impermeable shale barrier separates the two zones except at the fracture. Each zone is 25 ft thick, the fracture half-length (L_f) is 50 ft, and the fracture is conductive enough so that leakoff in a given zone is uniform along the length of the fracture (i.e., $CL_f<1$). The water zone is effectively ten-times more permeable than the oil zone, the aqueous phase porosity (at S_{or}) is 0.15 in both zones, and the oil/water mobility ratio is about 1. This well is roughly 1,000 ft from the nearest well (so $r_e\approx500$ ft). Using a core from each zone, laboratory studies identified a gel that will reduce permeability to water by a factor of 100 (i.e., $F_{rrw}=100$) and permeability to oil by a factor of 10 (i.e., $F_{rro}=10$). Before gelation, the gelant is 20 times more viscous than water ($F_r=20$). How much gelant should be injected, and what effect should be seen from the gel treatment?

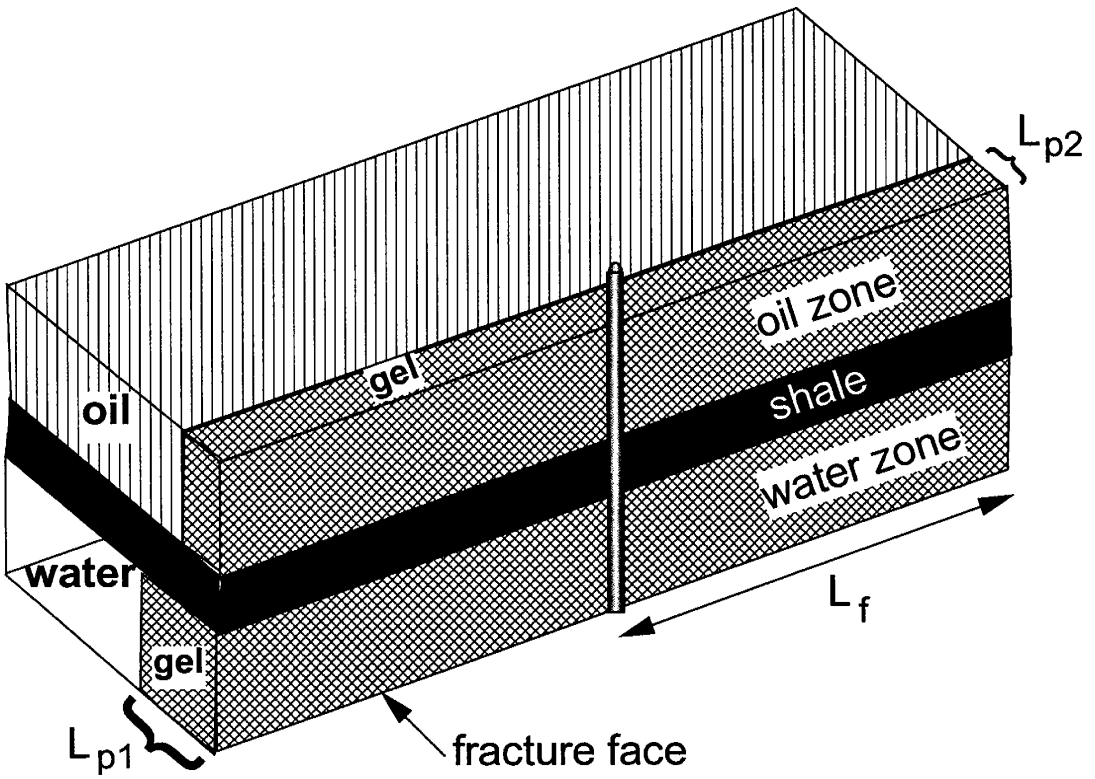

Fig. 40. A gel treatment in a vertical fracture that cuts through oil and water zones.

In solving this problem, losses to oil productivity should be minimized while maximizing losses to water productivity. For example, we may want the oil productivity after the gel treatment to retain at least 90% of its original value. Using either Eq. 20 or Fig. 37, we determine (see Eq. 22)

that a gel with F_{ro}=10 provides a 10% loss of oil productivity if the leakoff distance in the oil zone (L_{p2}) is 6.2 ft.

$$0.9 = \frac{1}{1+(6.2/500)(10-1)} \tag{22}$$

For this distance of gelant penetration in the oil zone, the distance of gelant penetration in the water zone (L_{p1}) can be estimated using Eq. 1 of Ref. 25 (i.e., Eq. 23).

$$\frac{L_{p2}}{L_{p1}} = \frac{\sqrt{1+(F_r^2-1)(\phi_1 k_2)/(\phi_2 k_1)}-1}{F_r-1} \tag{23}$$

This calculation estimates L_{p1} to be 21.8 ft in the water zone (see Eq. 24).

$$\frac{6.2}{21.8} = \frac{\sqrt{1+(20^2-1)(1/10)}-1}{20-1} \tag{24}$$

Using Eq. 20, the productivity retained in the water zone is 19% for F_{rw}=100 and L_p=21.8 ft (see Eq. 25).

$$0.19 = \frac{1}{1+(21.8/500)(100-1)} \tag{25}$$

Before the gel treatment, the producing water/oil ratio (WOR) was 10. After the treatment, the final WOR expected is (10x0.19)/(1x0.9) or 2.1.

The total volume of gelant injected is given by Eq. 26.

$$V = 4L_f(h_{fo}\phi_i L_{p2} + h_{fw}\phi_i L_{p1})$$
$$V = 4(50)[25(0.15)6.2 + 25(0.15)21.8]/5.61 = 3{,}750 \text{ bbl} \tag{26}$$

Therefore, using 3,750 bbl of gelant, the WOR was reduced from 10 to 2.1 while maintaining 90% of the original oil productivity.

Of course, if more than two zones are present, the total volume of gelant injected is the sum of the gelant volumes in all zones.

$$V = 4\sum_i L_{fi} L_{pi} h_{fi} \phi_i \tag{27}$$

In Eq. 27, the i subscripts refer to individual zones.

[This example assumed that retention of gelant components by the rock did not significantly affect the L_p values. This is a reasonable assumption for concentrated gelants (e.g., containing

≥0.5% HPAM). For dilute gelants, the effects of retention and inaccessible pore volume can easily be taken into account using Eq. 21 of Ref. 25 instead of Eq. 23 above. The example also assumed that placement could be approximated using single-phase flow calculations. Refs. 2 and 25 show that this is a reasonable assumption for most light-to-medium gravity oils. For heavy oils, two-phase flow effects can be taken into account using the methods described in Ref. 2.]

What would happen if different gelant volumes were used? This question can easily be answered using Eqs. 20-26. The results from these calculations are summarized in Fig. 41. For reference, if the gelant volume was 1,875 bbl (instead of 3,750 bbl), the oil productivity would be reduced to 95% of the original (before gel) value, and the final WOR would be 3.3. If the gelant volume was 7,500 bbl, the oil productivity would be reduced to 82% of the original value, and the final WOR would be 1.3. Fig. 41 suggests that the gelant volume should be at least 1,000 bbl to cause a significant reduction in the WOR. However, the gelant volume should not be greater than 10,000 bbl because losses in oil productivity then become substantial.

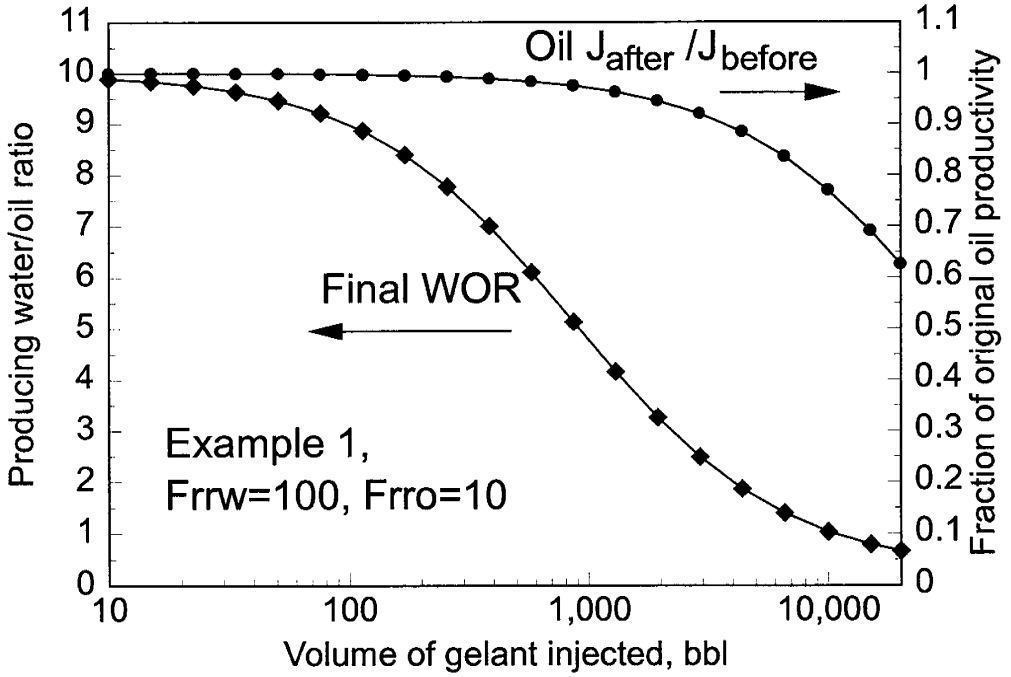

Fig. 41. Sensitivity of Example 1 to gelant volume. F_{rrw}=100, F_{rro}=10.

What would happen if a different gelant was used—for example, one with F_{rrw}=1,000 and F_{rro}=100? This question is answered in Fig. 42. This figure shows that increasing the water and oil residual resistance factors by a factor of 10 reduced the volume of gelant required by a factor of 10. For example, for this second gelant system, only 370 bbl of gelant were needed to reduce the WOR from 10 to 2.1 while maintaining 90% of the original oil productivity—the same effect that was produced by the 3,750-bbl treatment described above. Thus, in hydraulically fractured production wells, a substantial incentive exists to identify relatively strong gels that reduce permeability to water much more than that to oil. Careful consideration of Eq. 20 reveals that for

a given F_{rrw}/F_{rro} ratio, the gelant volume required to achieve a given WOR reduction is inversely proportional to F_{rro}, if F_{rro} is not too small (i.e., close to 1). Our analysis reveals that a critical step in this design process is determining the water and oil residual resistance factors using gelant, oil, brine, rock, and temperature that are representative of the intended application.

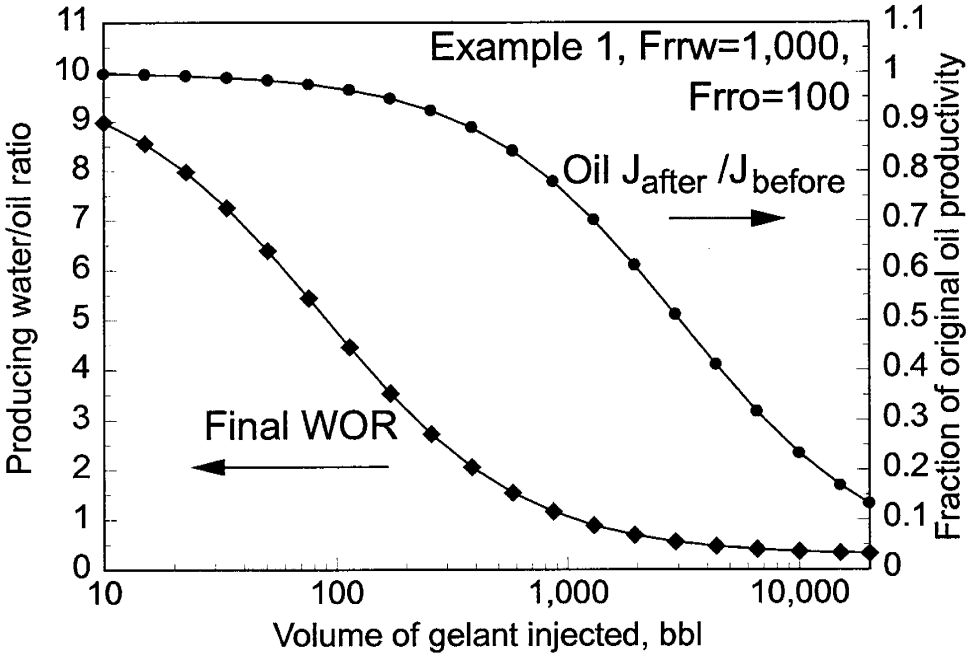

Fig. 42. Sensitivity of Example 1 to gelant volume. F_{rrw}=1,000, F_{rro}=100.

Example 2—Gel Covers Only Part of the Fracture Face. Next, consider an example where the gel does not cover the entire distance along the fracture. In particular, assume that the fracture from Example 1 becomes extended by 50% (e.g., from a stimulation operation) sometime after the 3,750-bbl gel treatment was applied. What effect would be seen on the WOR and productivities? In both zones, the fracture half-length, L_f, grows from 50 ft to 75 ft. (The gel still exists along only the first 50 ft of the fracture in both zones.) By inputting numbers from Example 1 into Eq. 21, Eq. 28 calculates that the fraction of the original (before gel) productivity in the oil zone will be 0.93.

$$0.93 = \frac{1+(6.2/500)(10-1)(1-50/75)}{1+(6.2/500)(10-1)} \tag{28}$$

Thus, stimulation increases J_a/J_b from 0.9 to 0.93 for the oil zone. A similar calculation can be made for the water zone.

$$0.46 = \frac{1+(21.8/500)(100-1)(1-50/75)}{1+(21.8/500)(100-1)} \tag{29}$$

So, stimulation increases J_a/J_b from 0.19 to 0.46 for the water zone. After the stimulation, the WOR is given by Eq. 30.

$$WOR_{final} = (WOR_{initial}) \frac{(J_a / J_b)_{water}}{(J_a / J_b)_{oil}} \tag{30}$$

In this particular case, Eq. 30 provides a WOR of (10x0.46)/(1x0.93) or 4.9. Therefore, stimulation increases the WOR from 2.1 to 4.9—a significant increase.

Determining CL_f Values

The previous sections demonstrated that the CL_f value must be below a value of 1 to ensure that leakoff is uniform along the length of the fracture. How are CL_f values determined in field applications? At least three methods are available—(1) productivity data, (2) pressure transient analysis, and (3) reservoir simulation (history matching).

For those circumstances where operators have the time and resources to characterize their wells, pressure transient analysis or reservoir simulation can provide more accurate estimates of formation permeabilities, fracture conductivities, and fracture lengths than those available from productivity data.[30] We encourage the use of the more sophisticated methods when practical.

If these methods are not practical, then we recommend that simple calculations using productivity data should be used. McGuire and Sikora[28] and Holditch[29,30] have produced charts that predict the increase in productivity caused by a hydraulic fracture as a function of fracture conductivity and fracture length. Fig. 43 illustrates one of these charts.

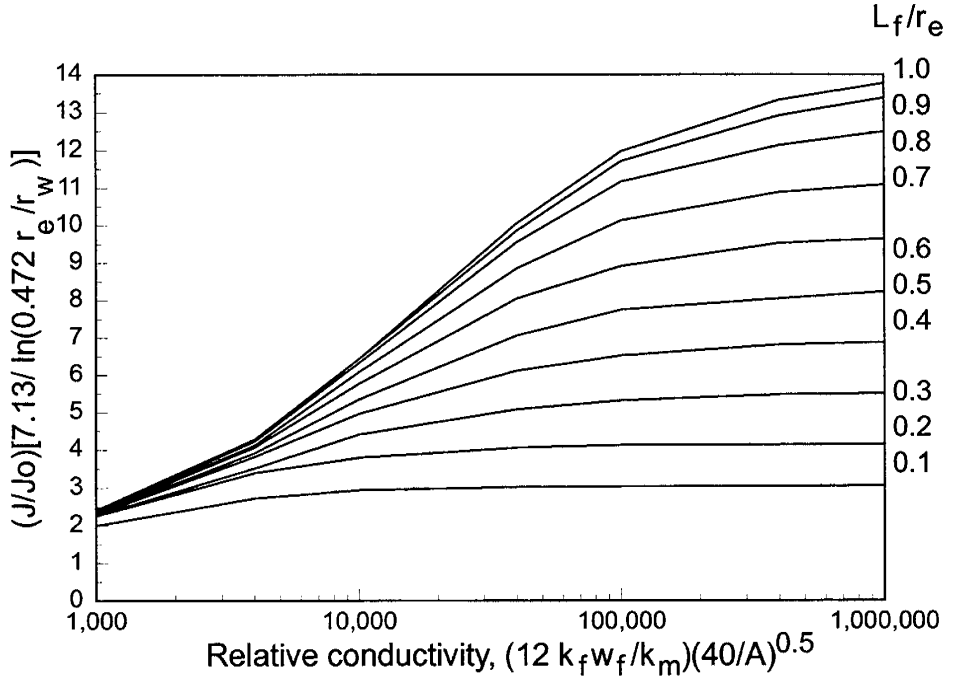

Fig. 43. Productivity increase from hydraulic fracturing (from Refs. 29 and 30).

Fig. 43 can be used to act in a manner reverse to that originally intended. In particular, field productivity data can be used to estimate C and L_f values. This method requires knowledge of rock permeabilities (i.e., from core analysis), flowing and static wellbore pressures, and well spacing. The first step in this process is to estimate the well productivity in the absence of the fracture. This calculation is made using the simple Darcy equation for radial flow (Eq. 31).

$$J_o = \frac{\sum kh}{141.2\mu \ln(r_e / r_w)} \tag{31}$$

In Eq. 31, the permeability to water (k_w) should be corrected so that it reflects the permeability at the resident oil saturation (e.g., at S_{or}). (Of course, the permeability to oil should also be corrected if needed.)

Second, the actual well productivity, J, is the total production rate divided by the downhole pressure drop (reservoir pressure minus the wellbore pressure).

$$J = q / \Delta p \tag{32}$$

Next, the term on the y-axis of Fig. 43 is calculated.

$$y = \frac{J}{J_o} \frac{7.13}{\ln(0.472 r_e / r_w)} \tag{33}$$

Then, Fig. 43 is used to look up an x-value associated with the upper left envelope of curves. This x-value provides the minimum relative conductivity.

$$x = \frac{12 k_f w_f}{k_m} \sqrt{40 / A} \tag{34}$$

Once the minimum x-value is known, the minimum fracture conductivity, $k_f w_f$, can be found from Eq. 34. For example, if the y-value is 8, Fig. 43 indicates that the minimum x-value is about 20,000. If the well spacing, A, is 40 acres and the rock permeability is 10 md, the fracture conductivity is 16.7 darcy-ft. The external drainage radius can be estimate from Eq. 35.

$$r_e = \sqrt{A(43{,}560) / (2\pi)} \tag{35}$$

For 40-acre spacing, r_e is 527 ft. The maximum C value can be calculated using Eq. 15. In this example, the maximum C value is given by Eq. 36.

$$C = \sqrt{\frac{2(0.01)}{16.7(527)}} = 0.0015 \text{ ft}^{-1} \tag{36}$$

Fig. 43 can also be used to estimate the minimum fracture length, L_f. This can be done by extending a line from the given y-value horizontally to the right side of Fig. 43 to determine the corresponding L_f/r_e value. In our example, where the y-value is 8, the corresponding L_f/r_e value is 0.5. So, if the r_e value is 527 ft, the L_f value is 0.5(527) or 263 ft. Thus, the estimated CL_f value for this example is (0.0015)(263) or 0.4. This value is less than 1, so fluid leakoff should be uniform over the length of the fracture.

Actually, one can use Fig. 43 to demonstrate that the fluid leakoff from the fracture should be uniform if the well productivity is at least five times the value for an unfractured well. Eqs. 15, 34, and 35 can be combined to produce Eq. 37.

$$x = 12{,}640\left(\frac{L_f}{r_e}\right)^2\left(\frac{1}{CL_f}\right)^2 \tag{37}$$

From Figs. 34 and 35, we noted that uniform leakoff occurs from the fracture faces if $CL_f \leq 1$. Thus, Eq. 37 suggests that if $CL_f \leq 1$, uniform leakoff should occur if $x > 12{,}640$. In Fig. 43, this x-value corresponds to a y-value (on the upper-left envelope) of about 6. The y-axis term, $7.13/[\ln(0.472\, r_e/r_w)]$, has a value typically near 1.15. Dividing 6 by 1.15 provides a J/J_o value of about 5. Therefore, fluid leakoff from the fracture should be uniform if the well productivity is at least five times greater than that for an unfractured well.

Fig. 43 also suggests that if $J/J_o \geq 5$, then $L_f/r_e \geq 0.3$. For higher J/J_o values, the right side of Fig. 43 provides greater estimates for the minimum fracture length. Note that Fig. 43 does not generally provide the actual fracture length. Even so, knowledge of the minimum fracture length could be useful when designing the gelant volume to be injected. To explain, Figs. 41 and 42 suggest that the performance of a gel treatment is not particularly sensitive to the treatment volume, so long as that volume is roughly in the proper range. For example, in Fig. 41, we suggested that the gelant volume should be 3,750 bbl. Fig. 41 indicates that the treatment results would not be catastrophic if the treatment size was as little as half or as much as twice the proposed volume of 3,750 bbl. Therefore, if information on fracture length is not available, a reasonable approximation is to assume that the fracture length is half the external drainage radius ($L_f = 0.5r_e$). Alternatively, the right side of Fig. 43 can be used to make the following approximation.

$$L_f \approx [(J/J_o)(0.09) - 0.14]r_e \tag{38}$$

Eq. 38 is the result of a linear least-squares regression of the relation between the J/J_o values on the y-axis of Fig. 43 and the L_f/r_e values on the right sight of Fig. 43.

What range of CL_f values is commonly encountered in field applications? This range can be estimated using Eq. 15 and results from a survey of field gel treatments.[6] In previous field applications, formation permeabilities varied from 4 to 5,000 md, with a median permeability of 100 md.[6] Well spacings varied from 10 to 160 acres, so r_e values ranged from 250 to 1,050 ft. We suspect that fracture conductivities typically varied from 1 to 1,000 darcy-ft. Inserting these

values into Eq. 15 suggests that C values can range from 0.0001 to 0.2 ft^{-1}. If fracture lengths vary from 10 to 500 ft, CL_f values could range from 0.001 to 100. Assuming that k_m=100 md, r_e=500 ft, and L_f=100 ft, CL_f will be less than 1 if the fracture conductivity is greater than 4 darcy-ft.

Limitations

An unfortunate reality for many operators is that they do not have the time, information, or resources to adequately diagnose the nature of their excess water-production problem or to adequately engineer the best solution. For those cases, this paper provides a very simple method to screen and engineer a reasonable gel treatment in hydraulically fractured production wells. In this method, we emphasize that water and oil residual resistance factors must be determined in advance. These values can be determined either from laboratory measurements or by calculation of in-situ residual resistance factors from a prior field test. Also, the reader should note that our method assesses (1) whether fractures are conductive enough to allow uniform leakoff along the fracture and (2) the minimum fracture length. (The method does not determine the actual conductivity or length of the fracture.) In many cases, these determinations are adequate to design a satisfactory gel treatment. The reader should also note that this method assumes that a reasonable estimate can be made of the undamaged rock permeabilities in the zones of interest in a well (e.g., through core analysis). If the near-wellbore region or fracture faces are known to be damaged and this damage can be quantified, methods are available to take this damage into account.[30] Also, our method assumes that the resistance to flow provided by gel in the fracture is small compared to that provided by gel in the porous rock adjacent to the fracture. Concern about the effects of gel in the fracture may be mitigated by using a postflush to displace gelant from the fracture before gelation.

Method for Sizing Gelant Treatments in Hydraulically Fractured Production Wells

1. Estimate the rock permeabilities (k_i in md), porosities (ϕ_i), and thicknesses (h_{fi} in ft) for the oil and water zones of interest. Core analysis data on unfractured cores are preferred. Correct the k_w values so they reflect the permeability at the resident oil saturation (e.g., at S_{or}).

2. Estimate the productivity of an unfractured, undamaged well, J_o in bbl/D-psi, using Eq. 39.
$$J_o = \sum kh / [141.2\mu \ln(r_e / r_w)] \quad (39)$$

3. Calculate the actual total well productivity for the fractured well, J in bbl/D-psi, and determine the ratio, J/J_o. The well may be a good candidate for a gel treatment if all five of the following conditions are met: a) J/J_o is greater than 5, b) the WOR is high, c) the fracture cuts through distinct water and hydrocarbon zones, d) barriers to vertical flow exist except in the fracture, and e) a satisfactory mobile oil target exists.

4. In the laboratory, determine the water and oil residual resistance factors (F_{rrw} and F_{rro}) using gelant, oil, brine, rock, and temperature that are representative of the intended application.

Alternatively, F_{rrw} and F_{rro} values may be back-calculated from a prior treatment using the same gelant in a nearby well.

5. Estimate the external drainage radius, r_e in ft, for the well spacing, A in acres.
$$r_e = \sqrt{A(43{,}560)/(2\pi)} \quad (40)$$

6. Calculate the desired distance of gelant leakoff in the oil zone(s), L_{p2} in ft, for the target final oil-productivity level(s), J_a/J_b (e.g., J_a/J_b=0.9). ($J_a/J_b=J_{after}/J_{before}$.)
$$L_{p2} = r_e[(J_b/J_a)-1]/(F_{rro}-1) \quad (41)$$

7. Use Eq. 42 (or use Eq. 21 of Ref. 25 if chemical retention must be considered and/or use the methods in Ref. 2 if two-phase flow effects must be considered) to estimate the target distance of gelant penetration into the water zone(s), L_{p1} in ft. If more than two zones are present, repeat this step for each zone. (F_r is the gelant resistance factor.)
$$L_{p1} = (F_r-1)L_{p2}/[\sqrt{1+(F_r^2-1)(\phi_1 k_2)/(\phi_2 k_1)}-1] \quad (42)$$

8. Use Eq. 43 and F_{rrw} to calculate J_a/J_b values for the water zone(s).
$$J_a/J_b = 1/[1+(L_{p1}/r_e)(F_{rrw}-1)] \quad (43)$$

9. Find L_f, assume that L_f=0.5 r_e, or use Eq. 44.
$$L_f \approx [(J/J_o)(0.09)-0.14]r_e \quad (44)$$

10. Determine the gelant volume to be injected.
$$V = 4L_f \sum_i L_{pi} h_{fi} \phi_i \quad (45)$$

11. Estimate the final expected WOR.
$$WOR_{final} = (WOR_{initial})(J_a/J_b)_{water}/(J_a/J_b)_{oil} \quad (46)$$

Conclusions

Based on the work described in this chapter, the previous page presents a simple 11-step procedure for sizing gel treatments in hydraulically fractured production wells. A critical step in designing a gel treatment using this method is to determine water and oil residual resistance factors for the selected gelant using the fluid, rock, and temperature conditions representative of the actual application. Our procedure has been incorporated in user-friendly graphical-user-interface software that can be made available upon request (especially for those who will help us test the validity of our model).

To test the utility of our procedure, we need field data coupled with results from two simple laboratory experiments. The needed field data includes: (1) fluid production rates before and after the gel treatment, (2) downhole static and flowing pressures before and after the gel treatment, (3) permeabilities, porosities, and thicknesses of the relevant zones, (4) water and oil

viscosities at reservoir temperature, (5) well spacing or distance between wells, and (6) the volume of gelant injected. These parameters are normally available during conventional gel treatments. To properly test our model, we also need oil and water residual resistance factors (F_{rro} and F_{rrw} values) from laboratory core experiments. These experiments are easy to perform;[26,27] however, they must be conducted using the gelant, oil, brine, rock, and temperature that are representative of the intended application.

In the absence of laboratory oil and water residual resistance factors, our model can use field data to back-calculate the F_{rro} and F_{rrw} values in situ after a gel treatment. This information may be useful when designing similar treatments in nearby wells. Since our model quite definitively predicts oil and water productivity losses and WOR changes, its validity can be tested in a straightforward fashion. Therefore, oil and gas producers and gel vendors are encouraged to test our procedure in their field applications. We emphasize that our method is specifically directed at hydraulically fractured production wells. Work is currently underway to design gel treatments for other circumstances (including naturally fractured reservoirs).

4. THE POTENTIAL OF GEL TREATMENTS FOR REDUCING CHANNELING THROUGH NATURALLY FRACTURED RESERVOIRS

Some of the most successful gel treatments have been applied in naturally fractured reservoirs.[3,4,33] This chapter considers some of the reservoir variables that affect the severity of channeling and the potential of gel treatments for reducing channeling through naturally fractured reservoirs.

At least three books describe reservoir engineering in naturally fractured reservoirs.[34-36] These books concentrate on oil and gas recovery during primary production. In contrast, our interest in this chapter focuses on correcting channeling problems during secondary recovery operations.

Various logging methods have been used to detect and characterize fractures (Chapter 3 of Ref. 34, Chapter 2 of Ref. 35, and Chapter 5 of Ref. 36). Caution must be used with these methods, especially since they usually measure properties at or very near the wellbore. The value of these methods can be increased if the wellbore is deviated to cross the different fracture systems (i.e., fractures with different orientations).

Pressure transient analyses have often been used to characterize fractured reservoirs (Chapter 4 of Ref. 34, Chapter 4 of Ref. 35, Chapters 6-8 of Ref. 36, and Ref. 37). Reportedly, these methods can estimate the fracture volume, the fracture permeability, and, possibly under some circumstances, the minimum spacing between fractures. Pressure interference tests can also indicate fracture orientation. In addition to unsteady-state methods, steady-state productivity indexes were also suggested as a means to estimate fracture permeability.

Interwell tracer studies provide valuable characterizations of fractured reservoirs, especially in judging the applicability of gel treatments to reduce channeling.[38-41] Interwell tracer data provides much better resolution of reservoir heterogeneities than pressure transient analysis.[42] Tracer results can indicate (1) whether fractures are present and if those fractures are the cause of a channeling problem, (2) the location and direction of fracture channels, (3) the fracture volume, (4) the fracture conductivity, and (5) the effectiveness of a remedial treatment (e.g., a gel treatment) in reducing channeling. Several models are available to analyze tracer results.[41-47]

In this chapter, we present some simple concepts to assess the applicability of gel treatments in naturally fractured reservoirs—in particular, when channeling occurs between injector-producer pairs.

Representation of a Naturally Fractured Reservoir

When modeling naturally fractured reservoirs, the fracture systems generally have been envisioned as (1) slabs (i.e., one set of parallel fractures), (2) columns (i.e., two intersecting sets of parallel vertical fractures), and (3) cubes (i.e., three intersecting sets of parallel fractures—two vertical and one horizontal). (See Fig. 44.)

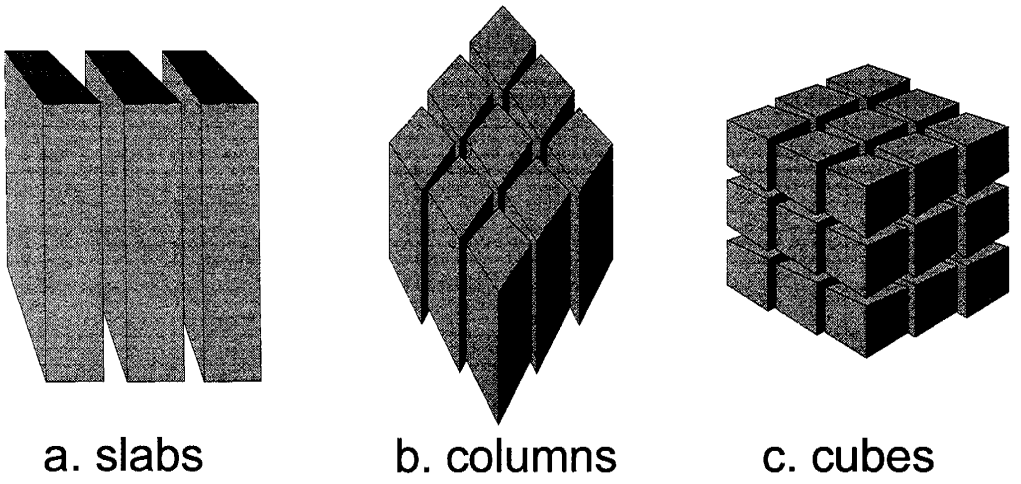

Fig. 44. Models of naturally fractured reservoirs.

In this chapter, we focus on the column model. For simplicity, assume that a naturally fractured reservoir consists of a regular pattern of north-south fractures intersected by east-west fractures (see Fig. 45). For a given number, n, of fractures that are oriented in the north-south direction (the y-direction), 2n-1 fractures are oriented in the east-west direction (the x-direction). As shown in Fig. 45, one injection well and one production well are located at either end of the central east-west fracture. Also assume that flow through the rock is negligible compared with that through the fractures and that the system is incompressible. Furthermore, fractures in the y-direction are assumed to have a conductivity, $(k_f w_f)_y$, and fractures in the x-direction are assumed to have a different conductivity, $(k_f w_f)_x$. A conductivity ratio, R, is defined using Eq. 47.

$$R = \frac{(k_f w_f)_x}{(k_f w_f)_y} \tag{47}$$

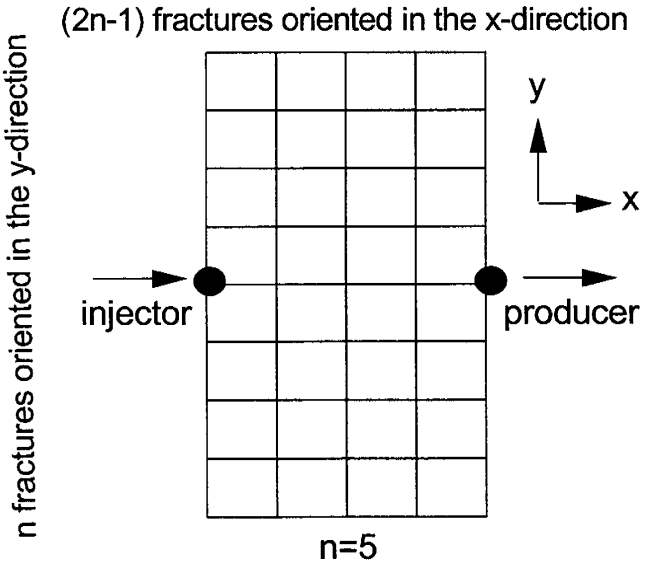

Fig. 45. Plan view of an injector-producer pair in a simple naturally fractured reservoir.

Appendixes C, D, and E list Fortran computer programs that were used to determine pressures, flow rates, and front positions when a water tracer or a gelant with a water-like viscosity was injected into a fracture pattern. In these programs, a unit-mobility displacement was assumed. The program in Appendix C is relatively simple and assumes that gelant or tracer is injected continuously and that no dispersion occurs. In contrast, the programs in Appendixes D and E are more sophisticated—allowing injection of banks of gelant or tracer and also accounting for dispersion of the banks. The program in Appendix D allows dispersion at the rear of a tracer bank but not at the front. In contrast, the program in Appendix E allows dispersion at both the front and the rear of the bank. All three programs were used in this work. The programs in Appendixes D and E were most useful for systems with relatively few fractures (i.e., with n-values of 21 or less). For systems with greater fracture densities, these program were too slow. The program in Appendix C was required for systems with large numbers of fractures (i.e., with n-values up to 101).

Tracer Transit Times In a Single Fracture

During a unit-mobility displacement, the time required for a tracer to travel between an injector-producer pair often provides a useful characterization of a fractured reservoir.[38-41] Of course, the tracer transit time depends on a number of variables, including the pressure drop between the wells (Δp), the distance between wells (L), the number, orientation, and conductivity of the connecting fractures, and the viscosity of the fluid in the fractures (μ). We use the transit time associated with a single direct fracture as a means to normalize transit times for our fractured systems. If a reservoir contains only one fracture (with fracture height, h_f) that leads directly from the injector to the producer and flow through the rock matrix can be neglected, the Darcy equation determines the volumetric flow rate (q).

$$q = \frac{\Delta p k_f w_f h_f}{L\mu} \tag{48}$$

The transit time (t) for a tracer is estimated from the fracture volume ($h_f w_f L \phi_f$) divided by q.

$$t = \frac{h_f w_f L \phi_f}{q} = \frac{w_f L^2 \mu \phi_f}{\Delta p (k_f w_f)} \tag{49}$$

Given the fracture conductivity, the effective average fracture width, w_f, can be estimated using Eq. 50 if w_f is expressed in feet and $k_f w_f$ is expressed in darcy-ft.[48]

$$w_f = 5.03 \times 10^{-4} (k_f w_f)^{1/3} \tag{50}$$

Fig. 46 plots expected tracer transit times from Eq. 49 versus fracture conductivity and pressure drop when L=1,000 ft, μ=1 cp, and ϕ_f=1. As an example, for a pressure drop of 80 psi, Fig. 46 predicts a transit time of one day for a 1,000-ft-long fracture with a conductivity of 1 darcy-ft.

Although the above analysis provides a simple and useful means to roughly estimate tracer transit times, one should recognize that dispersion affects the profile of produced tracer concentrations versus time or volume throughput. For example, Fig. 47 (taken from Ref. 41) shows field results from two interwell tracer tests that were performed before and after application of a gel treatment in a limestone reservoir. For both tests, a slug of radioactive tracer was injected over a short time period, but the tracer was produced over the course of 140 days. In both cases, the first tracer was produced only four days after tracer injection into a well that was 450 feet from the producer. The peak concentration was observed after 10 days for the tracer study before the gel treatment and after 37 days for that after the gel treatment.

Using tracer results, Tester *et al.*[39] considered several methods to estimate the volume associated with a fracture channel. They suggested that the best estimate of the volume of a fracture path is provided by the modal volume. This volume is associated with the peak concentration in the produced tracer distribution. For example, in Fig. 47, the peak concentration during a tracer study before the gel treatment was noted about 10 days after tracer injection. Based on other information provided in Ref. 41, about 20% of the production rate of 550 BWPD was attributed to the well where tracer was injected. Thus, the estimated volume of the dominant fracture path was 0.2 x 550 x 10 or 1,100 bbls.

Tester *et al.*[39] noted that other volume measures could be determined from the tracer curves, including integral mean volumes and median volumes. However, they observed that these volumes are usually weighted to overestimate the fracture volume in most circumstances.

If dispersion during flow through a single fracture (with no leakoff) was caused only by laminar mixing, a tracer would first arrive at the end of a fracture after injecting two-thirds of one fracture volume.[49,50] In the examples shown in Fig. 47, tracer breakthrough occurred at 40% and 11% of the volumes and times associated with the peak concentrations. These results suggest that considerable dispersion occurred in the field examples. Also, the tracer front should completely pass after injection of a few fracture volumes (i.e., a few thousand barrels). Instead the tracer profile was dispersed over 140 days ($\approx$ 70 fracture volumes). This dispersion reflects the range of pathways from the injection well to the production well.[39,41] Early tracer production reflects the most rapid pathways, while late tracer production indicates long or circuitous pathways, dead ends, or possibly chemical exchange in the reservoir.[39,41] As will be evident in the next section, a wide range of pathways are available in naturally fractured reservoirs.

Transit Times In a Fracture System

The program listed in Appendix C was used to determine times required for a tracer to travel from an injection well to a production well in a naturally fractured system. These calculated transit times reflect the most rapid pathways between the wells. In all cases, the "reservoir" looked like Fig. 45. Also, a unit-mobility displacement was used, and a fixed pressure drop was applied between the wells. The transit times from this program were normalized by dividing by the time calculated using Eq. 49. These dimensionless transit times are plotted in Fig. 48. In this figure, the fracture conductivity ratios, R, ranged from 0.001 to 1,000. The number of fractures oriented in the y-direction, n, ranged from 3 to 101.

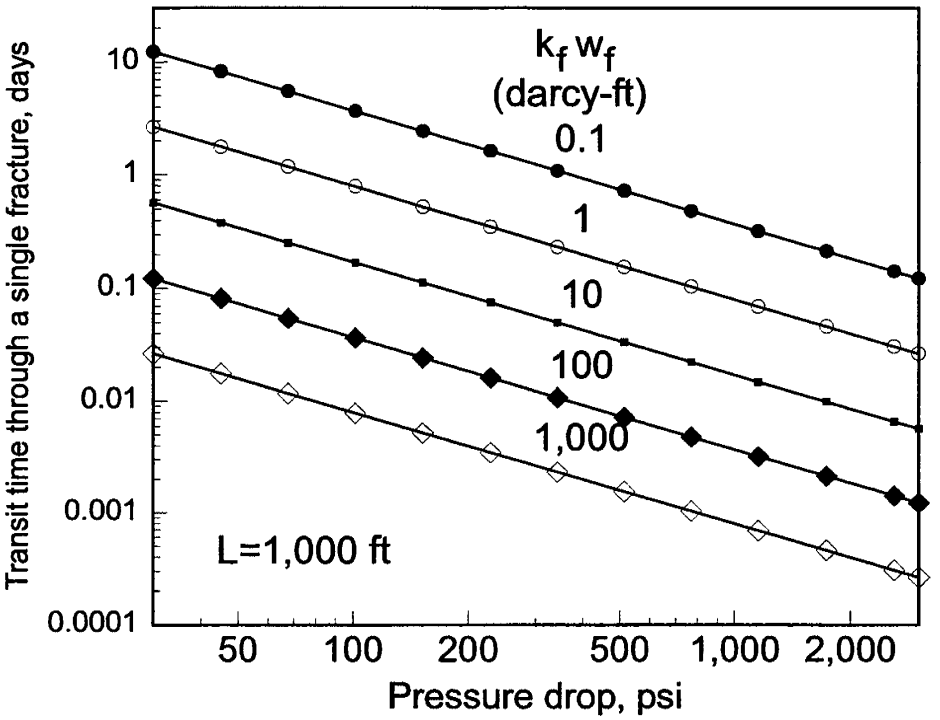

Fig. 46. Transit times through a single 1,000-ft-long fracture.

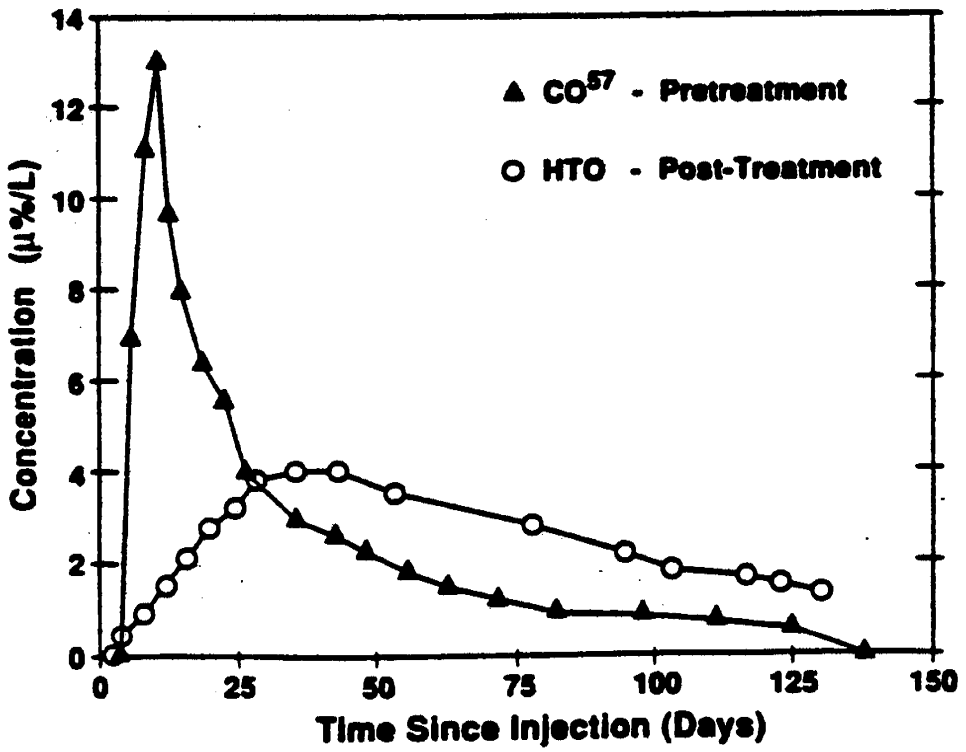

Fig. 47. Results of interwell tracer tests conducted before and after a gel treatment (taken from Ref. 41). Injection rate = 250 BWPD. Production rate = 550 BWPD.

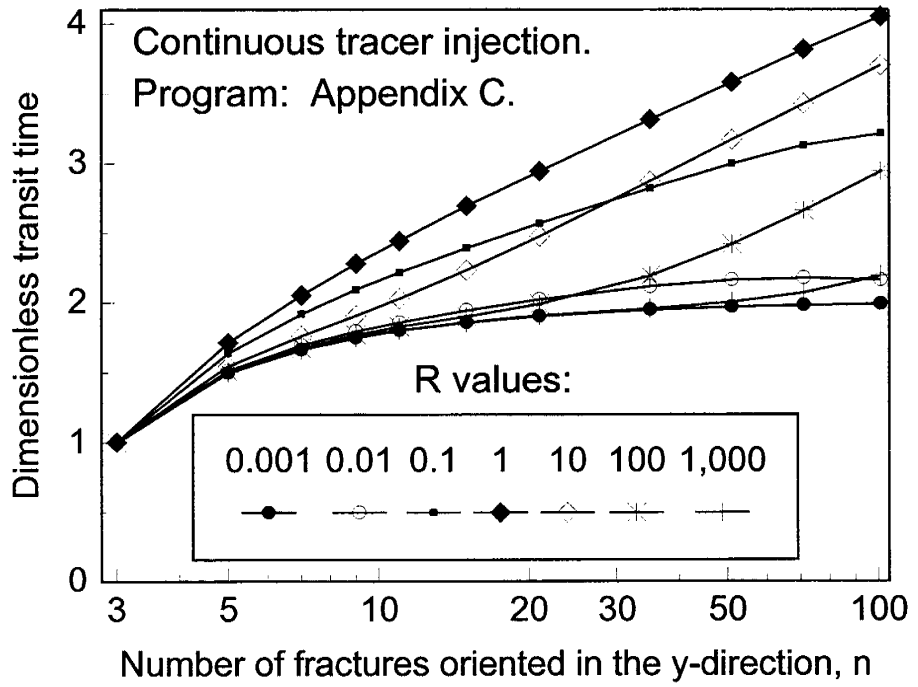

Fig. 48. Injector-producer tracer transit times in naturally fractured systems relative to that for a single direct fracture (unit-mobility displacement, fixed pressure drop, continuous injection, no dispersion).

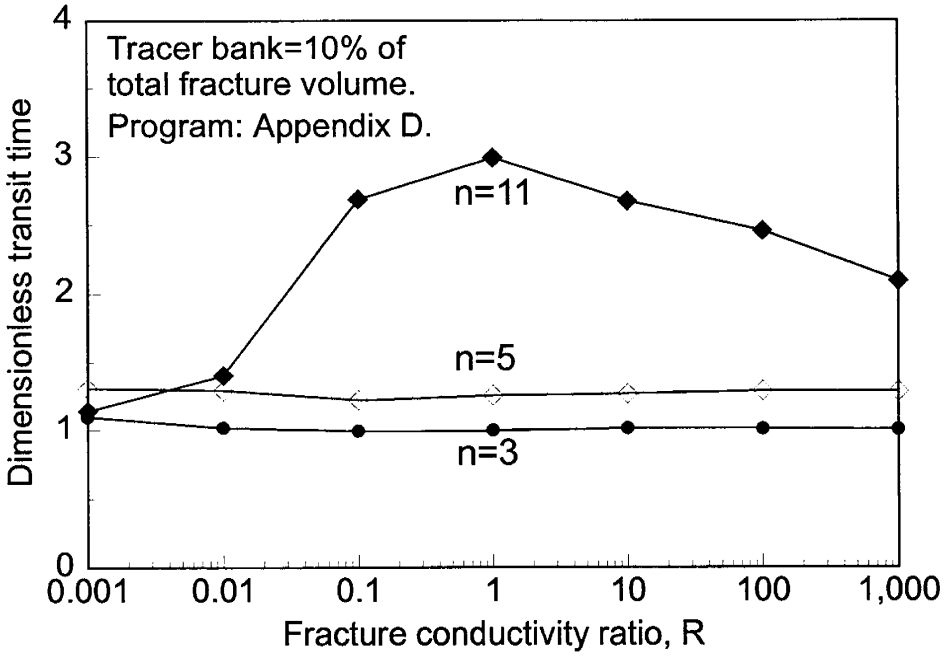

Fig. 49. Injector-producer tracer transit times in naturally fractured systems relative to that for a single direct fracture (unit-mobility displacement, fixed pressure drop, 10% fracture-volume tracer bank, with dispersion at the rear of the tracer bank).

The programs listed in Appendixes D and E were used as a check for the results shown in Fig. 48. The same conditions were applied for both sets of simulations. As mentioned earlier, the programs in Appendixes D and E consider injection of a tracer bank that can experience dispersion, while the program in Appendix C only considers continuous tracer injection with no dispersion. Fig. 49 plots the results using the program from Appendix D. For these simulations, the volume of the injected tracer bank was 10% of the total fracture volume of the system. Fig. 49 plots the dimensionless tracer transit time versus the R-value for n-values ranging from 3 to 11.

For the range of conditions examined, Figs. 48 and 49 suggest that the transit time is not greatly sensitive to the R- or n-values. In particular, we see, at most, only a four-fold variation in dimensionless transit times. Our results indicate that tracer transit times will not help much in determining R- or n-values in field applications. With increasing n-values, the greatest variations occur when R=1 (fractures in the x-direction have the same conductivity as those in the y-direction). The smallest variations occur when R is very large or when R is near zero. Incidentally, under our conditions, the dimensionless transit time is unity when $n \leq 3$.

The fact that tracer transit times are not sensitive to R- or n-values suggests that transit times can be very useful when estimating the permeability or conductivity of the most direct fracture. To explain, Figs. 48 and 49 indicate that the tracer transit time in a naturally fractured reservoir is usually between one and four times the value for a single direct fracture (if $n \leq 101$). Therefore, if the tracer transit time is measured, that value can be used in Eq. 51 (obtained by rearranging Eq. 49) to estimate the effective fracture permeability (within a factor of four).

$$k_f = \frac{L^2 \mu \phi_f}{t \Delta p} \tag{51}$$

If k_f is known in darcy units, Eq. 52 (obtained by rearranging Eq. 50) can be used to convert fracture permeability to fracture conductivity (in darcy-ft).

$$k_f w_f = 1.13 x 10^{-5} (k_f)^{1.5} \tag{52}$$

Sweep Efficiency

The sweep efficiency in our model systems can be assessed by comparing flow rates through specific fractures. For example, an effective method to judge the severity of channeling is to compare the flow rate in the most direct fracture with the total injection rate. This comparison is made in Fig. 50 for R-values ranging from 0.001 to 1,000 and for n-values ranging from 2 to 101. The y-axis in Fig. 50 shows the flow rate in the most direct x-direction fracture (i.e., the central east-west fracture in Fig. 45) divided by the total injection rate. More specifically, the flow rate in the most direct fracture was determined at the midpoint between the two wells. (In Figs. 50 through 53, all flow rates in the fractures were determined at an x-position that was midway between the two wells.)

As expected, Fig. 50 shows that the most severe channeling occurs with the largest R-values (i.e., when fracture conductivity in the x-direction is much greater than that in the y-direction). When the R-values are 0.1 or less, the fraction of flow in the most direct fracture is low and nearly independent of the R-value—indicating that sweep efficiency is quite good. Fig. 50 suggests that channeling is not severe unless the R-value is 10 or greater.

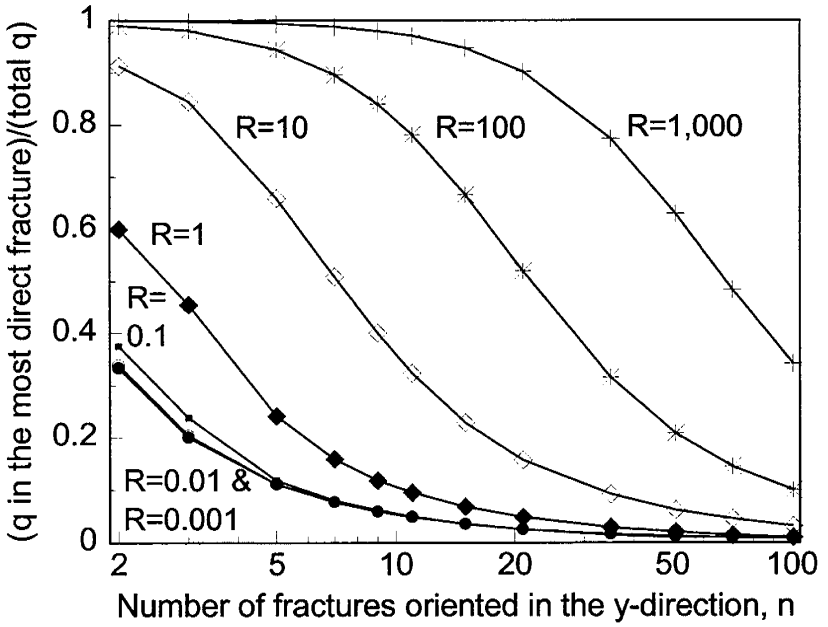

Fig. 50. Severity of channeling through the most direct x-direction fracture.

Fig. 50 also indicates that the severity of channeling through the most direct fracture decreases with increased n-value. Recall from Fig. 45 that n is the number of fractures oriented in the y-direction, while 2n-1 fractures are oriented in the x-direction. In all figures in this chapter, the distance between the two wells is fixed. So, as the n-value increases, the distance between fractures decreases. For example, if n=11, the distance between fractures will be 10 times greater than that when n=101.

Fig. 50 suggests a method to make interwell tracer studies useful when assessing the R- and n-values in field applications. When R is large and n is low to intermediate, the production rate is dominated by flow through the most direct fracture. Thus, if a tracer is injected continuously, the tracer concentration in the production well should stabilize at a high value under these conditions. Fig. 50 suggests that if the produced tracer concentration was 90% of the injected value, the R-value must be at least 10. However, this suggestion assumes that our production well is fed only by the fracture system to the left of the producer in Fig. 45. In a naturally fractured system, we expect a similar fluid supply from a fracture pattern to the right of the producer in Fig. 45. Thus, the expected tracer concentrations would be half of the values suggested by Fig. 50. Then, in the example above, if the produced tracer concentration was 45% of the injected value, the R-value must be at least 10.

As will be shown shortly, gel treatments in naturally fractured reservoirs have the greatest potential when R-values are high and n-values are low to intermediate. In searching for a guideline to distinguish when a reservoir meets these conditions, perhaps a useful indicator is a stabilized produced tracer concentration of at least 30% of the injected value. A produced tracer concentration of at least this value suggests that flow through the most direct fracture accounts for at least 60% of the total flow from the pattern shown in Fig. 45. This 60%+ value, in turn, suggests that the R-value is at least 1 and is probably at least 10 (from Fig. 50). Of course, the potential for a gel treatment becomes greater as the produced tracer concentration increases above 30% of the injected value. When produced tracer concentrations are low, gel treatments are unlikely to be effective.

The sweep efficiency can also be assessed by comparing the flow rates in various x-direction fractures with that in the most direct fracture. These comparisons are made in Figs. 51 through 53. In Fig. 51, the numerator of the y-axis is the flow rate in the second most direct fracture between the wells. Since our "reservoir" is symmetric, two of these fractures exist—one just above and one just below the central x-direction fracture in Fig. 45. (As a reminder, the flow rates are determined at the midpoint x-positions between the two wells.) In Fig. 52, the numerator of the y-axis is the flow rate in the x-direction fractures at the top or the bottom of Fig. 45. Thus, these are the least direct fractures between the wells. Fig. 53 applies to the x-direction fractures that are halfway (in the y-direction) between the most direct fracture and the least direct fractures.

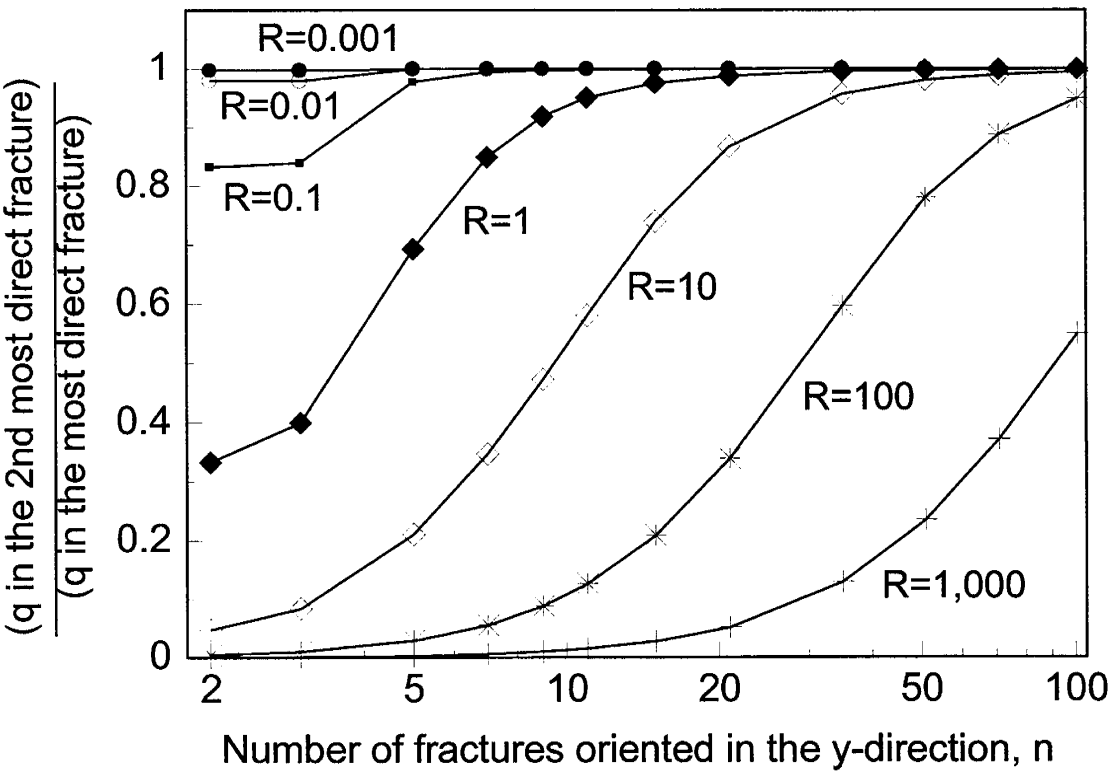

Fig. 51. Flow rate in the second most direct fracture relative to that in the most direct fracture.

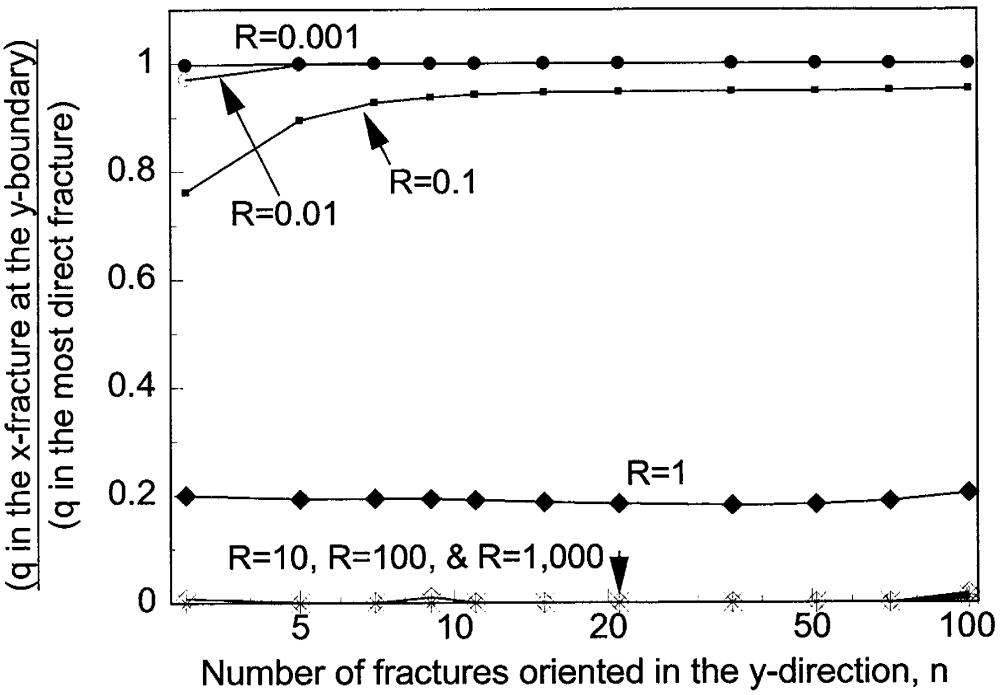

Fig. 52. Flow rate in the least direct fracture relative to that in the most direct fracture.

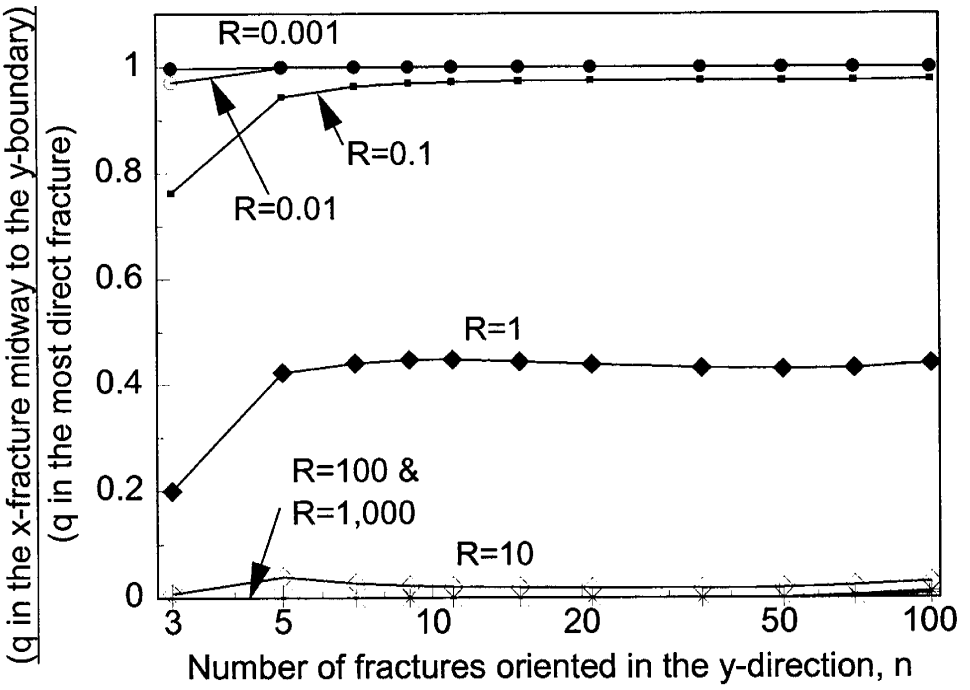

Fig. 53. Flow rate in the midway fractures relative to that in the most direct fracture.

When $R \leq 0.1$, Figs. 51 to 53 show that the flow rate is basically the same through all x-direction fractures, regardless of the n-value. The sweep efficiency is very high when the conductivity of the x-direction fractures is much less than that of the y-direction fractures. Obviously, no gel treatment is needed in this type of reservoir, since no significant channeling exists.

In contrast, when $R \geq 10$, Figs. 52 and 53 show that virtually no flow occurs through most of the x-direction fractures. In these cases, Figs. 50 and 51 confirm that most flow occurs through the most direct fracture or through fractures close to the most direct fracture. Of course, these are the conditions where a gel treatment is expected to work best.

When R=1 (all fractures have the same conductivity), Fig. 52 indicates that the flow rate in the least direct fracture is about 20% of that in the most direct fracture. Thus, the sweep efficiency is still reasonably good, and we suspect that a gel treatment may not provide much benefit.

Figs. 50 through 53 were generated using the program in Appendix C. As a check for these results, simulations were also performed using the programs in Appendixes D and E. These programs calculated the tracer concentrations that were produced after injecting a tracer bank equivalent to 10% of the total fracture volume. Fig. 54 plots the maximum (peak) tracer concentrations that were produced during simulation (using the program in Appendix D) of tracer propagation through a given fracture system. Fig. 54 considers R-values ranging from 0.001 to 1,000 and n-values ranging from 3 to 11.

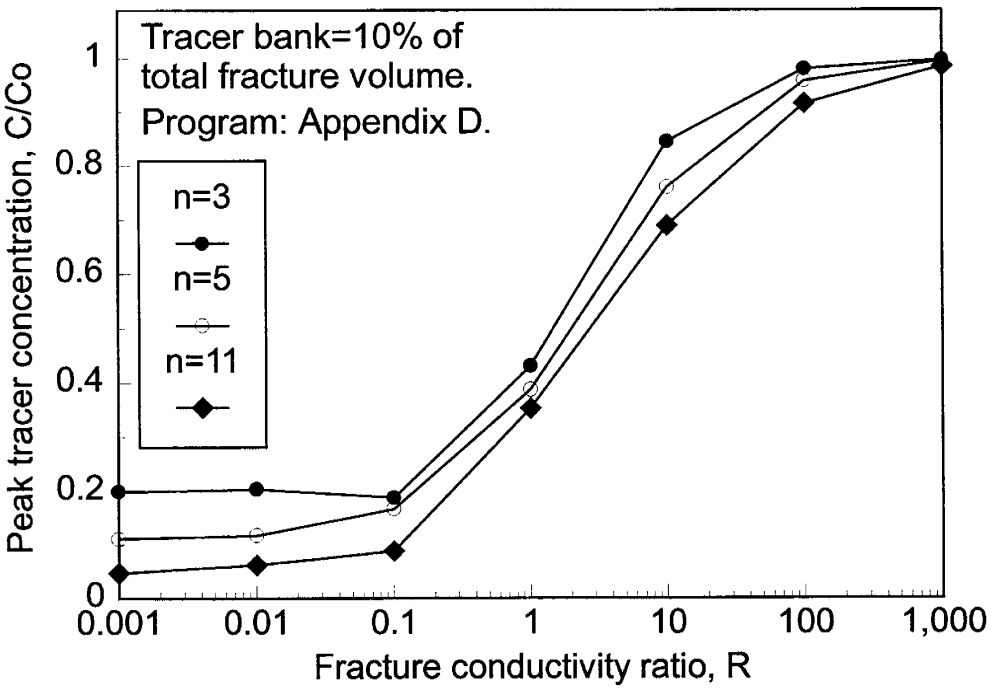

Fig. 54. Maximum produced tracer concentration when injecting a tracer bank. (Results determined using the program in Appendix D.)

In agreement with the results shown in Fig. 50, Fig. 54 indicates that high tracer concentrations are expected when the fracture conductivity ratio is 10 or greater. Also, low tracer concentrations are expected when the fracture conductivity ratio is less than 1. However, Fig. 54 suggests that the peak tracer concentrations may be less sensitive to n-values than indicated by Fig. 50.

Fig. 55 was generated using the program in Appendix E. This figure plots the produced tracer concentration when n=11 for R-values ranging from 0.001 to 1,000. In agreement with the previous results and conclusions, Fig. 55 demonstrates that (1) the tracer transit time (as determined by tracer breakthrough) is not sensitive to R-value, (2) produced tracer concentrations are low (less than 10% of the injected values) when $R \leq 1$, and (3) peak produced tracer concentrations are relatively high when $R \geq 10$. We note that the predicted peak tracer concentrations in Fig. 55 are generally lower than those in Fig. 54. For example, for the case where n=11 and R=10, the peak C/Co value is 0.35 in Fig. 55, compared to 0.69 in Fig. 54. This result occurs because the program that generated Fig. 55 (Appendix E) allows more dispersion than the program that generated Fig. 54 (Appendix D). However, simulations using all three of our programs qualitatively give the same results and support the same conclusions.

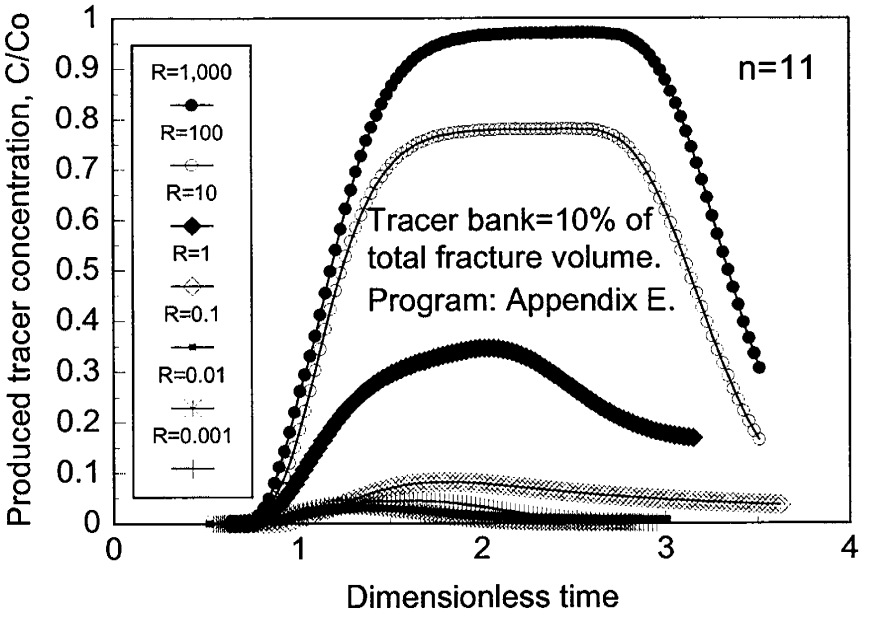

Fig. 55. Produced tracer concentrations when injecting a tracer bank with n=11. (Results determined using the program in Appendix E.)

Gelant Front Profiles

We also determined the front positions when injecting a gelant with a water-like viscosity to displace water from our fractured systems. In these simulations, we assumed a piston-like displacement, and we neglected dispersion, gravity, retention, and flow through the rock matrix. Our results are illustrated in Figs. 56 through 58. These figures plot plan views of the x- and y-positions of the gelant fronts at the time the gelant reached the production well. We only plot the north quadrant, since the profile in the south quadrant was symmetric.

Fig. 56 shows gelant front profiles versus n-value when R=1. For all n-values, at the time the gelant reached the production well, the gelant reached about 57% of the distance to the north and south boundaries of the reservoir along the y-direction fracture that intersects the injection well (i.e., the y-axis in Fig. 56). For n-values of at least 7 and x-positions less than 0.44, the profiles appear very similar. Depending on the n-value, the profiles depart from the common trend by abruptly dropping to the x-axis at a certain x-value. As shown in Fig. 56, these x-values are 0.25. 0.44, 0.58, 0.66, 0.82, and 0.92, for n-values of 5, 7, 9, 11, 21, and 51, respectively.

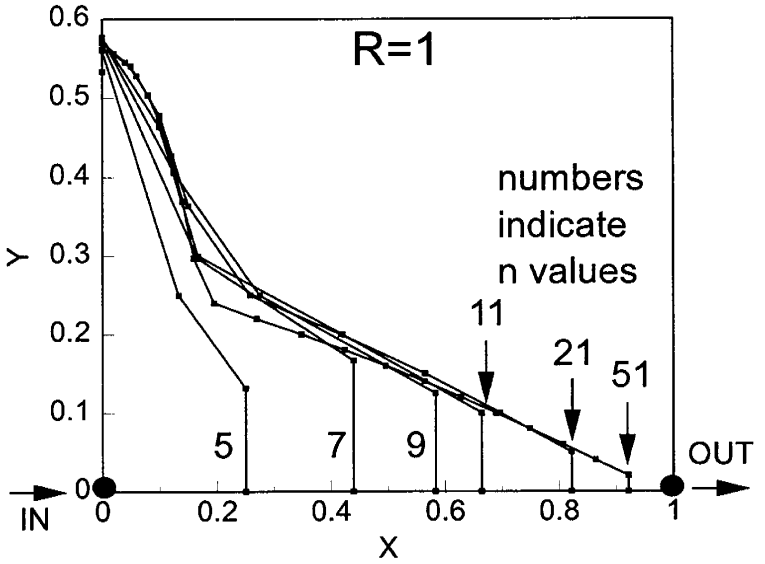

Fig. 56. Front profiles at gelant breakthrough in the producer when all fractures have the same conductivity. (Unit-mobility displacement.)

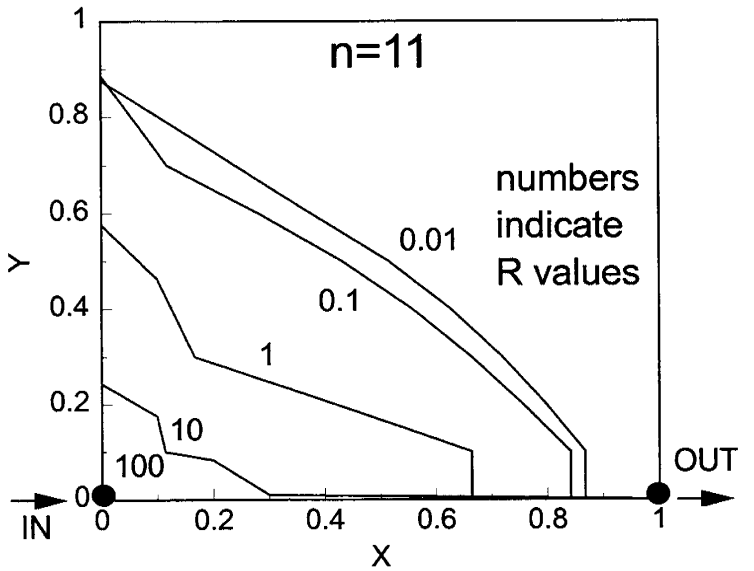

Fig. 57. Gelant front profiles versus R when n=11. (Unit-mobility displacement.)

For an n-value of 11, Fig. 57 plots the gelant front profiles for R-values ranging from 0.01 to 100. (The profile for R=100 lies on the axes). As expected, the profiles cover a larger area as the R-value decreases. However, there is a limit to this trend. Note that the profile for R=0.1 is not much different from that for R=0.01. Upon first consideration, one might expect the profiles to be vertical and to show nearly 100% sweep efficiency for the low R-values. This result is not observed because of the relation between fracture volume and fracture conductivity. At low R-values, fracture conductivity is much greater in the y-direction than in the x-direction, causing uniform east-west *velocity* profiles across the pattern. However, low R-values also mean that the y-direction fractures have significantly greater volumes than the x-direction fractures. For R=0.01, at the time the gelant front reaches the production well along the small-volume fracture on the x-axis, the gelant only fills 87% of the larger-volume fracture that lies on the y-axis.

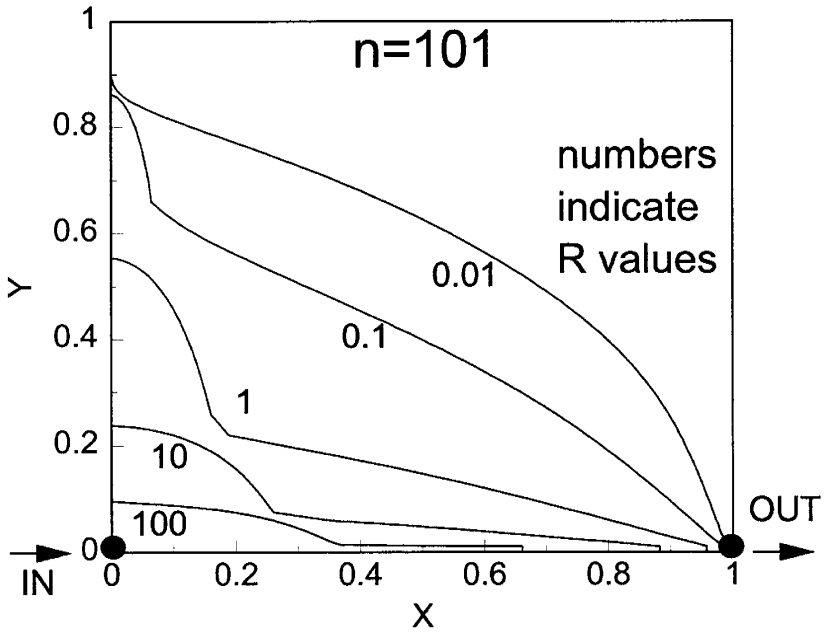

Fig. 58. Gelant front profiles versus R when n=101. (Unit-mobility displacement.)

Fig. 58 provides a similar plot for n=101. For a given R-value, note that the profiles are not radically different for the two n-values. For R-values of 1 or less, both figures raise concern that the gel will damage the secondary fracture pathways. Recall that our objective with a gel treatment is to plug the most direct x-direction fracture while leaving the secondary fracture pathways open. In this way, when fluid (water or gas) is injected after the gel treatment, the secondary fractures will allow a relatively high injectivity, and the injected fluid will sweep more uniformly through the reservoir. Thus, Figs. 57 and 58 suggest that R-values of 10 or greater are needed during a gel treatment to prevent excessive damage to the secondary fractures.

Effect of Plugging the Most Direct Fracture

Ideally, a gel treatment should plug the most direct fracture without entering or damaging the secondary fractures. If this gel placement could be achieved, how would sweep efficiency be affected? More specifically, how rapidly would a water tracer travel between an injector and a

producer after versus before a gel treatment? This question is addressed in Fig. 59 for R-values ranging from 1 to 1,000 and for n-values ranging from 3 to 101. The y-axis plots the ratio of breakthrough times—i.e., the transit time for a tracer injected after the most direct fracture was plugged divided by the tracer transit time before the most direct fracture was plugged.

Fig. 59 suggests that gel treatments have the greatest potential for reservoirs with high R-values and low to intermediate n-values. Gel treatments can be effective in reservoirs with high n-values, but the R-values must be very high. Gel treatments are not expected to provide much sweep improvement when $R \leq 1$.

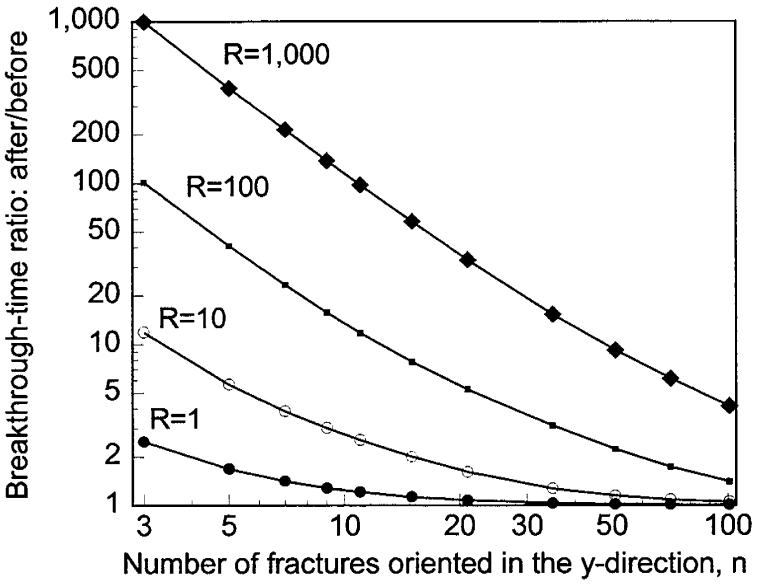

Fig. 59. Effect of plugging the most direct fracture.

Injection and Production Rates

Our work indicates that gel treatments have their greatest potential in naturally fractured reservoirs with high R-values. In particular, the most direct fracture between the wells should be at least ten times more conductive than those for the secondary fractures. Also, reservoirs with low n-values (low fracture intensities) are preferred. The discussion associated with Figs. 50 and 54 suggested that high R-values probably exist when interwell tracer studies yield produced tracer concentrations greater than 30% of the injected value.

In earlier work (Ref. 6 and Chapter 3), we used injectivity and productivity calculations to characterize whether a well was fractured. We also used these calculations to estimate the minimum conductivity of a hydraulic fracture. Can these calculations be useful in characterizing wells in naturally fractured reservoirs? Using the program listed in Appendix C, we determined injection rates, q, relative to that for a single direct fracture, q_o. Figs. 60 and 61 plot q/q_o values versus R- and n-values. In Fig. 60, R-values ranged from 1 to 1,000, while in Fig. 61, they ranged from 0.001 to 1. In all cases, a fixed pressure drop was applied between the wells, and the wells were separated by a fixed distance.

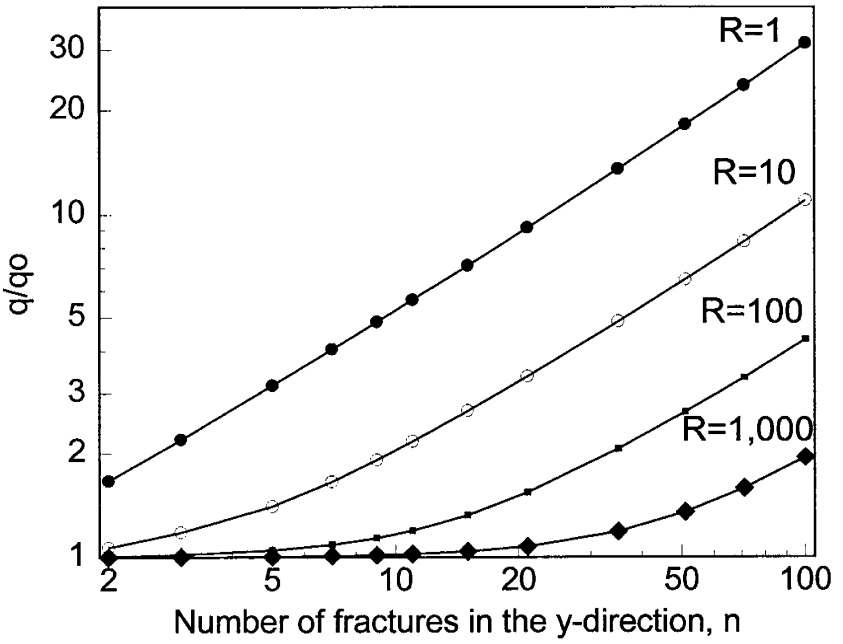

Fig. 60. Injectivity in a naturally fractured system relative to that for a single fracture that directly connects an injector-producer pair. $R \geq 1$.

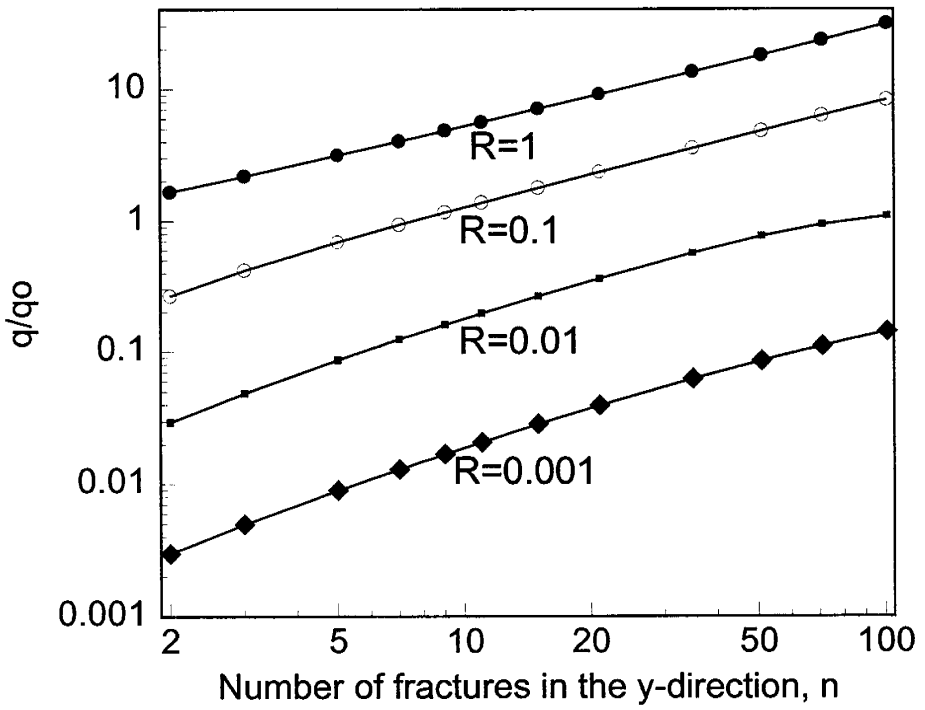

Fig. 61. Injectivity in a naturally fractured system relative to that for a single fracture that directly connects an injector-producer pair. $R \leq 1$.

As expected, Figs. 60 and 61 indicate that q/q_o increases as the n-value increases. This result is not surprising since the flow capacity of the system should increase as the fracture intensity (i.e., the concentration of fractures) increases.

In Fig. 60, the conductivity of the x-direction fractures were the same for all four R-values [i.e., $(k_f w_f)_y$ values were varied while the $(k_f w_f)_x$ values were fixed]. Under these circumstances, q/q_o decreases with increasing R-value. In particular, q/q_o approaches 1 as R approaches large values. This result is not surprising since, at large R-values, flow is dominated by the central east-west fracture (see Fig. 45), and the behavior is expected to approach that of a single direct fracture.

In Fig. 61, the conductivity of the y-direction fractures were the same for all four R-values [i.e., $(k_f w_f)_y$ values were fixed while the $(k_f w_f)_x$ values varied]. Also, q_o values were based on the R=1 case. As expected, Fig. 61 shows that injection rates decreased in proportion to the R-values.

From Eqs. 48 through 52, we have a means to estimate the denominator, q_o, in the y-axis of Figs. 60 and 61, based on tracer breakthrough times. However, careful consideration of these equations (especially Eqs. 51 and 52) reveals that our estimates of $k_f w_f$ could be in error by a factor of eight. Thus, our estimate of q_o could be in error by a factor of eight. This error is too large to allow a reliable distinction between R- and n-values using Figs. 60 and 61. Therefore, injection and production rates, by themselves, have limited value in characterizing fractured systems.

Diagonally Oriented Fractures

We have focused on fractured systems where one central x-direction fracture directly connects the injector-producer pair. How would our results be affected if the fractures were oriented diagonally relative to the wells (see Fig. 62)? This question is addressed in Fig. 63 for R-values ranging from 1 to 1,000 and for n-values ranging from 2 to 101. In this figure, the injection rates, q, are plotted relative to q_o, the injection rate for a single fracture that was used as the basis for comparison in Figs. 61 and 63. A comparison reveals that Fig. 63 is very similar to Fig. 61, except that the R-values in Fig. 61 correspond to the reciprocal R-values in Fig. 63. The most important point to be taken from this comparison is that diagonally oriented fractures (i.e., those illustrated in Fig. 62) act like direct-fracture systems with low R-values. Careful consideration reveals that systems like those shown in Fig. 62 should provide acceptable sweep efficiencies, and they are poor candidates for gel treatments.

The fracture orientations shown in Figs. 45 and 62 represent two possible extremes. Intermediate orientations (relative to the injector-producer pair) are illustrated in Fig. 64 for the case where n=11. Fig. 64 also illustrates a numbering scheme for the fractures.

Figs. 65 and 66 plot q/q_o values versus row location of the production well, using the fracture-numbering scheme illustrated in Fig. 64. In these figures, the reference flow rate, q_o, is the same value used in Figs. 60, 61, and 63 (i.e., the flow rate in a single direct fracture between the two wells). Fig. 65 applies to cases where $R \geq 1$, while Fig. 66 applies to cases where $R \leq 1$.

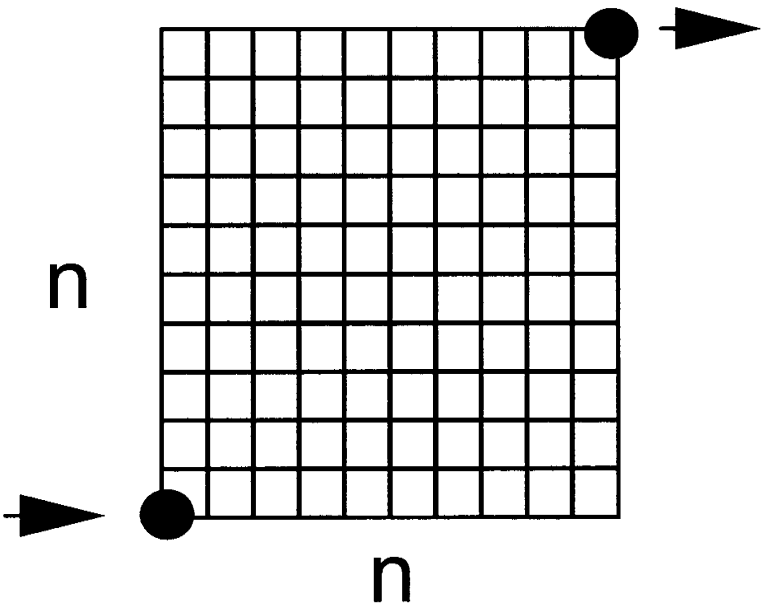

Fig. 62. Fractures oriented diagonally relative to the wells.

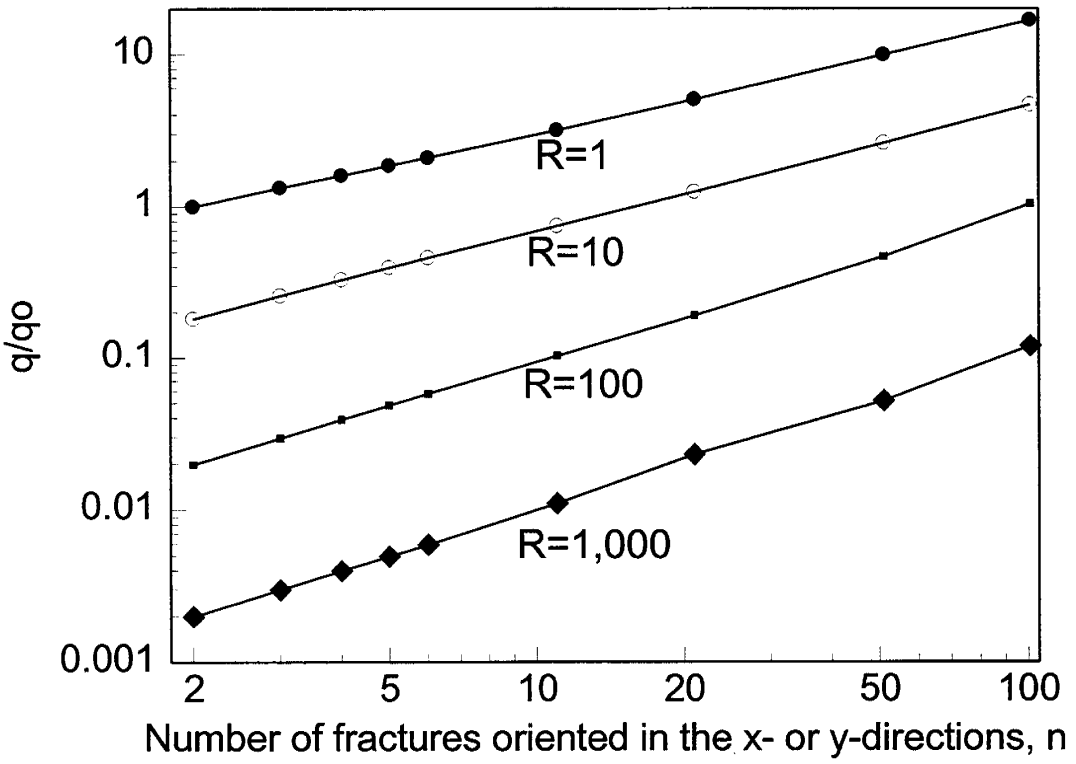

Fig. 63. Relative injection rates for diagonally oriented fractures.

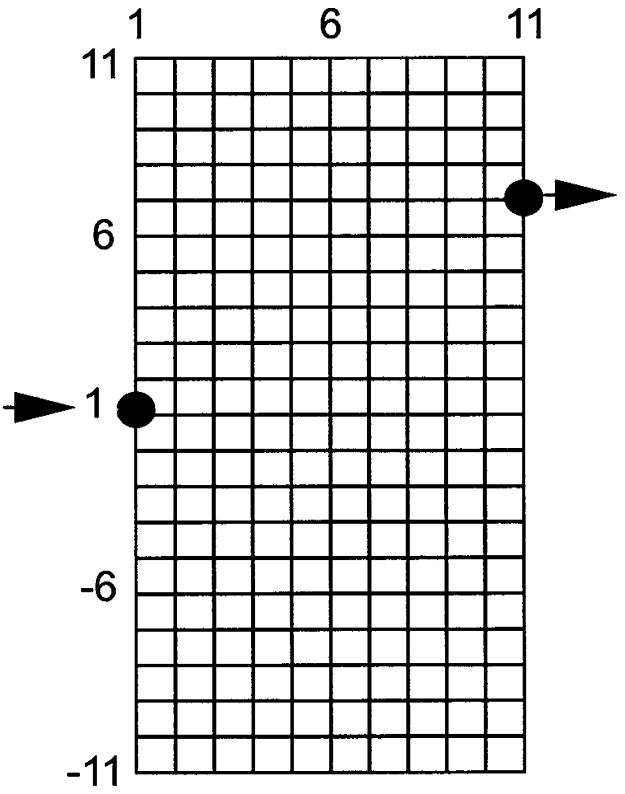

Fig. 64. Intermediate fracture orientations relative to the injector-producer pair.

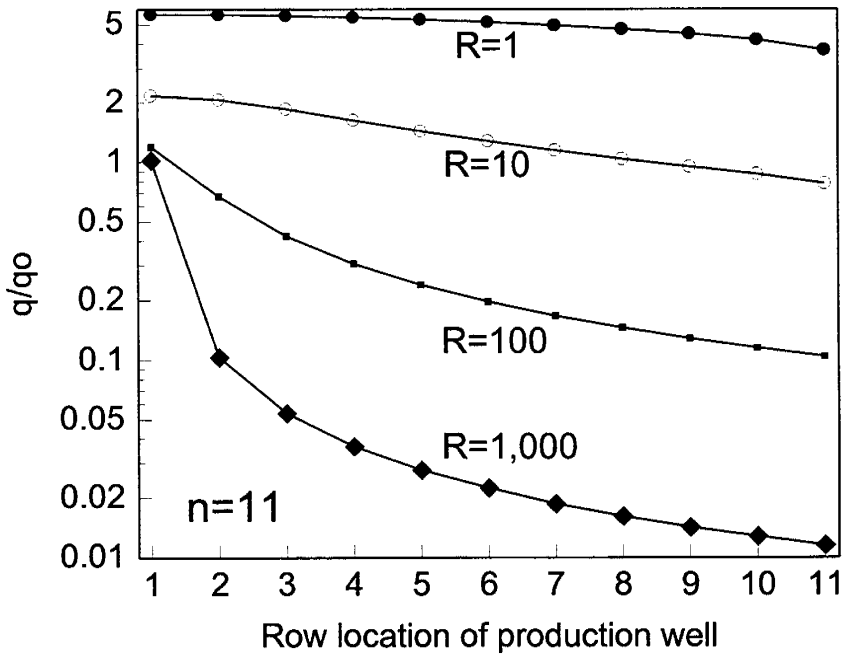

Fig. 65. Relative injection rates for intermediate fracture orientations. $R \geq 1$.

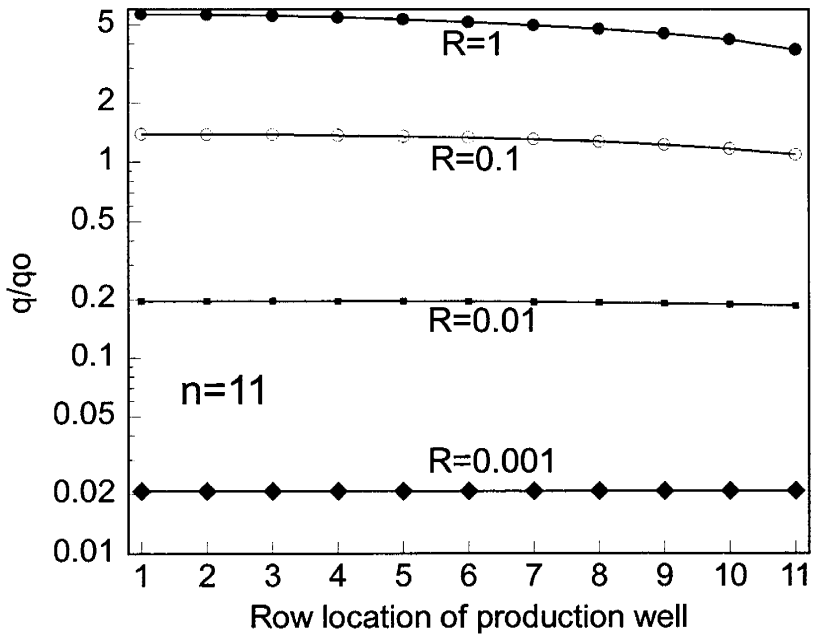

Fig. 66. Relative injection rates for intermediate fracture orientations. $R \leq 1$.

Fig. 67 shows the effects of injecting a 0.1 fracture-volume tracer bank when n=11 and the producer was slightly off the direct east-west path. In this case, the injection well was located on the central x-direction fracture, and the production well was located one fracture north of the central x-direction fracture. In other words, in Fig. 64, the production well was located at coordinates (11,2), while the injection well was located at (1,1). Fig. 67 plots the relative produced tracer concentration (C/C_o) versus dimensionless time for R-values ranging from 1 to 1,000. The denominator used to determine the dimensionless time was the same for all four curves. Specifically, the denominator was the same transit time used when determining dimensionless times for Fig. 55.

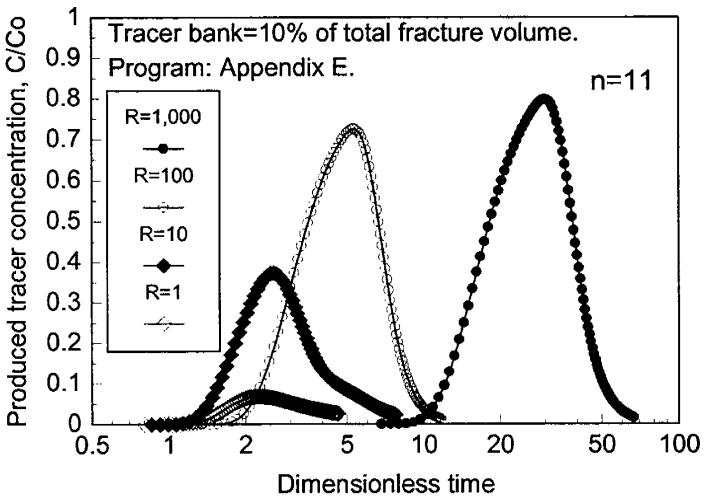

Fig. 67. Tracer curves when injector and producer were located at (1,1) and (11,2), respectively.

For cases where the injector-producer pair were located at opposite ends of the central x-direction fracture, Fig. 55 shows that breakthrough times all occurred at dimensionless times around 0.8 and the peak-concentration times occurred at dimensionless times roughly around 2, regardless of the R-value. In contrast, when the producer was located one fracture off center, at (11,2), Fig. 67 shows that the breakthrough times and peak-concentration times increased with increased R-value.

The behavior in Fig. 55 can be readily understood by remembering that in all cases, the central x-direction fracture had the same conductivity. Also, all injector-producer pairs represented in Fig. 55 were effectively separated by the same distance and experienced the same pressure drop. Therefore, we expected the interwell tracer transit time to be fairly insensitive to R-value. Recall that the results in Figs. 48 and 49 were consistent with this idea. As mentioned earlier, the tracer transit times provide an excellent means to estimate the conductivity of the most direct fracture (i.e., using Eq. 51).

The behavior in Fig. 67 can be understood by recognizing that the most direct injector-producer pathways were slightly longer (specifically, 10% longer) than those associated with Fig. 55. Depending on the R-value, the resistance to flow added by the additional 10% of fracture pathway could significantly increase the transit time.

Interestingly, the tracer curves in Fig. 67 appear more peaked than those in Fig. 55, but the peak concentration values are fairly similar for the two figures. The R=1,000 case appears to be a slight exception, with the peak value in Fig. 67 being about 16% lower than that in Fig. 55. Simulations using larger tracer banks revealed that this is a dispersion effect—the peak values for the R=1,000 cases would have been much closer if a 0.5-fracture-volume tracer bank had been injected.

Uneven Fracture Spacing

In the work described so far, the distance between adjacent x-direction fractures was the same as that for y-direction fractures. How would our results change if fracture spacing was different in the x- and y-directions? This question is addressed in Figs. 68 through 73. Figs. 68 and 69 plot gelant front profiles when the gelant has just reached the production well for the case where R=1 (x- and y-direction fractures have the same conductivity). In Fig. 68, the reservoir contained 11 fractures that were oriented in the y-direction. The number of fractures oriented in the x-direction was varied from 21 to 321. As a reminder, the case with 11 y-direction fractures and 21 x-direction fractures has the same fracture spacing in both directions (see Fig. 45). Also recall that the dimensions of the reservoir are fixed, so we simply change the fracture spacing or intensity when the number of fractures are varied. The case with 321 x-direction fractures has 16 times greater distance between fractures in the y-direction than in the x-direction. In Fig. 68, three other cases are considered where the distance between y-direction fractures is 2, 4, and 8 times the distance between x-direction fractures. These cases correspond to 41, 81, and 161 fractures, respectively, oriented in the x-direction.

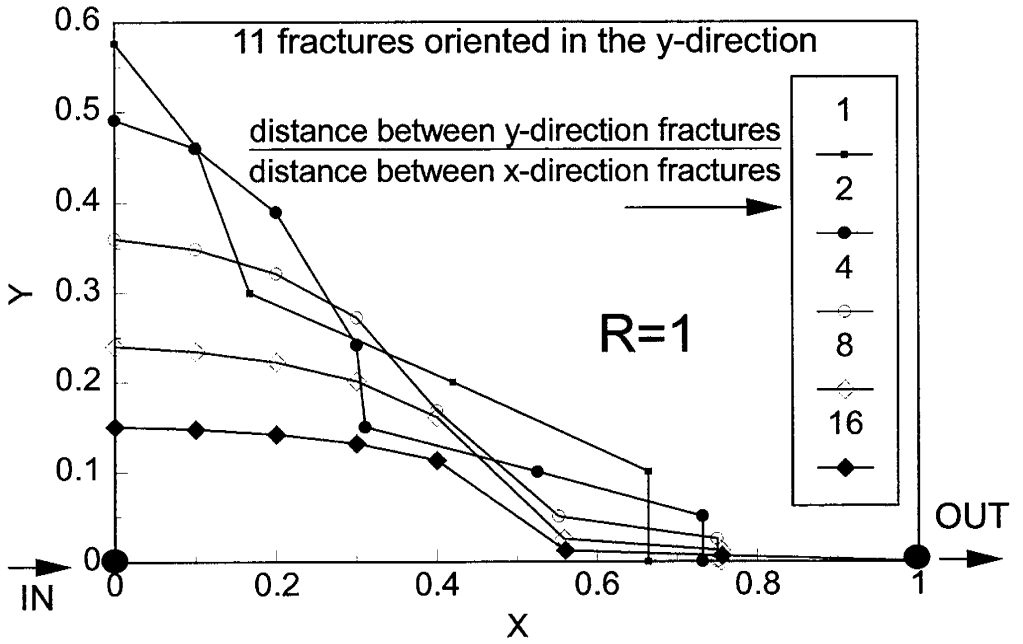

Fig. 68. Gelant front profiles when fracture spacing for y-direction fractures is greater than that for x-direction fractures. Number of y-direction fractures is fixed at 11. R=1.

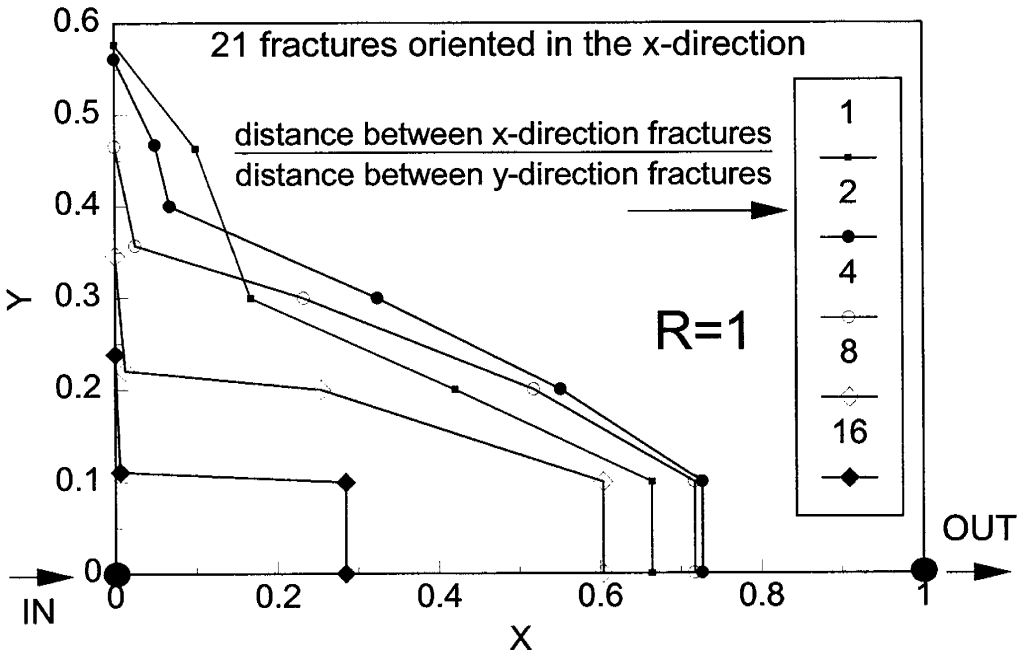

Fig. 69. Gelant front profiles when fracture spacing for x-direction fractures is greater than that for y-direction fractures. Number of x-direction fractures is fixed at 21. R=1.

Fig. 68 shows that the main effect of decreasing the fracture spacing in the x-direction is to decrease the distance of gelant penetration in the y-direction (away from the most direct x-direction fracture). In a sense, making the fracture spacing more anisotropic is equivalent to increasing the R-value (compare Figs. 57 and 68). Thus, increasing the anisotropy of the fracture spacing decreases the sweep efficiency and increases the need for a gel treatment.

Fig. 69 confirms the above observations for the case where fracture spacing is varied in the y-direction instead of the x-direction. In Fig. 69, the number of x-direction fractures was fixed at 21, while the number of y-direction fractures was varied from 11 to 161. Correspondingly, the distance between x-direction fractures varied from 1 to 16 times the distance between y-direction fractures. Like Fig. 68, Fig. 69 also shows that increasing the anisotropy of the fracture spacing decreases the sweep efficiency.

Figs. 70 and 71 show the effect of fracture-spacing anisotropy on the breakthrough-time ratio. In both figures, the y-axis plots the tracer transit time after an ideal gel treatment divided by that before the gel treatment. The gel treatment is ideal because we assume that the gel plugs the most direct fracture without damaging secondary fracture pathways. In Fig. 70, the number of y-direction fractures is fixed at 11, while the x-direction fractures are varied from 11 to 321. For R-values ranging from 1 to 1,000, Fig. 70 shows that the breakthrough-time ratio is remarkably insensitive to the number of fractures oriented in the x-direction.

In contrast, in Fig. 71, the number of x-direction fractures is fixed at 21 while the y-direction fractures are varied from 5 to 161. Fig. 71 indicates that the breakthrough-time ratio is sensitive to y-direction fracture spacing, especially for high R-values. The trends in Fig. 71 are similar to those in Fig. 59. This similarity suggests that variation in the spacing of y-direction fractures is responsible for the sensitivity to n-values seen in Fig. 59. Both Figs. 70 and 71 confirm that gel treatments have their greatest potential in reservoirs with high R-values (i.e., $R \geq 10$).

Figs. 72 and 73 show the effects of fracture-spacing anisotropy on injection rates. Recall that q/q_o is the injection rate relative to that for a single direct fracture between the wells. Fig. 72 shows that q/q_o is insensitive to the spacing for x-direction fractures. In contrast, q/q_o shows a greater sensitivity to the spacing for y-direction fractures (Fig. 73).

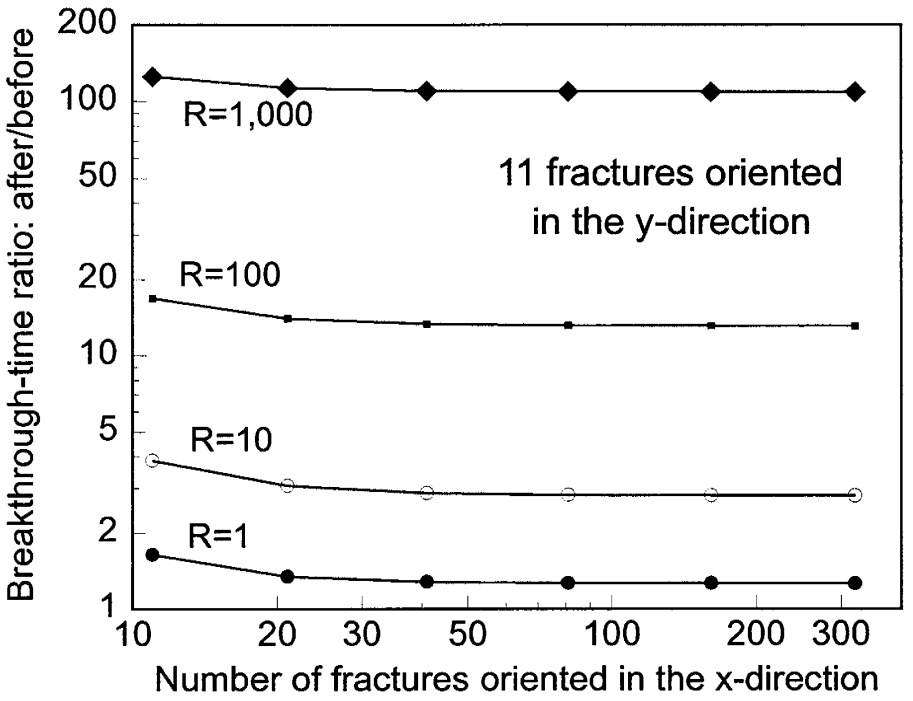

Fig. 70. Effect of plugging the most direct fracture when fracture spacing for y-direction fractures is greater than for x-direction fractures. Number of y-direction fractures is fixed at 11.

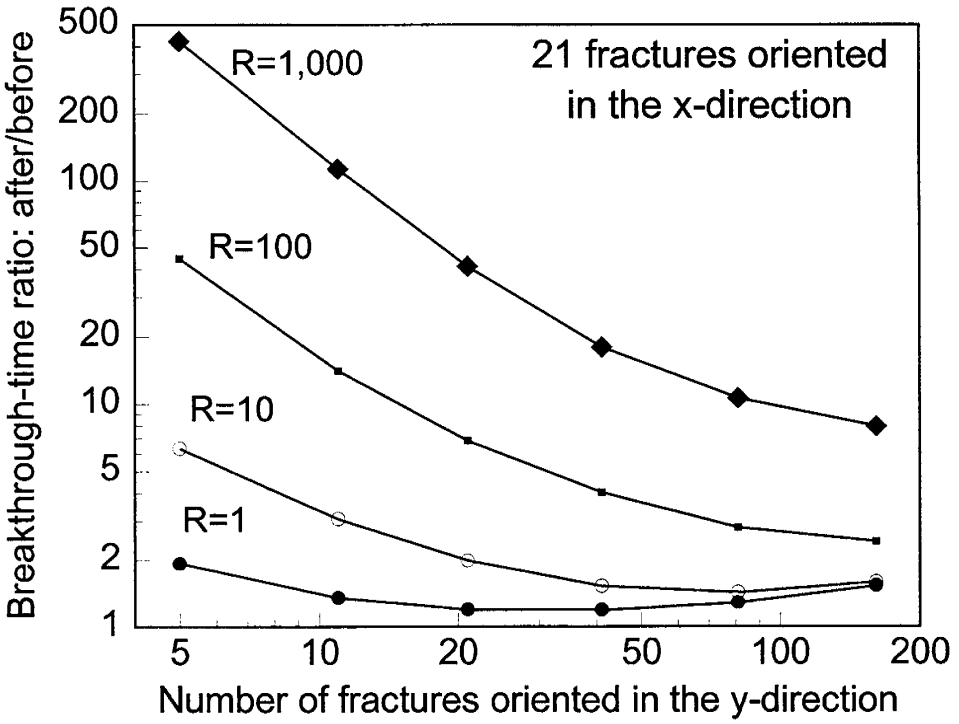

Fig. 71. Effect of plugging the most direct fracture when fracture spacing for x-direction fractures is greater than for y-direction fractures. Number of x-direction fractures is fixed at 21.

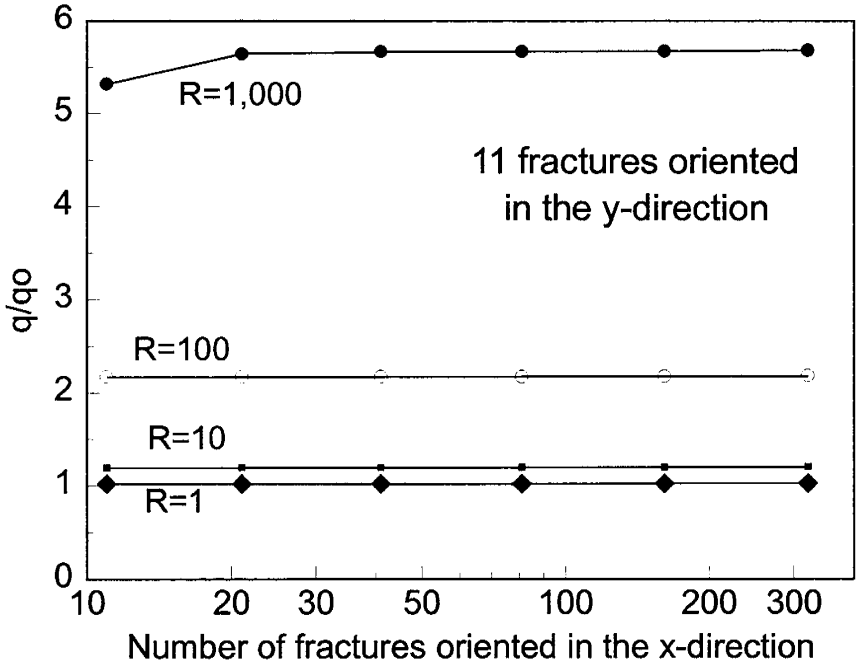

Fig. 72. Relative injection rates when fracture spacing for y-direction fractures is greater than that for x-direction fractures. Number of y-direction fractures is fixed at 11.

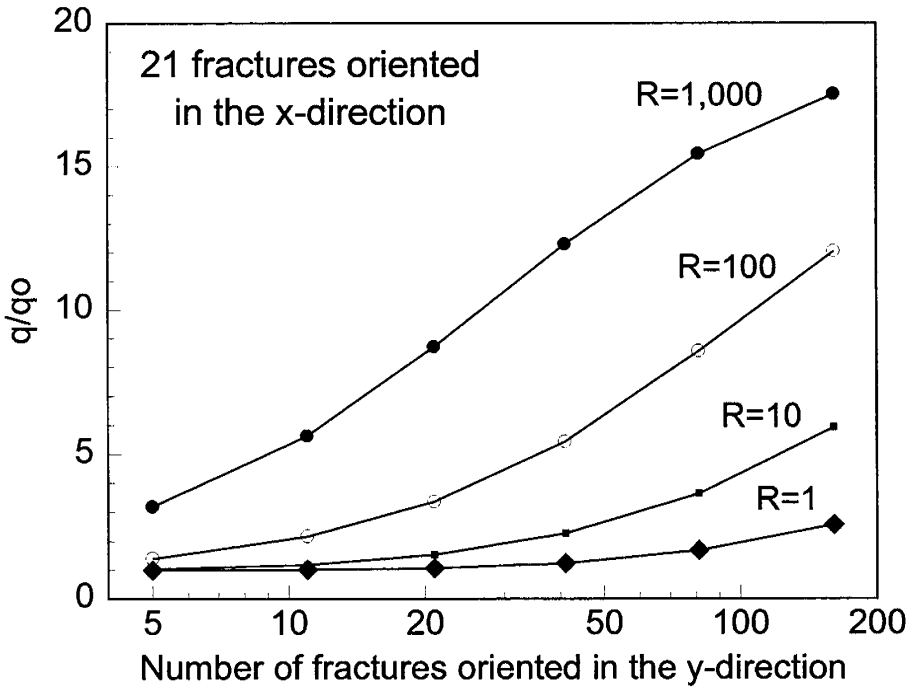

Fig. 73. Relative injection rates when fracture spacing for x-direction fractures is greater than that for y-direction fractures. Number of x-direction fractures is fixed at 21.

Future Work

In the next step of our examination of gel treatments in naturally fractured reservoirs, we will explore placement of gels that exhibit a strong shear-thinning behavior and dehydration during extrusion through fractures (i.e., gel properties reported in Ref. 48). Ultimately, we hope to develop a methodology for sizing gel treatments in naturally fractured reservoirs.

Conclusions

In a naturally fractured reservoir, we define an R-value as the conductivity of fractures that are aligned with direct flow between an injector-producer pair divided by the conductivity of fractures that are not aligned with direct flow between wells. We also define an n-value as the fracture density or intensity. More specifically, the n-value is the number of fractures between an injector-producer pair, where these fractures are not aligned with the direct flow direction.

1. Gel treatments in naturally fractured reservoirs have the greatest potential when R-values are high (greater than 10).
2. Produced tracer concentrations from interwell tracer studies can be useful in identifying reservoirs with high R-values. We propose that the potential for a gel treatment becomes greater as the produced tracer concentration increases above 30% of the injected value. When produced tracer concentrations are low, gel treatments are unlikely to be effective.
3. Because tracer transit times are not sensitive to R- or n-values, they can be very useful when estimating the permeability or conductivity of the most direct fracture.
4. Injection and production rates have limited value in characterizing fractured systems.
5. The potential of gel treatments is insensitive to fracture spacing for fractures that are not aligned with the direct flow direction.
6. The potential of gel treatments decreases with increased fracture spacing for fractures that are aligned with the direct flow direction.

5. GEL PROPERTIES IN FRACTURES

Gels have often been used to reduce fluid channeling in reservoirs.[6] The objective of these gel treatments is to substantially reduce flow through high-permeability channels without damaging hydrocarbon-productive zones. The most successful applications for this purpose have occurred when treating linear flow problems—either fractures[3,4,33,51,52] or flow behind pipe.[53,54] In fractured reservoirs, some of the most successful treatments used relatively large volumes (e.g., 10,000 to 37,000 bbl/well) of Cr(III)-acetate-HPAM gel.[4,33,51] In these applications, the gel injection times were substantially longer than the gelation time (e.g., by factors ranging from 10 to 100). Since these gels (after gelation) do not flow through porous rock,[55] they must extrude through fractures during the placement process. Therefore, we are investigating the properties of gels during placement in fractures.

Gel Extrusion Through Fractures

Gel Dehydration. In previous work,[48] we reported that gel extrusion through fractures can occur at an unexpectedly low rate if the fracture conductivity or width is sufficiently small. We suggested that this low rate of gel propagation occurred because the gel dehydrated as it extruded through the fracture. In other words, water left the gel and leaked off into the porous rock or flowed through the fracture ahead of the gel, while the crosslinked polymer remained behind in the fracture to propagate at a much slower rate.

Recently, we performed several additional experiments to characterize the gel dehydration effect. The questions that we addressed in these experiments were:

1. What concentrations of polymer [HPAM] and crosslinker [Cr(III)] are found in the core effluent as a function of gel throughput?
2. How much are the polymer and crosslinker concentrated in the dehydrated gel?
3. Will gel extrude through fractures when low pressure gradients are applied?

Our experiments used an aqueous gel that contained 0.5% Allied Colloids Alcoflood 935 HPAM, 0.0417% Cr(III)-acetate, 1% NaCl, and 0.1% $CaCl_2$ at pH=6. All experiments were performed at 41°C (105°F). The gelant formulations were aged at 41°C for 24 hours (5 times the gelation time) before injection into a fractured core. Preparation of the fractured cores was described earlier.[48,55] The fractured cores (Berea sandstone) were 2.7 to 4 feet (81 to 122 cm) in length and 1.5 inches (3.8 cm) in height and width. Each core had four internal pressure taps that were spaced equidistant along the fracture—thus dividing the core into five equal sections. Table 1 lists the properties of these fractured cores. Before gel injection, all fractured cores were completely saturated with brine. All fractures were oriented vertically during our experiments.

In Fractured Core 15, we injected 43 fracture volumes (440 ml) of gel using a fixed injection rate of 2 ml/hr. Considering the dimensions of this fracture (average width of 0.0324 cm or 0.013 inches), the average fluid velocity in the fracture would be about 13 ft/d if all injected fluid stayed in the fracture. Even though 43 fracture volumes of gel were injected, no significant polymer or chromium were produced (see Fig. 74). The pressure gradient in the first section (i.e., the first 20%) of the core was fairly stable at 160 psi/ft during the last 40 fracture volumes of gel

injection (see Fig. 75). In contrast, the pressure gradients in the last three sections (the last 60%) of the core were very low. After gel injection, the core was disassembled to determine how far gel had propagated through the fracture. A rubbery gel was found in the first 25% (30 cm or 1 ft) of the fracture length. These findings all suggest that the gel only propagated one-quarter of the distance through the 4-ft-long fracture.

Table 1. Properties of Long Fractured Cores

Fractured Core #	Length, cm	Fracture volume, cm^3	Average w_f, inches	Average $k_f w_f$, darcy-ft
15	122	10.2*	0.013♦	9.5
16	122	17.5*	0.014♦	12.6
17	122	18.6*	0.011♦	5.8
18	81.3	17.4*	0.0063♦	1.14
19	122	44.4*	0.038♦	242
20	81.3	12.2*	0.0073♦	1.75
21	122	100**	0.084	2,730**
22	81.3	13.0*	0.0072♦	1.72
23	122	230**	0.20	34,700**
24	122	465**	0.4	277,000**
25	122	139**	0.12	7,500**

* Estimated from tracer studies. ** Calculated from fracture width.

♦ Calculated from fracture conductivity.

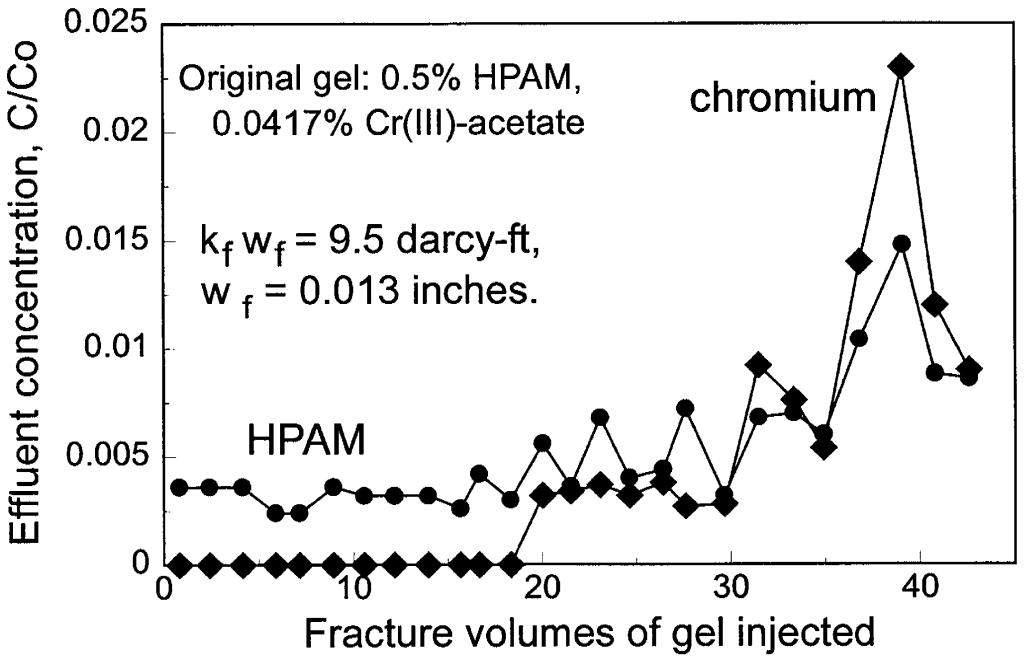

Fig. 74. Chromium and HPAM effluent concentrations during gel injection into Core 15.

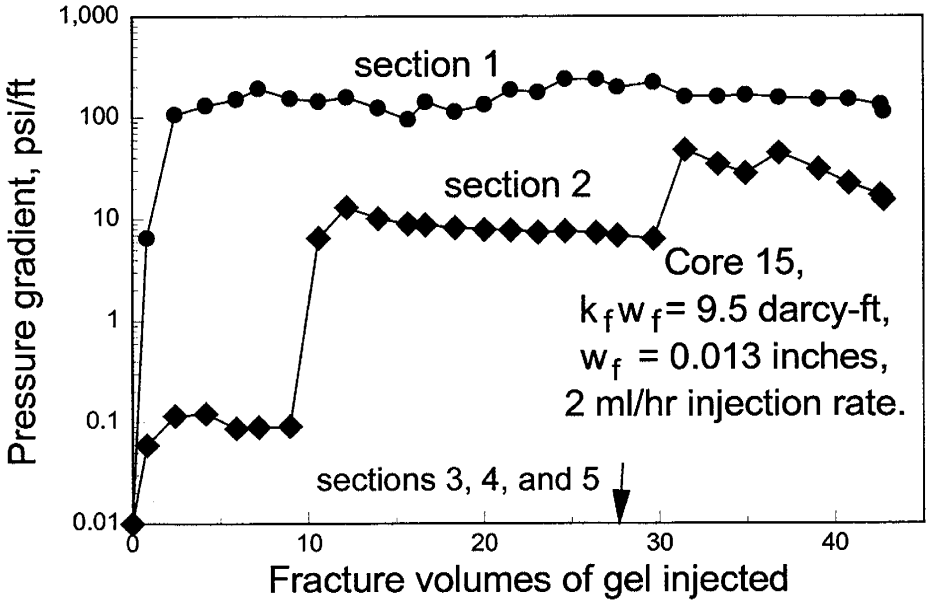

Fig. 75. Pressure gradients during gel injection into Core 15.

The gel in the fracture was analyzed for HPAM and chromium as a function of distance along the fracture. The results are shown in Fig. 76. Note that gel at the inlet sandface contained 22 times the HPAM concentration and 39 times the chromium concentration of the original gel. To a distance of 25 cm within the fracture, the gel contained between 8 and 28 times the HPAM concentration and between 18 and 45 times the chromium concentration of the original gel. In summary, our results demonstrate that the gel was concentrated (or dehydrated) by a factor typically between 10 and 40 during the extrusion process.

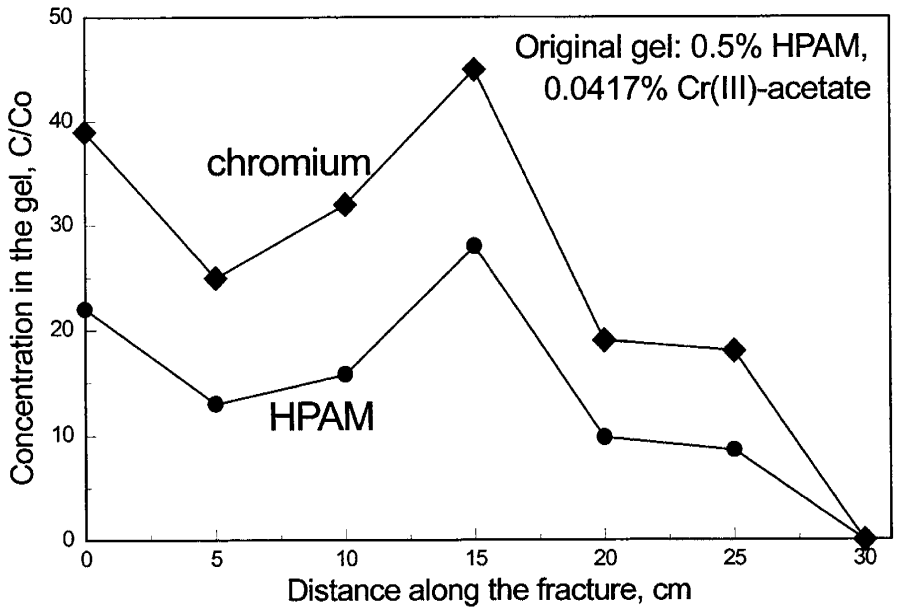

Fig. 76. Chromium and HPAM concentrations for gel in the fracture of Core 15 (relative to the concentrations of the injected gel) versus distance along the fracture (122-cm total length).

Gel Extrusion at Low Pressure Gradients. Our results using Core 15 suggested that a pressure gradient of 160 psi/ft was required to propagate gel through a 9.5-darcy-ft fracture when injecting at a fixed rate of 2 ml/hr. For comparison, in earlier work,[48] we noted that a pressure gradient of 65.4 psi/ft was required to extrude this gel through a 4.5 darcy-ft fracture when injecting at a fixed rate of 200 ml/hr. Also, a pressure gradient of 10.8 psi/ft was required to extrude this gel through a 568 darcy-ft fracture when injecting at a fixed rate of 200 ml/hr. These pressure gradients are quite high compared to values expected in many field applications. Typically, we expect pressure gradients around 1 psi/ft in reservoirs. In a previous paper,[48] we demonstrated that low-pressure gradients can be attained (during constant-rate injection tests) if the fracture conductivity is very high. However, will gel propagate through low-to-medium-conductivity fractures if a fixed, low-pressure gradient is applied?

To answer the above question, constant-pressure experiments were performed using Fractured Cores 16 and 17. In Core 16, a pressure drop of 35 psi was applied across the 4-ft-long core. As with our other experiments, the Cr(III)-acetate-HPAM gel was aged for 24 hours before attempting injection. Fig. 77 shows that after 10 days exposure to a 35-psi pressure drop, less than 4 fracture volumes of gel were injected (apparently) and flow had effectively stopped. The concentrations of HPAM and chromium in the core effluent were insignificant during this time (see Fig. 78). After the experiment, the core was disassembled and concentrations were determined along the fracture length. No sign of gel was found in the fracture. Gel was found on the inlet sandface. This gel contained 30 times the HPAM concentration and 47 times the chromium concentration of the original gel. Thus, a pressure drop of 35 psi was insufficient to extrude gel into this 12.6-darcy-ft (0.014-inch average width) fracture.

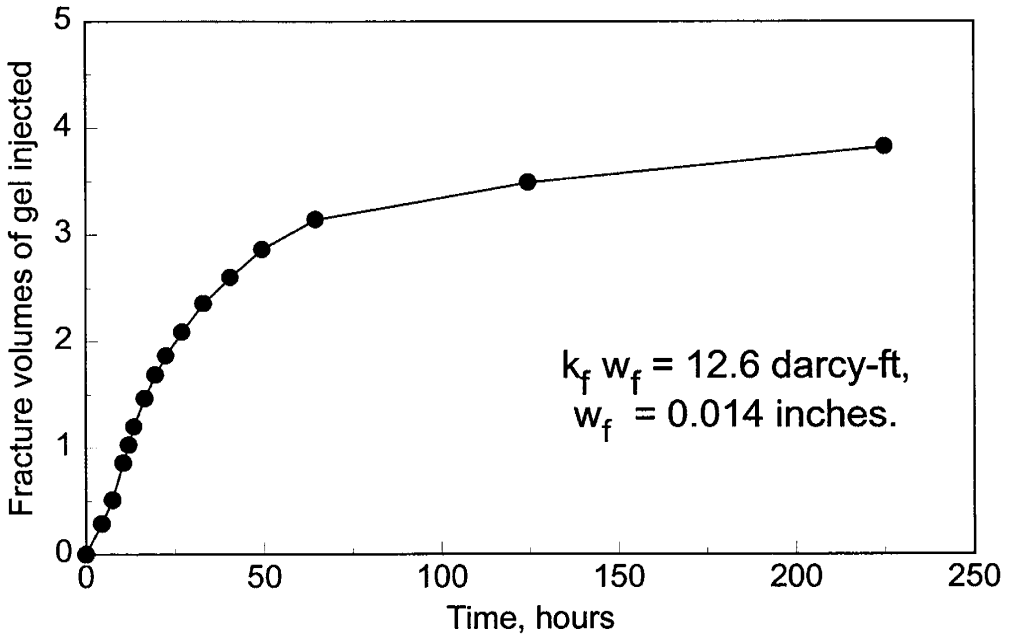

Fig. 77. After applying a constant pressure drop of 35 psi across a 4-ft-long core (Core 16), gel flow effectively stopped after 10 days or less than 4 fracture volumes of gel injection.

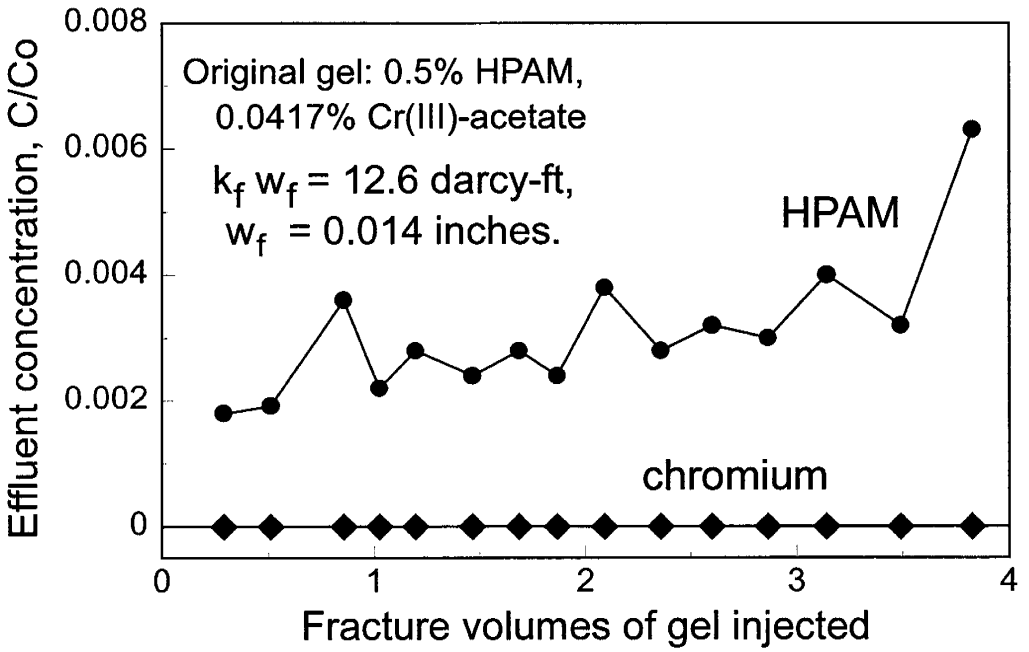

Fig. 78. Chromium and HPAM effluent concentrations during gel injection into Core 16.

A similar experiment was performed using Fractured Core 17. However, in this case, a constant pressure drop of 1 psi was applied across the 4-ft-long core (5.8 darcy-ft fracture conductivity and 0.011-inch average fracture width). After 19 days, less than one fracture volume was injected. Upon disassembly of the core, no evidence of gel was found in the fracture. Fluid samples at the core inlet contained 1.36 times the HPAM concentration and 3.0 times the chromium concentration of the original gel.

In summary, the Cr(III)-acetate-HPAM gel did not extrude through low-to-medium-conductivity fractures when low pressure gradients were applied. Some gel dehydration occurred even when relatively low pressure gradients were applied.

Effluent Compositions After Gel Breakthrough. In the above experiments, the gel did not propagate completely through the fractured core. Therefore, we performed several experiments to examine the effluent when gel was produced. One experiment was performed using Fractured Core 18, which was 2.7 ft (81.3 cm in length). The average conductivity was 1.14 darcy-ft, and the effective average fracture width was 0.0063 inches (0.016 cm). We injected 114 fracture volumes (1,980 ml) of 24-hr-old Cr(III)-acetate-HPAM gel using an injection rate of 200 ml/hr (effective average velocity in the fracture of 2,600 ft/d). Fig. 79 indicates that HPAM and chromium fronts arrived at the core outlet after injecting 25 to 30 fracture volumes of gel. The maximum effluent concentrations (relative to the original concentrations in the gel) were 0.72 for HPAM and 1.42 for chromium. Gel taken from the core inlet contained an HPAM concentration that was 6.8 times the original value and a chromium concentration that was 36 times the original value. Unfortunately, because of the method used for constructing Core 18 (it was cast in a metal alloy), we could not determine gel compositions along the length of the fracture.

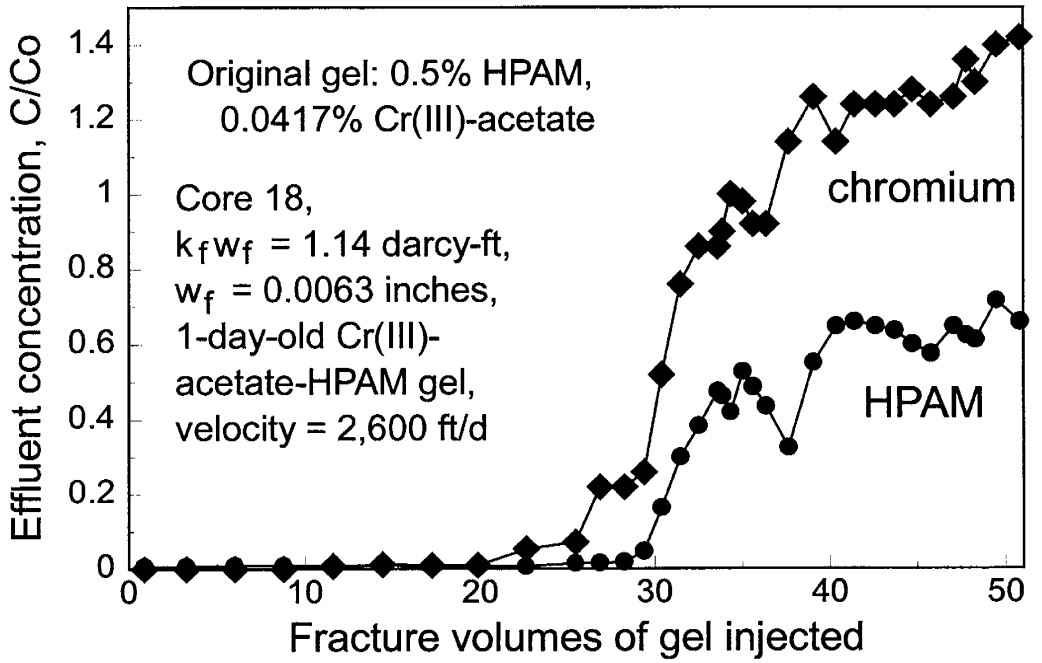

Fig. 79. Chromium and HPAM effluent concentrations during gel injection into Core 18.

In Fig. 79, one might have expected the effluent chromium and HPAM concentrations to be much higher than the injected concentrations, since we indicated that the gel was concentrated by roughly a factor of 30 when extruding through the fracture. However, remember that the effluent stream consists of the fluid that flows through the porous rock as well as the gel that extrudes through the fracture. When a steady state is reached, a mass balance indicates that the chromium and HPAM concentrations in the effluent must equal the injected concentrations. In other words, we ultimately expect the chromium and HPAM concentrations in the effluent to approach values of unity (relative to the injected values). To a rough approximation, Fig. 79 supports this expectation—i.e., the effluent relative concentrations for both polymer and chromium are much closer to a value of 1 than to 30. However, upon closer examination, we were somewhat surprised that after injecting 51 fracture volumes of gel, the relative chromium concentration appeared to level out at twice the relative HPAM concentration (1.42 versus 0.72).

Our first reaction after viewing Fig. 79 was that a greater volume of gel throughput was required to achieve a steady state. Therefore, we repeated this experiment using Cores 20 and 22. The lengths, fracture widths, and fracture conductivities of Core 18, 20, and 22 were very similar (see Table 1). Also, the experimental procedures were the same for these experiments, except that 110 fracture volumes (1,350 ml) of gel were forced through Core 20, and 59 fracture volumes (770 ml) were injected through Core 22 (compared to 51 fracture volumes through Core 18). Figs. 80 and 81 show the results from Cores 20 and 22, respectively. In agreement with the Fig. 79, these figures indicate that the gel arrived at the fracture outlet after injecting 25 to 40 fracture volumes of gel. Also, in Fig. 80, the relative effluent chromium and HPAM concentrations level out at values of 1.38 and 0.82, respectively. In Fig. 81, the relative effluent chromium and HPAM concentrations level out at values of 1.10 and 0.80, respectively. Thus, in all three experiments

(Figs. 79-81), the effluent chromium concentrations appear higher than expected, while the HPAM concentrations appear lower than expected.

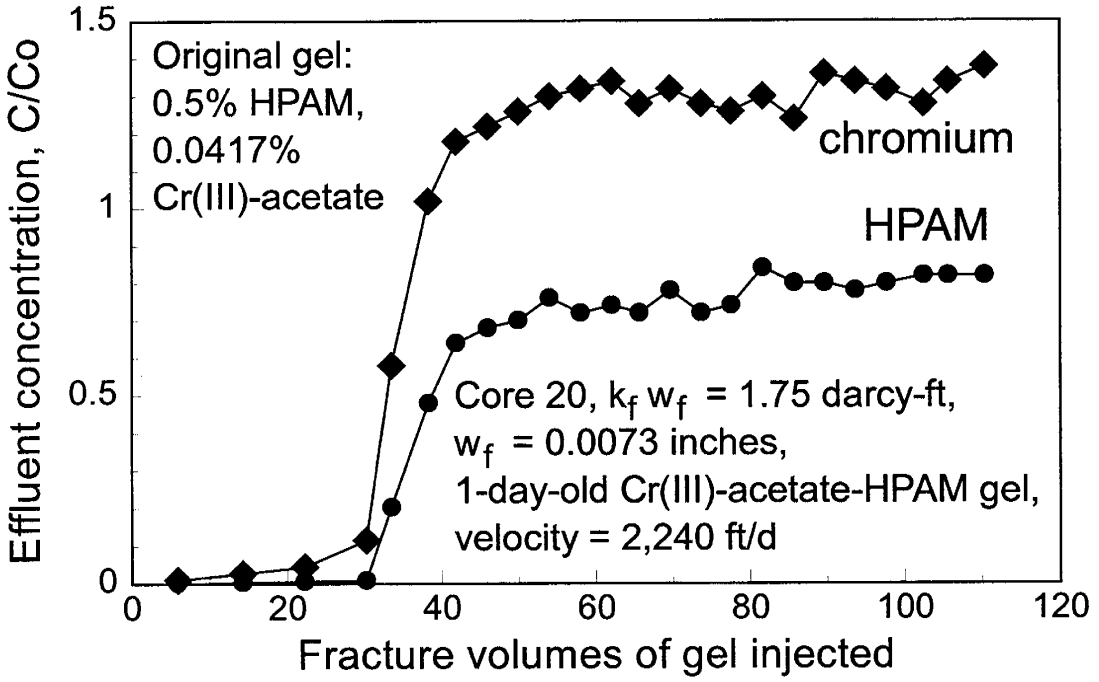

Fig. 80. Chromium and HPAM effluent concentrations during gel injection into Core 20.

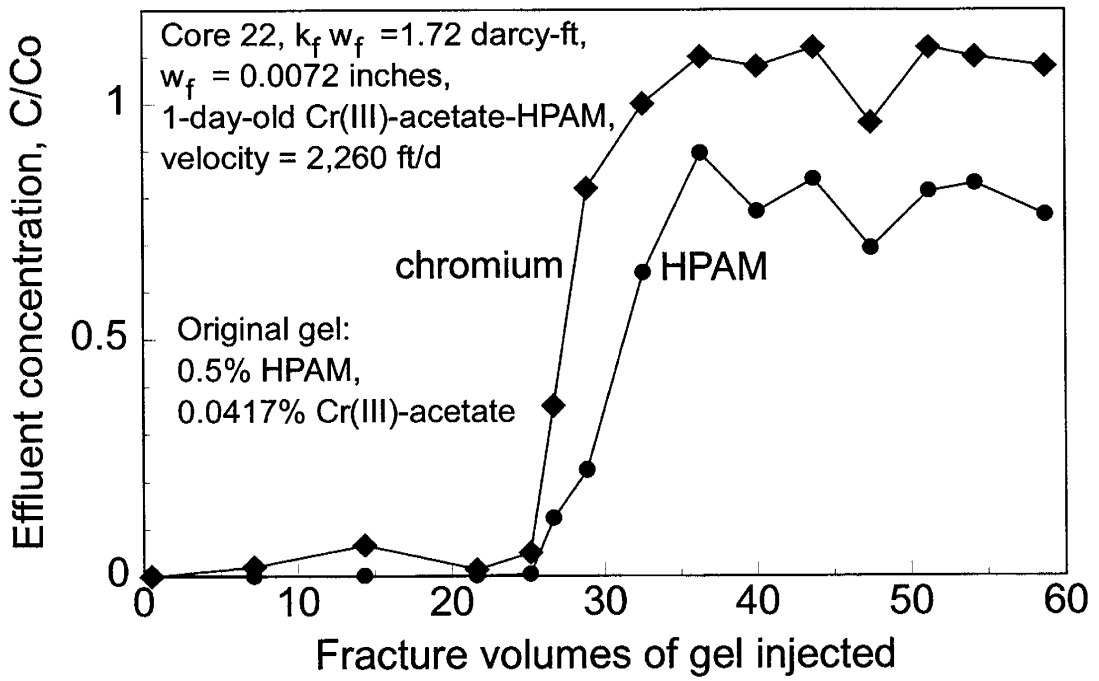

Fig. 81. Chromium and HPAM effluent concentrations during gel injection into Core 22.

To explain why the effluent relative chromium concentration was higher than the relative HPAM concentration, a number of possibilities come to mind. For example, perhaps HPAM is retained in the concentrated gel more than chromium. This explanation is contradicted by the analysis of the retained gel. Analysis of the gel taken from the inlet of Core 20 (after gel injection) revealed a chromium concentration 44.4 times that of the injected gel and an HPAM concentration 26 times that of the injected gel. In agreement with our other observations (e.g., Fig. 76), we consistently observed that the dehydration process concentrated chromium by a greater factor than HPAM.

A second possible explanation is that perhaps the differences were caused by experimental errors associated with our determinations of chromium and HPAM concentrations. However, this explanation is contradicted by detailed examination of the error bars and interferences associated with our analytical procedures. We find that our error bars were typically ± 5% for HPAM concentrations and ± 5% for chromium concentrations. These uncertainty levels were too low to explain the 10% to 40% deviations from the expected steady state values in Figs. 79 through 81.

A third explanation is that some of the chromium and HPAM leaches from the gel and propagates slowly through the porous rock. If the HPAM is retained in porous rock by a greater factor than the chromium, one might be able to rationalize the results in Figs. 79 through 81. Additional work is needed to test this and other ideas.

Gel Behavior in Wider Fractures. The fractures examined to this point have been fairly narrow—i.e., 0.014 inches or less in width. Will the dehydration effect be less pronounced if wider fractures are used? To answer this question, additional experiments were performed using long fractured cores. The core properties, core dimensions, gel composition, gel age, and experimental procedures were similar in all cases. With these experiments, we extended our range of fracture widths examined from 0.0063 to 0.4 inches. The corresponding range of fracture conductivities extends from 1.14 to 277,000 darcy-ft. During these experiments, we noted (1) the average pressure gradients, (2) the gel breakthrough volumes, (3) chromium and HPAM concentrations in the effluent, and (4) chromium and HPAM concentrations in gel along the fracture (after disassembling the core at the end of an experiment). The results from these experiments are summarized in Table 2, while some details are shown in Figs. 82 through 89.

Table 2. Effect of Fracture Conductivity on Gel Propagation

Conductivity, darcy-ft	Fracture width, inches	Pressure gradient, psi/ft	Gel breakthrough, fracture volumes
1.14	0.0063	750	40
4.5	0.010	65	35
242	0.038	20	21
586	0.051	11	7.7
2,730	0.084	6.5	4.8
7,500	0.12	2.0	5.4
34,700	0.2	0.28	1.8
277,000	0.4	0.14	1.1

Several important conclusions become evident after examining Table 2 and Figs. 82 through 89. First, the pressure gradient required to extrude the gel through a fracture decreases with increasing fracture conductivity and width. Fig. 82 quantifies this point by plotting the results from 33 separate experiments. The solid line in Fig. 82 shows a least squares fit, suggesting that the average pressure gradient during extrusion of this gel is proportional to fracture conductivity raised to the -0.58 power.

A second important point is that relatively wide fractures (> 0.1 inches) are needed for this gel to propagate using typical reservoir pressure gradients (e.g., ~1 psi/ft). This result implies that the gel simply may not enter fractures with widths less than 0.1 inches. Thus, in naturally fractured reservoirs with a range of fracture conductivities, the gel may selectively be confined to the wider fractures.

A third important point (from Table 2) is that the degree of gel dehydration (as judged by gel breakthrough) decreases with increased fracture width and with decreased pressure gradient. At pressure gradients around 1 psi/ft, this gel may concentrate (dehydrate) by a factor less than 6. However, since near-wellbore pressure gradients could be much greater than 1 psi/ft, much greater degrees of gel dehydration could be observed near the well.

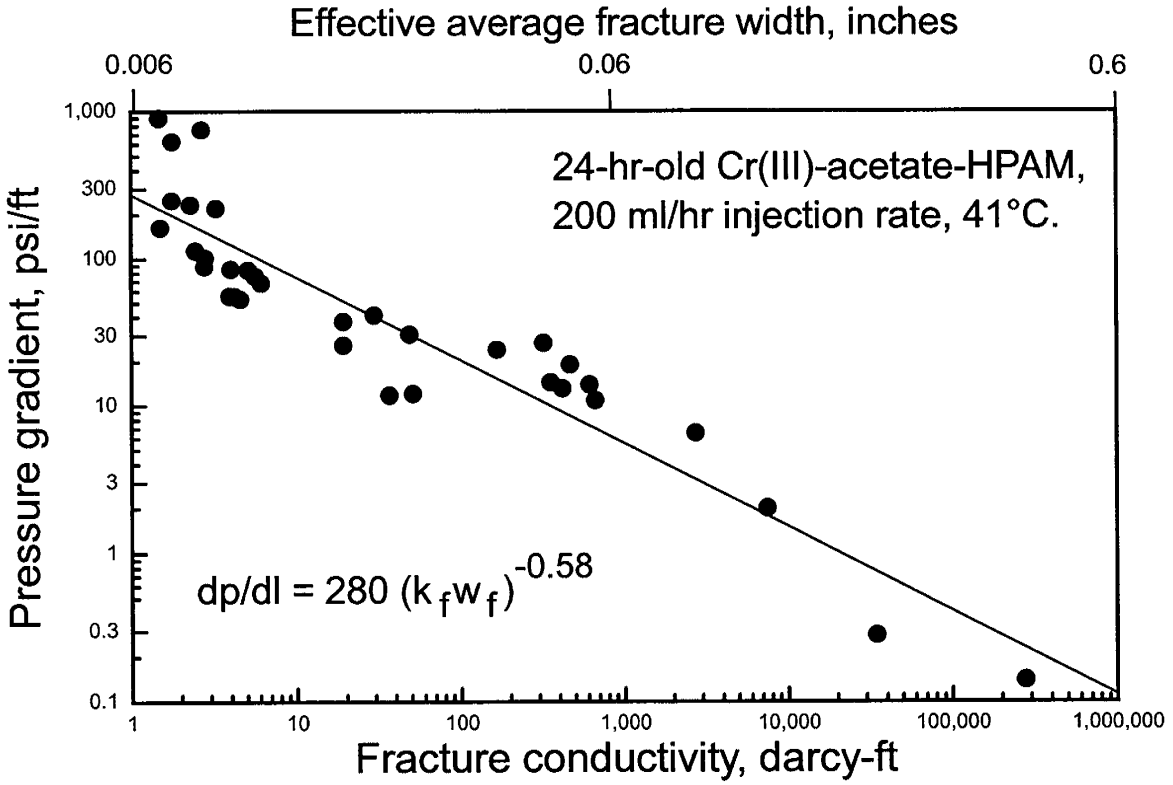

Fig. 82. Pressure gradient versus fracture conductivity for a fixed volumetric injection rate.

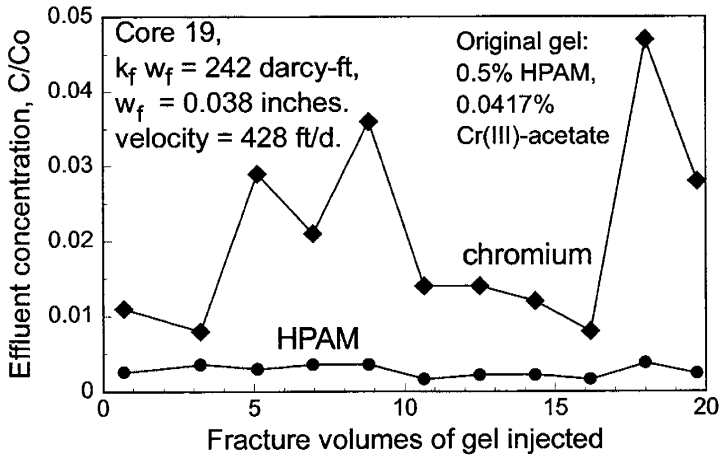

Fig. 83. Chromium and HPAM effluent concentrations during gel injection into Core 19.

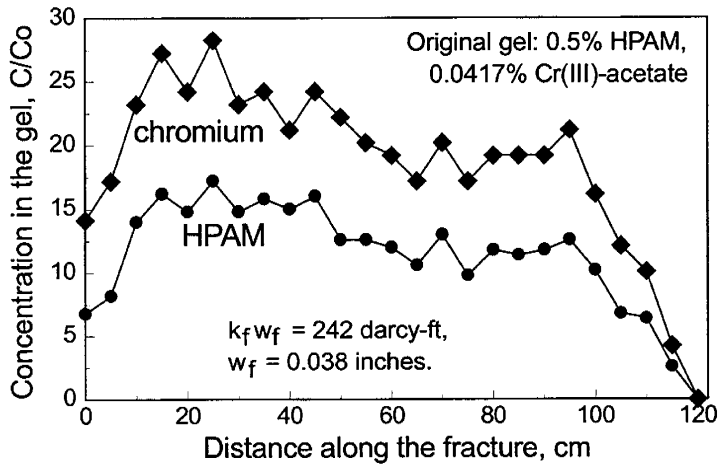

Fig. 84. Chromium and HPAM concentrations for gel in the fracture of Core 19. (relative to the concentrations of the injected gel. 122-cm total length.)

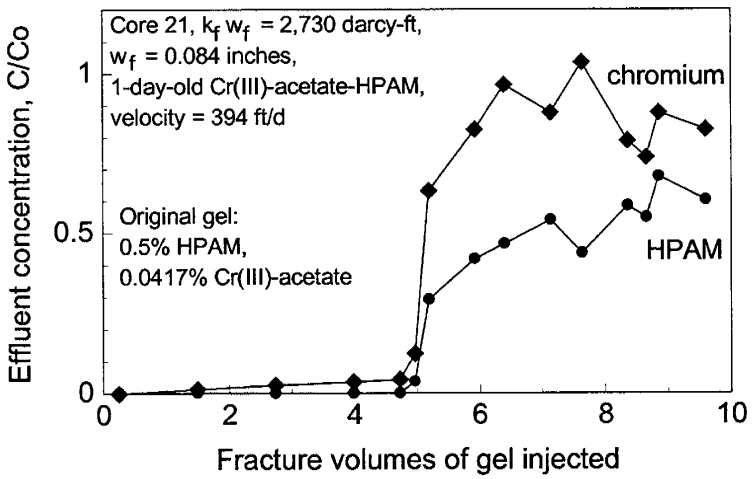

Fig. 85. Chromium and HPAM effluent concentrations during gel injection into Core 21.

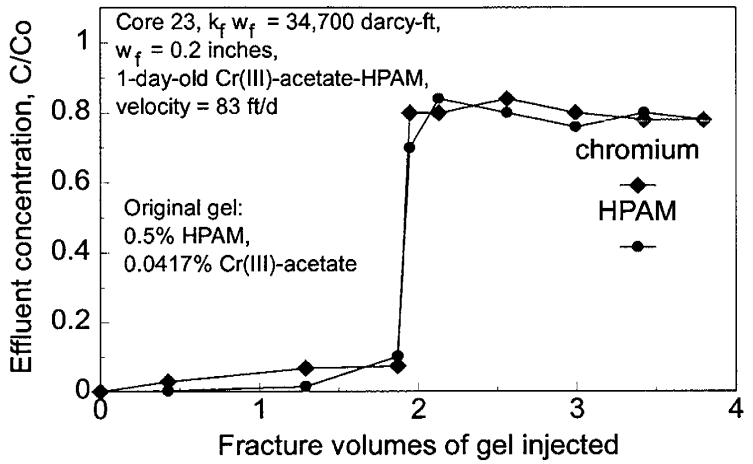

Fig. 86. Chromium and HPAM effluent concentrations during gel injection into Core 23.

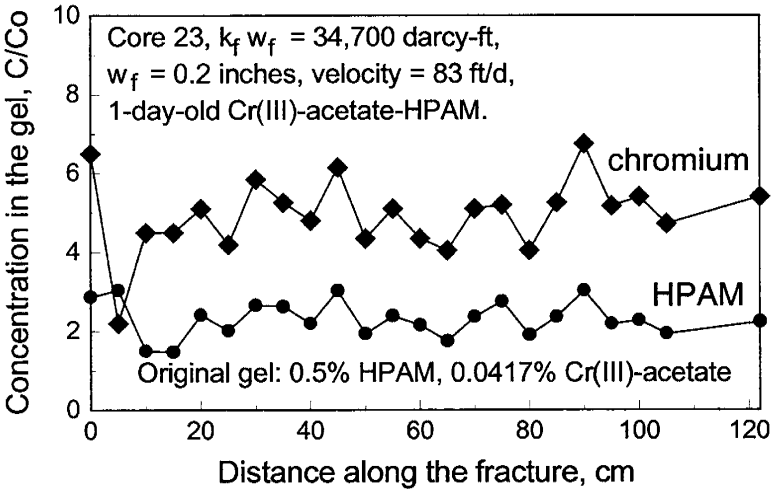

Fig. 87. Chromium and HPAM concentrations for gel in the fracture of Core 23. (relative to the concentrations of the injected gel. 122-cm total length.)

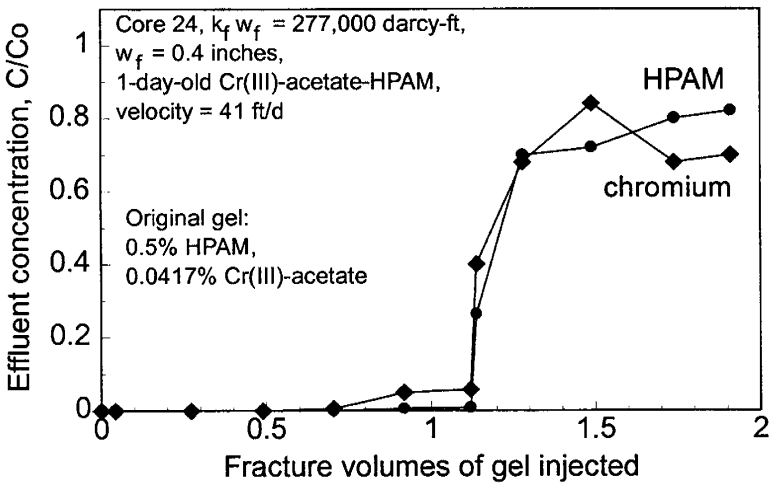

Fig. 88. Chromium and HPAM effluent concentrations during gel injection into Core 24.

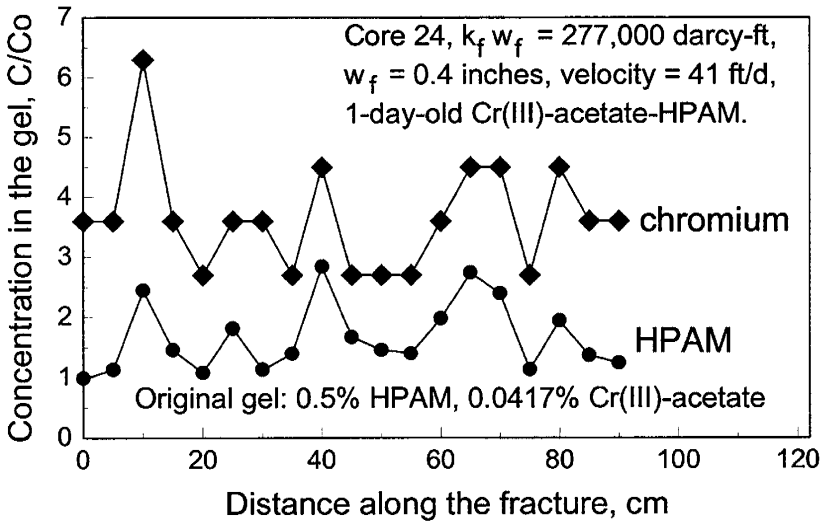

Fig. 89. Chromium and HPAM concentrations for gel in the fracture of Core 24. (relative to the concentrations of the injected gel. 122-cm total length.)

Water Flow After Gel Placement

How effectively does the gel reduce fracture conductivity after gel placement? This question is addressed in Fig. 90 for fractures with conductivities ranging from 1 to 277,000 darcy-ft (corresponding to fracture widths ranging from 0.006 to 0.4 inches). The brine injection rates during these experiments were generally the same as those used during gel placement (typically 200 ml/hr). These studies were routinely performed after the gel injection experiments described above.

For reference, the horizontal line (at a y-value of 0.081 darcy-ft) in Fig. 90 gives the conductivity associated with a fresh, unfractured 650-md Berea sandstone core. For fractures with initial conductivities (before gel placement) below 5,000 darcy-ft, the final conductivities (after gel placement) were less than or equal to 0.081 darcy-ft. This result indicates that the gels effectively healed the fractures when the initial conductivities were less than 5,000 darcy-ft (i.e., fracture widths less than about 0.1 inches). We noted (Table 2) that the gel placement process concentrated gel in the fracture by a factor of 5 or more when the initial conductivities were less than 5,000 darcy-ft. Incidentally, final core conductivity values less than 0.081 darcy-ft indicated that the permeability of the porous rock was reduced along with the conductivity losses experienced by the fracture. Much of this damage to the porous rock was simply gel that was not completely removed from the injection sand face before beginning brine injection.

For fractures with initial conductivities greater than 5,000 darcy-ft, Fig. 90 shows that the gel did not completely heal the fracture (because the final conductivities were greater than 0.081 darcy-ft). For these cases, the final conductivity after gel placement increased with increased initial fracture conductivity. Even so, the gel substantially reduced the fracture conductivities for all cases. For the 277,000-darcy-ft fracture, the gel reduced fracture conductivity by a factor of 600,000.

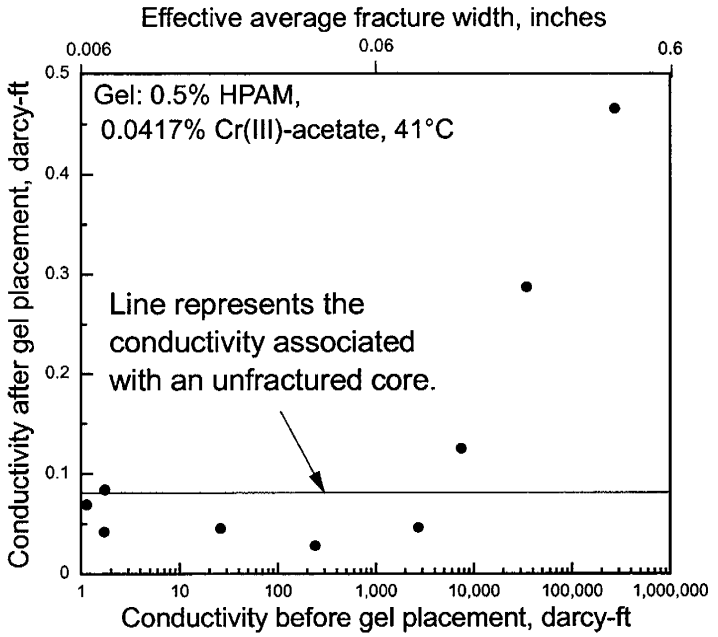

Fig. 90. Core conductivity during brine injection after gel placement versus fracture conductivity before gel placement.

For all tests that we performed to date, virtually no gel, polymer, or chromium was produced from the fractured cores during brine injection after gel placement. This result is demonstrated in Fig. 91 for the three most conductive fractures that we used to date (Cores 23, 24, and 25 with conductivities of 34,700, 277,000, and 7,500 darcy-ft, respectively). Within about 0.2 fracture volumes of brine throughput, the HPAM and chromium concentrations in the effluent were reduced below two percent of the concentrations in the original gel. Thus, we observed virtually no gel washout under the conditions that we tested.

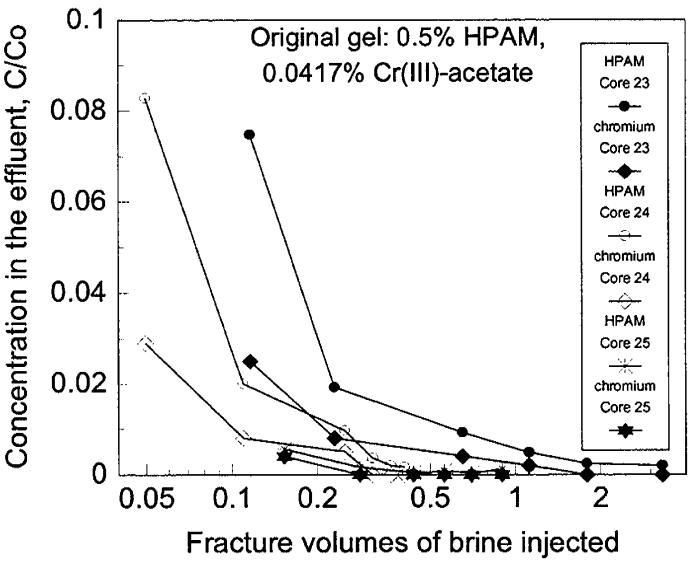

Fig. 91. Chromium and HPAM concentrations produced from Cores 23 and 24 (relative to the original values) during brine injection after gel placement.

Interpreting the Rheological Behavior of Gels in Fractures

In earlier work,[48] we showed that gels show an extremely strong apparent shear-thinning behavior when extruding through fractures and tubes (see Fig. 92).

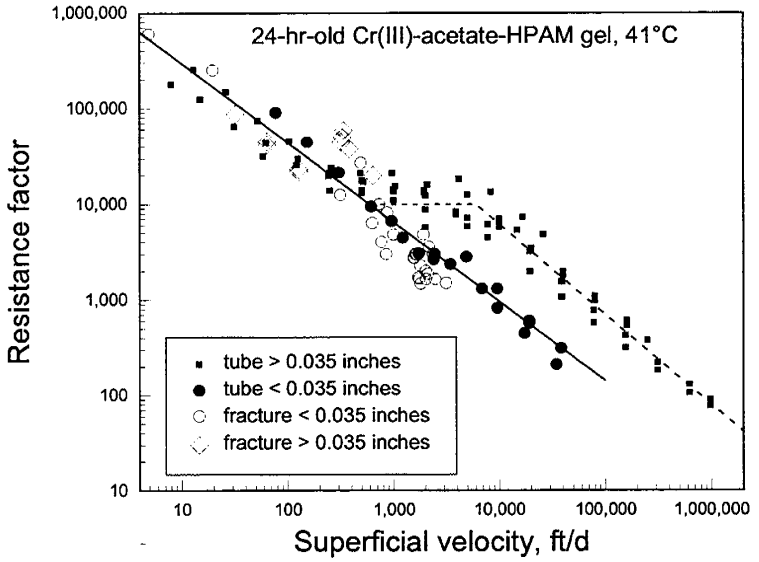

Fig. 92. Correlating behavior in short tubes (3 to 15 ft) and short fractures (0.5 to 4 ft).

For tubes with diameters less than 0.035 inches or fractures with estimated widths less than 0.035 inches, the resistance factors, F_r, were described fairly well using Eq. 53,

$$F_r = 2 \times 10^6 \, u^{-0.83} \quad \text{if} \quad w_f < 0.035 \text{ inches}, \tag{53}$$

where u was the superficial velocity in ft/d. The solid line in Fig. 92 illustrates Eq. 53.

For tubes with diameters greater than 0.035 inches (and presumably, for fractures with widths greater than 0.035 inches), the resistance factors were described using Eq. 54.

$$\begin{aligned} F_r &= 2 \times 10^6 \, u^{-0.83} \quad \text{if} \quad u \le 600 \text{ ft/d} \\ F_r &= 10{,}000 \quad \text{if} \quad 600 < u < 6{,}200 \text{ ft/d} \\ F_r &= 4 \times 10^7 \, u^{-0.95} \quad \text{if} \quad u \ge 6{,}200 \text{ ft/d} \end{aligned} \tag{54}$$

The dashed curve in Fig. 90 illustrates Eq. 54 for velocities above 600 ft/d. Below 600 ft/d, Eq. 54 predicts the same values as Eq. 53.

The steep slope of the curves in Fig. 92 indicates that the pressure gradient is fairly insensitive to fluid velocity over much of the velocity range. In other words, a minimum pressure gradient appears necessary to extrude the gel through a given fracture (or tube). This suggestion is consistent with our observations associated with Figs. 75-78—gel will not enter a fracture if the pressure gradient is not sufficiently high.

This behavior indicates that a Bingham model might be appropriate when describing extrusion of gels through fractures. In the Bingham rheological model,[50] the fluid will not move until a minimum shear stress or "yield" stress, τ_o, is exceeded. (For the Cr(III)-acetate-HPAM gel, Fig. 82 provides a good indication of the magnitude of this yield stress for a wide range of fracture conductivities and fracture widths.) Above this minimum shear stress, the model assumes that flow is basically Newtonian. In the Bingham model, the fluid velocity profile is flat (the velocity gradient is zero) between the center of the fracture and some distance, x_o, from the fracture center. In other words, the gel flows like a solid plug in this region. Between x_o and the fracture wall, the Bingham model assumes Newtonian flow. In effect, the Bingham model assumes that a Newtonian fluid flowing near the fracture wall lubricates the flow of the plug through the fracture. In our experiments, since the gel dehydrates as it extrudes through fractures, we suspect that the water leaving the gel during the dehydration process may be the key component of the lubricating layer.

In Appendix F, an analysis is performed using the Bingham model to determine x_o as a function of gel resistance factor. Eq. 55 provides this relation.

$$F_r = \left[1 - \frac{3x_o}{w_f} + \frac{4x_o^3}{w_f^3}\right]^{-1} \tag{55}$$

This relation can be coupled with Eq. 54 to provide an estimate of the thickness of the lubricating layer relative to the fracture width. (Appendix F shows details of this determination.) Fig. 93 shows the results.

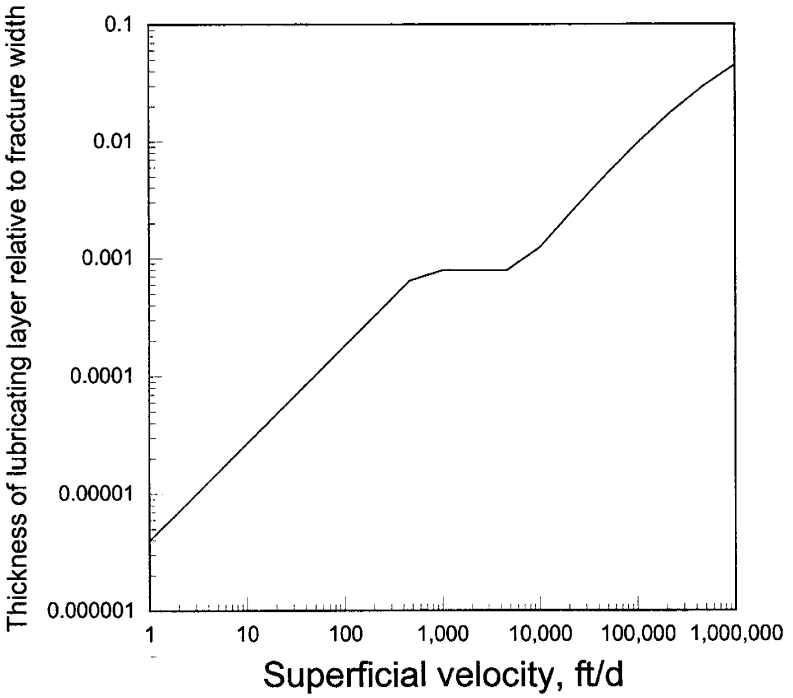

Fig. 93. Use of the Bingham model to predict the thickness of the lubricating layer based on Fig. 92, Eq. 54, and Eq. 55.

Fig. 93 reveals two important observations. First, the relative thickness of the lubricating layer is very small for the range of velocities shown. Second, the thickness of the lubricating layer increases with increased superficial velocity. If a means could be devised to physically measure the thickness of the lubricating layer (perhaps using interferometry), one could test whether the thickness of the lubricating layer actually does increase with increased velocity.

Yield Stress and Creep Stress. At a recent workshop, Elise Allen (with Smedvig of Stavanger, Norway) suggested that flow of gels through fractures could be analyzed using concepts of yield stress and creep stress. From the experimental results and the analysis presented in this chapter, the concept of yield stress certainly seems valuable. A minimum pressure gradient and shear stress do appear necessary to extrude gel through a given fracture.

However, to date, we have not seen evidence of gel "creep" during our experiments. In other words, when a fixed pressure gradient is applied that is below the yield stress, we see no evidence that the gel slowly deforms, flows, or extrudes through the fracture. Perhaps, we may see evidence of creep if we perform experiments with other gel compositions, at higher temperatures, or for much longer time periods.

Schemes To Optimize Gel Placement In Fractures

Part of our project focuses on schemes to optimize placement of blocking agents in fractures. Ideally, we desire schemes that will provide the placement illustrated by the upper left part of Fig. 94. To achieve this objective, the blocking agent must possess three properties. First, during the placement process, it must flow readily through the fracture without screening out or developing excessive pressure gradients. Second, it must become immobile at a predictable and controllable time. Third, some mechanism must be available to remove the blocking agent from the near-wellbore portion of the fracture without damaging the blocking agent in the far-wellbore part of the fracture.

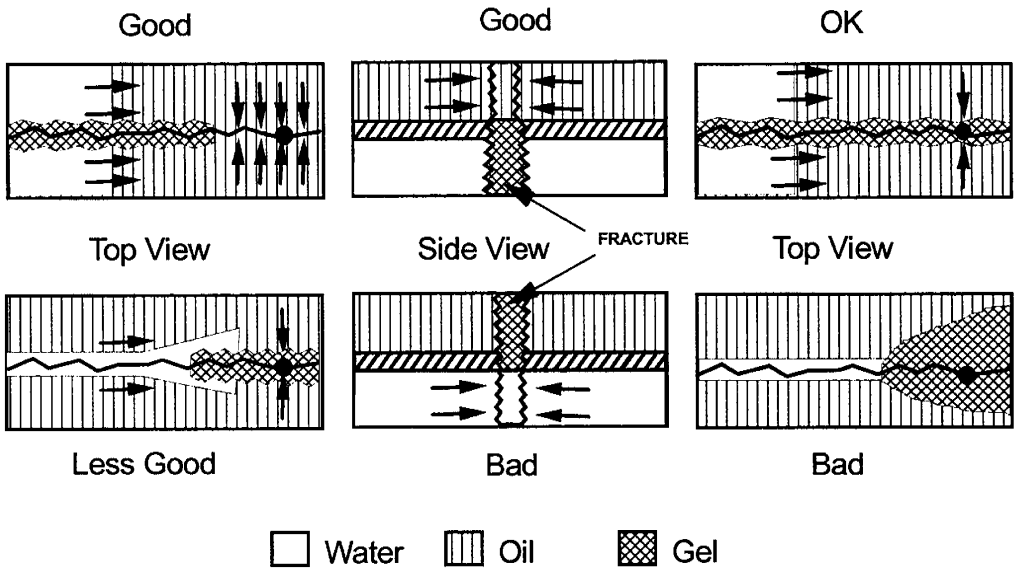

Fig. 94. Idealized locations for gels in fractures.

Chapter 5 of Ref. 1 discusses our investigations of several schemes. Table 3 outlines the schemes that we have examined to date. Categories 1 and 2 in Table 3 are directed at allowing the gel to propagate as far as possible along a fracture without developing excessive pressure gradients. Categories 3 and 4 are directed at plugging the far-wellbore portions of fractures while leaving the near-wellbore segments of the fractures open to flow.

In this section, we consider Category 4b in Table 3: Inclusion of an encapsulated breaker (degrading agent) at the end of gel placement in a fracture. The specific objective of this experiment was to fill most of the fracture with gel, but incorporate a breaker in the last gel injected to keep the near-wellbore part of the fracture open.

Table 3. Schemes to Optimize Gel Placement in Fractures

1. Use of mechanically degraded gels.

2. Two-stage reactions: Injection of Cr(III) after placement of:
   a. mechanically degraded Cr(III)-acetate-HPAM,
   b. hydroquinone-HMT-HPAM,
   c. HPAM water-in-oil emulsion.

3. Mobility-matched postflushes:
   a. water postflush displacing a water-like gelant,
   b. viscous postflush displacing a viscous gelant.

4. Use of degrading agents:
   a. sodium pyrophosphate postflush after a Cr(III)-acetate-HPAM gel,
   b. inclusion of an encapsulated breaker at the end of gel placement.

In these experiments, we used the same procedures and one-day old Cr(III)-acetate-HPAM gel that were described above. The fractured core (Core 19) was 4 ft (122 cm) long, with a conductivity of 242 darcy-ft, an effective average fracture width of 0.038 inches, and a fracture volume of 44.4 ml. The breaker that we used was an encapsulated persulfate (Halliburton Optiflo-II). At 41°C, we found that 0.1% breaker destroys the Cr(III)-acetate-HPAM gel over a 2- to 5-day period.

In this experiment, we first injected 20 fracture volumes of 1-day-old Cr(III)-acetate-HPAM gel, followed by 0.2 fracture volumes of gel that contained 0.1% breaker. The injection rate was 200 ml/hr or 4.5 fracture volumes/hr. Next, the core was shut in for 6 days. Then, brine was injected to determine permeability reduction values, and a tracer study was performed to find if the breaker destroyed gel in the first section of the fracture. Finally, we disassembled the core to examine gel in the fracture.

During gel injection, we observed a pressure gradient averaging about 20 psi/ft. Results from tracer studies indicated that the gel effectively plugged the fracture. However, effluent analysis (Fig. 83) indicated that the gel did not quite propagate all the way through the fracture. After disassembly of the core and analysis of gel along the length of the fracture (Fig. 84), we found that the gel propagated 96% of the distance through the 4 ft long fracture. We also noted red husks (the encapsulating material for the breaker) had propagated 10% of the distance through the fracture, compared to the 20% distance that was expected. Analysis of gel along the fracture (Fig. 84) suggested that the breaker was only marginally effective in destroying the gel in the first part of the fracture. Perhaps, this result occurred because the gel was concentrated too much by the dehydration effect. Table 2 and Fig. 84 indicate that the gel was concentrated by a factor of 20 during the extrusion process. In contrast, our breaker was designed and tested to destroy the original (not concentrated) gel. More work of this type will be performed in the future.

Effect of Length on Gel Propagation Through Tubes

Most of our experiments to date used relatively short fractured cores (0.5 to 4 ft) and tubes (3 to 15 ft). Since fractures in field applications are typically more than 100 ft in length, we wish to determine gel properties as a function of fracture length. Unfortunately, creating very long fractures is difficult in the laboratory. However, long tubes are readily available. If a satisfactory relation between the behavior of gels in fractures versus tubes could be found, gel-extrusion experiments in long tubes might indicate the performance of gels in long fractures.

To explore this possibility, we performed several experiments in a 0.03-inch-ID, 100-ft-long tube. The tube had four equally spaced internal pressure taps that divided the tube into five 20-ft sections. The total tube volume was 0.85 in^3 or 13.9 cm^3. Fig. 95 plots resistance factors and pressure gradients observed in the five 20-ft sections versus tube volumes of gel injected.

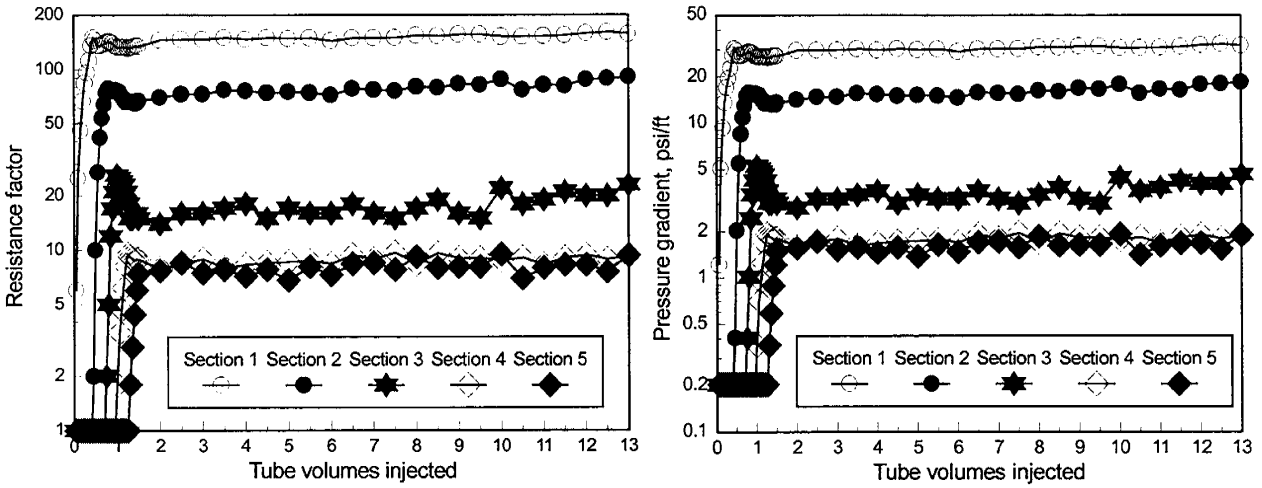

Fig. 95. Extrusion of a 24-hr-old Cr(III)-acetate-HPAM gel through a 100-ft-long, 0.03-inch-ID tube at 35,000 ft/d. 41°C.

We noted that the gel arrived at the tube outlet after injecting only 1.3 tube volumes, instead of 6 tube volumes, as observed in 6-ft and 15-ft tubes (Figs. 36 and 38 of Ref. 1). As mentioned in

Ref. 1, we suspect that in the 6-ft and 15-ft tubes, the water expelled from the gel flowed ahead of the less-mobile gel—allowing the water front to flow about 6 times faster than the gel front. However, in the 100-ft tube, the water that was expelled from the gel had insufficient opportunity to flow ahead of the gel. Instead, it was forced to mix and form a dispersion with the gel.

After injecting two tube volumes of gel, the pressure gradients in the five tube sections averaged 29.2, 15.3, 3.7, 1.8, and 1.6 psi/ft, respectively, while the resistance factors averaged 144, 75.6, 18.2, 8.9, and 8.0, respectively. Thus, the gel apparently experienced severe degradation during extrusion through the 100-ft-long tube. Two explanations could account for this behavior. First, the gel could experience continuous mechanical degradation as it extrudes farther down the tube. Second, water expelled from the gel during the gel-dehydration process could lubricate the flow of gel in the down-stream sections of the tube. Since the ratio of free water to gel increases with increased tube length, the resistance factor decreases with increasing tube length.

If the second mechanism mentioned above is correct, gel extrusion experiments in long tubes are not representative of gel extrusion through long fractures. In fractures, water that leaves the gel can leak off into the porous rock, leaving the concentrated gel behind to extrude through the fracture. However, in tubes, water that is expelled from the gel must flow along with the more concentrated gel. If the dehydration effect occurs soon after the gel enters a tube and if the free water could be removed early in the extrusion process, perhaps, the gel behavior in the tube may satisfactorily imitate that in a fracture. To test this idea, we repeated the extrusion experiment with the 0.03-inch-ID, 100-ft-long tube, except that a 0.5 μm steel filter was placed at the end of each of the first three internal pressure taps. These filters did not interfere with gel flow through the tube, but they allowed free water to leave the tube at these points. During extrusion of 10 tube volumes (139 cm^3) of 24-hr-old Cr(III)-acetate-HPAM gel through the tube at 35,000 ft/d, the volumes of filtrate collected at the first (20-ft), second (40-ft), and third (60-ft) taps were only 3.2 cm^3, 2.6 cm^3, and 2.7 cm^3, respectively. Thus, only about 2% of the total throughput left the tube at each of the three filters. If the gel was dehydrated by a factor of 6 (as suggested by Figs. 36 and 38 in Ref. 1), our filters were very ineffective at removing the free water from the tube.

Analysis of the three filtrates revealed HPAM concentrations of 68 ppm (C/C_o=1.4%), 190 ppm (C/C_o=3.8%), and 380 ppm (C/C_o=7.6%), respectively. These results suggest that very little polymer passed through the filters. However, since the polymer concentrations in the filtrates increased with increased length along the tube, perhaps, mechanical degradation of the polymer and gel was important as they flowed through the tube.

Analysis of the filtrates also revealed chromium concentrations of 13.3 ppm (C/C_o=14.1%), 14.4 ppm (C/C_o=15.2%), and 10.5 ppm (C/C_o=11.1%), respectively. Thus, the free water contained about the same level of chromium, regardless of the distance along the tube.

Table 4 compares the resistance factors in the five tube sections for this experiment with those from the previous experiment. For a given tube section, the resistance factors were about the same for both experiments. This result also indicates that our filters were ineffective at removing free water from the tube.

Table 4. Extrusion of 24-hr-old Cr(III)-Acetate-HPAM Gels Through 0.03-inch-ID, 100-ft-long Tubes. 41°C

	Resistance factor				
Experiment	Section 1	Section 2	Section 3	Section 4	Section 5
No filters	144	75.6	18.2	8.9	8.0
0.5 μm filters at 20, 40, and 60 ft	135	62.1	11.1	7.2	6.3
2.5-inch Berea sandstone core with 0.04-inch hole at tube inlet	134	62.2	12.3	8.9	7.9
6-inch fracture Berea core at tube inlet	149	82.1	18.7	14.1	

We performed another experiment where a 650-md Berea core with a 0.04-inch-ID hole was mounted at the inlet of a 0.03-inch-ID, 100-ft-long tube (see Fig. 96). The core was 1.4 inches (3.6 cm) in diameter and 2.5 inches (6.37 cm) in length, with a pore volume of 0.836 in^3 (13.7 cm^3). A 0.04-inch-ID hole was drilled axially through the center of the core. The outlet from the 0.04-inch-ID hole led directly into a 0.03-inch-ID, 100-ft-long tube. The core was cast in epoxy so that gel could be forced through the 0.04-inch-ID hole and the 100-ft-long tube in series. A tap was drilled to penetrate a short distance into the porous rock, so that leakoff fluid could drain from the core. Thus, the core acted as a tangential filter to remove water that emanated from the gel during the first part of the flow path. As with all of our experiments, the tube and core were saturated with brine at the beginning of the gel experiment.

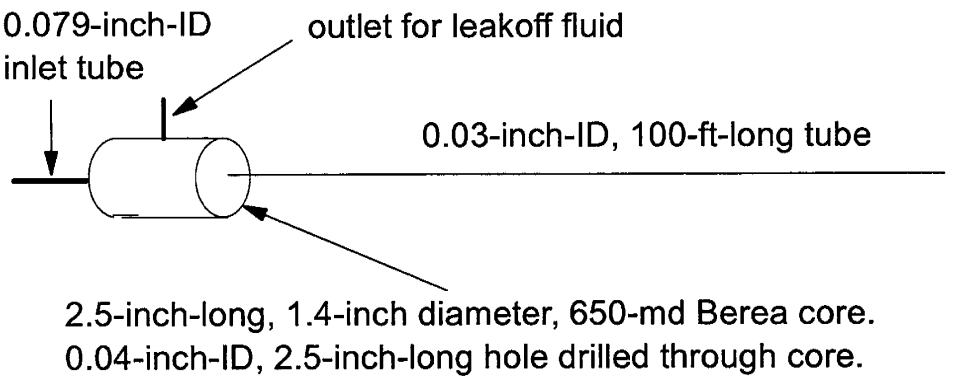

Fig. 96. Schematic of the core-tube experiment.

Fifteen tube volumes of a 24-hr-old Cr(III)-acetate-HPAM gel were forced through this core and tube using the same rate used in the previous experiments (35,000 ft/d in the 0.03-inch-ID tube). The third data row of Table 4 lists the average resistance factors observed in the five sections of the 0.03-inch-ID, 100-ft-long tube. Table 4 shows that the behavior observed during this experiment was not significantly different from that seen during the two previous experiments.

After observing the above results, we were concerned that the rock area available for leakoff was too small to effectively remove the water of dehydration before the gel entered the 100-ft-long tube. For example, we noted that the sandface area available for leakoff was only 0.314 in^2 for the 2.5-inch-long core with the 0.04-inch-ID hole. Therefore, we performed an additional experiment with a substantially increased leakoff area in the initial core. In particular, we replaced the 2.5-inch-long core with a 6-inch-long fractured Berea sandstone core. Details of the preparation of this fractured core can be found in Ref. 1. As with the previous core, this core had an internal pressure tap (located away from the fracture) to allow filtrate water to drain from the porous rock.

The sandface area available for leakoff was 19.9 in^2 or 63 times greater than that for the 2.5-inch-long core. As with the previous experiments, a one-day-old Cr(III)-acetate-HPAM gel was forced through a 100-ft-long, 0.03-inch-ID tube, after passing through the 6-inch-long fractured core. The bottom line of Table 4 lists the gel resistance factors along the length of the tube. Note that these values are not significantly different than those associated with the other experiments. These results indicate that removal of the early water of dehydration during an extrusion experiment does not prevent deterioration of the gel as it extrudes through long tubes. Therefore, we conclude that extrusion of gels through long tubes cannot adequately imitate the behavior of gels during extrusion through long fractures.

Conclusions

During experiments where one-day-old Cr(III)-acetate-HPAM gels were extruded through 2.7- to 4-ft-long fractures, we observed the following results:

1. In fractures with conductivities between 1 and 242 darcy-ft (effective average widths between 0.006 and 0.04 inches), the gel was concentrated (or dehydrated) by a factor typically between 20 and 40 during the extrusion process. This dehydration effect delayed propagation of the gel through fractures by factors ranging from 20 to 40.
2. The gel dehydration effect became less pronounced as the fracture width increased. However, a fracture width around 0.4 inches was required to completely eliminate the effect.
3. For a given fracture conductivity and width, a minimum pressure gradient (i.e., a yield stress) appears to be required to extrude gel through the fracture. For fractures with conductivities ($k_f w_f$, in darcy-ft) between 1 and 1,000,000 darcy-ft (widths between 0.006 and 0.6 inches), the required pressure gradient (dp/dl, in psi/ft) can be estimated using the relation: $dp/dl=280(k_f w_f)^{-0.58}$. To extrude this gel with a pressure gradient of only 1 psi/ft (a typical pressure gradient in a reservoir), the fracture width should be at least 0.1 inches.
4. During brine injection after gel placement, we saw no evidence of significant gel washout for fractures with widths up to 0.4 inches. For fractures with widths greater than 0.1 inches, the gel did not completely heal the fracture (i.e., reduce its flow capacity to near zero). However, the fracture conductivities were reduced substantially.
5. Extrusion of gels through long tubes cannot adequately imitate the behavior of gels during extrusion through long fractures.

6. DISPROPORTIONATE PERMEABILITY REDUCTION

Introduction

The ability of blocking agents to reduce the permeability to water much more than to oil is critical to the success of water-shutoff treatments in production wells if hydrocarbon-productive zones cannot be protected during placement.[2,26] Results from the literature and our own experimental work[27,56-66] have shown that many polymers and gels exhibit this disproportionate permeability reduction. In our previous studies, we extensively examined several possible mechanisms for this disproportionate permeability reduction.[1,27,65,66] Although we still do not have a plausible explanation for this phenomenon, many interesting leads have been generated during the course of the study. Our previous studies ruled out gravity and lubrication effects as possible mechanisms. Also, gel shrinking and swelling are unlikely to be responsible for this phenomenon. Our experimental results indicate that wettability may play a role; however its effect is unclear.

This chapter describes the results from several new experiments that were designed to elucidate the mechanism responsible for the disproportionate permeability reduction. One new experiment examined whether the disproportionate permeability reduction varies with core length. In this study, we performed an oil-water experiment in a 2-ft Berea core. In contrast, in our previous oil-water experiments, we routinely used 6-in Berea cores.[65] In another set of experiments, we conducted constant-pressure oil-water experiments using different pressure gradients during residual-resistance-factor measurements to study the effect of pressure drawdown on the disproportionate permeability reduction.

We also performed additional core experiments to test whether the disproportionate permeability reduction is caused by a balance between capillary forces and gel elasticity.[67,68] Results from our previous studies suggested that this mechanism is valid only in micromodels and small glass tubes, not in porous rock.[1,68]

Finally, we examine whether the disproportionate permeability reduction is caused by oil and water following segregated pathways on a microscopic scale. We speculated that if this theory is valid, a simultaneous injection of oil and an aqueous gelant during placement should enhance disproportionate permeability reduction. However, our previous annual report[1] showed that the injection of oil with an aqueous gelant using gelant/oil volume ratios of 50/50 and 30/70 did not enhance the disproportionate permeability reduction. One possible explanation is that the volume fraction of oil injected with the gelant might be too high during placement. Therefore, in this study, we used a higher gelant/oil ratio (95/5) during placement (i.e., lower volume fraction of oil) to examine the effect of simultaneous gelant-oil injection on the disproportionate permeability reduction. Also, we investigated the possibility that capillary redistribution of fluids during the shut-in period closed the open oil channels maintained during the simultaneous gelant-oil injection.

Oil-Water Experiments in a 2-ft Berea Core

In our previous oil-water experiments, we routinely used 6-in Berea cores.[65] We wondered if the disproportionate permeability reduction varies with core length. To answer this question, we performed an oil-water experiment in a 2-ft Berea core. The core was 2 ft long and 1.5 inches in height and width (Fig. 97). The core had four internal pressure taps. Among the five core sections, we focused our experimental measurements on the three 6.3-in. internal sections. The experiment was conducted at 41°C.

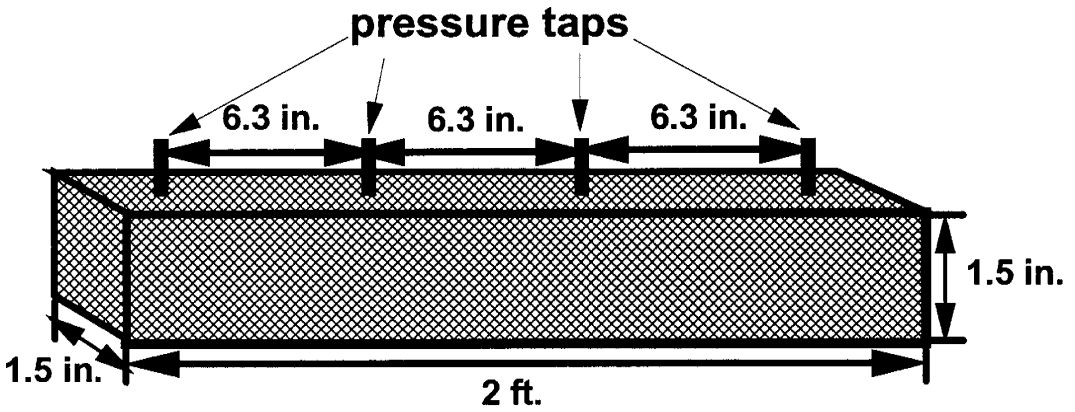

Fig. 97. Long Berea core.

Table 5 shows that the core was fairly homogeneous with an average permeability to water of 1,034±16 md for the three 6.3-in. internal sections. The average endpoint permeabilities to oil and water for the internal sections were 852±38 md and 216±5 md, respectively. (Detailed permeability and saturation data are listed in Table G.1h)

Table 5. Summary of Permeabilities for a 2-ft Berea Core (SSH-156) Before Gel

	Internal Section 1	Internal Section 2	Internal Section 3
k_w, md @S_w=1.0	1,018	1,035	1,049
k_o, md @S_{wr}=0.30	893	845	817
k_w, md @S_{or}=0.23	218	211	220

The gel contained 0.5% HPAM (Allied Colloids Alcoflood 935®, Mw=5×10^6 daltons, degree of hydrolysis: 5-10%), 0.0417% Cr(III)-acetate, 1% NaCl, and 0.1% $CaCl_2$ at pH 6. (Most experiments described in this chapter used this Cr(III)-acetate-HPAM gel.) The brine had the same composition as that used for gelant preparation. A refined oil (Soltrol 130) was used as the oil phase. Ten PV of gelant were injected into the core at residual oil saturation. To delay the gelation during placement, the gelant was injected at room temperature (26°C). After gelant injection, the temperature was raised to 41°C, and the core was then shut in for 5 days to allow the gelation to complete. After the shut-in period, multiple cycles of oil/water injections were performed to determine the residual resistance factors.

After shut-in, we first injected oil to determine the residual resistance factors for oil, F_{rro}. The F_{rro} was measured at a single rate of 1.21 ft/d. The first data row of Table 6 shows that the F_{rro} (for the three internal core sections) had an average value of 48±10. Next, we injected brine at a single rate of 0.019 ft/d to measure the residual resistance factor for water, F_{rrw}. The second data row of Table 6 shows that the F_{rrw} values were also fairly uniform averaging 8600±690 across the three internal core sections. A comparison of the first and second data rows in Table 6 shows that disproportionate permeability reduction was observed throughout the 2-ft Berea core, and the magnitude of this effect was relatively uniform across the three 6.3-in. internal sections. (The F_{rrw}/F_{rro} values for the three internal sections during the first oil/water injection cycle were 231, 170, and 155.) During the next oil/water injection cycle, brine was injected using different flow rates to determine the flow behavior of water after treatment. As shown in the fourth data row of Table 6, F_{rrw} exhibited a strong shear-thinning behavior, which can be described by power-law equations. Finally, oil was injected again using different injection rates. During oil flow, Newtonian behavior was observed. (At present, we cannot explain why the F_{rro} values in the third data row are significantly greater than those in the first and fifth data rows.) In summary, Table 6 shows that throughout the oil/water injection cycles, the gel reduced the permeability to water significantly more than that to oil. The disproportionate permeability reduction was relatively uniform across the three internal sections (18.9 inches total length) of a 2-ft Berea core. (Detailed residual-resistance-factor data are listed in Table G.2e.)

Table 6. Summary of F_{rrw} and F_{rro} for a 2-ft Berea Core (SSH-156) After Gel
Gel: 0.5% HPAM, 0.0417% Cr(III)-acetate, 1% NaCl, and 0.1% $CaCl_2$

	Internal Section 1	Internal Section 2	Internal Section 3
1st F_{rro}	39	46	58
1st F_{rrw}	9,000	7,800	9,000
2nd F_{rro}	83	107	134
2nd F_{rrw}	$1{,}047u^{-0.41}$	$831u^{-0.48}$	$783u^{-0.56}$
3rd F_{rro}	27	39	54

Constant-Pressure Experiments

Disproportionate Permeability Reduction Under Constant-Pressure Drive. For most of our oil-water experiments, residual resistance factors were measured using constant flow rates.[65] However, in field applications, the water and oil zones are often subject to a constant-pressure drawdown when the well is returned to production. An unanswered question is, Do gels reduce the permeability to water more than that to oil under a constant-pressure drawdown? To answer this question, we performed an oil-water experiment in a 737-md Berea core. In this experiment, the residual resistance factors were determined using constant-pressure drive. The gel contained 0.5% HPAM, 0.0417% Cr(III)-acetate, and 1% NaCl. Soltrol 130 was the oil phase. During placement, 10 PV of gelant were injected at 26°C to delay gelation. Then, the core was shut in at 41°C for 5 days to allow the gelation to proceed to completion.

After shut-in, oil was first injected into the core at a constant pressure gradient of 90 psi/ft. Table 7 shows that F_{rro} was 14. Next, brine was injected using the same pressure gradient, and F_{rrw} was

321. After brine injection, oil was injected again using the same pressure gradient, and F_{rro} was 11. During the next oil-water injection cycle, different pressure gradients were used during residual-resistance-factor measurements to examine the flow behavior of water and oil. For each F_{rr} measurement performed under a given pressure gradient, we measured the corresponding flow rate after a steady state was reached. The sixth column of Table 7 shows that F_{rrw} exhibited a strong shear-thinning behavior that can be described by a power-law equation. However, F_{rro} was Newtonian (seventh column of Table 7). These results are consistent with our observations during constant-rate experiments.[65] Table 7 also shows that under the same pressure gradient, the gel reduced the permeability to water much more than that to oil in a 737-md Berea core.

Table 7. Summary of F_{rrw} and F_{rro} for a Constant-Pressure Experiment (SSH-138)
Gel: 0.5% HPAM, 0.0417% Cr(III)-acetate, 1% NaCl

k_w, md @S_w=1.0	Pressure Gradient, psi/ft	1st F_{rro}	1st F_{rrw}	2nd F_{rro}	2nd F_{rrw}	3rd F_{rro}
737	90	14	321	11	$37u^{-0.26}$	6

In production-well treatments, gelants penetrate into both the water and oil zones during placement.[2] When the well is returned to production, the gel in the water zones contacts water while the gel in the oil zones contacts oil. Both zones are commonly subjected to about the same pressure drawdown. Therefore, it is important to perform two experiments using the same pressure gradient; one simulating what happens in the water zones (i.e., by injecting water into the core immediately after shut-in) and the other simulating what happens in the oil zones (i.e., by injecting oil into the core immediately after shut-in). The F_{rrw} and F_{rro} values determined this way are representative of the resistance to water and oil flow in the formation after treatment, respectively. The experiment summarized in Table 7 simulates what happens in the oil zone after treatment by injecting oil immediately after shut-in using a constant pressure gradient of 90 psi/ft. The F_{rro} value in the third column of Table 7 indicates that the gel in the oil zone reduced the permeability to oil by a factor of 14.

Next, we performed a similar experiment in a 705-md Berea core to simulate what happens in the water zone after treatment. The Cr(III)-acetate-HPAM gel had the same composition as that used in the previous experiment. In this new experiment, water was injected instead of oil immediately after shut-in. The third column of Table 8 shows that under the same pressure gradient (90 psi/ft), the gel reduced the permeability to water by a factor of 10,085 in the water zone—much more than the factor of 14 in the oil zone (third column of Table 7). This level of disproportionate permeability reduction could be very beneficial in treating fractured production wells.[2,26]

Table 8. Summary of F_{rrw} and F_{rro} for a Constant-Pressure Experiment (SSH-137)
Gel: 0.5% HPAM, 0.0417% Cr(III)-acetate, 1% NaCl

k_w, md @S_w=1.0	Pressure Gradient, psi/ft	1st F_{rrw}	1st F_{rro}	2nd F_{rrw}	2nd F_{rro}	3rd F_{rrw}
705	90	10,085	20	140	10	13

In this experiment, oil was injected after the first water injection using the same pressure gradient. Table 8 shows that the F_{rro} was 20. Then, brine was injected again. As shown in Table 8, the F_{rrw} was reduced from 10,085 to 140 after the first oil injection. Additional gel breakdown was observed after the second oil injection (sixth and seventh columns of Table 8).

Effect of Pressure Drawdown on Disproportionate Permeability Reduction. To study the effect of pressure drawdown on the disproportionate permeability reduction, we performed three sets of oil-water experiments using different pressure gradients during residual-resistance-factor measurements. For each pressure gradient, we performed two similar oil-water experiments; one with oil injected immediately after shut-in to measure F_{rro} and the other with brine injected immediately after shut-in to measure F_{rrw}. The gel contained 0.5% HPAM, 0.0417% Cr(III)-acetate, and 1% NaCl. Soltrol 130 was the oil phase. The residual resistance factors listed in Table 9 were those measured immediately after shut-in. (Detailed residual-resistance-factor data are listed in Tables G.2a, G.2b, and G.2h through G.2k.)

Table 9. Effect of Pressure Drawdown on Disproportionate Permeability Reduction
Gel: 0.5% HPAM, 0.0417% Cr(III)-acetate, 1% NaCl
Cores: High-permeability Berea sandstone (SSH-137, 138, 168, 169, 170, 171)

Pressure Gradient, psi/ft	F_{rrw}	F_{rro}	F_{rrw}/F_{rro}
90	10,085	14	720
135	4,510	16	282
180	9	5	1.8

Table 9 shows that the disproportionate permeability reduction decreases with increasing pressure drawdown. A comparison of the residual resistance factors measured at 135 psi/ft and those measured at 180 psi/ft shows a significant drop in both F_{rrw} and F_{rro}. This result indicates that the gel suffered severe breakdown at 180 psi/ft. Also, the ratio of F_{rrw} and F_{rro}, which is a measure of the disproportionate permeability reduction, was only 1.8. As shown in Table 9, the ratio of F_{rrw} and F_{rro} was reduced from 720 to 282 when we increased the pressure gradient from 90 to 135 psi/ft. A comparison of the second and the third data rows of Table 9 reveals that the increase in pressure gradient resulted in a lower F_{rrw} while the F_{rro} remained relatively unchanged. More work (especially at lower pressure gradients) is underway to investigate this phenomenon.

Effect of Capillary Forces and Gel Elasticity on Disproportionate Permeability Reduction

After viewing the results from the micromodel experiments of Dawe and Zhang,[67] we wondered whether capillary forces and gel elasticity might contribute to the disproportionate permeability reduction.[65] In a video from Dawe and Zhang, we observed that during oil injection, oil drops squeezed through an elastic, aqueous gel. During water injection, most of the water flowed through the pathways created by oil, except the pathways were more constricted. Dawe and Zhang [67] reported that the gel reduced the permeability to water significantly more than that to oil. We suspect that the disproportionate permeability reduction was caused by the balance between capillary forces and gel elasticity. As illustrated in Fig. 98, when an oil droplet extrudes

through an aqueous gel, two opposing forces act. On the one hand, a capillary force acts to maintain a minimum droplet radius, which in turn, forces open a channel through the gel. On the other hand, the gel exerts an elastic confining force to close the channel. The final radius of the oil droplet and the size of the oil pathway depend on the balance between the two forces. The effective permeability to oil increases with increasing radius of the flow path around the oil droplet. In contrast, when water flows through the same channel, no capillary force acts to open the channel. Therefore, the effective permeability to water should be less than that to oil.

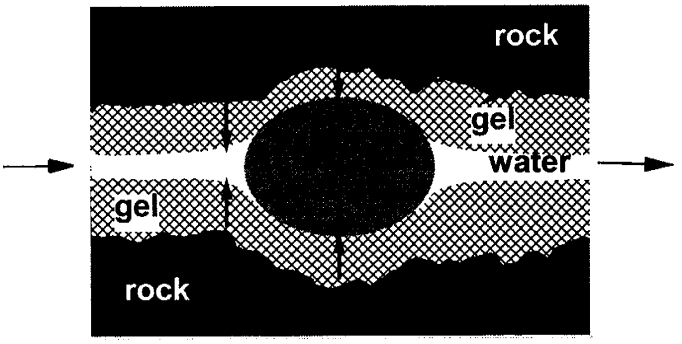

Fig. 98. Balance between capillary forces and gel elasticity when forcing oil or water through an aqueous gel.

Review of Previous Work. Two possible ways exist to test this theory: (1) vary the capillary force and (2) change the gel elasticity. In our previous annual report,[1] we first performed oil-water experiments in small glass conduits (3 cm × 0.5 cm × 0.05 cm) to reproduce what we observed in the micromodel experiments by Dawe and Zhang.[67] We found that a Cr(III)-acetate-HPAM gel reduced the permeability to water more than that to oil in small glass conduits.

In a small glass conduit that was filled with a Cr(III)-acetate-HPAM gel, lowering the oil-water interfacial tension from 42.5 dyne/cm to 8 dyne/cm resulted in a decreased permeability to oil.[1] This finding supports the theory that capillary forces and gel elasticity contribute to the disproportionate permeability reduction. However, a similar experiment in a Berea sandstone core did not show a decrease in permeability to oil when the oil-water interfacial tension was reduced.[1] Thus, we suspect that a capillary-elastic-force balance may not be the dominant mechanism in porous rock.

In Berea sandstone, the disproportionate permeability reduction was very similar for a Cr(III)-acetate-HPAM gel and a Cr(III)-acetate-HPAM-nitrogen gelled foam.[65] This finding also does not support the theory that capillary forces and gel elasticity contribute to the disproportionate permeability reduction in porous rock. (However, we recognize that gelled foams may not be a good analogy for studying the elastic mechanism.) In this report, we continue our study of the capillary-force-gel-elasticity mechanism.

Effect of Gel Treatment on Residual Oil Saturation. In the micromodel study by Dawe & Zhang,[67] they observed that the residual oil saturation trapped by the gel after treatment was quickly connected with the injected oil drops and helped in forcing open additional flow channels. Does the residual oil saturation play a similar role in porous rock?

In earlier work,[69] results from tracer studies and material-balance calculations indicated that strong water-based gels could encapsulate the residual oil in Berea cores and render it immobile after treatment. This finding contradicts what Dawe and Zhang[67] observed in their micromodel experiments where the residual oil saturation was re-connected during oil injection after gel treatment.

To resolve this issue, we performed a specially designed oil-water experiment using a Cr(III)-acetate-HPAM gel. The experiment was conducted in a 725-md Berea core (SSH-145). The gel contained 0.5% HPAM, 0.0417% Cr(III)-acetate, and 1% NaCl. Soltrol 130 was the oil phase. In this experiment, we added 0.1% trans-stilbene to the oil phase as a tracer. The core was first saturated with brine. Then, the core was flooded to residual water saturation using the oil with tracer. Next, water was injected until no more oil was produced. The produced oil was collected and analyzed for tracer content to determine the oil remaining in the core before gelant injection. Next, 10 pore volumes of the gelant were injected into the core. After shut-in, oil without tracer was injected to measure the F_{rro}. During the process, the produced oil was carefully collected. After the F_{rro} measurement, the produced oil was analyzed for tracer content. Results indicate that only 7% of the residual oil saturation was produced during the F_{rro} measurement. In other words, 93% of the residual oil saturation was trapped by the gel and remained inaccessible after treatment. These findings support our conclusion that the mechanism for the disproportionate permeability reduction is different in micromodels than in porous rock.

Pressure Spikes During Oil Injection Immediately After Shut-in. In the micromodel study by Dawe & Zhang[67] and our own glass-conduit experiments,[1] we observed an initial pressure surge before the oil drops broke through a water-based gel. However, we did not observe similar initial pressure surges in our previous core experiments.[65] During our regular oil-water experiments, we usually take pressure readings in 0.1-PV fluid increments.[65] We suspect that the pressure spike might have happened before the first pressure reading was taken. To determine when and if a pressure spike occurred, we performed two core experiments in 700-md Berea cores, one with residual oil present during gelant injection and one without. After shut-in, oil was injected using a constant flow rate of 1ml/hr. Fig. 99 shows that in both cases, a pressure spike (40 psi with residual oil and 34 psi without residual oil) was observed between 0.03 to 0.04 PV of oil injected. The pressure drop then decreased and leveled off at around 12 psi after injecting only 0.08 PV of oil. This explains why we did not observe any significant pressure surges during oil injections immediately after shut-in. (Remember that we usually take the first pressure reading after injecting 0.1 PV of oil.) If the residual oil saturation was accessible and re-connected during the oil injection, we expected a much smaller pressure spike when residual oil was present. However, the pressure spike observed with residual oil (40 psi) was actually higher than that when residual oil was absent (34 psi). This finding again supports our conclusion that the mechanism for the disproportionate permeability reduction is different in micromodels than in porous rock.

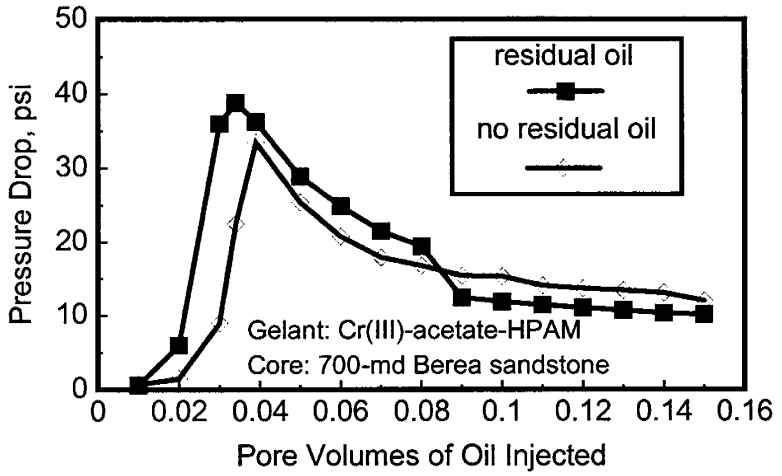

Fig. 99. Pressure spike during oil injection immediately after shut-in (SSH-154, 155).

Segregated Oil and Water Pathways

In our previous studies,[27,65] we proposed that the disproportionate permeability reduction might be caused by water and oil following segregated pathways. If (on a microscopic scale) a water-based gelant follows primarily the pathways available to water, then many of the oil pathways could remain open (relatively gel-free) after treatment while most of the water pathways would be blocked by the gel (Fig. 100). In this way, the water-based gel could reduce permeability to water more than to oil.

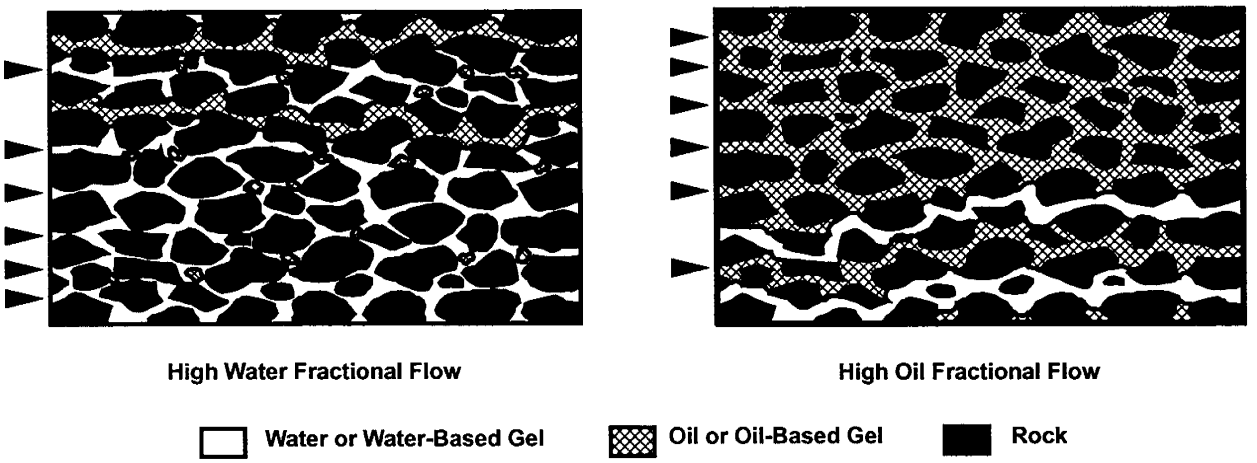

Fig. 100. Segregated oil and water pathways.

Following the same logic, during high oil fractional flow, if an oil-based gel follows primarily the pathways available to oil on a microscopic scale, then many of the water pathways could remain open after treatment while most of the oil pathways would be blocked by the gel.

If this segregated-pathway theory is valid, we speculate that the disproportionate permeability reduction could be enhanced by simultaneously injecting oil with a water-based gelant or water with an oil-based gelant. Presumably, simultaneous injection of oil and a water-based gelant should allow a larger fraction of oil pathways to remain open than if a water-based gelant is injected by itself. Using similar logic, simultaneous injection of water and an oil-based gelant should allow a larger fraction of water pathways to remain open than if an oil-based gelant is injected by itself.

Review of Previous Work. In previous studies, [27,65] we found that an oil-based gel (12-hydroxystearic acid in Soltrol 130) reduced permeability to oil much more than to water. Also, simultaneous injection of water with an oil-based gel (using a 50/50 gelant/water volume ratio) in Berea sandstone enhanced the disproportionate permeability reduction. These findings support the segregated-oil-and-water-pathway theory. In contrast, our previous annual report[1] showed that simultaneous injection of oil with an aqueous gel (using gelant/oil volume ratios of 50/50 and 30/70) did not enhance the disproportionate permeability reduction. These findings do not support this theory. We suspected that the reason that this simultaneous injection of oil and a water-based gelant failed to enhance the disproportionate permeability reduction was because the volume fraction of oil injected with the gelant was too high during placement. Therefore, in this study, we used a higher gelant/oil ratio (95/5) (i.e., lower volume fraction of oil) to study the effect of simultaneous gelant/oil injection on the disproportionate permeability reduction.

Effect of Gelant/Oil Volume Ratio During Placement on Disproportionate Permeability Reduction. The purpose of the simultaneous injection of oil with an aqueous gelant was to allow a larger fraction of oil pathways to remain open than if a water-based gelant was injected by itself. Since the gel reduced the permeability to water significantly more than to oil, a small increase in the number of open pathways after treatment could significantly increase the permeability to oil while maintaining a similar level of permeability reduction to water. However, if too many pathways remained open after treatment, the effectiveness of the gel in reducing both the permeability to water and to oil should increase.

To test this theory, we conducted a core experiment using a higher gelant/oil volume ratio of 95/5 during placement. The core experiment was performed in a 655-md Berea sandstone core using a Cr(III)-acetate-HPAM gel. This water-based gel contained 0.5% HPAM, 0.0417% Cr(III) acetate, and 1% NaCl. Soltrol 130 was the oil phase. Results from this experiment along with three other experiments from our previous annual report[1] are summarized in Table 10. Table 10 shows that in all four cases, the gel reduced permeability to water significantly more than to oil. The ratio, F_{rw}/F_{ro}, provides a measure of the disproportionate permeability reduction. This ratio was 58 (i.e., 2,450/42), 28, 46, and 41 for gelant/oil injection ratios of 100/0, 95/5, 50/50, and 30/70, respectively. In other words, a gelant/oil ratio of 95/5 failed to enhance the disproportionate permeability. These findings do not support the segregated-pathway theory.

Why did the simultaneous injection of oil with an aqueous gelant fail to enhance the disproportionate permeability reduction? One possible explanation is that capillary redistribution of fluids closed the open oil channels during the shut-in period.

Table 10. F_{rrw} and F_{rro} Values For a Water-Based Gel
Gel: 0.5% HPAM, 0.0417% Cr(III)-acetate, 1% NaCl
Core: Berea sandstone (SSH-122, 129, 135, 151)

Gelant/oil volume ratio during placement	k_w, md	1st F_{rro}	1st F_{rrw}	2nd F_{rro}	$(F_{rrw}/F_{rro})_{1st}$
100/0	793	42	2,450	37	58
95/5	655	390	11,100	500	28
50/50	520	27	1,255	16	46
30/70	622	26	1,075	20	41

Capillary Redistribution of Fluids During Shut-in. For a water-based gelant, the balance between capillary and viscous forces keeps the oil pathways open during simultaneous gelant/oil injection in a strongly water-wet rock. During the shut-in period, the capillary force allows the water-based gelant to imbibe into and block some of the open oil pathways. In contrast, the capillary force may not allow an oil-based gelant to imbibe into the open pathways during shut-in (in a strongly water-wet rock). This concept might explain why simultaneous injection of water with an oil-based gel enhanced the disproportionate permeability reduction while simultaneous injection of oil with a water-based gel failed to do so. One possible way to prevent the capillary redistribution of fluids from closing the oil channels is to maintain the oil flow during the gelation period.

50/50 Gelant/Oil Volume Ratio During Placement with Continuous Oil Injection During Gelation. To test the above theory, we first conducted an oil-water experiment using a 50/50 gelant/oil volume ratio during placement (41°C). The gelant contained 0.5% HPAM, 0.0417% Cr(III) acetate, 1% NaCl, and 0.1% $CaCl_2$. Soltrol 130 was the oil phase. After injecting 10 PV of gelant, the pressure drop started to increase indicating the onset of the gelation reaction. In this experiment, we maintained the simultaneous gelant-oil injection until the pressure drop across the center section of the core approached the pressure constraint of 600 psi/ft. At this point, we stopped the gelant injection and switched the oil injection to constant-pressure drive—maintaining a 32.5 psi pressure drop across the center section of the core. (This was the pressure drop across the center section of the core at the end of the simultaneous gelant-oil injection.) A total of 15 PV of gelant was injected when we stopped gelant injection. The continuous oil injection was maintained for another 5 days to allow the gelation to proceed to completion. At the end of the 5-day gelation period, we measured the F_{rro} using a constant fluid velocity of 6.3 ft/d. (The third row of Table 11 shows that the F_{rro} was 22.) After the F_{rro} measurement, we disassembled the end caps and cleaned the core faces. After we reassembled the end caps, brine was injected at 0.202 ft/d to determine the F_{rrw}. The F_{rrw} was 465 (the fourth row of Table 11). After brine injection, oil was injected again, and the F_{rro} was 59. Comparing with the case where the gelant was injected by itself[1] (the first data row of Table 11), continuous oil flow during the gelation period did not enhance the disproportionate permeability reduction. Table 11 shows that in this case, both the F_{rrw} and F_{rro} values were lower than those when gelant was injected by itself. Also, the ratio of F_{rrw} to F_{rro} during the first oil-water injection cycle was reduced from 58 to 21. These findings do not support the capillary redistribution concept. We

wondered whether the 50/50 gelant/oil injection ratio caused too many pathways to remain open after treatment. Thus, we repeated this experiment using a 95/5 gelant/oil ratio.

Table 11. F_{rrw} and F_{rro} Values For a Water-Based Gel
Gel: 0.5% HPAM, 0.0417% Cr(III)-acetate, 1% NaCl, 0.1% $CaCl_2$
Core: Berea sandstone (SSH-122, 160)

Gelant/oil volume ratio during placement	k_w, md	1st F_{rro}	1st F_{rrw}	2nd F_{rro}	$(F_{rrw}/F_{rro})_{1st}$
100/0	793	42	2,450	37	58
50/50 (w/continuous oil)	784	22	465	59	21

95/5 Gelant/Oil Volume Ratio During Placement with Continuous Oil Injection During Gelation. Next, we performed a similar experiment using 95/5 gelant/oil volume ratio. During simultaneous gelant/oil injection, we reduced the core temperature to 26°C to delay the gelation reaction. After injecting 10 PV of gelant, we stopped gelant injection and increased the core temperature to 41°C to allow the gelation to proceed to completion. During the 5-day gelation period, we maintained oil injection using a constant rate of 1 ml/hr. (About 0.03 PV (1 ml) of the gelant was produced during the 5-day period of continuous oil injection.) A comparison of the first and second data rows of Table 12 shows that with 95/5 gelant/oil volume ratio, continuous oil injection during the gelation period enhanced the disproportionate permeability reduction. (The ratio, F_{rrw}/F_{rro}, was increased from 58, when the gelant was injected by itself, to 103 when the gelant was injected using the 95/5 gelant/oil ratio with continuous oil injection during the gelation period.)

Table 12. F_{rrw} and F_{rro} Values For a Water-Based Gel
Gel: 0.5% HPAM, 0.0417% Cr(III)-acetate, 1% NaCl, 0.1% $CaCl_2$
Core: Berea sandstone (SSH-122, 152)

Gelant/oil volume ratio during placement	k_w, md	1st F_{rro}	1st F_{rrw}	2nd F_{rro}	$(F_{rrw}/F_{rro})_{1st}$
100/0	793	42	2,450	37	58
95/5 (w/continuous oil)	711	23	2,380	28	103

These findings suggest that we might be able to enhance the disproportionate permeability reduction by using a high gelant/oil ratio during placement while maintaining continuous oil flow during the gelation period. More experiments are underway to understand this interesting phenomenon.

One might argue that the experiments with oil-based gelants are not directly comparable to those with water-based gelants because both sets of experiments used strongly water-wet cores. Nevertheless, with any wettability, the segregated pathway theory predicts that oil and water

phases basically take different flow paths on a microscopic scale. Thus, the appropriate method to test this theory is to perform oil and water flow experiments in a system of fixed wettability (as we have done). Even so, to further probe the disproportionate permeability reduction, our future plans include experiments in systems with other wettabilities.

Conclusions

1. Results from an oil-water experiment in a 2-ft Berea sandstone core showed that the disproportionate permeability reduction did not vary with core length. Flow behavior of water and oil after treatment in the 2-ft Berea core was consistent with our observations in 6-in Berea cores.[65]
2. Disproportionate permeability reduction was observed using constant-pressure-drive experiments. The disproportionate permeability reduction decreased with increasing pressure drawdown. More work is underway to determine if this phenomenon can be exploited during field applications.
3. A strong water-based gel encapsulated the residual oil saturation in a Berea core and rendered it immobile after treatment. This finding supports our conclusion that the mechanism for the disproportionate permeability reduction is different in micromodels than in porous rock.
4. Simultaneous gelant-oil injection using a 95/5 volume ratio during placement did not enhance the disproportionate permeability reduction. This finding does not support the segregated-oil-and-water-pathway theory. However, we suspect that this result was caused by the capillary redistribution of fluids closing the open oil channels during the shut-in period.
5. One possible way to prevent the capillary redistribution of fluids from closing the open oil channels is to maintain the oil flow during the gelation period. Results from oil-water experiments suggest that with the proper gelant/oil volume ratio, continuous oil injection during the gelation period could enhance the disproportionate permeability reduction. More experiments are underway to understand this interesting phenomenon.

NOMENCLATURE

A	well spacing, acres [m^2]
B_p	phase formation volume factor, RB/STB [Rm^3/Sm^3]
C	constant defined by Eq. 15, ft^{-1} [m^{-1}]
C'	constant defined by Eq. 18, ft^{-1} [m^{-1}]
F_r	resistance factor (brine mobility before gelant placement divided by gelant mobility)
F_{rr}	residual resistance factor (mobility before gel placement divided by mobility after gel placement)
F_{rro}	oil residual resistance factor
F_{rrw}	water residual resistance factor
h_f	fracture height, ft [m]
G_{shape}	G-shape scaling group defined by Eq. 1
g	acceleration of gravity, ft/s^2 [m/s^2]
h	reservoir layer thickness or effective reservoir thickness, ft [m]
h_e	thickness of oil zone, ft [m]
h_f	fracture height, ft [m]
h_w	depth of well penetration, ft [m]
J	productivity, bbl/D-psi [m^3/s-Pa]
J_a	productivity after gel placement, bbl/D-psi [m^3/s-Pa]
J_b	productivity before gel placement, bbl/D-psi [m^3/s-Pa]
J_o	initial productivity for an undamaged well before fracturing, bbl/D-psi [m^3/s-Pa]
k	absolute permeability, md [μm^2]
k_f	fracture permeability, md [μm^2]
$(k_f w_f)_x$	fracture conductivity in the x-direction, darcy-ft [m^3]
$(k_f w_f)_y$	fracture conductivity in the y-direction, darcy-ft [m^3]
k_h	horizontal permeability, md [μm^2]
k_i	permeability in Zone i, md [μm^2]
k_m	matrix permeability, md [μm^2]
k_{rp}	relative permeability to phase p
k_{ro}	oil relative permeability
k^0_{ro}	endpoint oil relative permeability
k_{rw}	water relative permeability
k^0_{rw}	endpoint water relative permeability
k_v	vertical permeability, md [μm^2]
k_w	permeability to water, md [μm^2]
L	distance along a fracture or between wells, ft [m]
L_f	length of one wing of a fracture, ft [m]
L_{pi}	distance of gelant penetration (leakoff) from a fracture face in Zone i, ft [m]
M	water/oil mobility ratio
n	number of fractures oriented in the y-direction
n_o	exponent for oil relative permeability equation (Eq. 3)
n_w	exponent for water relative permeability equation (Eq. 2)
P_b	bubble-point pressure, psi [Pa]
p	pressure, psi [Pa]

p_{cell} pressure in gridcell containing a well, psi [Pa]
p_{well} wellbore pressure, psi [Pa]
Δp pressure drop between two wells, psi [Pa]
q volumetric rate at a given point in a fracture, bbl/D [m^3/s]
q_c critical oil rate, bbl/D [m^3/s]
q_o total volumetric rate, bbl/D [m^3/s]
q_p well flow rate of a produced phase, bbl/D [m^3/s]
R ratio of fracture conductivities defined by Eq. 47
r_e external drainage radius, ft [m]
r_o equivalent well-block radius, ft [m]
r_w wellbore radius, ft [m]
r_{wa} apparent wellbore radius, ft [m]
r_1 distance from center of wellbore to center of first gridblock, ft [m]
s skin factor
S_{or} residual oil saturation
S_w water saturation
S_{wr} residual water saturation
t tracer transit time, days
u superficial or Darcy velocity or flux, ft/d [m/s]
u_o flux at the wellbore, ft/d [m/s]
v velocity, ft/d [m/s]
V gelant volume, bbl [m^3]
V_f fracture volume, bbl [m^3]
V_m gelant volume in the rock matrix, bbl [m^3]
WC well constant defined by Eq. 5
w_f fracture width, inches [m]
w_l width of the lubricating layer in the Bingham model, inches [m]
x abscissa value
x_o half-width of the region of plug flow in the Bingham model, inches [m]
Δx grid spacing in x direction, ft [m]
ΔX total length of reservoir, ft [m]
y ordinate value
Δy grid spacing in y direction, ft [m]
ΔZ total height of reservoir, ft [m]
μ fluid viscosity, cp [mPa-s]
μ_p viscosity of fluid phase p, cp [mPa·s]
μ_o oil viscosity, cp [mPa·s]
μ_w water viscosity, cp [mPa-s]
ρ_o oil density, g/cm^3
ρ_w water density, g/cm^3
τ shear stress, psi [Pa]
τ_o yield stress in the Bingham model, psi [Pa]
ϕ_f porosity in the fracture
ϕ_i effective aqueous-phase porosity in Zone i
ϕ_m porosity in the rock matrix

REFERENCES

1. Seright, R.S.: "Improved Methods for Water Shutoff," DOE Report DOE/PC/91008-1, Contract No. DE-AC22-94PC91008, BDM-Oklahoma Subcontract No. G4S60330, U.S. Department of Energy (Aug. 1997).

2. Liang, J., Lee, R.L., and Seright, R.S: "Placement of Gels in Production Wells," *SPEPF* (Nov. 1993) 276-84; *Trans.*, AIME, **295**.

3. Moffitt, P.D.: "Long-Term Production Results of Polymer Treatments in Production Wells in Western Kansas," *JPT* (April 1993) 356-62.

4. Sydansk, R.D. and Moore, P.E.: "Gel Conformance Treatments Increase Oil Production in Wyoming," *Oil & Gas J.* (Jan. 20, 1992) 40-45.

5. Woods, P. *et al.*: "In-Situ Polymerization Controls CO_2/Water Channeling at Lick Creek," paper SPE/DOE 14958 presented at the 1986 SPE/DOE Symposium on Enhanced Oil Recovery, Tulsa, April 20-23.

6. Seright, R.S. and Liang, J.: "A Survey of Field Applications of Gel Treatments for Water Shutoff," paper SPE 26991 presented at the 1994 SPE III Latin American & Caribbean Petroleum Engineering Conference, Buenos Aires, April 27-29.

7. Chan, K.S.: "Water Control Diagnostic Plots," paper SPE 30775 presented at the 1995 SPE Annual Technical Conference and Exhibition, Dallas, Oct. 22-25.

8. Chan, K.S. *et al.*: "Diagnostic Plots Evaluate Gas Shut-Off Gel Treatments at Prudhoe Bay, Alaska," paper SPE 36614 presented at the 1996 SPE Annual Technical Conference and Exhibition, Denver, Oct. 6-9.

9. Stanley, F.O. *et al.*: "Improving Hydrocarbon/Water Ratios in Producing Wells - An Indonesian Case History Study," paper SPE 36615 presented at the 1996 SPE Annual Technical Conference and Exhibition, Denver, Oct. 6-9.

10. Craig, F.F., Jr.: *The Reservoir Engineering Aspects of Waterflooding,* Monograph Series, SPE, Richardson, TX (1971) **3**, 62-76.

11. Sorbie, K.S. and Seright, R.S.: "Gel Placement in Heterogeneous Systems with Crossflow," paper SPE 24192 presented at the 1992 SPE/DOE Symposium on Enhanced Oil Recovery, Tulsa, April 22-24.

12. Zapata, V.J. and Lake, L.W.: "A Theoretical Analysis of Viscous Crossflow," paper SPE 10111 presented at the 1981 SPE Annual Technical Conference and Exhibition, San Antonio, Oct. 5-7.

13. Lake, L.W.: *Enhanced Oil Recovery,* Prentice-Hall Inc., Englewood Cliffs, NJ (1989) 58-62.

14. *Documentation for Reservoir Simulators SABRE and COALGAS,* S.A. Holditch & Associates, Inc., (1993) 236-37.

15. Peaceman, D.W.: "Interpretation of Well-Block Pressures in Numerical Reservoir Simulation With Nonsquare Grid Blocks and Anisotropic Permeability," *SPEJ* (June 1983) 531-43; *Trans.*, AIME, **275.**

16. Muskat, M.: *Flow of Homogeneous Fluids Through Porous Media*, McGraw-Hill Book Co. Inc., New York City (1937) 480-86.

17. Muskat, M.: *Physical Principles of Oil Production*, McGraw-Hill Book Co. Inc., New York City (1949) 226-40.

18. Abass, H.H. and Bass, D.M.: "The Critical Production Rate in Water-Coning System," paper SPE 17311 presented at the 1988 SPE Permian Basin Oil and Gas Recovery Conference, Midland, March 10-11.

19. MacDonald, R.C. and Coats, K.H.: "Methods for Numerical Simulation of Water and Gas Coning," *SPEJ* (Dec. 1970) 425-36; *Trans.*, AIME, **249**.

20. Guo, B. and Lee, R.L-H.: "A Simple Approach to Optimization of Completion Interval in Oil/Water Coning Systems," *SPERE* (Nov. 1993) 249-55.

21. Mattax, C.C. and Dalton, R.L.: *Reservoir Simulation*, Monograph Series, SPE, Richardson, TX (1990) **13**, 127-28.

22. Willhite, G.P.: *Waterflooding*, Textbook Series, SPE, Richardson, TX (1986), **3**, 167-70.

23. Dake, L.P.: *Fundamentals of Reservoir Engineering*, 11th edition, Elsevier Science Publishing Co. Inc., New York City (1990) 372-76.

24. Lane, R.H. and Sanders, G.S.: "Water Shutoff Through Fullbore Placement of Polymer Gel in Faulted and in Hydraulically Fractured Producers of the Prudhoe Bay Field," paper SPE 29475 presented at the 1995 SPE Production Operations Symp., Oklahoma City, April 2-4.

25. Seright, R.S.: "Placement of Gels to Modify Injection Profiles," paper SPE/DOE 17332 presented at the 1988 SPE/DOE Enhanced Oil Recovery Symposium, Tulsa, April 17-20.

26. Seright, R.S., Liang, J., and Sun, H.: "Gel Treatments in Production Wells with Water-Coning Problems," *In Situ* (1993) **17**(3), 243-72.

27. Liang, J., Sun, H., Seright, R.S.: "Why Do Gels Reduce Water Permeability More Than Oil Permeability?," *SPERE* (Nov. 1995) 282-286.

28. McGuire, W.J. and Sikora, V.J.: "The Effect of Vertical Fractures on Well Productivity," *Petr. Trans.* AIME (1960) **219**, 401-403.

29. Holditch, S.A.: *Quarterly Low-Permeability Gas Well Research Report for Fall 1975*, quarterly report, Petroleum Engineering Dept., Texas A&M U., College Station.

30. Lee, J.W.: "Postfracture Formation Evaluation," in *Recent Advances in Hydraulic Fracturing*, Monograph Series, SPE, Richardson, TX (1989) **12**, 316-340.

31. Ross, S.H.: *Introduction to Ordinary Differential Equations*, Xerox College Publishing, Toronto (1966) 226-227.

32. Gradshteyn, I.S. and Ryzhik, I.W.: *Table of Integrals, Series and Products*, Academic Press, New York (1965) 92.

33. Borling, D.C.: "Injection Conformance Control Case Histories Using Gels at the Wertz Field CO_2 Teriary Flood in Wyoming, USA," paper SPE 27825 presented at the 1994 SPE/DOE Symposium on Improved Oil Recovery, April 17-20.

34. Aguilar, R.: *Naturally Fractured Reservoirs*, Pennwell, Tulsa, OK (1980).

35. Saidi, A.M.: *Reservoir Engineering of Fractured Reservoirs*, General Printing, Singapore (1987).

36. Van Golf-Racht, T.D.: *Fundamentals of Fractured Reservoir Engineering*, Elsevier Scientific Publishing, Amsterdam (1982).

37. Gilman, J.R, Hinchman, S.B., and Svaldi, M.A.: "Using Polymer Injectivity Tests to Estimate Fracture Porosity in Naturally Fractured Reservoirs," paper SPE 25880 presented at the 1993 Rocky Mountain Regional/Low Permeability Reservoirs Symposium, Denver, April 12-14.

38. Wagner, O.R.: "The Use of Tracers in Diagnosing Interwell Reservoir Heterogeneities—Field Results," *JPT* (Nov. 1977) 1410-1416.

39. Tester, J.W., Bivins, R.L., and Potter, R.M.: "Interwell Tracer Analyses of a Hydraulically Fractured Granitic Geothermal Reservoir," *SPEJ* (Aug. 1982) 537-554.

40. Beier, R.A. and Sheely, C.Q.: "Tracer Surveys to Identify Channels for Remedial Work Prior to CO_2 Injection at MCA Unit, New Mexico," paper SPE 17371 presented at the 1988 SPE/DOE Enhanced Oil Recovery Symposium, Tulsa, April 17-20.

41. Lichtenberger, G.J.: "Field Applications of Interwell Tracers for Reservoir Characterization of Enhanced Oil Recovery Pilot Areas," paper SPE 21652 presented at the 1991 SPE Production Operations Symposium, Oklahoma City, April 7-9.

42. Datta-Gupta, A. Vasco, D.W., and Long, J.C.S.: "Sensitivity and Spacial Resolution of Transient Pressure and Tracer Data for Heterogeneity Characterization," paper SPE 30589 presented at the 1995 SPE Annual Technical Conference and Exhibition, Dallas, Oct. 22-25.

43. Hagoort, J.: "The Response of Interwell Tracer Tests in Watered-Out Reservoirs," paper SPE 11131 presented at the 1982 SPE Annual Technical Conference and Exhibition, New Orleans, Sept. 26-29.

44. Agca, C., Pope, G.A., and Sepehrnoori, K.: "Modelling and Analysis of Tracer Flow in Oil Reservoirs," *J. Petroleum Science and Engineering*, **4** (1990) 3-19.

45. Shinta, A.A., and Kazemi, H.: "Tracer Transport in Characterization of Dual-Porosity Reservoirs," paper SPE 26636 presented at the 1993 SPE Annual Technical Conference and Exhibition, Houston, Oct. 3-6.

46. Datta-Gupta, A. *et al.*: "Detailed Characterization of a Fractured Limestone Formation by Use of Stochastic Inverse Approaches," *SPEFE* (Sept. 1995) 133-140.

47. Jetzabeth, R. *et al.*: "Tracer-Test Interpretation in Naturally Fractured Reservoirs," *SPEFE* (Sept. 1995) 186-192.

48. Seright, R.S.: "Use of Preformed Gels for Conformance Control in Fractured Systems," *SPEPF* (Feb. 1997) 59-65.

49. Perkins, T.K., and Johnston, O.C.: "A Review of Diffusion and Dispersion in Porous Media," *SPEJ* (March 1963) 70-84.

50. Bird, R.B., Stewart, W.E., and Lightfoot, E.N.: *Transport Phenomena*, John Wiley & Sons, New York (1960) 11, 42-63.

51. Fullbright, G.D. *et al.*: "Evolution of Conformance Improvement Efforts in a Major CO_2 WAG Injection Project," paper SPE/DOE 35361 presented at the 1996 SPE/DOE Symposium on Improved Oil Recovery, Tulsa, April 21-24.

52. Tweidt, L.I. *et al.*: "Improving Sweep Efficiency in the Norman Wells Naturally Fractured Reservoir Through the Use of Polymer Gels: A Field Case History," paper SPE 38901 presented at the 1997 SPE Annual Technical Conference and Exhibition, San Antonio, Oct. 5-8.

53. Sanders, G.S., Chambers, M.J., and Lane, R.H.: "Successful Gas Shutoff with Polymer Gel Using Temperature Modeling and Selective Placement in the Prudhoe Bay Field," paper SPE

28502 presented at the 1994 SPE Annual Technical Conference and Exhibition, New Orleans, Sept. 25-28.

54. Odorisio, V.G. and Curtis, S.C.: "Operational Advances from Field Application of Short-Radius Horizontal Drilling in the Yates Field Unit," paper SPE 24612 presented at the 1992 SPE Annual Technical Conference and Exhibition, Washington, D.C., Oct. 4-7.

55. Seright, R.S.: "Gel Placement in Fractured Systems," *SPEPF* (Nov. 1995), 241-248.

56. Liang, J., Sun, H., Seright, R.S.: "Reduction of Oil and Water Permeabilities Using Gels," paper SPE 24195 presented at the 1992 SPE/DOE Symposium on Enhanced Oil Recovery, Tulsa, April 22-24.

57. Needham, R.B., Threlkeld, C.B., and Gall, J.W.: "Control of Water Mobility Using Polymers and Multivalent Cations," paper SPE 4747 presented at the 1974 SPE-AIME Improved Oil Recovery Symposium, Tulsa, April 22-24.

58. Avery, M.R. and Wells, T.A.: "Field Evaluation of a New Gelant for Water Control in Production Wells," paper SPE 18201 presented at the 1988 SPE Annual Technical Conference and Exhibition, Houston, Oct. 2-5.

59. Sandiford, B.B. and Graham, G.A.: "Injection of Polymer Solutions in Producing Wells," AIChE Symposium Series, (1973) **69**, No. 127, 38.

60. Schneider, F.N. and Owens, W.W.: "Steady-State Measurements of Relative Permeability for Polymer/Oil Systems," *SPEJ* (Feb. 1982) 79.

61. Sparlin, D.D.: "An Evaluation of Polyacrylamides for Reducing Water Production," *JPT* (Aug. 1976) 906-914.

62. White, J.L., Goddard, J.E., and Phillips, H.M.: "Use of Polymers To Control Water Production in Oil Wells," *JPT* (Feb. 1973) 143-150.

63. Zaitoun, A. and Kohler N.: "Two-Phase Flow Through Porous Media: Effect of an Adsorbed Polymer Layer," paper SPE 18085 presented at the 1988 SPE Annual Technical Conference and Exhibition, Houston, Oct. 2-5.

64. Zaitoun, A. and Kohler N.: "Thin Polyacrylamide Gels for Water Control in High-Permeability Production Wells" paper SPE 22785 presented at the 1991 SPE Annual Technical Conference and Exhibition, Dallas, Oct. 6-9.

65. Seright, R.S.: "Improved Techniques for Fluid Diversion in Oil Recovery Processes," final report, DOE/BC/14880-15, U.S. DOE (Jan. 1996) 62-89.

66. Seright, R.S.: "Reduction of Gas and Water Permeabilities Using Gels," *SPEPF* (Nov. 1995) 103-108.

67. Dawe, R.A. and Zhang, Y.: "Mechanistic study of the selective action of oil and water penetrating into a gel emplaced in a porous medium," *Journal of Petroleum Science and Engineering* (1994) **12**, 113-125.

68. Liang, J. and Seright, R.S.: "Further Investigations of Why Gels Reduce k_w More Than k_o," *SPEPF* (Nov. 1997).

69. Seright, R.S. and Martin, F.D.: "Fluid Diversion and Sweep Improvement with Chemical Gels in Oil Recovery Processes," final report, DOE/BC/14447-15, U.S. DOE (Sept. 1992) 28-58.

APPENDIX A: Data and Figure Supplement for Chapter 2

Table A.1. Channeling base case reservoir and fluid data.

Wellbore radius, ft	0.25
Drainage area, acres	40
Reservoir dip, degrees	0
Grid dimensions, crossflow case (x×y×z)	(42×1×3)
Grid dimensions, no crossflow case (x×y×z)	(42×1×5)
Distance between wells, ft	933
Pressure drop between wells, psi	1,000
Producing layer thickness, ft	30
Impermeable layer thickness, ft	3
Porosity (producing layers)	0.20
Permeability (producing layers), md	variable
Permeability (impermeable layers), md	0
Average water gradient from surface to reservoir, psi/ft	0.42
Oil density, psi/ft	0.33
Water density, psi/ft	0.425
Oil viscosity, cp	1.1
Water viscosity, cp	0.44
Bubblepoint pressure, psia	1,800
Residual oil saturation	0.20
Residual water saturation	0.20
Endpoint oil relative permeability	1
Endpoint water relative permeability	0.1
Exponent for oil relative permeability equation	2
Exponent for water relative permeability equation	2

Table A.2. Coning model reservoir and fluid data.

Wellbore radius, ft	0.25
Reservoir dip, degrees	0
Drainage area, acres	160
Total thickness of reservoir, ft	280
Thickness of oil zone, ft	100
Perforated interval, ft	20
Skin factor	0
Grid dimensions (r×θ×z)	(11×1×16)
Porosity	.20
Radial permeability in oil zone, md	1,000
Radial permeability in water zone, md	1,000
Vertical permeability, md	1,000
Average water gradient from surface to reservoir, psi/ft	0.435
Water density @ P_b, psi/ft	0.42
Oil density @ P_b, psi/ft	0.35
Water viscosity @ P_b, cp	0.41
Oil viscosity @ P_b, cp	2.00
Water FVF @ P_b, RB/STB	1.021
Oil FVF @ P_b, RB/STB	1.108
Bubble point pressure, psia	1,000

Table A.3. Coning model saturation, relative permeability and capillary pressure data.

S_w	.160	.200	.300	.400	.500	.600	.700	.800
k_{ro}	.950	.750	.450	.240	.120	.050	.005	0
k_{rw}	0	.005	.020	.030	.065	.080	.130	.190
P_c	4.000	.800	.470	.380	.320	.250	.170	0

The following diagnostic plots show similar behavior as the multi-layer channeling base case described in Chapter 2. Data for all the cases are listed in the tables below. They only differ from each other in the number of layers (three or six) and the permeability contrast among the layers.

Case A:

Layer	1	2	3
Permeability [md]	200	25	20

Case B:

Layer	1	2	3
Permeability [md]	200	180	25

Case C:

Layer	1	2	3	4	5	6
Permeability [md]	250	200	150	100	50	25

Case D:

Layer	1	2	3	4	5	6
Permeability [md]	400	200	50	40	30	20

Case E:

Layer	1	2	3	4	5	6
Permeability [md]	400	40	35	30	25	20

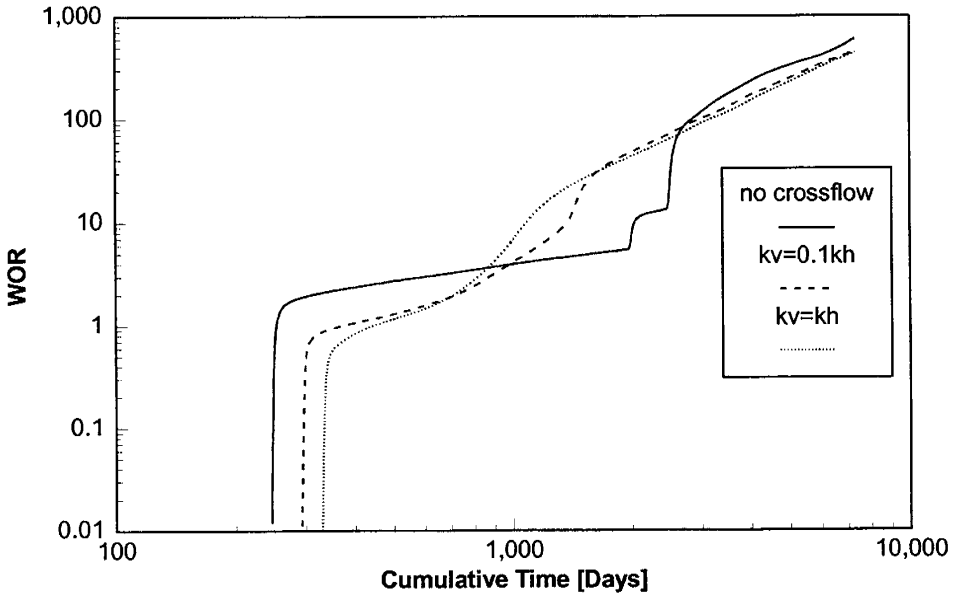

Fig. A.1. Case A channeling WOR behavior for varying degrees of vertical communication.

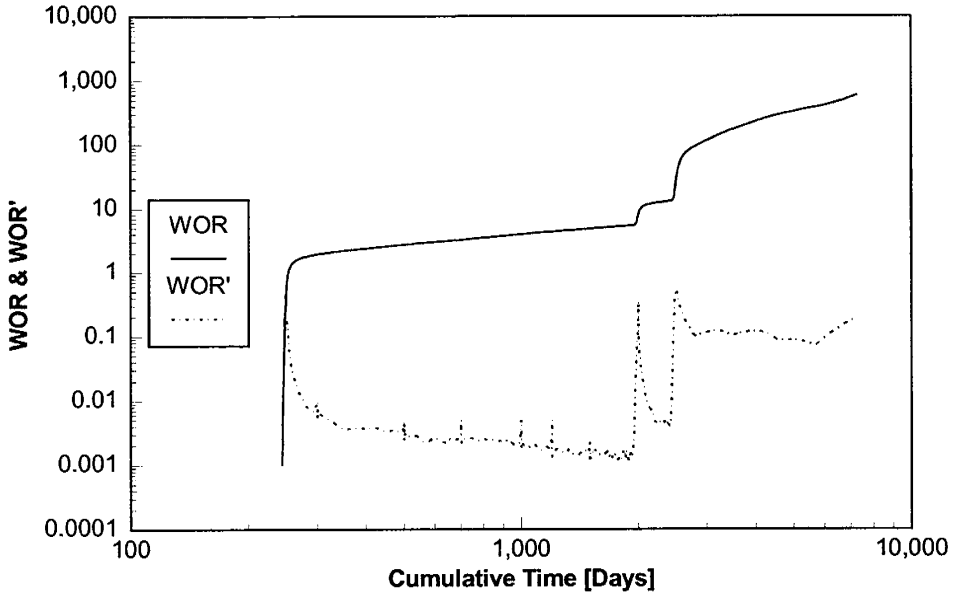

Fig. A.2. WOR and WOR' behavior for the no-crossflow case shown in Fig. A.1.

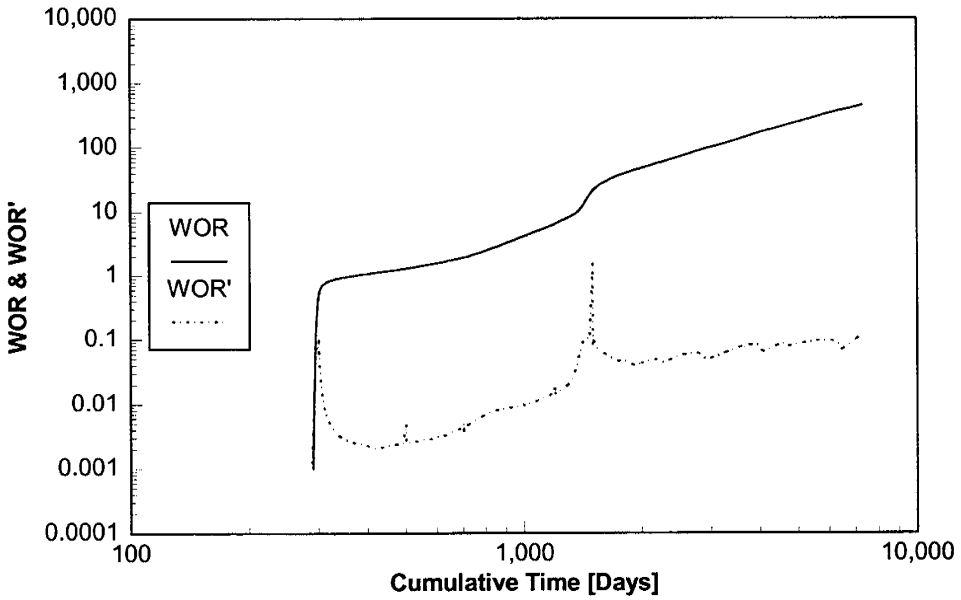

Fig. A.3. WOR and WOR' behavior for the $k_v=0.1k_h$ case shown in Fig. A.1.

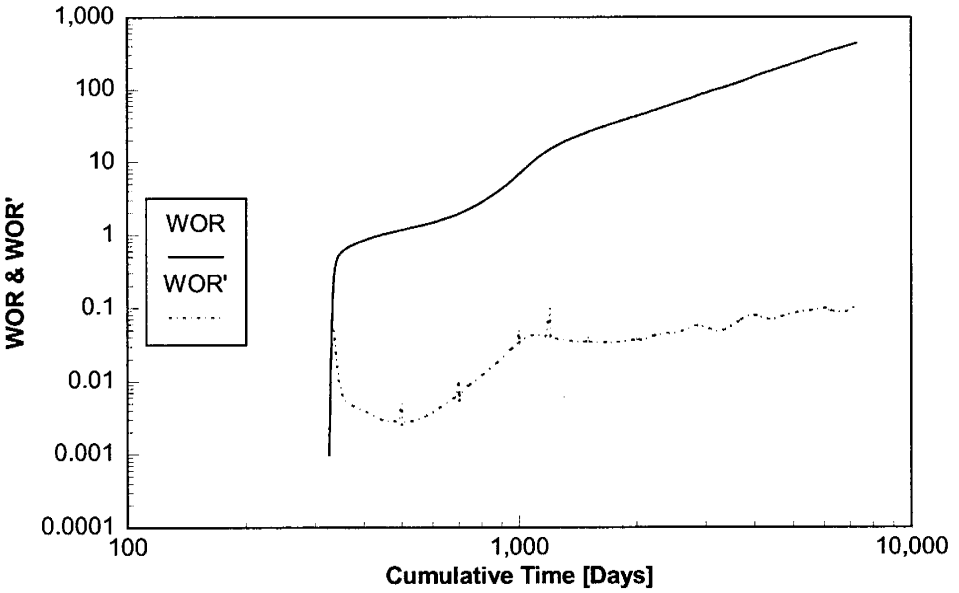

Fig. A.4. WOR and WOR' curves for the vertical equilibrium case shown in Fig. A.1.

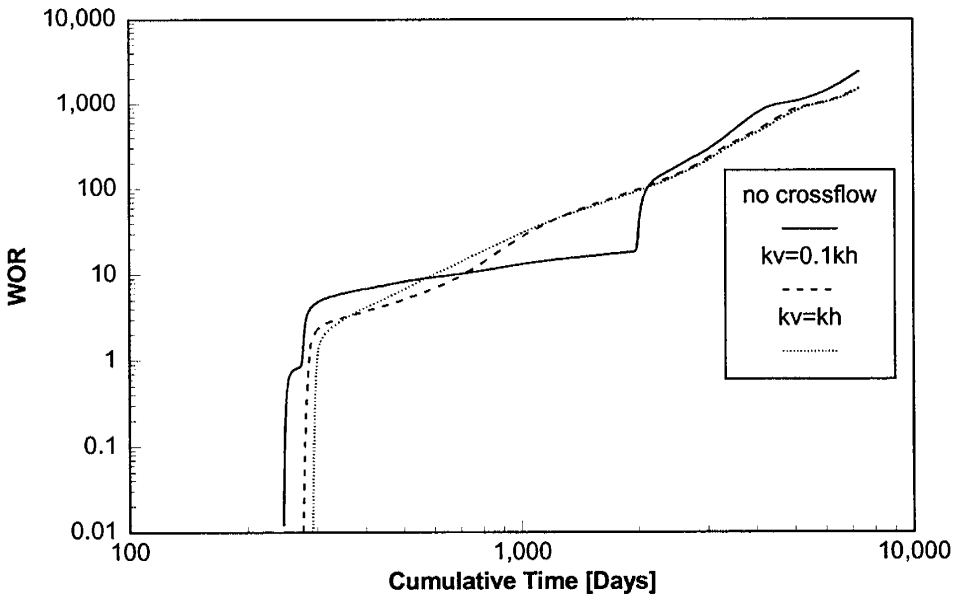

Fig. A.5. Case B channeling WOR behavior for varying degrees of vertical communication.

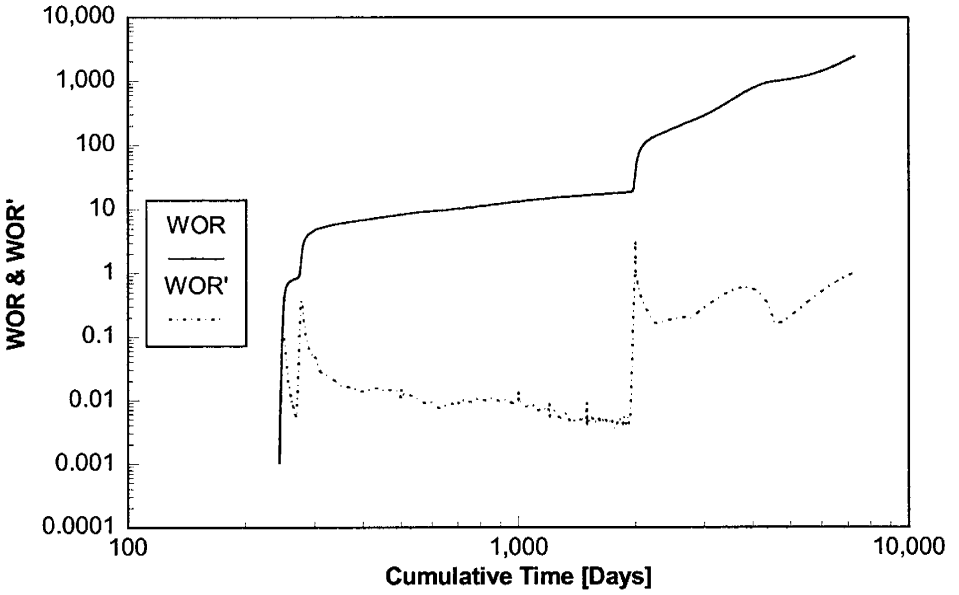

Fig. A.6. WOR and WOR' behavior for the no-crossflow case shown in Fig. A.5.

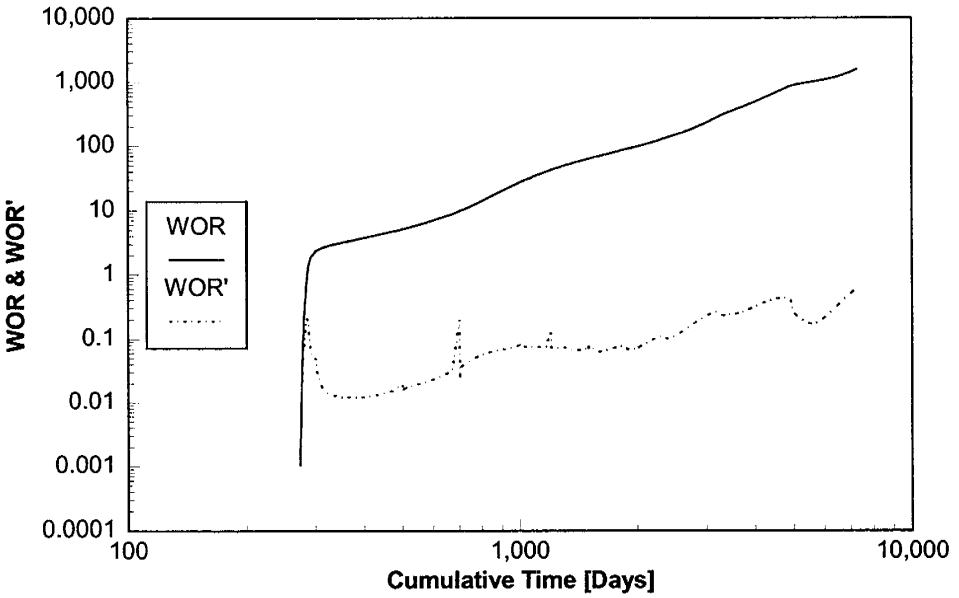

Fig. A.7. WOR and WOR' curves for the $k_v=0.1k_h$ case shown in Fig. A.5.

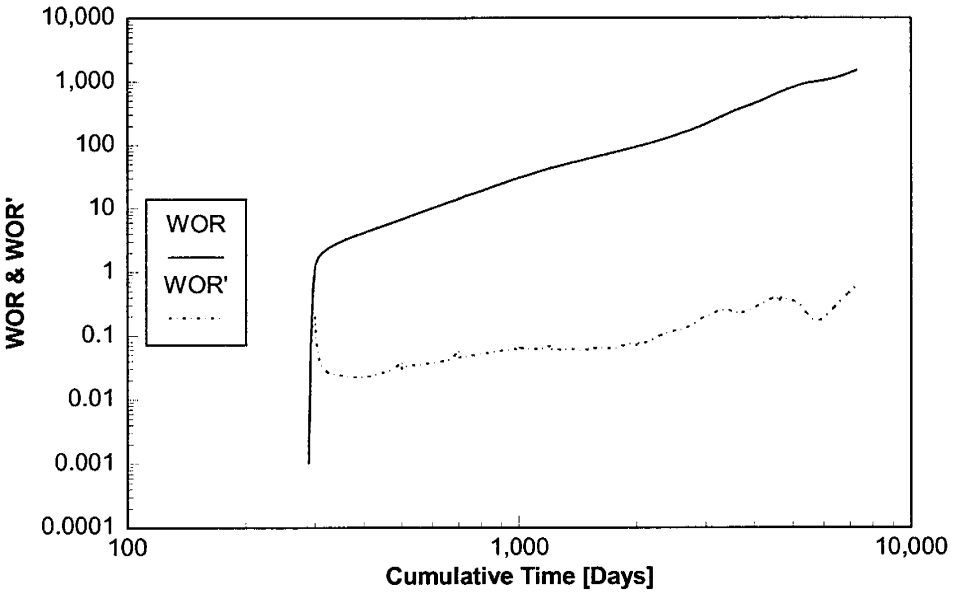

Fig. A.8. WOR and WOR' curves for the vertical equilibrium case shown in Fig. A.5.

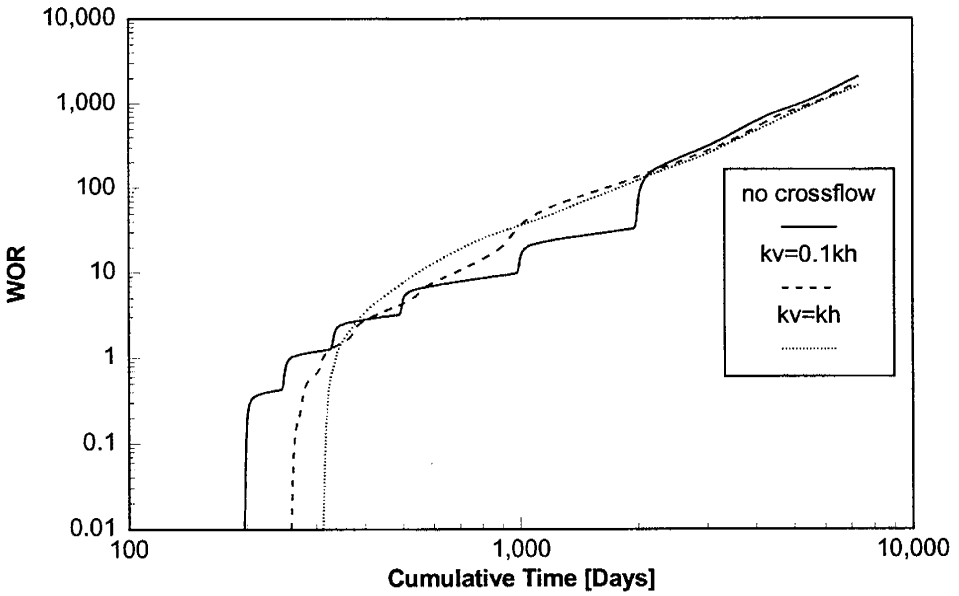

Fig. A.9. Case C channeling WOR behavior for different degrees of vertical communication.

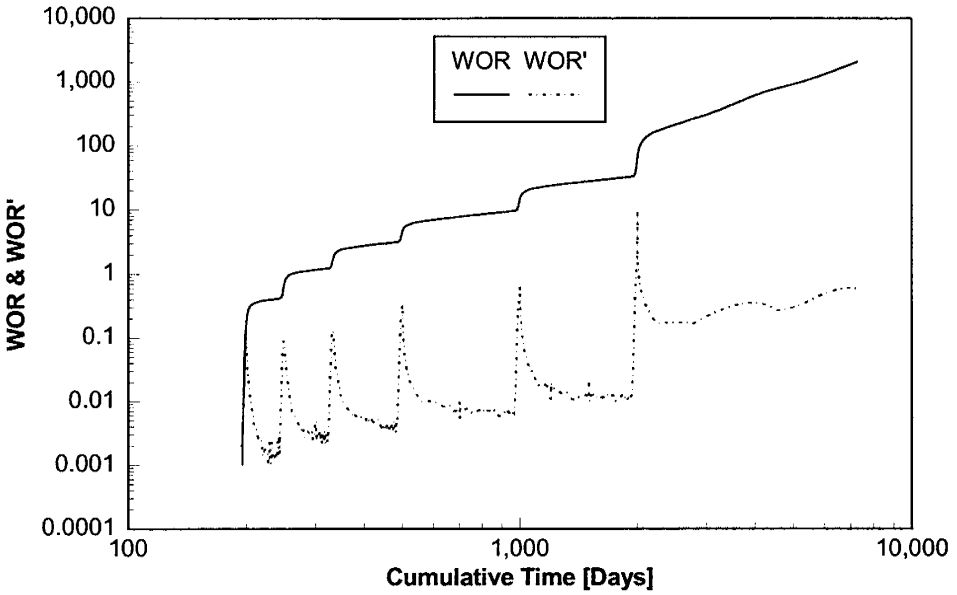

Fig. A.10. WOR and WOR' behavior for the no-crossflow case shown in Fig. A.9.

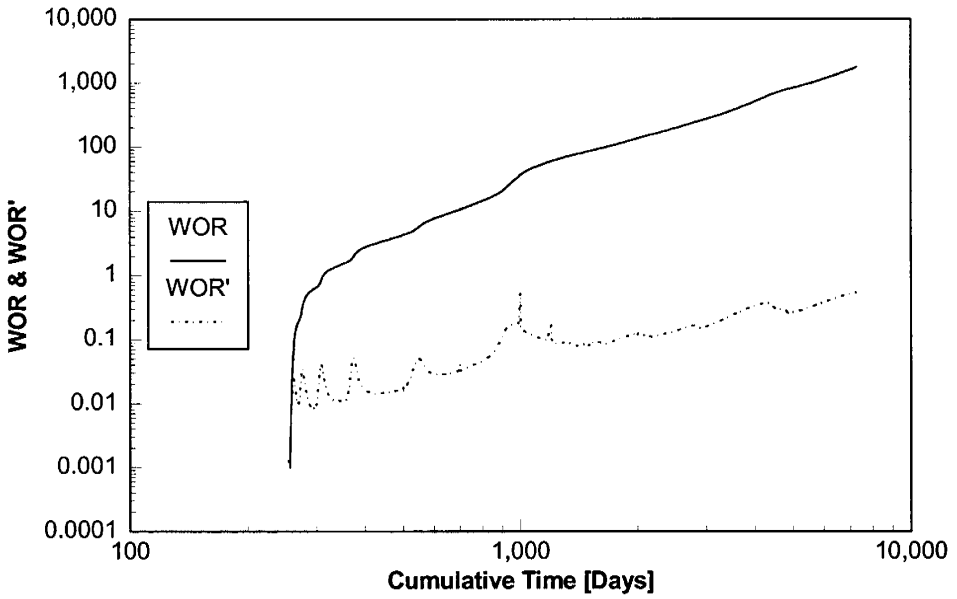

Fig. A.11. WOR and WOR' behavior for the k_v=0.1k_h case shown in Fig. A.9.

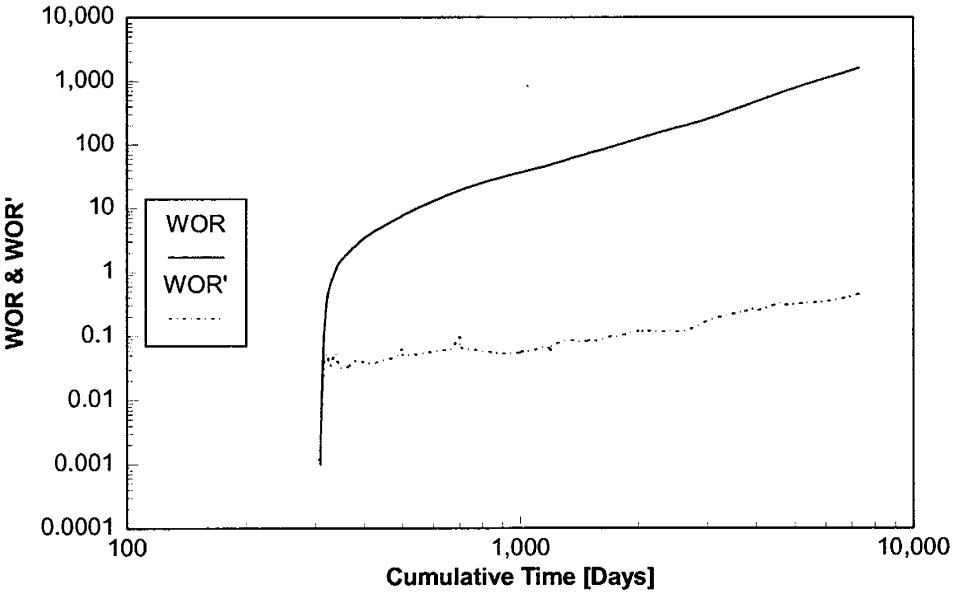

Fig. A.12. WOR and WOR' curves for the vertical equilibrium case shown in Fig. A.9.

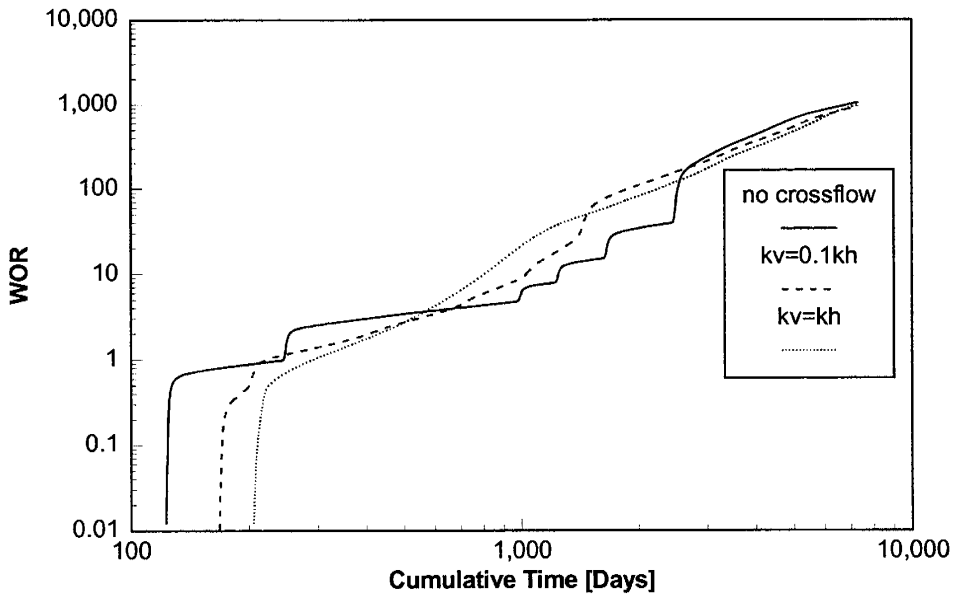

Fig. A.13. Case D channeling WOR behavior for different degrees of vertical communication.

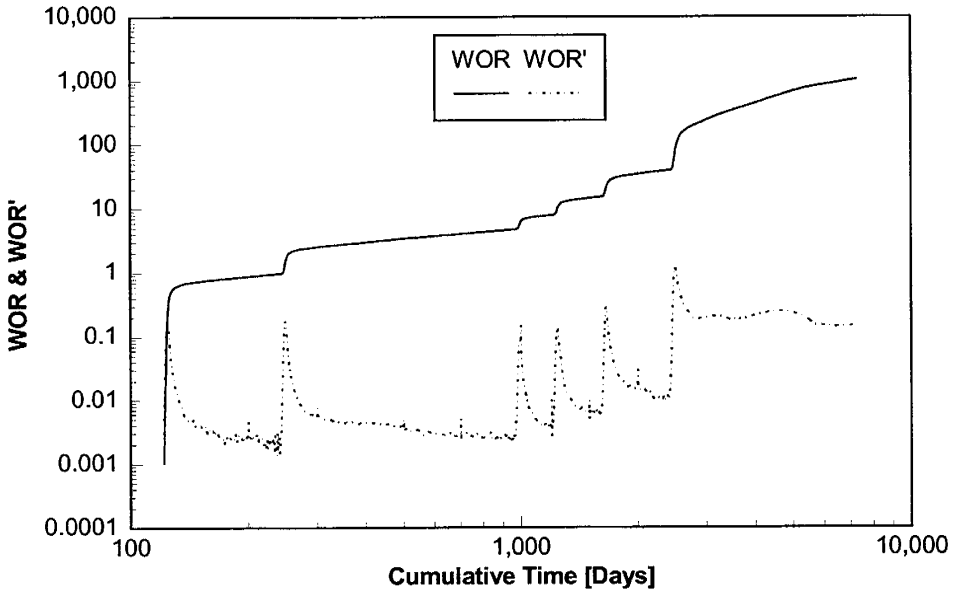

Fig. A.14. WOR and WOR' curves for the no-crossflow case shown in Fig. A.13.

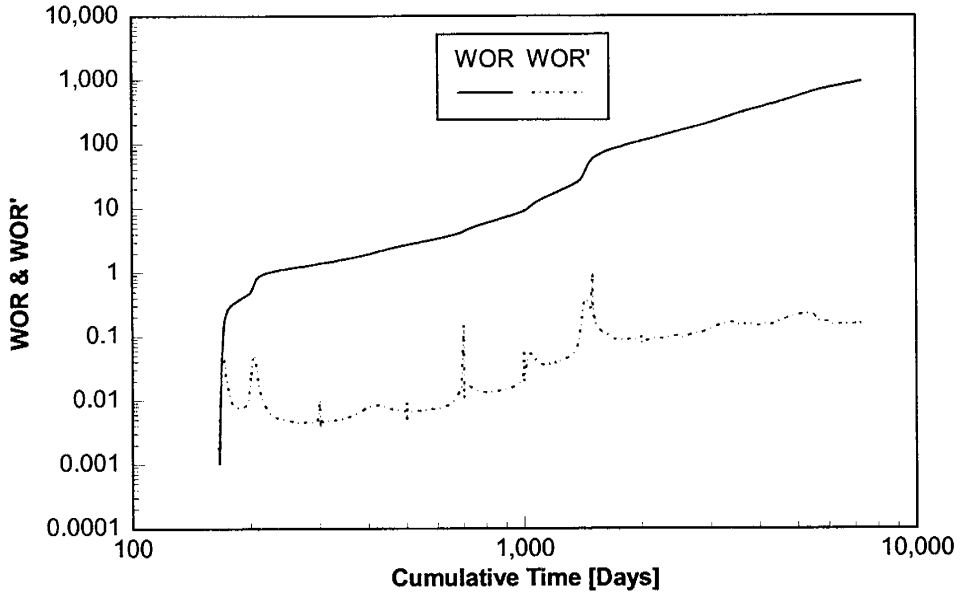

Fig. A.15. WOR and WOR' curves for the $k_v=0.1k_h$ case shown in Fig. A.13.

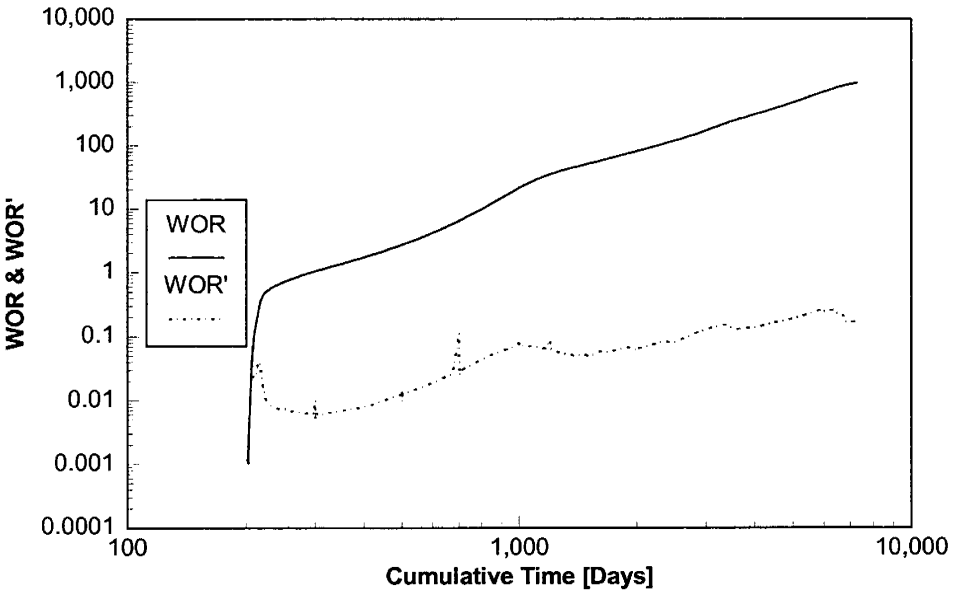

Fig. A.16. WOR and WOR' curves for the vertical equilibrium case shown in Fig. A.13.

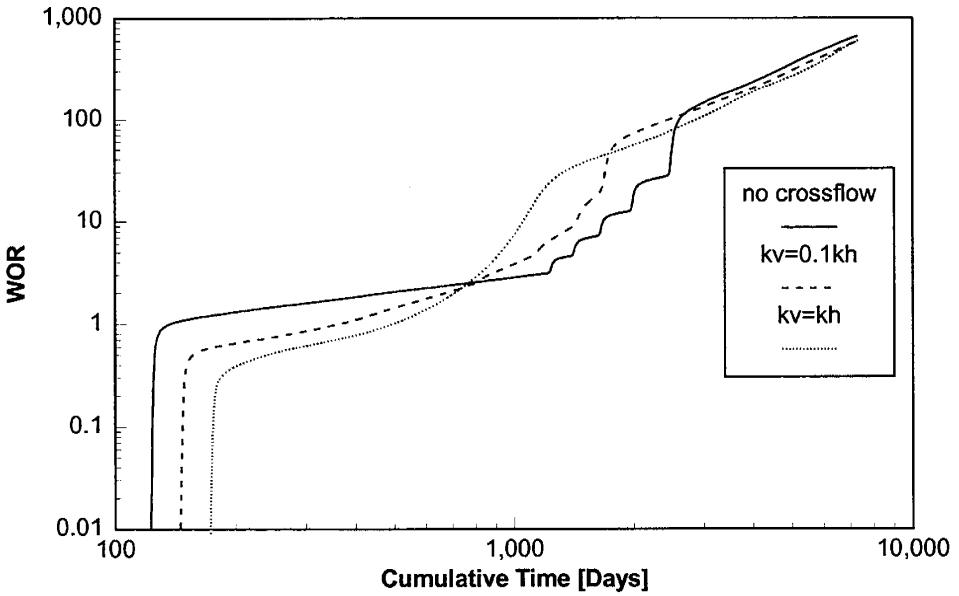

Fig. A.17. Case E channeling WOR behavior for varying degrees of vertical communication.

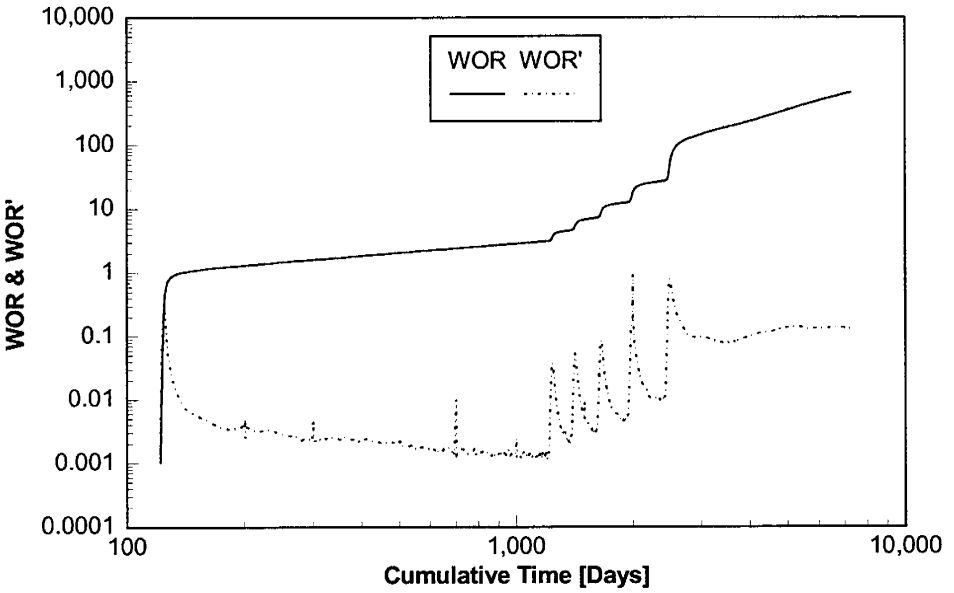

Fig. A.18. WOR and WOR' curves for the no-crossflow case shown in Fig. A.17.

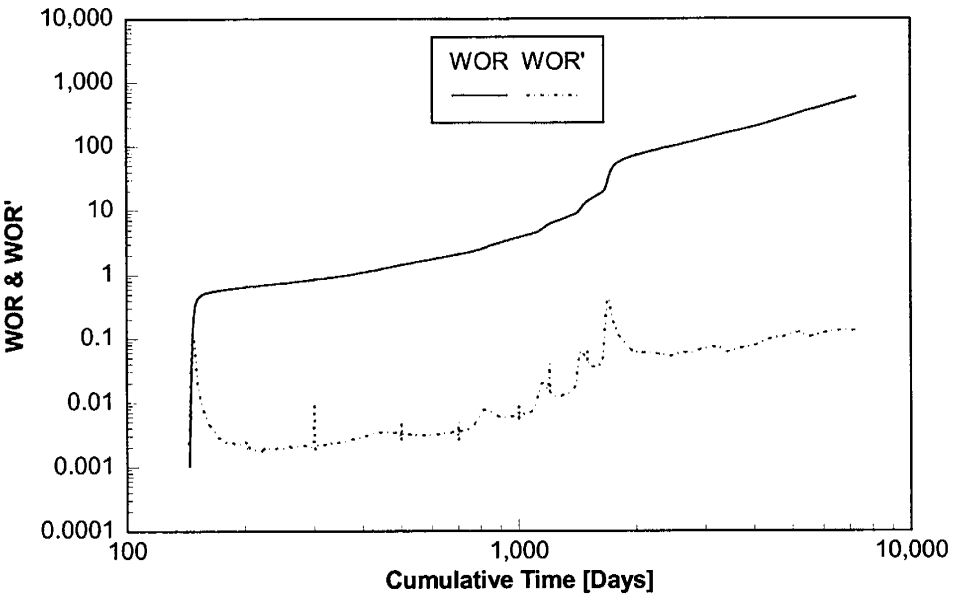

Fig. A.19. WOR and WOR' curves for the $k_v=0.1k_h$ case shown in Fig. A.17.

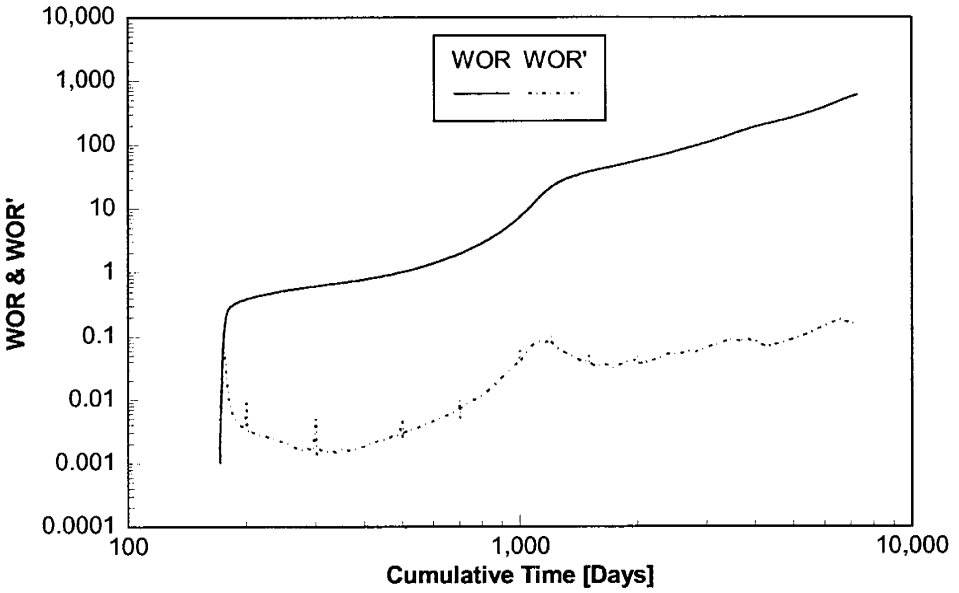

Fig. A.20. WOR and WOR' curves for the vertical equilibrium case shown in Fig. A.17.

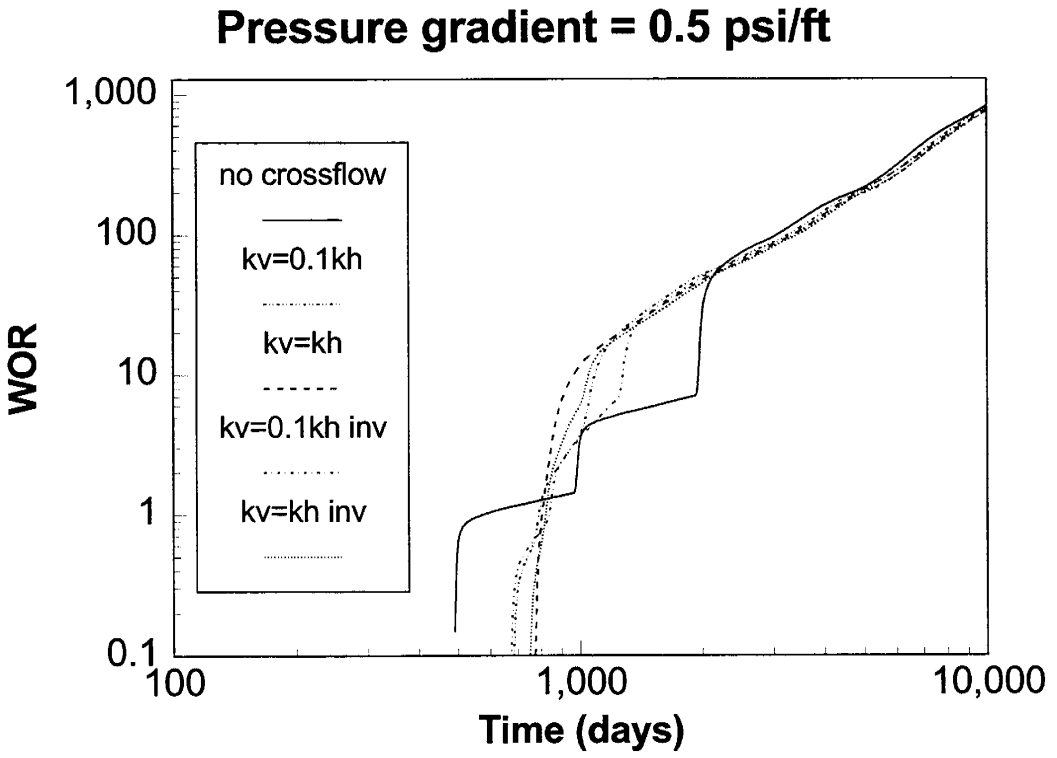

Fig. A.21. Effect of layer ordering and crossflow when pressure gradient = 0.5 psi/ft.

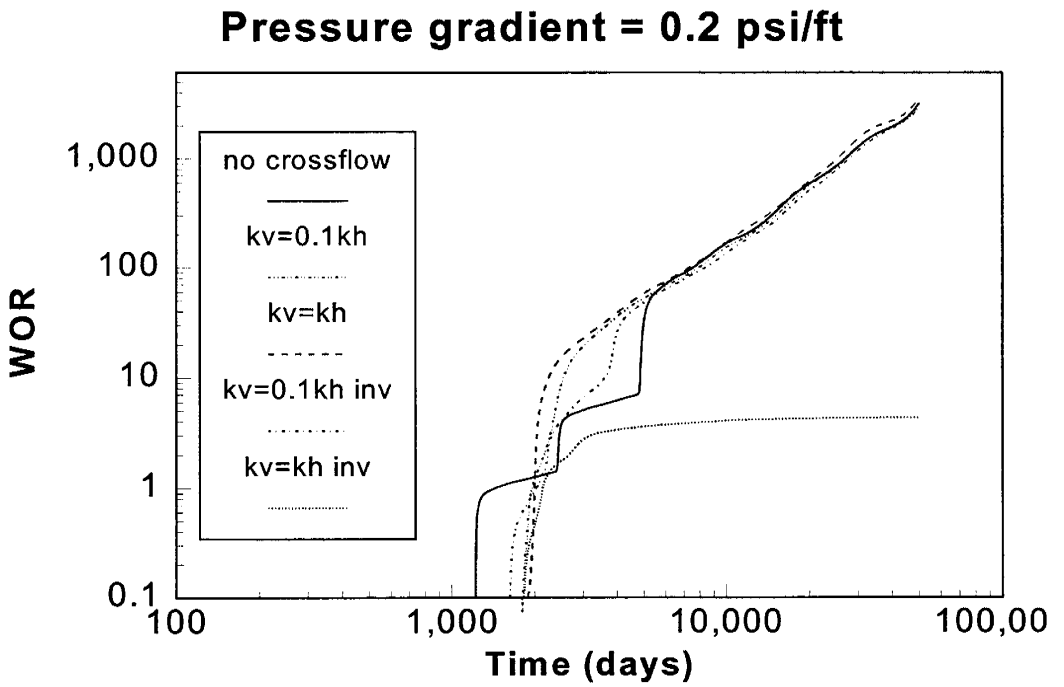

Fig. A.22. Effect of layer ordering and crossflow when pressure gradient = 0.2 psi/ft.

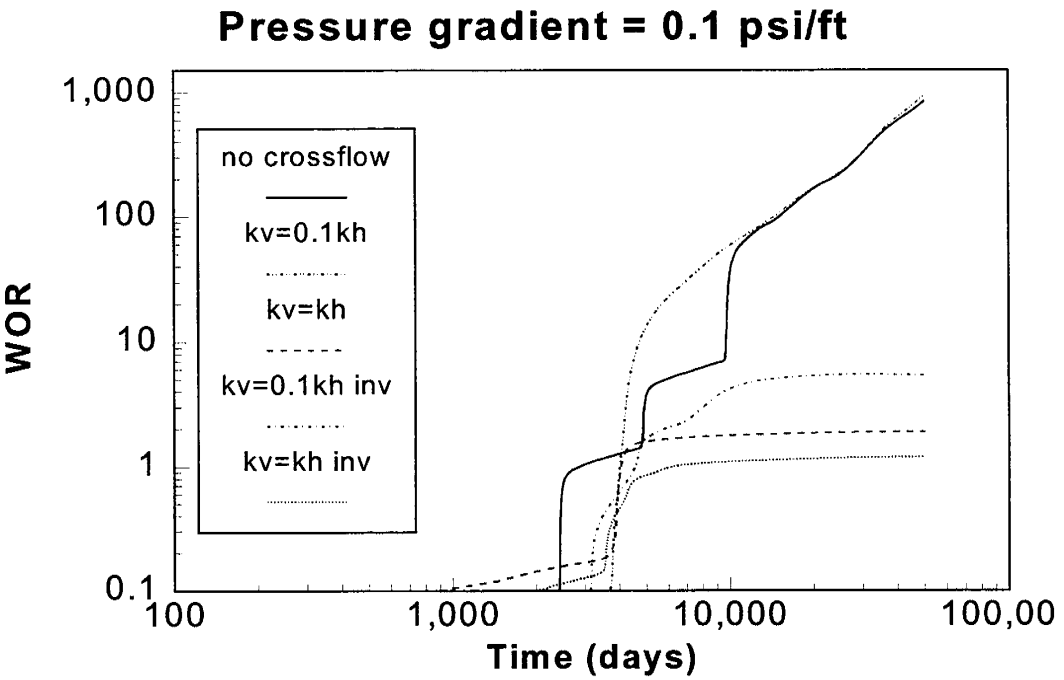

Fig. A.23. Effect of layer ordering and crossflow when pressure gradient = 0.1 psi/ft.

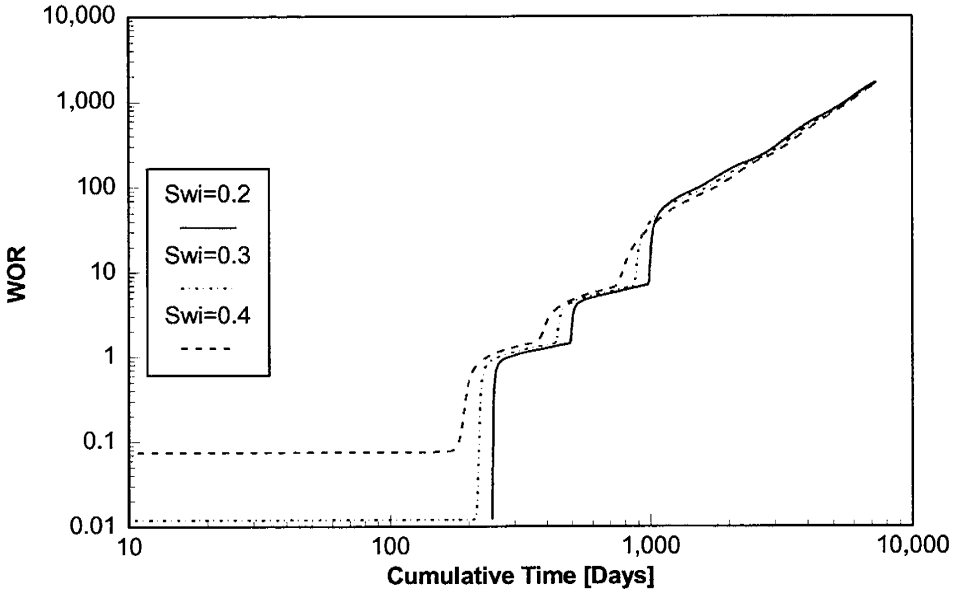

Fig. A.24. Effect of changing initial water saturation, no-crossflow case. The irreducible water saturation is 20%.

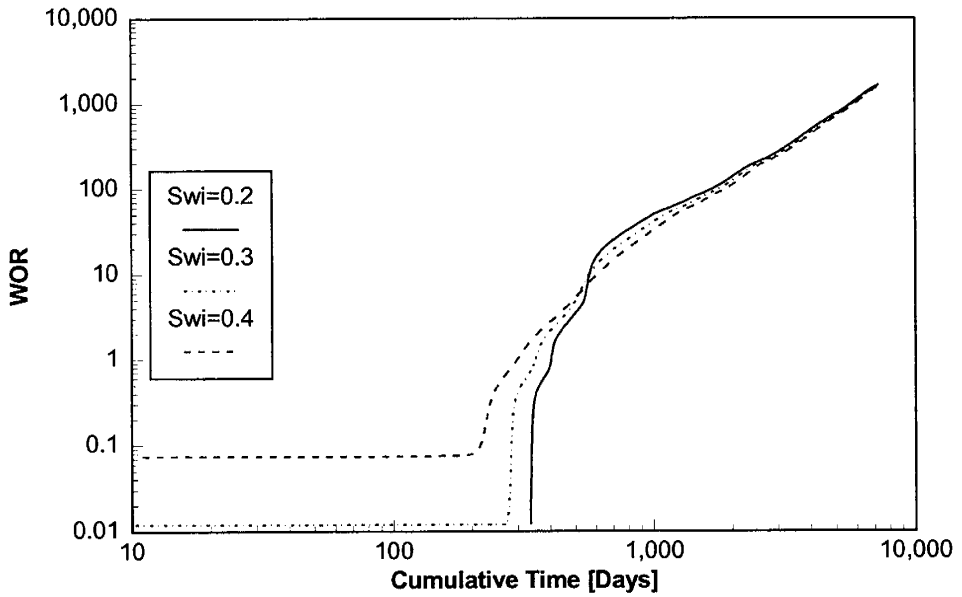

Fig. A.25. Effect of changing initial water saturation, $k_v=0.1k_h$ case. The irreducible water saturation is 20%.

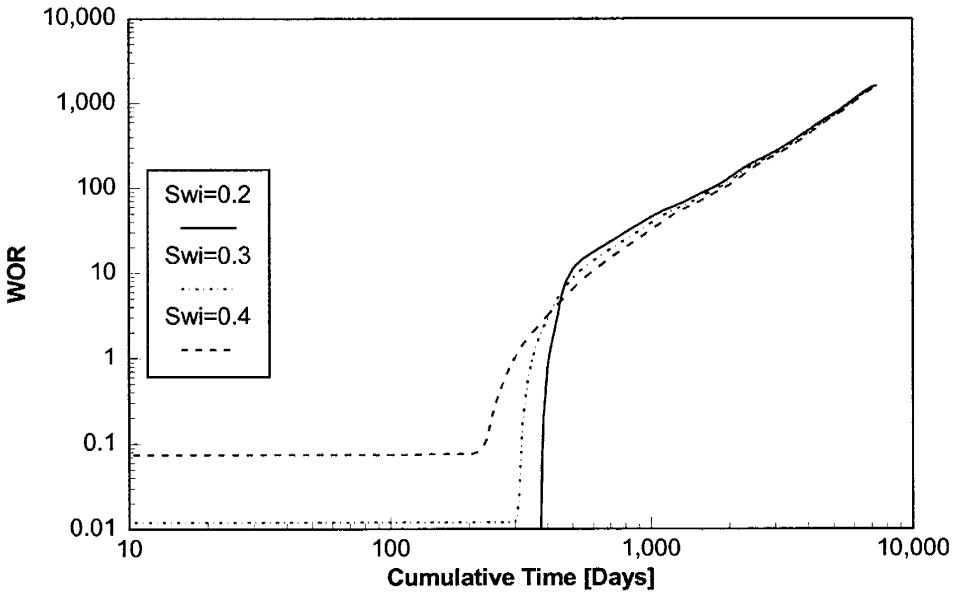

Fig. A.26. Effect of changing initial water saturation, vertical equilibrium case. The irreducible water saturation is 20%.

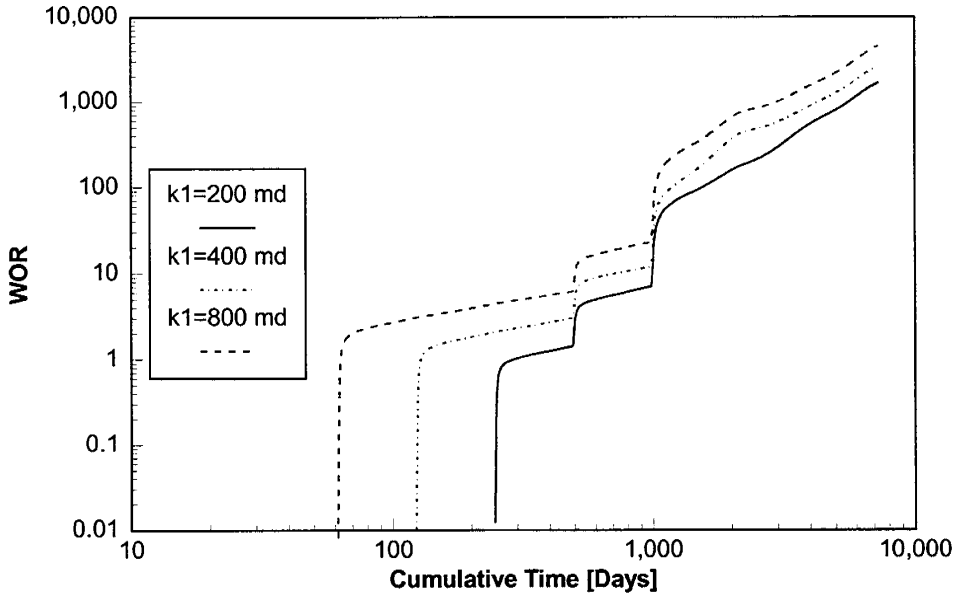

Fig. A.27. Increasing the permeability of the most permeable layer, no-crossflow case.

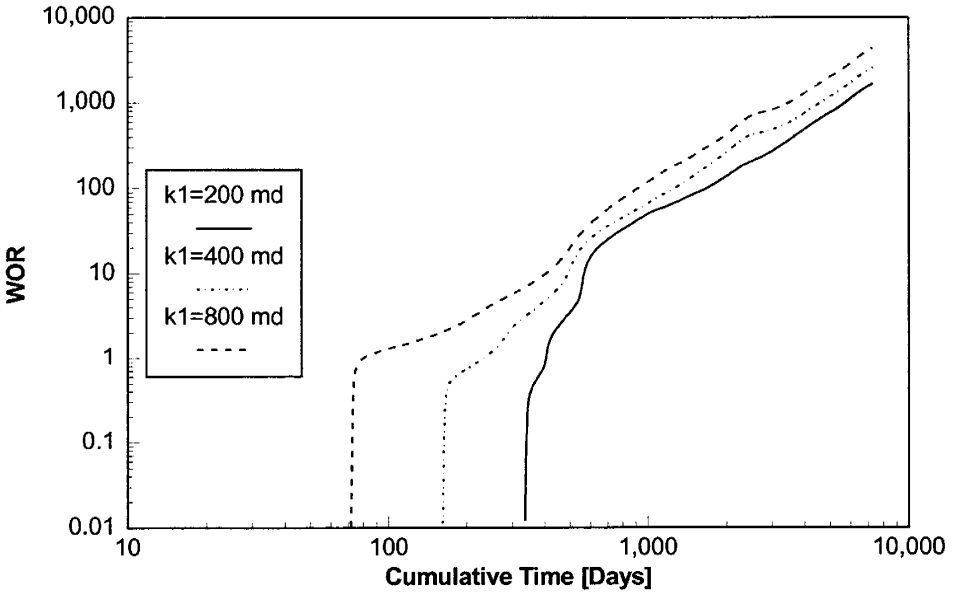

Fig. A.28. Increasing the permeability of the most permeable layer, $k_v=0.1k_h$ case.

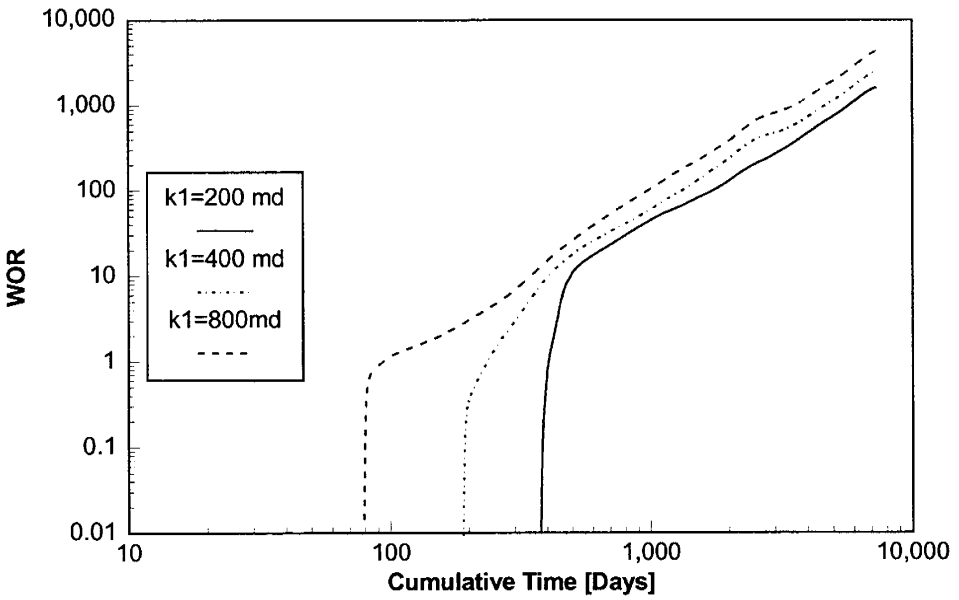

Fig. A.29. Increasing the permeability of the most permeable layer, vertical equilibrium case.

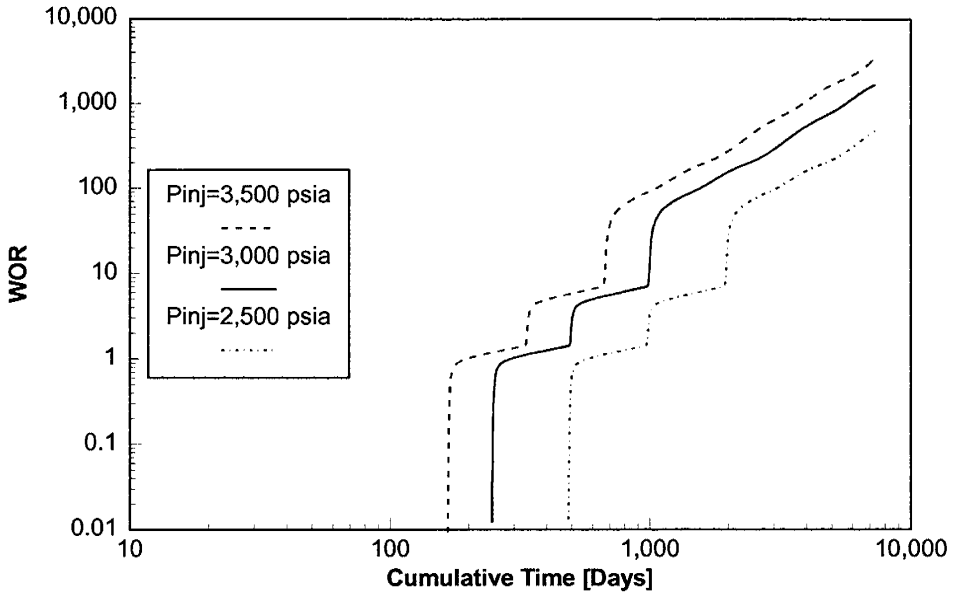

Fig. A.30. Effect of changing the injection pressure, no-crossflow case. The production pressure is 2,000 psia for all cases.

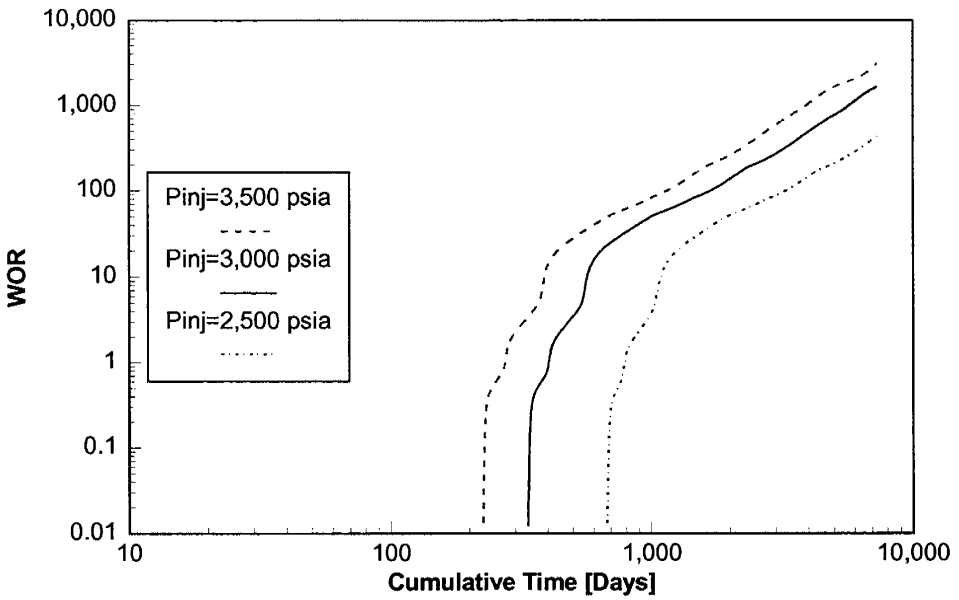

Fig. A.31. Effect of changing the injection pressure, $k_v=0.1k_h$ case. The production pressure is 2,000 psia for all cases.

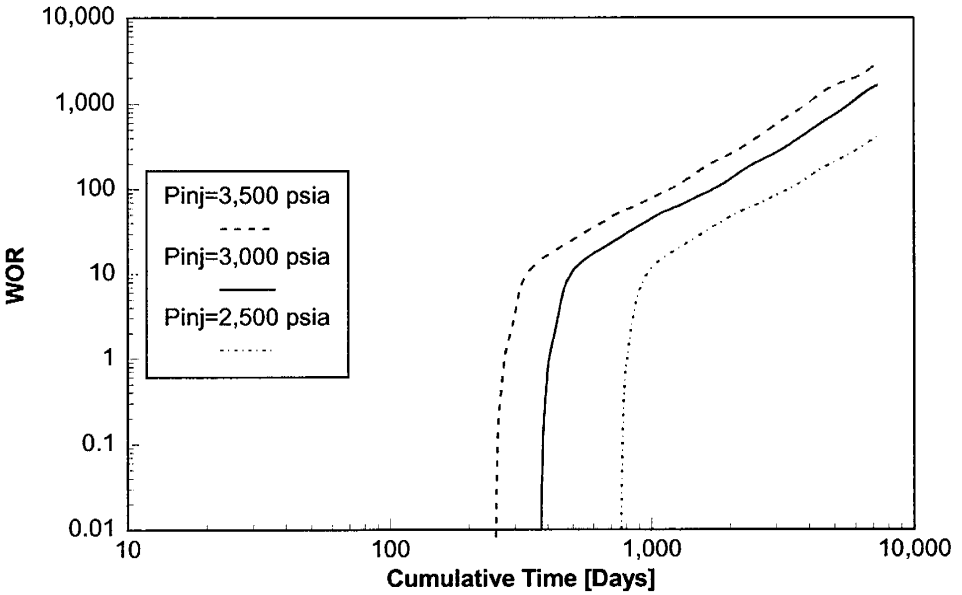

Fig. A.32. Effect of changing the injection pressure, vertical equilibrium case. The production pressure is 2,000 psia for all cases.

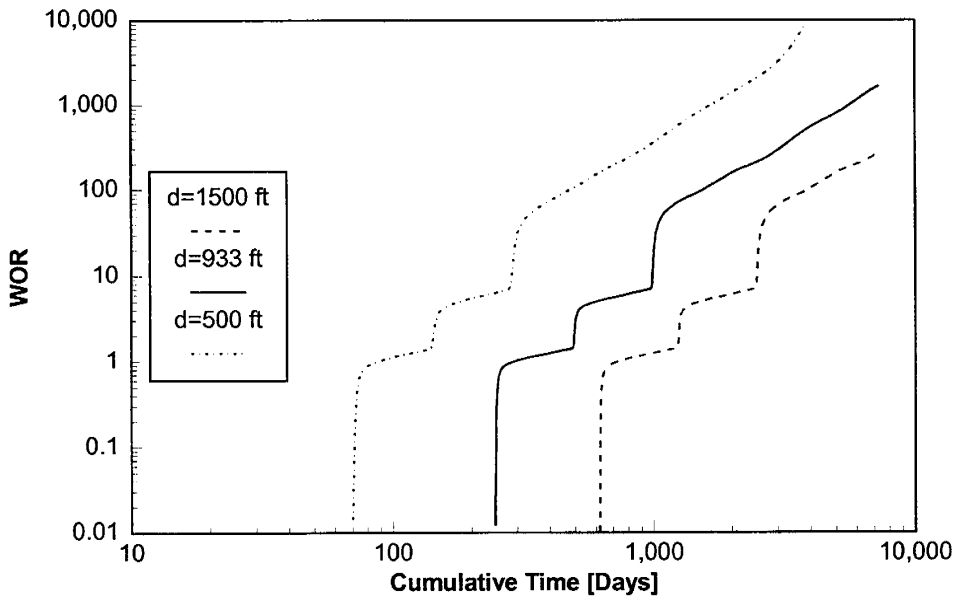

Fig. A.33. Changing the well spacing, no-crossflow case. The pressure differential between the injector and producer is kept constant at 1,000 psia.

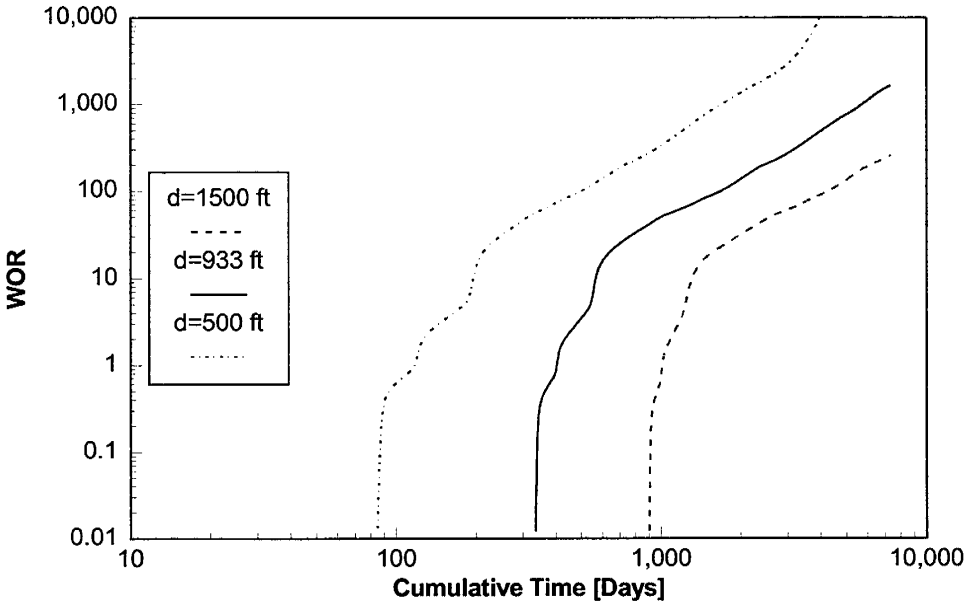

Fig. A.34. Changing the well spacing, $k_v=0.1k_h$ case. The pressure differential between the injector and producer is kept constant at 1,000 psia.

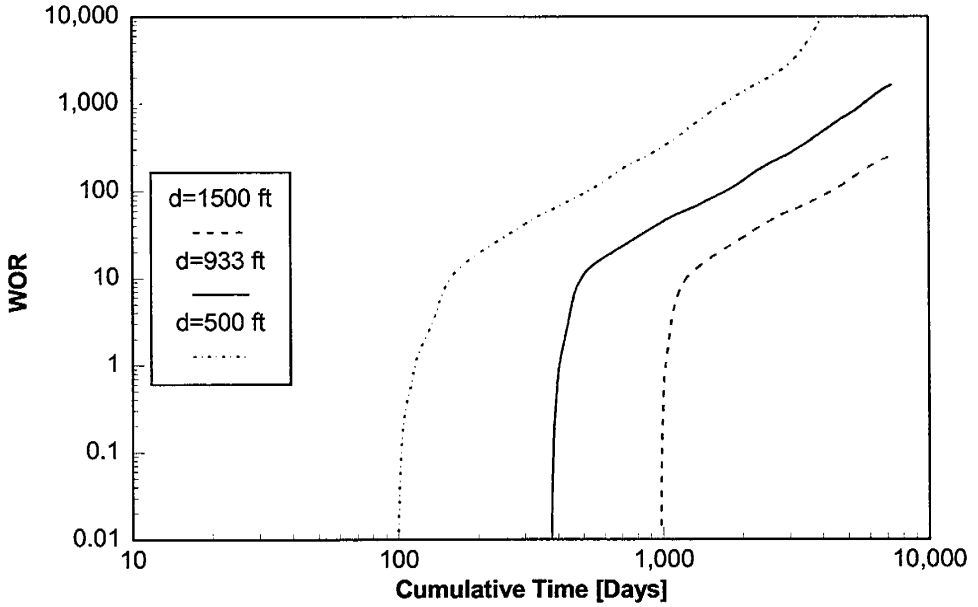

Fig. A.35. Changing the well spacing, vertical equilibrium case. The pressure differential between the injector and producer is kept constant at 1,000 psia.

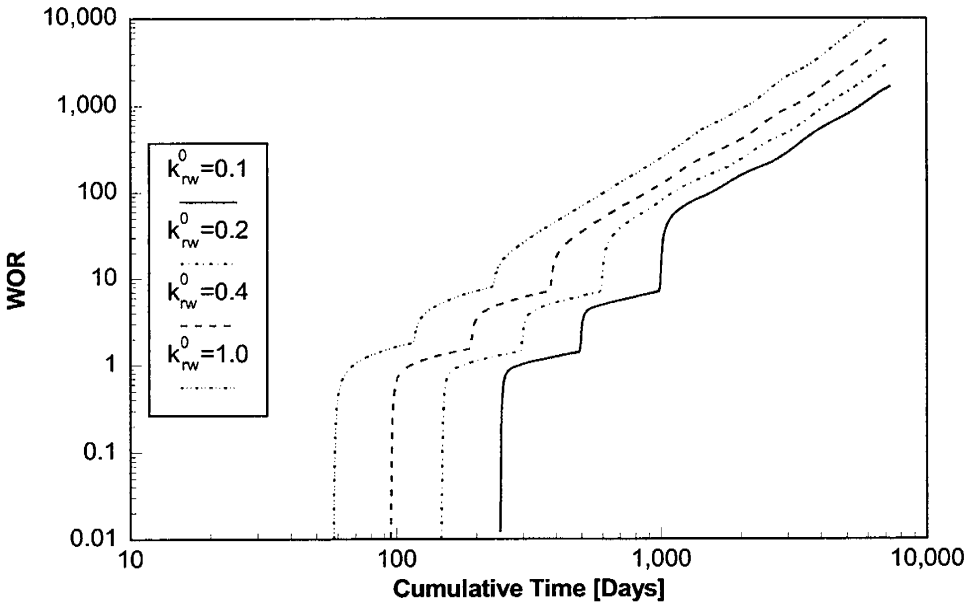

Fig. A.36. Changing the endpoint relative permeability to water, no-crossflow case. All other parameters are equal to those of the base case.

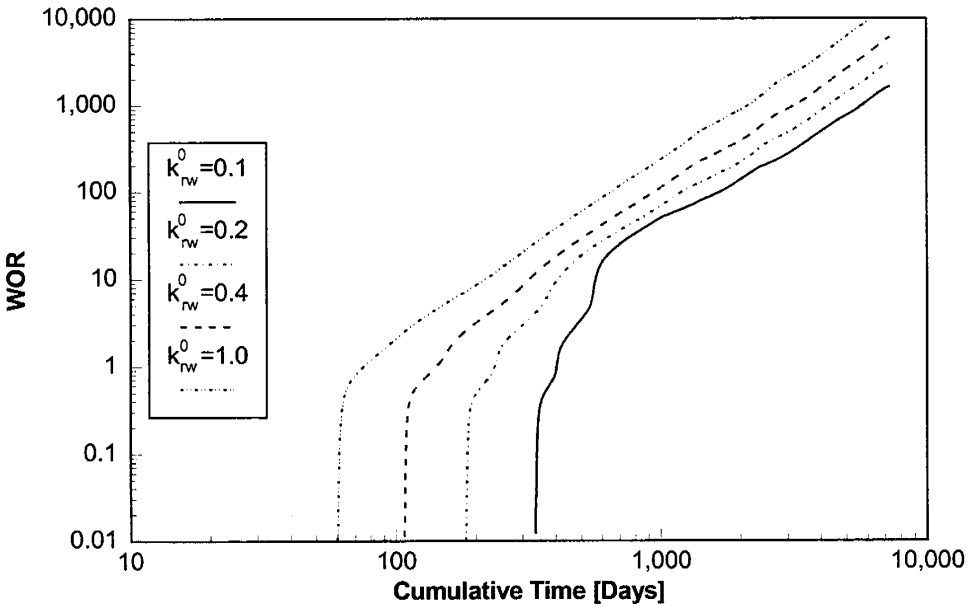

Fig. A.37. Changing the endpoint relative permeability to water, $k_v=0.1k_h$ case. All other parameters are equal to those of the base case.

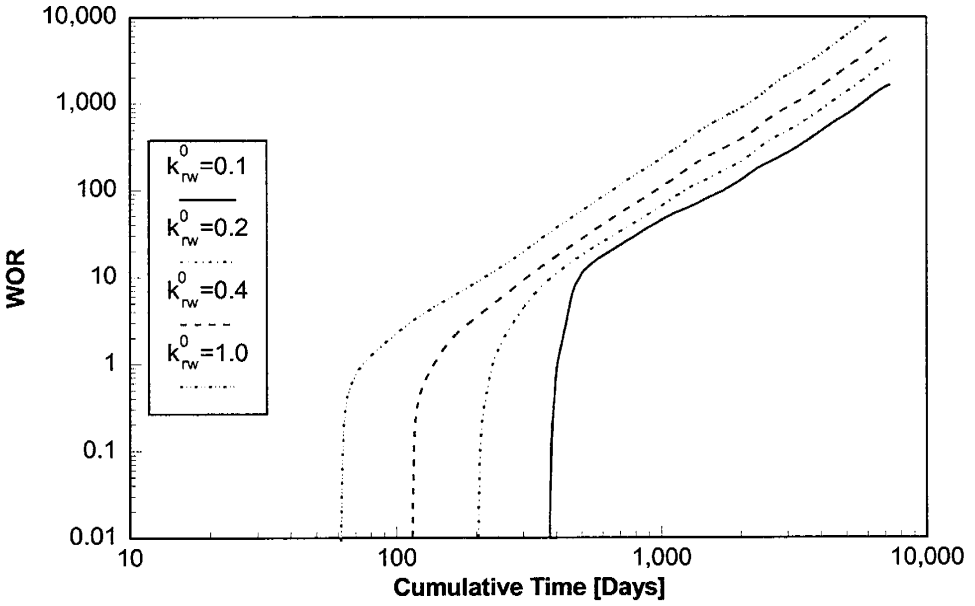

Fig. A.38. Changing the endpoint relative permeability to water, vertical equilibrium case. All other parameters are equal to those of the base case.

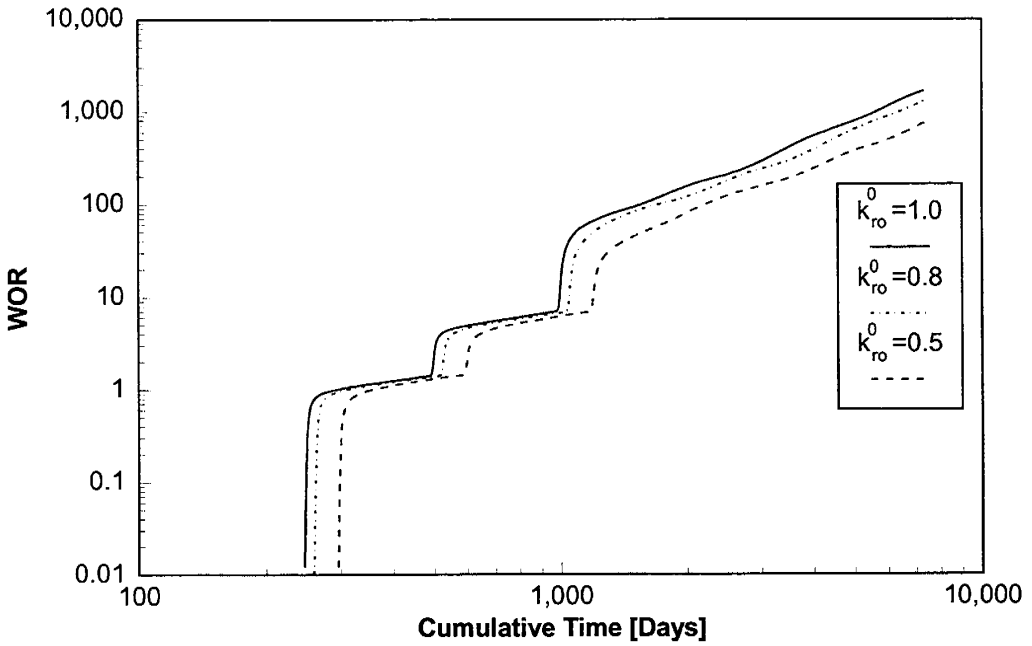

Fig. A.39. Changing the endpoint relative permeability to oil, no-crossflow case. All other parameters are equal to those of the base case.

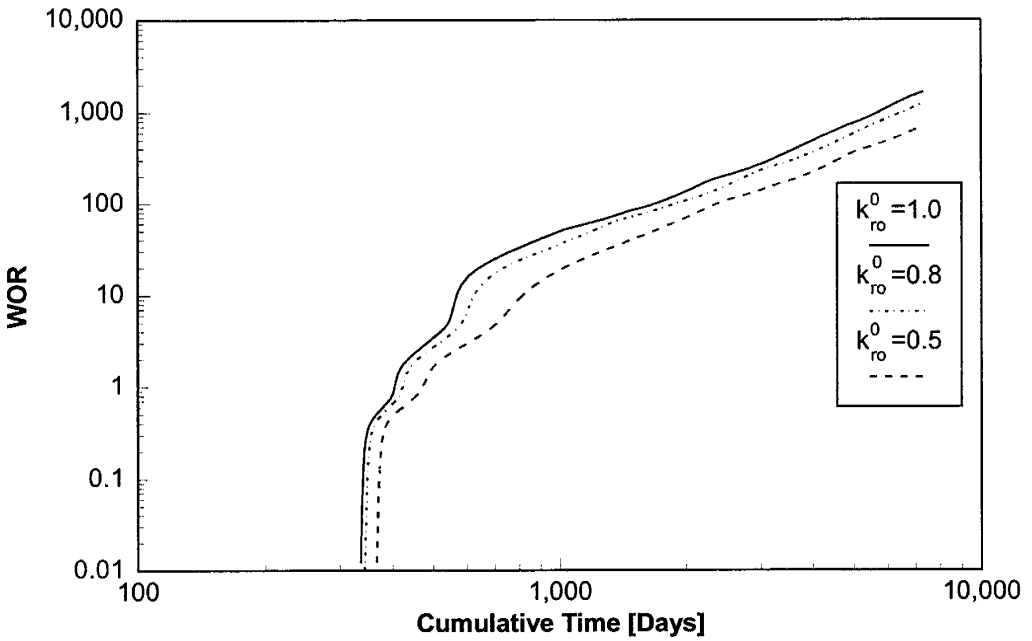

Fig. A.40. Changing the endpoint relative permeability to oil, $k_v=0.1k_h$ case. All other parameters are equal to those of the base case.

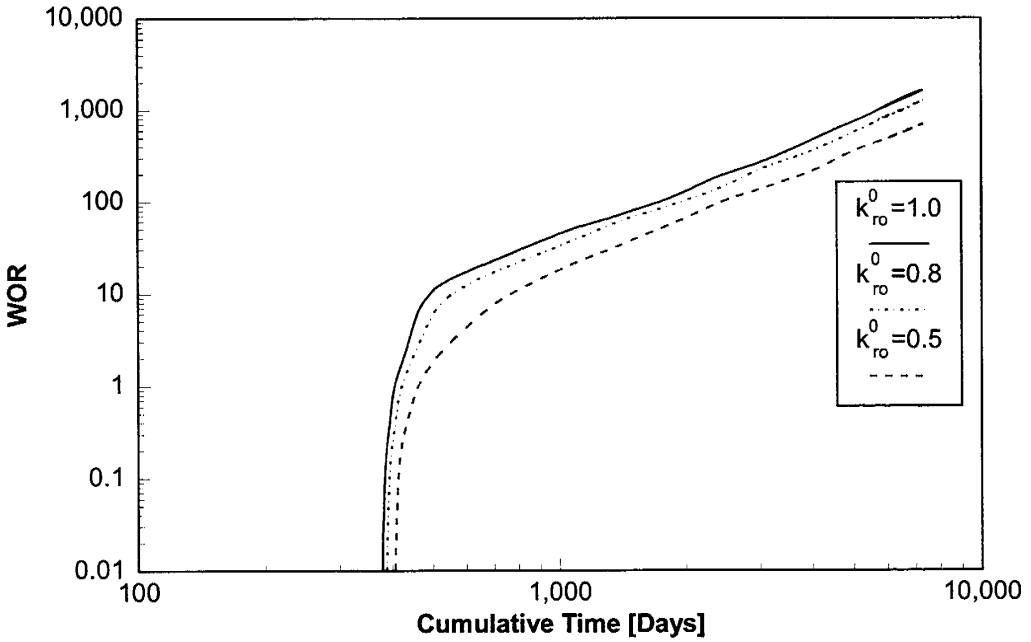

Fig. A-41. Changing the endpoint relative permeability to oil, vertical equilibrium case. All other parameters are equal to those of the base case.

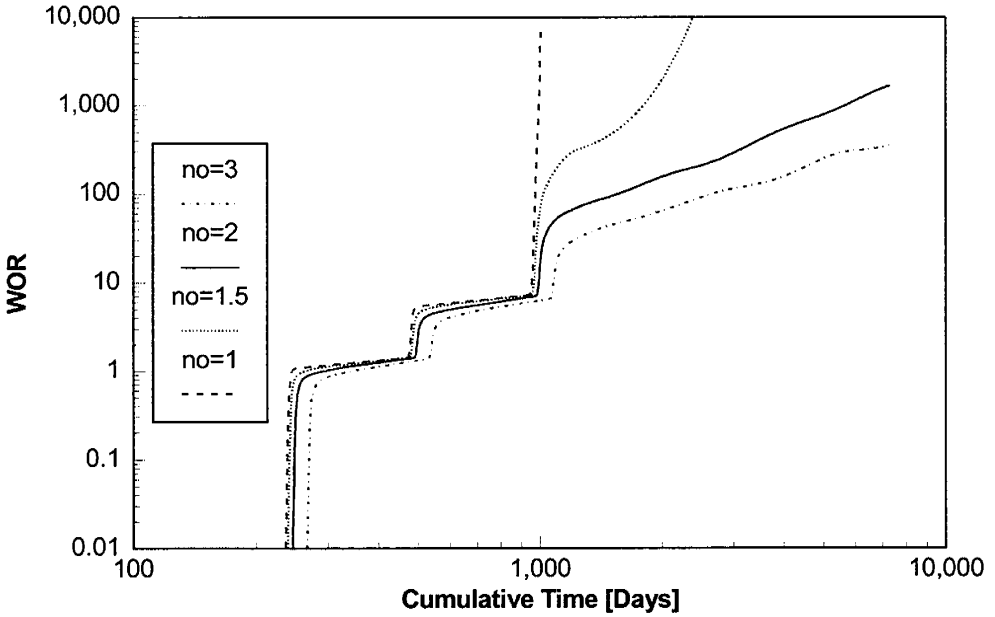

Fig. A.42. Changing the exponent for the oil relative permeability equation, no-crossflow case. All other parameters are equal to those of the base case.

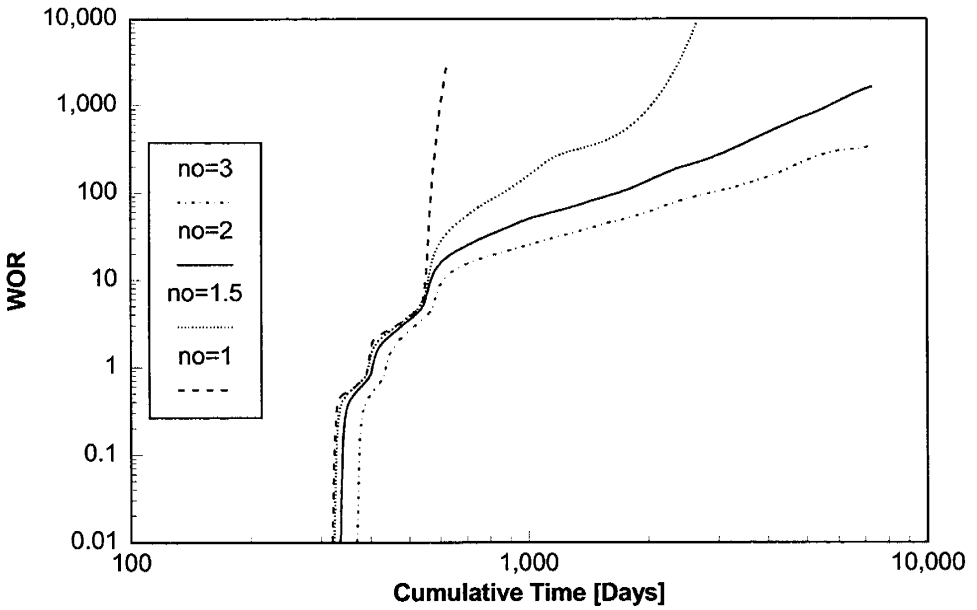

Fig. A.43. Changing the exponent for the water relative permeability equation, $k_v=0.1k_h$ case. All other parameters are equal to those of the base case.

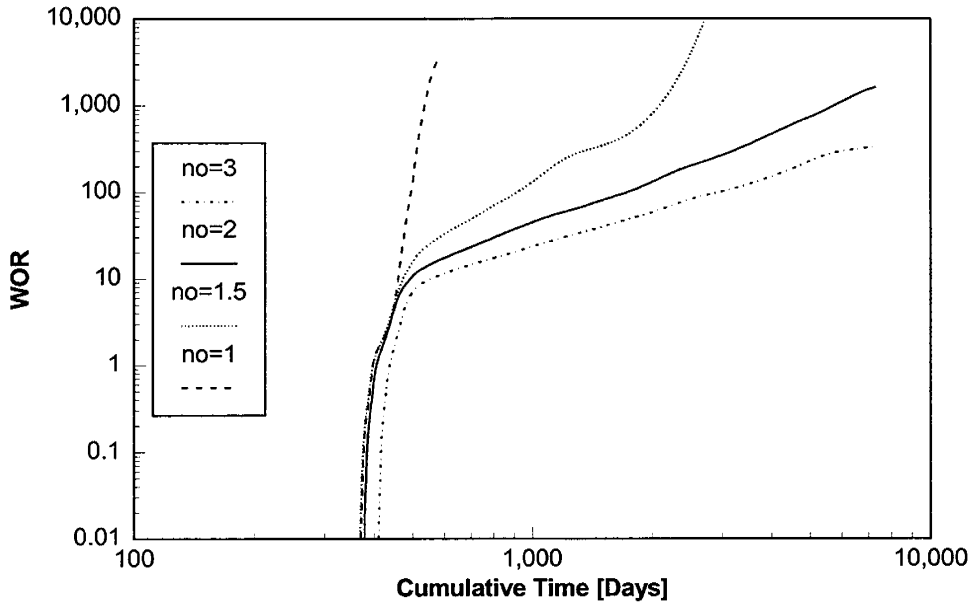

Fig. A-44. Changing the exponent for the water relative permeability equation, vertical equilibrium case. All other parameters are equal to those of the base case.

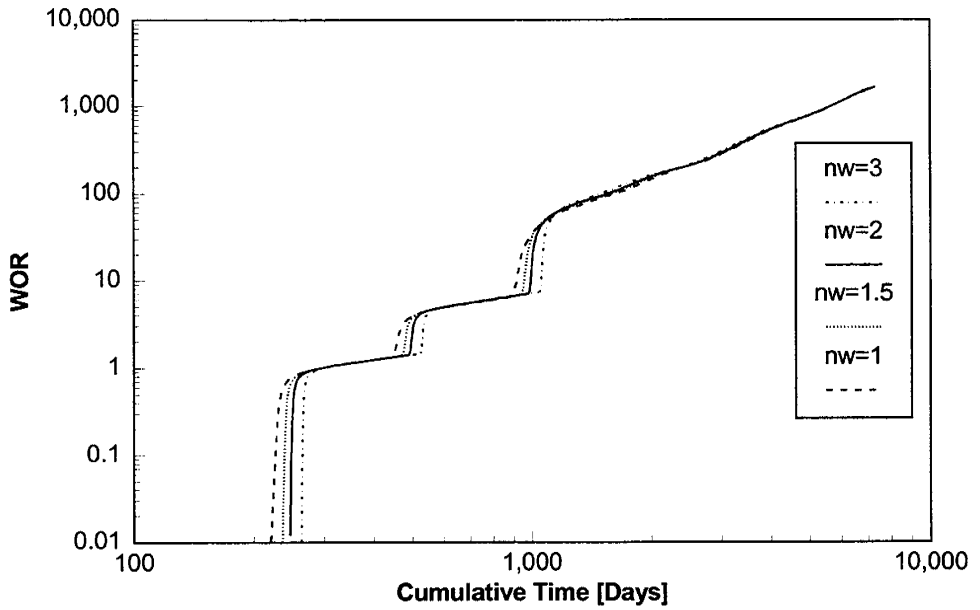

Fig. A.45. Changing the exponent for the water relative permeability equation, no-crossflow case. All other parameters are equal to those of the base case.

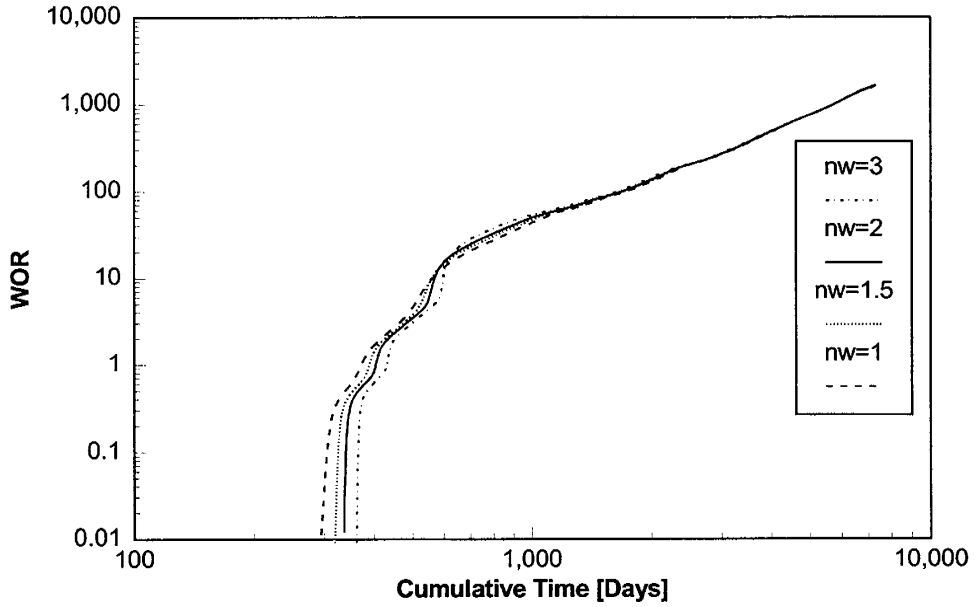

Fig. A.46. Changing the exponent for the water relative permeability equation, $k_v=0.1k_h$ case. All other parameters are equal to those of the base case.

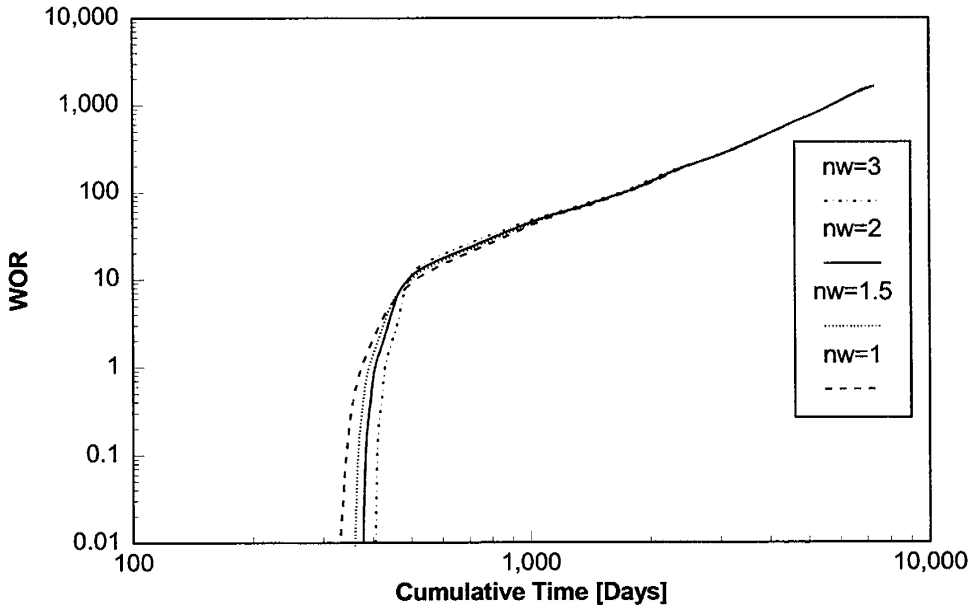

Fig. A.47. Changing the exponent for the water relative permeability equation, vertical equilibrium case. All other parameters are equal to those of the base case.

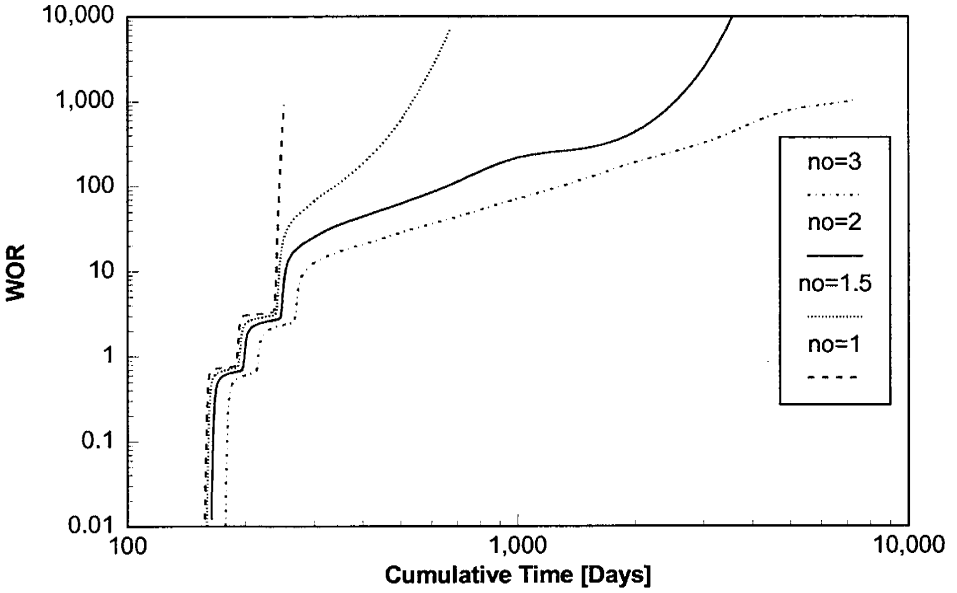

Fig. A.48. Changing the exponent of the oil relative permeability curve for layer permeabilities of 300, 250, and 200 md, no-crossflow case.

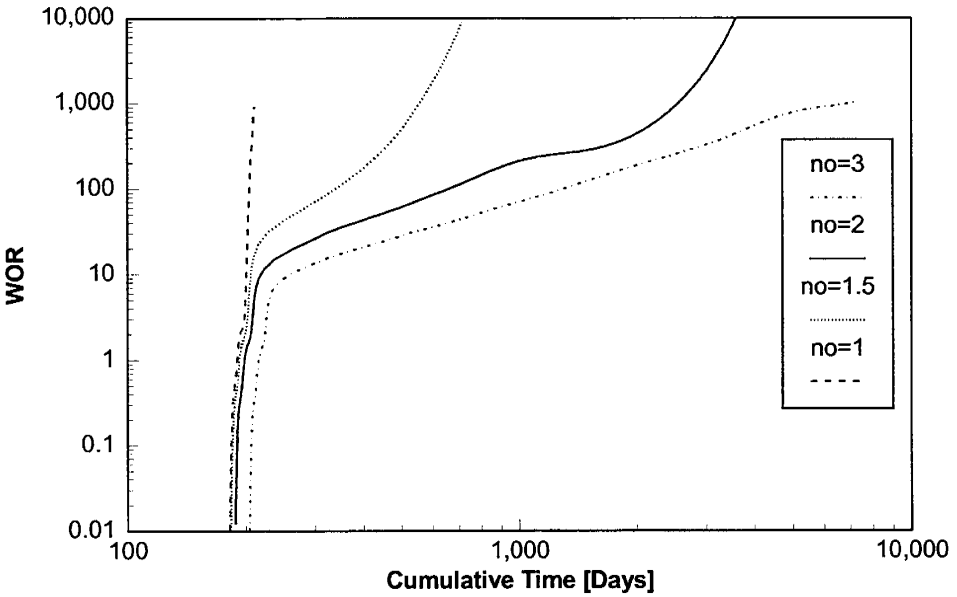

Fig. A.49. Changing the exponent of the oil relative permeability curve for layer permeabilities of 300, 250, and 200 md, $k_v=0.1k_h$ case.

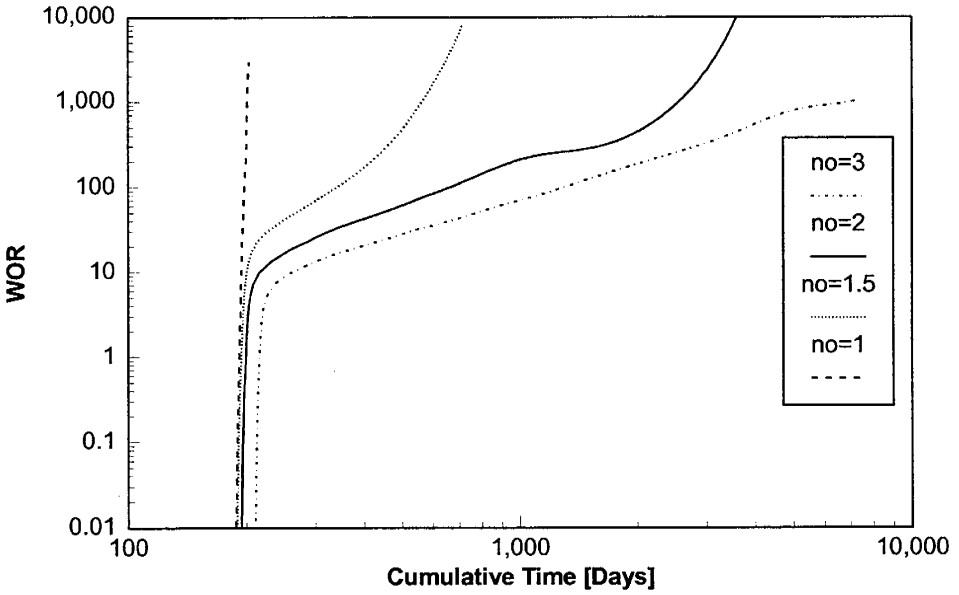

Fig. A.50. Changing the exponent of the oil relative permeability curve for layer permeabilities of 300, 250, and 200 md, k_v=k_h case.

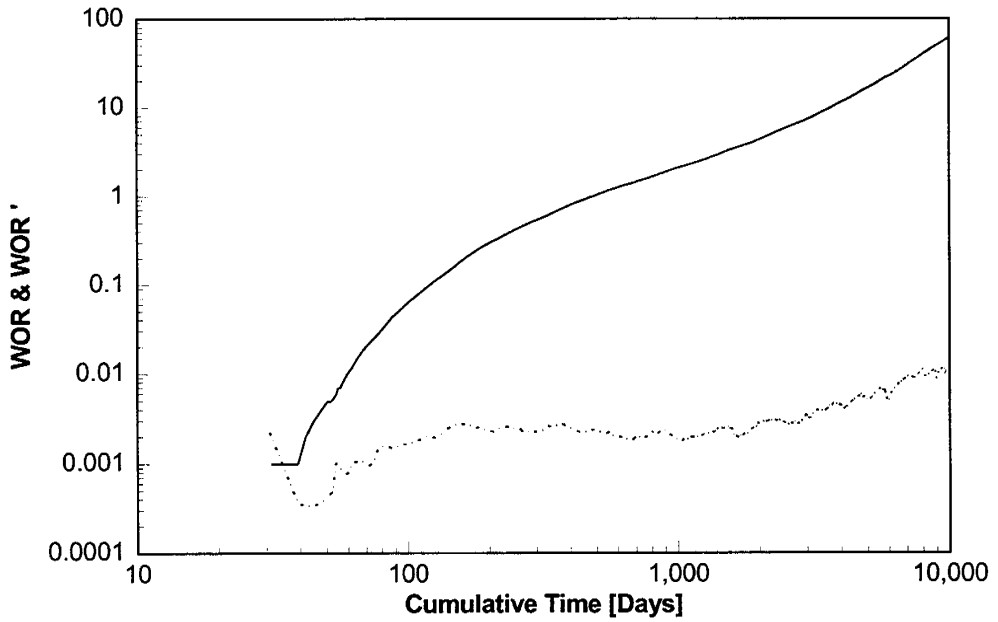

Fig. A.51. Diagnostic plot for the coning base case with 80-acre drainage area.

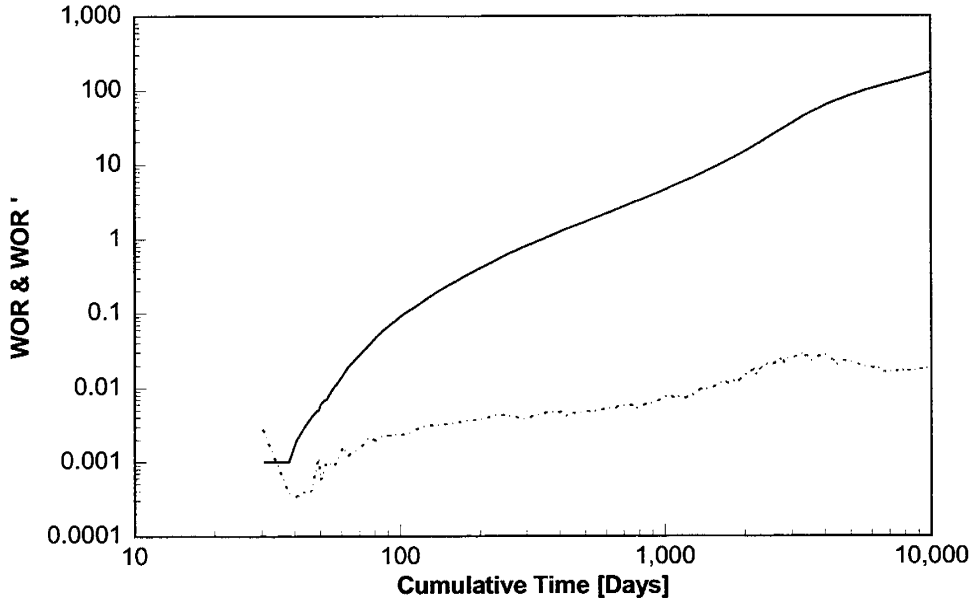

Fig. A.52. Diagnostic plot for the coning base case with 40-acre drainage area.

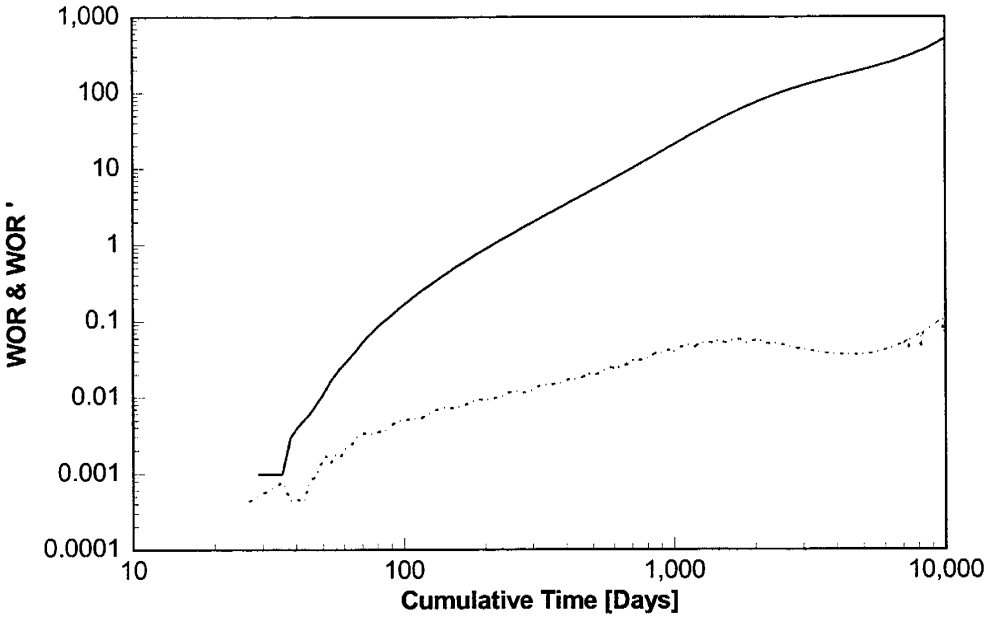

Fig. A.53. Diagnostic plot for the coning base case with 20-acre drainage area.

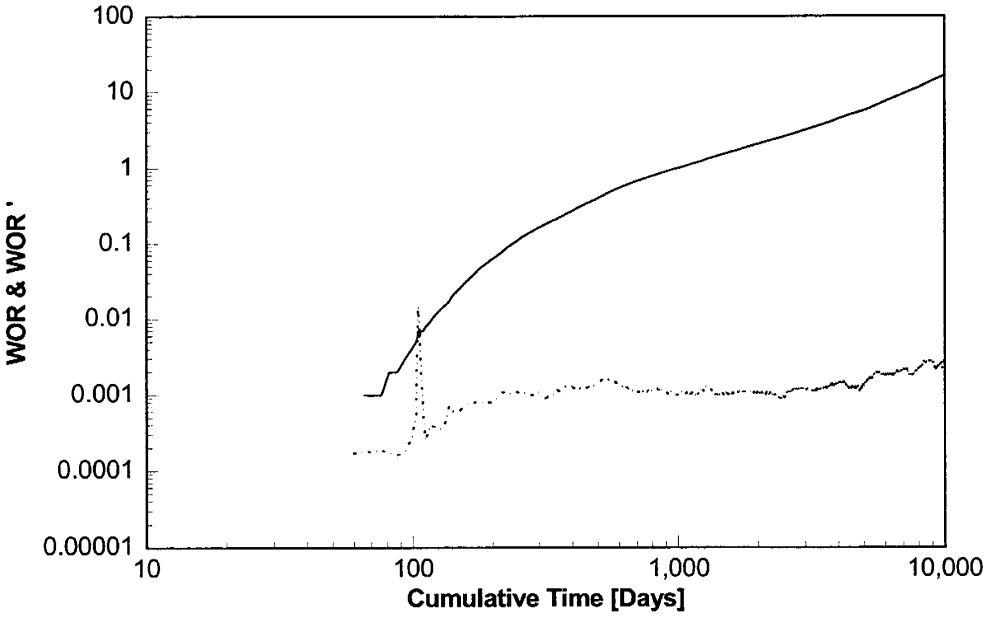

Fig. A.54. Diagnostic plot for the coning base case with $k_v=0.05k_h$.

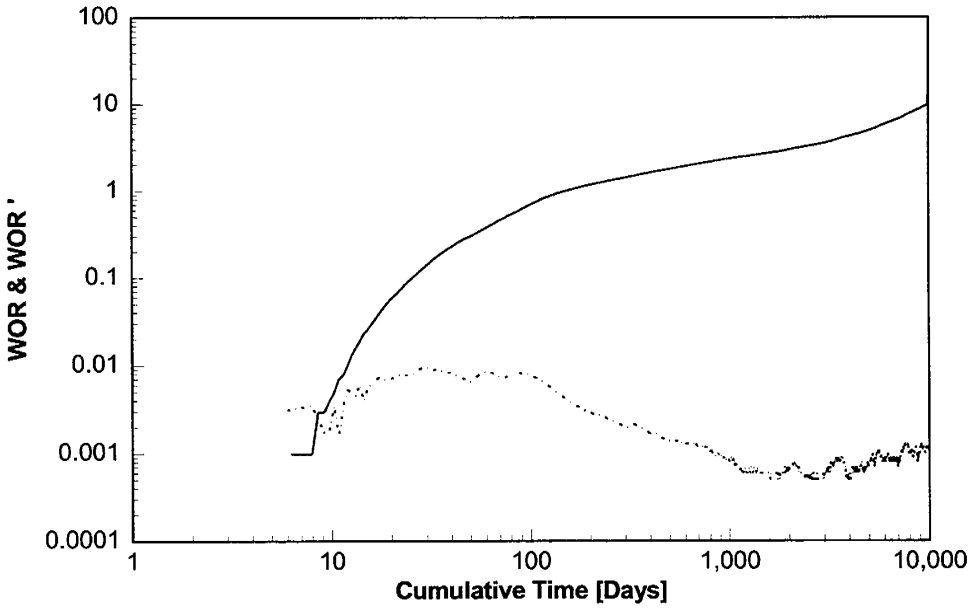

Fig. A.55. Diagnostic plot for the coning base case with $k_v=0.5k_h$.

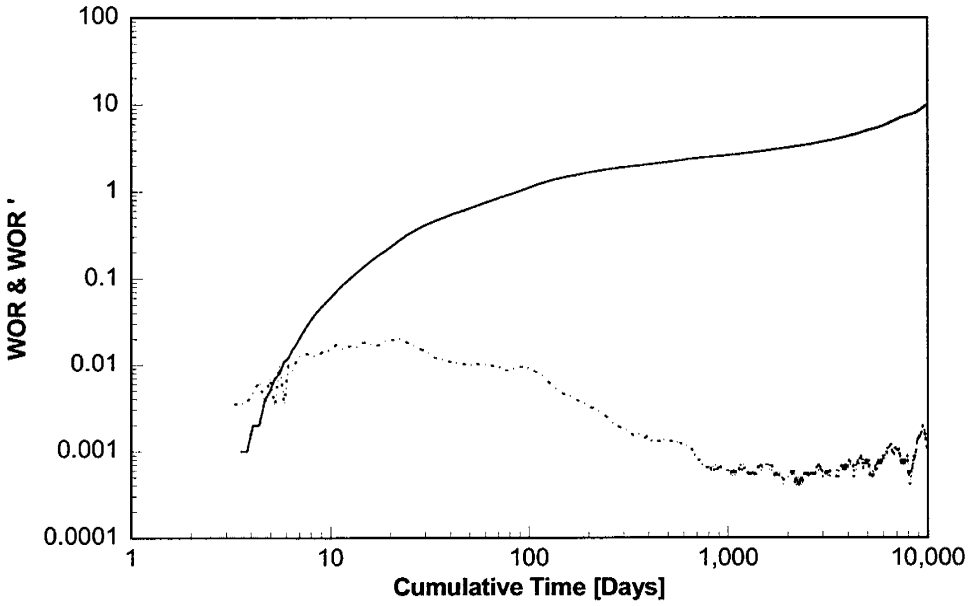

Fig. A.56. Diagnostic plot for base case with $k_v=k_h$.

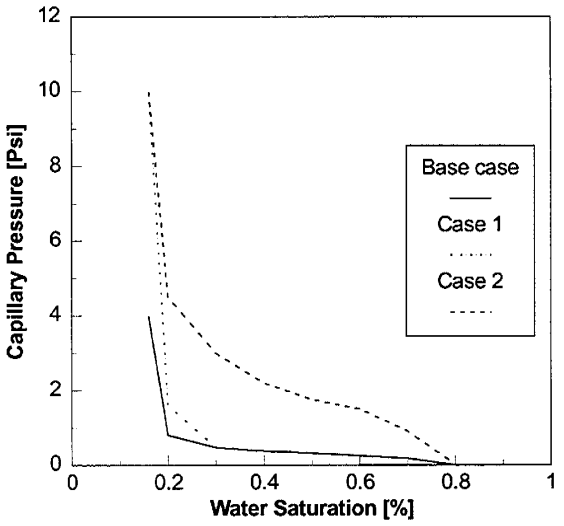

Fig. A.57. Capillary pressure curves corresponding to the cases shown in Fig. 29.

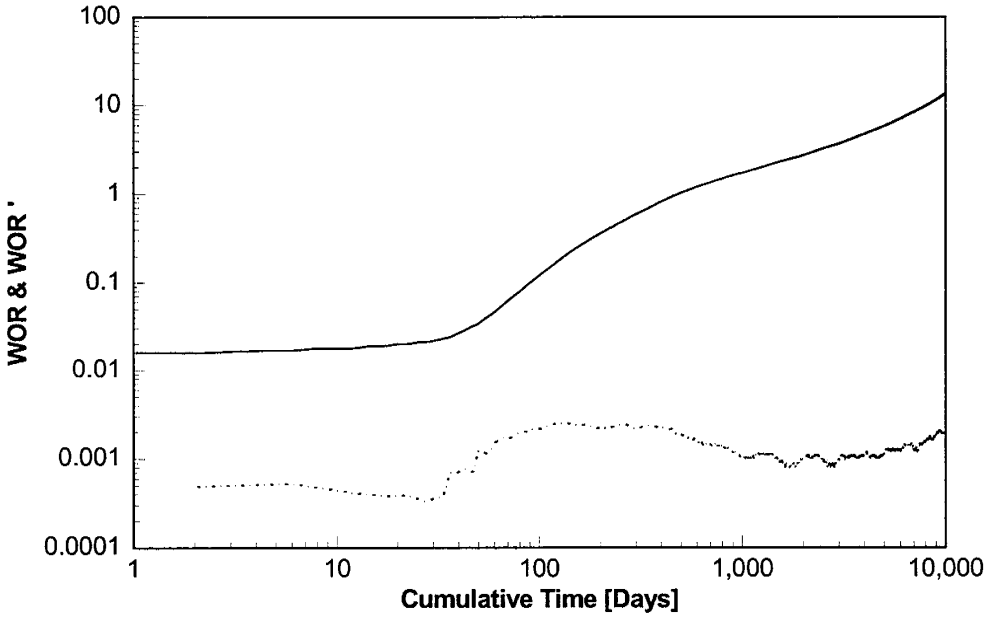

Fig. A.58. Diagnostic plot for base case with capillary pressure set 1.

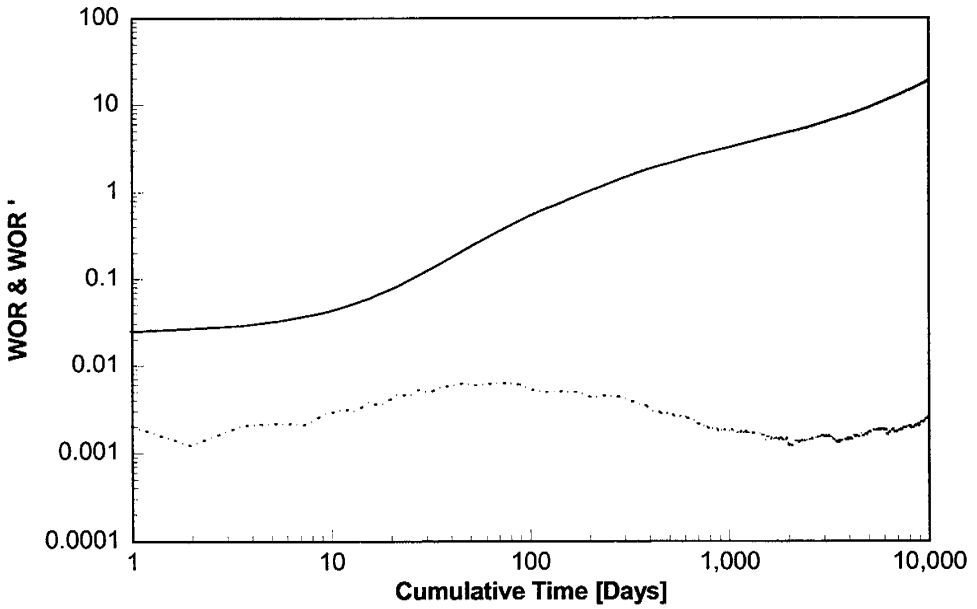

Fig. A.59. Diagnostic plot for base case with capillary pressure set 2.

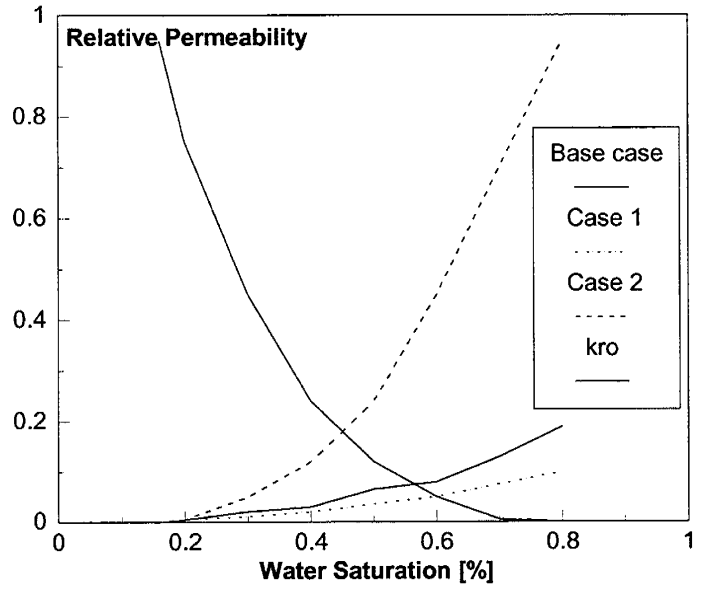

Fig. A.60. Different water relative permeability curves corresponding to the cases shown in Fig. 30. The oil relative permeability curve is kept unchanged.

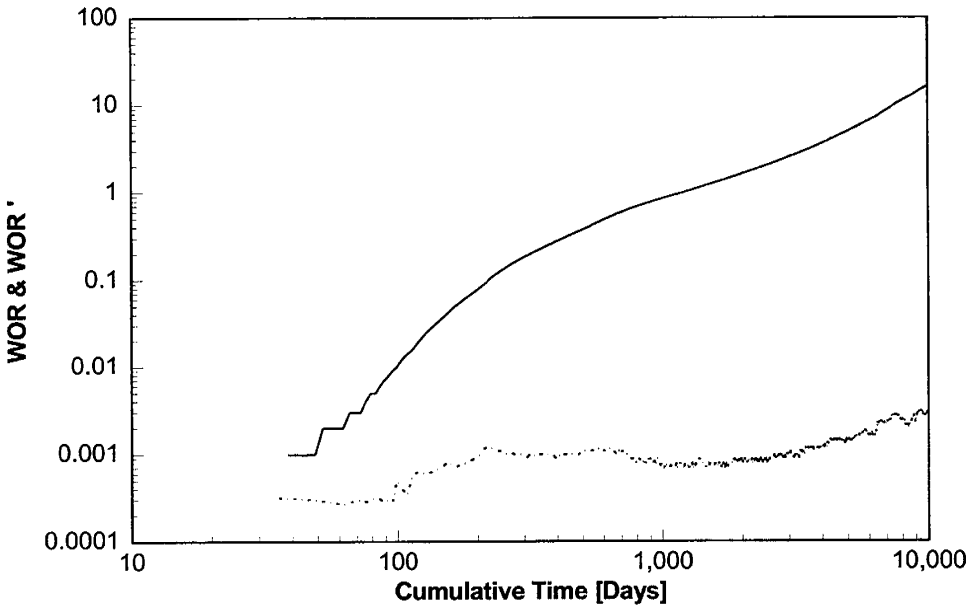

Fig. A.61. Diagnostic plot for base case with relative permeability set 1.

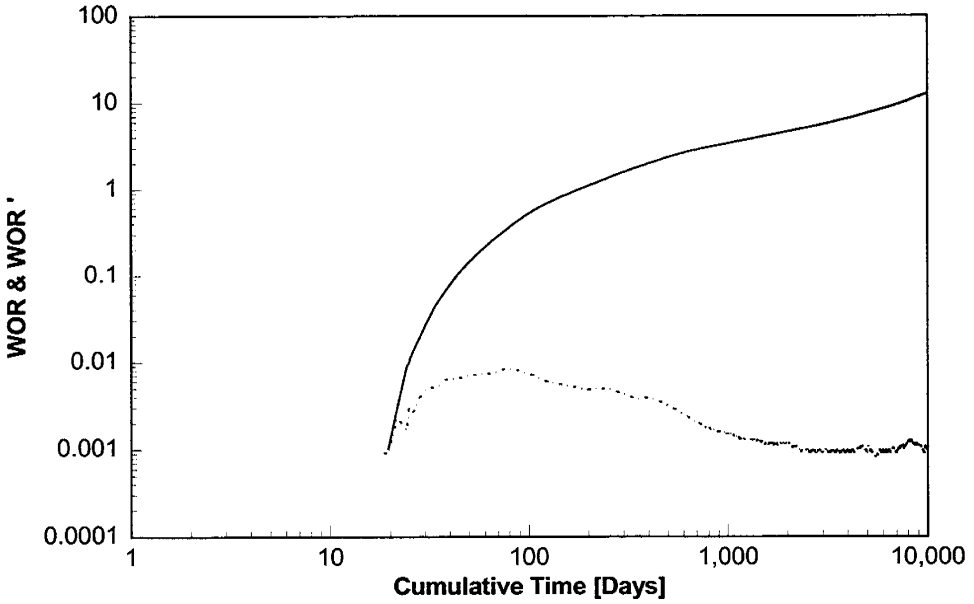

Fig. A.62. Diagnostic plot for base case with relative permeability set 2.

APPENDIX B: Derivation Supplement to Chapter 3

Derivation of Eq. 13.

How much gelant must be injected to reach a given distance along a fracture if the leakoff flux is independent of distance along the fracture?

The total injection rate equals the sum of leakoff over both faces of the fracture:

$$q_0 = 2\int_0^{h_f} \int_o^{L_f} u dL dh = 2uL_f h_f \tag{B1}$$

The rate of movement of the gelant front, dL/dt, is found from a mass balance:

$$h_f w_f \phi \frac{dL}{dt} = q_0 - 2uLh_f = 2u(L_f - L)h_f \tag{B2}$$

$$\frac{dL}{L_f - L} = \frac{2udt}{w_f \phi_f} \tag{B3}$$

Integrating the left side from 0 to L and the right side from 0 to t gives:

$$-\ln(L_f - L) - \ln(L_f) = \ln\left(\frac{L}{L_f - L}\right) = \frac{2ut}{h_f w_f \phi_f} = \frac{q_0 t}{h_f w_f \phi_f L_f} \tag{B4}$$

$$-\ln(1 - L/L_f) = V/V_f \tag{B5}$$

Eq. B5 is identical to Eq. 13 in Chapter 3.

Derivations of Eqs. 14, 15, 16, and 17.

If leakoff flux (u) is allowed to change with distance (L) along a fracture (of length, L_f, width, w_f, height, h_f, and permeability, k_f), what is the pressure (p), flow rate (q), and flux (u) as a function of L?

Let the pressure deep in the reservoir be p_e and the effective distance from the fracture to locations where $p=p_e$ is r_e. Each fracture has two faces. Matrix permeability is k_m. All fluids have the same mobility and viscosity (μ).

$$\frac{dp}{dL} = -\frac{q\mu}{k_f w_f h_f} = \frac{d(p-p_e)}{dL} \tag{B6}$$

$$\frac{dq}{dL} = -\frac{2h_f(p-p_e)k_m}{r_e\mu} \tag{B7}$$

Let $a = -2h_f k_m/(r_e\mu)$ and $b = -\mu/(k_f w_f h_f)$.

The general solution to this type of system of differential equations is given by Eqs. B8 and B9.[31]

$$p - p_e = c_1 A_1 e^{C_1 L} + c_2 B_1 e^{C_2 L} \tag{B8}$$

$$q = c_1 A_2 e^{C_1 L} + c_2 B_2 e^{C_2 L} \tag{B9}$$

Let's attempt a solution of the form:

$$p - p_e = Ae^{CL} \tag{B10}$$

$$q = Be^{CL} \tag{B11}$$

Substituting Eqs. B10 and B11 into Eqs. B6 and B7,

$$ACe^{CL} = bq = bBe^{CL} \tag{B12}$$

$$BCe^{CL} = a(p-p_e) = aAe^{CL} \tag{B13}$$

So,

$$AC = bB \text{ and } BC = aA \tag{B14}$$

$$AC = b(aA/C) \tag{B15}$$

$$C^2 = ab \tag{B16}$$

$$C = \pm\sqrt{ab} = \pm\sqrt{2k_m/(k_f w_f r_e)} \tag{B17}$$

Eq. B17 is equivalent to Eq. 15 in the report.

Let's call these roots C and -C.

Then, two possible solutions for A and B are

$$A = 1, \quad B = C/b \tag{B18}$$

and

$$A = 1, \quad B = -C/b \tag{B19}$$

Inserting Eqs. B18 and B19 into Eqs. B8 and B9 gives

$$p - p_e = c_1 e^{CL} + c_2 (C/b) e^{-CL} \tag{B20}$$

$$q = c_1 e^{CL} - c_2 (C/b) e^{-CL} \tag{B21}$$

Boundary conditions: At L=0, $p=p_w$ so

$$p - p_e = p_w - p_e = c_1 + c_2(C/b) \tag{B22}$$

At L=L_f, q=0, so

$$0 = c_1 e^{CL_f} - c_2(C/b)e^{-CL_f} \tag{B23}$$

$$c_2 = c_1(b/C)e^{2CL_f} \tag{B24}$$

Substituting Eq. B24 into Eq. B22 gives

$$c_1 = (p_w - p_e)/(1+e^{2CL_f}) \tag{B25}$$

and

$$c_2 = (b/C)(p_w - p_e)e^{2CL_f}/(1+e^{2CL_f}) \tag{B26}$$

So, Eqs. B20 and B21 become

$$\frac{p - p_e}{p_w - p_e} = \frac{e^{CL} + e^{2CL_f}e^{-CL}}{1+e^{2CL_f}} \tag{B27}$$

$$q = \frac{(p_w - p_e)[e^{CL} - e^{2CL_f}e^{-CL}]}{1+e^{2CL_f}} \tag{B28}$$

But

$$q_0 = \frac{(p_w - p_e)[1 - e^{2CL_f}]}{1+e^{2CL_f}} \tag{B29}$$

Dividing Eq. B28 by Eq. B29 gives Eq. B30.

$$\frac{q}{q_0} = \frac{[e^{CL} - e^{2CL_f}e^{-CL}]}{1-e^{2CL_f}} \tag{B30}$$

Now, let's find the leakoff flux, u, as a function of L. Start with a mass balance.

$$dq = -2uh_f dL \tag{B31}$$

We can also take the derivative of Eq. B30 with respect to L.

$$\frac{dq}{dL} = \frac{q_0 C[e^{CL} + e^{2CL_f}e^{-CL}]}{1-e^{2CL_f}} \tag{B32}$$

Combining Eqs. B31 and B32 gives Eq. B33

$$u = -\frac{q_0 C[e^{CL} + e^{2CL_f}e^{-CL}]}{2h_f(1-e^{2CL_f})} \tag{B33}$$

Eq. B33 is identical to Eq. 14 of Chapter 3.

At L=0, u=u_o.

$$u_0 = -\frac{q_0 C(1+e^{2CL_f})}{2h_f(1-e^{2CL_f})} \tag{B34}$$

Dividing Eq. B33 by Eq. B34 gives Eq. B35.

$$\frac{u}{u_0} = \frac{e^{CL} + e^{2CL_f}e^{-CL}}{1+e^{2CL_f}} \tag{B35}$$

Eq. B35 is identical to Eq. 16 of this report.

Now, let's determine L/L_f as a function of the volume of traced fluid that is injected. Again, start with a mass balance.

$$h_f w_f \frac{dL}{dt} = q_0 - 2\int_0^{h_f}\int_0^{L} u dL dh = q_0 - 2h_f \int_0^{L} u dL \tag{B36}$$

Combining Eqs. B33 and B36 gives Eq. B37.

$$h_f w_f \frac{dL}{dt} = q_0 + \frac{q_0 C}{1-e^{2CL_f}} \int_0^{L} [e^{CL} + e^{-CL} e^{2CL_f}] dL \tag{B37}$$

$$h_f w_f \frac{dL}{dt} = q_0 + \frac{q_0 C}{1-e^{2CL_f}} \left[\frac{e^{CL}}{C} - \frac{e^{-CL} e^{2CL_f}}{C} \right]_0^{L} \tag{B38}$$

$$h_f w_f \frac{dL}{dt} = q_0 + \frac{q_0}{1-e^{2CL_f}} [e^{CL} - e^{-CL} e^{2CL_f} - (1-e^{2CL_f})] \tag{B39}$$

$$\frac{h_f w_f}{q_0} \frac{dL}{dt} = 1 + \frac{e^{CL} - e^{-CL} e^{2CL_f}}{1-e^{2CL_f}} - 1 \tag{B40}$$

$$\frac{h_f w_f}{q_0} \frac{dL}{dt} = \frac{e^{CL} - e^{-CL} e^{2CL_f}}{1-e^{2CL_f}} \tag{B41}$$

$$\frac{dL}{e^{CL} - e^{-CL} e^{2CL_f}} = \frac{q_0 dt}{h_f w_f (1-e^{2CL_f})} \tag{B42}$$

The indefinite integral of Eq. B42 is given by Eq. B43.[32]

$$\frac{e^{-CL_f}}{2C} \ln\left[\frac{e^{CL_f} - e^{CL}}{e^{CL_f} + e^{CL}} \right] = \frac{q_0 t}{h_f w_f (1-e^{2CL_f})} \tag{B43}$$

Evaluating Eq. B43 between 0 and L gives Eq. B44.

$$\left[\frac{e^{-CL_f} - e^{CL_f}}{2C} \right] \ln\left[\left(\frac{e^{CL_f} - e^{CL}}{e^{CL_f} + e^{CL}} \right) \left(\frac{e^{CL_f} + 1}{e^{CL_f} - 1} \right) \right] = \frac{q_0 t}{h_f w_f} \tag{B44}$$

Dividing both sides of Eq. B44 by L_f gives Eq. B45.

$$\left[\frac{e^{-CL_f} - e^{CL_f}}{2CL_f} \right] \ln\left[\left(\frac{e^{CL_f} - e^{CL}}{e^{CL_f} + e^{CL}} \right) \left(\frac{e^{CL_f} + 1}{e^{CL_f} - 1} \right) \right] = \frac{q_0 t}{h_f w_f L_f} \tag{B45}$$

Realizing that $q_0 t$ is the total injection volume, V, and that $h_f w_f L_f$ is the fracture volume, V_f, leads to Eq. B46.

$$\frac{V}{V_f} = \left[\frac{e^{-CL_f} - e^{CL_f}}{2CL_f} \right] \ln\left[\left(\frac{e^{CL_f} - e^{CL}}{e^{CL_f} + e^{CL}} \right) \left(\frac{e^{CL_f} + 1}{e^{CL_f} - 1} \right) \right] \tag{B46}$$

Eq. B46 is identical to Eq. 17 in Chapter 3.

Derivations of Eqs. 18 and 19.

What if the gelant is more viscous than water (i.e., has a resistance factor of F_r)? Let L_p be the distance of gelant leakoff from the fracture at the distance, L, along the fracture.

$$\frac{dp}{dL} = -\frac{qF_r\mu_w}{k_f w_f h_f} = \frac{d(p-p_e)}{dL} \tag{B47}$$

$$\frac{dq}{dL} = -\frac{2h_f(p-p_e)k_m}{(r_e - L_p)\mu_w + F_r\mu_w L_p} \tag{B48}$$

From Eq. B17, Eq. B49 gives C, if F_r=1.

$$C = \sqrt{2k_m / (k_f w_f r_e)} \tag{B49}$$

However, if F_r>1, then C' is given by Eq. B50.

$$C' = \sqrt{\frac{2F_r k_m}{k_f w_f [(r_e - L_p) + F_r L_p]}} \tag{B50}$$

Eq. B50 is identical to Eq. 18 in Chapter 3.

Dividing Eq. B50 by Eq. B49 gives the term, C'/C.

$$\frac{C'}{C} = \sqrt{\frac{F_r r_e}{(r_e - L_p) + F_r L_p}} \tag{B51}$$

Eq. B51 is identical to Eq. 19 in this report.

Consideration of Eq. B51 reveals that increasing the resistance factor to 10 causes C'/C to increase from a value of 1 to a value of 3. Therefore, increased gelant viscosity or resistance factor has the effect of increasing C.

APPENDIX C: Fortran Program for Finding Pressures, Flow Rates, and Front Positions During a Unit-Mobility Displacement in a Simple Naturally Fractured Reservoir. Dispersion Not Included.

```
C
C .... program PROFILE 1/17/97
C
      PARAMETER (NCOL=11,NROW=2*(NCOL-1)+1)
      PARAMETER (NODE=NROW*NCOL)
      PARAMETER (OWELL=(NCOL*INT((NROW-1)/2)+1),PWELL=OWELL+NCOL-1)

      DIMENSION P2(NODE), P1(NODE)
      DIMENSION UXW(NODE), UXE(NODE), UYN(NODE), UYS(NODE)
      DIMENSION TSROW(NODE), TSCOL(NODE),DSROW(NROW),DSCOL(NCOL)
      DIMENSION DNCOL(NCOL),TNCOL(NODE),QRATIO(NROW)

          MIDROW=INT((NROW-1)/2+1)

          OPEN(61,FILE='OUT.DAT')
          DO 150 K=1,7
          IF (K.EQ.1) THEN
          WFXKX=0.1
          WFYKY=100.
          ELSEIF (K.EQ.2) THEN
          WFXKX=1.
          WFYKY=100.
          ELSEIF (K.EQ.3) THEN
          WFXKX=10.
          WFYKY=100.
          ELSEIF (K.EQ.4) THEN
          WFXKX=100.
          WFYKY=100.
          ELSEIF (K.EQ.5) THEN
          WFXKX=100.
          WFYKY=10.
          ELSEIF (K.EQ.6) THEN
          WFXKX=100.
          WFYKY=1.
          ELSEIF (K.EQ.7) THEN
          WFXKX=100.
          WFYKY=0.1
          ENDIF

       INDEX = 0
       DO 10 I = 1, NROW
       DO 10 J = 1, NCOL
       INDEX = INDEX + 1
```

```
      IF(J.EQ.1) THEN
       P1(INDEX) = 1000.0
       GOTO 10
      ENDIF
       P1(INDEX) = P1(INDEX-1)-1000./(NCOL-1)
10    CONTINUE
      P1(OWELL)  = 1000.0
      P1(PWELL) = 0.0
      R = WFXKX/WFYKY

      ITER = 0
1     CONTINUE
      ITER = ITER + 1
      WRITE(*,*) ' ITER = ', ITER

      H   = 1.0
      C1  = 6.3265
      XMU = 0.67
      DX  = 1000./(NCOL-1)
      DY  = 2000./(NROW-1)
      INDEX = 0
      DO 15 I  = 1, NROW
       DO 15 J = 1, NCOL
        INDEX = INDEX+1

        IF(INDEX.EQ.OWELL) THEN
         P2(INDEX) = 1000.0
         GOTO 15
        ELSEIF(INDEX.EQ.PWELL) THEN
         P2(INDEX) = 0.0
         GOTO 15
        ELSEIF(I.EQ.NROW .AND. J.EQ.1) THEN
         P2(INDEX) = R/(R+1)*P1(INDEX+1)+1./(R+1)*P1(INDEX-NCOL)
         GOTO 15
        ELSEIF(I.EQ.NROW .AND. J.EQ.NCOL) THEN
         P2(INDEX) = R/(R+1)*P1(INDEX-1)+1./(R+1)*P1(INDEX-NCOL)
         GOTO 15
        ELSEIF(I.EQ.1 .AND. J.EQ.NCOL) THEN
         P2(INDEX) = R/(R+1)*P1(INDEX-1)+1./(R+1)*P1(INDEX+NCOL)
         GOTO 15
        ELSEIF(I.EQ.1 .AND. J.EQ.1) THEN
         P2(INDEX) = R/(R+1)*P1(INDEX+1)+1./(R+1)*P1(INDEX+NCOL)
         GOTO 15
        ELSEIF(I.EQ.1) THEN
         P2(INDEX) = R/(2*R+1)*(P1(INDEX-1)+P1(INDEX+1))
     +           + 1/(2*R+1)*P1(INDEX+NCOL)
         GOTO 15
        ELSEIF(I.EQ.NROW) THEN
         P2(INDEX) = R/(2*R+1)*(P1(INDEX-1)+P1(INDEX+1))
```

```
     +          + 1/(2*R+1)*P1(INDEX-NCOL)
          GOTO 15
         ELSEIF(J.EQ.1) THEN
          P2(INDEX) = R/(R+2)*P1(INDEX+1)
     +          + 1/(R+2)*(P1(INDEX-NCOL)+P1(INDEX+NCOL))
          GOTO 15
         ELSEIF(J.EQ.NCOL) THEN
          P2(INDEX) = R/(R+2)*P1(INDEX-1)
     +          + 1/(R+2)*(P1(INDEX-NCOL)+P1(INDEX+NCOL))
          GOTO 15
         ENDIF

        P2(INDEX) = R/(2*R+2)*(P1(INDEX-1)+P1(INDEX+1))
     +        + 1/(2*R+2)*(P1(INDEX-NCOL)+P1(INDEX+NCOL))

15   CONTINUE

       DO 20 I = 1, NODE
        DIFF = ABS(P1(I)-P2(I))
         IF(DIFFGE.0.001) THEN
          DO 18 J = 1, NODE
          P1(J) = P2(J)
18         CONTINUE
          GOTO 1
         ENDIF
20   CONTINUE

       INDEX = 0
       DO 25 I  = 1, NROW
        DO 25 J = 1, NCOL
         INDEX = INDEX+1

          IF(I.EQ.NROW .AND. J.EQ.1) THEN
           UXW(INDEX) = 0.0
           UXE(INDEX) = C1*WFXKX*H/XMU*(P1(INDEX)-P1(INDEX+1))/DX
           UYS(INDEX) = 0.0
           UYN(INDEX) = C1*WFYKY*H/XMU*(P1(INDEX)-P1(INDEX-NCOL))/DY
           GOTO 25
               ENDIF
          IF(I.EQ.NROW .AND. J.EQ.NCOL) THEN
           UXW(INDEX) = C1*WFXKX*H/XMU*(P1(INDEX-1)-P1(INDEX))/DX
           UXE(INDEX) = 0.0
           UYS(INDEX) = 0.0
           UYN(INDEX) = C1*WFYKY*H/XMU*(P1(INDEX)-P1(INDEX-NCOL))/DY
           GOTO 25
          ENDIF
               IF(I.EQ.1 .AND. J.EQ.NCOL) THEN
           UXW(INDEX) = C1*WFXKX*H/XMU*(P1(INDEX-1)-P1(INDEX))/DX
           UXE(INDEX) = 0.0
```

```
      UYS(INDEX) = C1*WFYKY*H/XMU*(P1(INDEX)-P1(INDEX+NCOL))/DY
      UYN(INDEX) = 0.0
      GOTO 25
     ENDIF
         IF(I.EQ.1 .AND. J.EQ.1) THEN
      UXW(INDEX) = 0.0
      UXE(INDEX) = C1*WFXKX*H/XMU*(P1(INDEX)-P1(INDEX+1))/DX
      UYS(INDEX) = C1*WFYKY*H/XMU*(P1(INDEX)-P1(INDEX+NCOL))/DY
      UYN(INDEX) = 0.0
      GOTO 25
     ENDIF
         IF(I.EQ.1) THEN
      UXW(INDEX) = C1*WFXKX*H/XMU*(P1(INDEX-1)-P1(INDEX))/DX
      UXE(INDEX) = C1*WFXKX*H/XMU*(P1(INDEX)-P1(INDEX+1))/DX
      UYS(INDEX) = C1*WFYKY*H/XMU*(P1(INDEX)-P1(INDEX+NCOL))/DY
      UYN(INDEX) = 0.0
      GOTO 25
     ENDIF
         IF(J.EQ.1) THEN
      UXW(INDEX) = 0.0
      UXE(INDEX) = C1*WFXKX*H/XMU*(P1(INDEX)-P1(INDEX+1))/DX
      UYS(INDEX) = C1*WFYKY*H/XMU*(P1(INDEX)-P1(INDEX+NCOL))/DY
      UYN(INDEX) = C1*WFYKY*H/XMU*(P1(INDEX)-P1(INDEX-NCOL))/DY
      GOTO 25
     ENDIF
         IF(J.EQ.NCOL) THEN
      UXW(INDEX) = C1*WFXKX*H/XMU*(P1(INDEX-1)-P1(INDEX))/DX
      UXE(INDEX) = 0.0
      UYS(INDEX) = C1*WFYKY*H/XMU*(P1(INDEX)-P1(INDEX+NCOL))/DY
      UYN(INDEX) = C1*WFYKY*H/XMU*(P1(INDEX)-P1(INDEX-NCOL))/DY
      GOTO 25
     ENDIF
         IF(I.EQ.NROW) THEN
      UXW(INDEX) = C1*WFXKX*H/XMU*(P1(INDEX-1)-P1(INDEX))/DX
      UXE(INDEX) = C1*WFXKX*H/XMU*(P1(INDEX)-P1(INDEX+1))/DX
      UYS(INDEX) = 0.0
      UYN(INDEX) = C1*WFYKY*H/XMU*(P1(INDEX)-P1(INDEX-NCOL))/DY
      GOTO 25
     ENDIF

      UXW(INDEX) = C1*WFXKX*H/XMU*(P1(INDEX-1)-P1(INDEX))/DX
      UXE(INDEX) = C1*WFXKX*H/XMU*(P1(INDEX)-P1(INDEX+1))/DX
      UYS(INDEX) = C1*WFYKY*H/XMU*(P1(INDEX)-P1(INDEX+NCOL))/DY
      UYN(INDEX) = C1*WFYKY*H/XMU*(P1(INDEX)-P1(INDEX-NCOL))/DY

25  CONTINUE

        QTOT=0.0
        DENOM=UXE(NCOL*(MIDROW-1)+INT((NCOL-1)/2+1))
```

```
      DO 26 I=1,NROW
      QTOT=QTOT+UXE(2+(I-1)*NCOL)
      QRATIO(I)=UXE((I-1)*NCOL+INT((NCOL-1)/2+1))/DENOM
26    CONTINUE

      Q1REL=      DENOM/QTOT

   INDEX = 0
      TSHORT= 0.0
   DO 30 I  = 1, NROW
   DO 30 J = 1, NCOL
    INDEX = INDEX+1
      IF (UXE(INDEX).NE.0.) THEN
       TSROW(INDEX)=(DX*H*(5.03E-4)*(WFXKX**(1./3.))/UXE(INDEX))
      ENDIF
      IF (UYS(INDEX).NE.0.) THEN
       TSCOL(INDEX)=(DY*H*(5.03E-4)*(WFYKY**(1./3.))/UYS(INDEX))
      ENDIF
      IF (UYN(INDEX).NE.0.) THEN
       TNCOL(INDEX)=(DY*H*(5.03E-4)*(WFYKY**(1./3.))/UYN(INDEX))
      ENDIF

28    IF (I.EQ.MIDROW) THEN
       TSHORT=TSHORT+TSROW(INDEX)
      ENDIF
      IF (I.GE.MIDROW.AND.J.EQ.NCOL.AND.INDEX.LT.PWELL) THEN
       TSHORT=TSHORT+TSCOL(INDEX)
      ENDIF

30    CONTINUE

   TSHORT2=TSCOL(NCOL*(MIDROW-1)+1)+TNCOL(NCOL*(MIDROW+1))

      DO 31 J1=1,NCOL
            TSHORT2=TSHORT2+TSROW(NCOL*MIDROW+J1)

31          CONTINUE

   DO 40 J  = 1, NCOL
      DSCOL(J)=MIDROW
      TSTART=0.0
      IF (J.EQ.1) THEN
      GOTO 34
      ENDIF

      DO 33 I=1,J-1
       TSTART=TSTART+TSROW(I+NCOL*(MIDROW-1))
       IF (TSTART.GE.TSHORT) THEN
       GOTO 40
```

```
        ENDIF
33      CONTINUE

34      TCMIN=TSTART
       DO 38 I=MIDROW, NROW
        INDEX=J+(I-1)*NCOL
        IF (ABS(MIDROW-I).LT.(MIDROW-2).AND.TSCOL(INDEX).EQ.0.) THEN
        GOTO 40
        ENDIF
   IF (I.EQ.NROW.AND.TSCOL(INDEX).EQ.0.) THEN
        DSCOL(J)=NROW
        GOTO 40
   ENDIF
35      IF (TSCOL(INDEX).LT.0.) THEN
         GOTO 40
        ENDIF

              TCMAX=TCMIN+TSCOL(INDEX)

    IF (TCMAX.EQ.TSHORT) THEN
              DSCOL(J)=I
    ENDIF
               IF (TCMAX.GT.TSHORT) THEN
              DSCOL(J)=I+(TSHORT-TCMIN)/TSCOL(INDEX)
        GOTO 40
              ENDIF
              IF (TCMAX.LE.TSHORT) THEN
         TCMIN=TCMAX
         DSCOL(J)=I
         GOTO 38
              ENDIF

38            CONTINUE
40            CONTINUE

   DO 50 J  = 1, NCOL
        DNCOL(J)=MIDROW
        TSTART=0.0
        IF (J.EQ.1) THEN
        GOTO 44
        ENDIF

       DO 43 I=1,J-1
        TSTART=TSTART+TSROW(I+NCOL*(MIDROW-1))
        IF (TSTART.GE.TSHORT) THEN
        GOTO 50
        ENDIF
43      CONTINUE
```

```
44      TCMIN=TSTART
        DO 48 I=MIDROW, 1,-1
         INDEX=J+(I-1)*NCOL
        IF (I.LT.2.AND.TNCOL(INDEX).EQ.0.) THEN
         GOTO 50
        ENDIF
        IF (I.EQ.1.AND.TNCOL(INDEX).EQ.0.) THEN
         DNCOL(J)=1
         GOTO 50
        ENDIF
45      IF (TNCOL(INDEX).LE.0.) THEN
          GOTO 50
        ENDIF

         TCMAX=TCMIN+TNCOL(INDEX)

    IF (TCMAX.EQ.TSHORT) THEN
                DNCOL(J)=I
    ENDIF
        IF (TCMAX.GT.TSHORT) THEN
                DNCOL(J)=I-(TSHORT-TCMIN)/TNCOL(INDEX)
         GOTO 50
        ENDIF
        IF (TCMAX.LE.TSHORT) THEN
          TCMIN=TCMAX
          DNCOL(J)=I
          GOTO 48
        ENDIF

48      CONTINUE
50      CONTINUE

   DO 60 J  = 1, NROW
         DSROW(J)=1.0
         TSTART=0.0
        IF (J.EQ.MIDROW) THEN
         GOTO 54
        ENDIF
        IF (J.LT.MIDROW) THEN
         DO 52 I=MIDROW,J,-1
         TSTART=TSTART+TNCOL((I-1)*NCOL+1)
          IF (TSTART.GE.TSHORT) THEN
           GOTO 60
          ENDIF
52       CONTINUE
        ENDIF
        IF (J.GT.MIDROW) THEN
        DO 53 I=MIDROW,J
         TSTART=TSTART+TSCOL((I-1)*NCOL+1)
```

```
          IF (TSTART.GE.TSHORT) THEN
           GOTO 60
          ENDIF
53        CONTINUE
         ENDIF

54        TRMIN=TSTART

         DO 58 I=1, NCOL
          INDEX=I+(J-1)*NCOL
          IF (I.EQ.NCOL.AND.TSROW(INDEX).EQ.0.) THEN
                DSROW(J)=NCOL
            GOTO 60
          ENDIF
          IF (TSROW(INDEX).LT.0.) THEN
            GOTO 60
          ENDIF

          TRMAX=TRMIN+TSROW(INDEX)

     IF (TRMAX.EQ.TSHORT) THEN
                DSROW(J)=I
     ENDIF
          IF (TRMAX.GT.TSHORT) THEN
                DSROW(J)=I+(TSHORT-TRMIN)/TSROW(INDEX)
          GOTO 60
          ENDIF
          IF (TRMAX.LE.TSHORT) THEN
            TRMIN=TRMAX
            GOTO 58
          ENDIF

58        CONTINUE
60        CONTINUE

     WRITE(*,*) ' **** DATA IN FILE, OUT.DAT **** '
          WRITE(61,*)
          WRITE(61,*)
          WRITE(61,*)

          WRITE(61,95) NCOL,NROW
95        FORMAT(15X,'1000 ft x 2000 ft, MU=1, FRACTURE GRID=',I3,' x',I3)
     WRITE(61,100) R, OWELL, PWELL, WFXKX, DX, WFYKY, DY, TSHORT,
    + TSHORT2, QTOT


100  FORMAT(15X,'R=WfxKx/WfyKy=',F8.3,2X,'IWELL=',F5.0,2X,'PWELL=',F5.0,
    +     /15X,'Kfx Wx (darcy-ft)=', F7.1,',  Dx (ft) = ', F7.1,
    +     /15X,'Kfy Wy (darcy-ft)=', F7.1,',  Dy (ft) = ', F7.1,
```

```
     +      /15X,'Transit time (days)=',F10.5,' 2ND TIME (days)=',F10.5,
     +      /15X,'Qtot (ft3/d)=',F10.3)
            WRITE(61,*)
            WRITE(61,*)

            WRITE(61,*) '        QTOT    QMID/  QMID-1  QMID+1',
            +' QTOP  QBOT  Q(1/4)  Q(3/4)'
            WRITE(61,*) '        ft3/d   QTOT   /QMID   /QMID',
            +' /QMID  /QMID   /QMID   /QMID'

            WRITE(61,147) QTOT,Q1REL,QRATIO(MIDROW-1),QRATIO(MIDROW+1),
            +QRATIO(1),QRATIO(NROW),QRATIO(MIDROW-INT(MIDROW/2)),
     +QRATIO(MIDROW+INT(MIDROW/2))

147         FORMAT(7X,F10.2,3(2X,F7.3),1X,F7.3,1X,F7.3,2X,F7.3,2X,F7.3)
            WRITE(61,*)
            WRITE(61,*)


       WRITE(61,*)'     ********** GELANT FRONT **********'
            WRITE(61,*)
       WRITE(61,*)'     *EAST ROW ****** SOUTH COLUMN **** NORTH COLUMN'
            WRITE(61,*)'     X     Y     X     Y      X     Y'
            DO 120 J=1,NCOL
       WRITE(61,130) DSROW(J),J,J,DSCOL(J),J,DNCOL(J)
120         CONTINUE
130         FORMAT(6X,F7.3,2X,I3,5X,I3,5X,F7.3,4X,I3,5X,F7.3)
            DO 140 J=NCOL+1,NROW
       WRITE(61,145) DSROW(J),J
140         CONTINUE
145         FORMAT(6X,F7.3,2X,I3)


            WRITE(61,*)
            WRITE(61,*)
            WRITE(61,*)


150         CONTINUE
       STOP
       END
```

APPENDIX D: Fortran Program for Finding Pressures, Flow Rates, and Front Positions During a Unit-Mobility Displacement in a Simple Naturally Fractured Reservoir. Dispersion Included at the Rear but not the Front of the Tracer Bank.

```
PROGRAM FRAC1121
    INCLUDE 'INFRAC1.FOR'

C .... authors: Robert Lee & Randy Seright

C .... it should be noted that, W: injection fluid

    CALL DATAIN
    CALL WIP
    CALL GIP

    OWGIP  = CWIP+CGIP
    IPRINT  = 0
        ISWITCH = 1
    IDT    = 0
    INDEXP = 0
        TTOTAL = 0.0

        WRITE(*,*) '*** PVINJMAX = '
        READ (*,*) PVINJMAX

    DO 100 I = 1, ITMAX

    IF(IDT.EQ.1)   DT = 1.2*DT
    IF(IDT.EQ.-1)  DT = 0.8*DT
    IF(DT.GE.DTMAX) DT = DTMAX

    IDT = 0
    INDEXP = INDEXP+1
        TTOTAL = TTOTAL + DT

    IF(INDEXP.EQ.1000) THEN
         WRITE(*,*) '*** I,DT,PVINJ  = ', I, DT, PVINJ
         WRITE(*,*) '*** ISWITCH (1/0)= ', ISWITCH
         WRITE(*,*) '*** PVINJMAX    = ', PVINJMAX
         IF(ISWITCH.EQ.1) THEN
          WRITE(*,*) '*** not breakthru yet *** '
      WRITE(*,*) 'CTW2(IINJ+1)  = ', CTW2(IINJ+1)
          WRITE(*,*) 'CTW2(NBT1)   = ', CTW2(NBT1)
          WRITE(*,*) 'SW2 (NBT1)   = ', SW2 (NBT1)
         ENDIF
         IF(ISWITCH.EQ.0) THEN
          WRITE(*,*) '*** breakthru *** '
```

```
      WRITE(*,*) 'CT2(IINJ+1) = ', CT2(IINJ+1)
           WRITE(*,*) 'CT2(NBT1)  = ', CT2(NBT1)
           WRITE(*,*) 'SW2(NBT1)  = ', SW2(NBT1)
          ENDIF
     INDEXP = 0
    ENDIF

    IF(PVINJ.GT.PVINJMAX) THEN
          WRITE(*,*) '*** stop at PVINJMAX = ', PVINJMAX
          WRITE(*,*) '*** enter 1 to stop  = '
          READ (*,*) ISTOP
          IF(ISTOP.EQ.1) STOP
         ENDIF

    CALL PREXY

          IF(NROW.GT.9) GOTO 555
          IF(I.EQ.1) THEN
           WRITE(*,*) '*** Do you want to see the transmissibility? '
           WRITE(*,*) '*** 0/1 no/yes = '
           READ (*,*) ISEE
           IF(ISEE.EQ.0) GOTO 555
          ELSE
           GOTO 555
          ENDIF

          WRITE(*,*) '*** GTW+WTW ***'
          DO 51 IK = 1, NROW
51       WRITE(*,605)
     &   (GTW((IK-1)*NCOL+J)+WTW((IK-1)*NCOL+J),J=1,NCOL)
     WRITE(*,*) '*** 0/1 continue/stop = '
          READ (*,*) ISTOP
          IF(ISTOP.EQ.1) STOP

          WRITE(*,*) '*** GTE+WTE ***'
          DO 52 IK = 1, NROW
52       WRITE(*,605)
     &   (GTE((IK-1)*NCOL+J)+WTE((IK-1)*NCOL+J),J=1,NCOL)
     WRITE(*,*) '*** 0/1 continue/stop = '
          READ (*,*) ISTOP
          IF(ISTOP.EQ.1) STOP

          WRITE(*,*) '*** GTS+WTS ***'
          DO 53 IK = 1, NROW
53       WRITE(*,605)
     &   (GTS((IK-1)*NCOL+J)+WTS((IK-1)*NCOL+J),J=1,NCOL)
     WRITE(*,*) '*** 0/1 continue/stop = '
          READ (*,*) ISTOP
          IF(ISTOP.EQ.1) STOP
```

```
      WRITE(*,*) '*** GTN+WTN ***'
      DO 54 IK = 1, NROW
54    WRITE(*,605)
     & (GTN((IK-1)*NCOL+J)+WTN((IK-1)*NCOL+J),J=1,NCOL)
      WRITE(*,*) '*** 0/1 continue/stop = '
      READ (*,*) ISTOP
      IF(ISTOP.EQ.1) STOP

555   CONTINUE

      CALL SWEEP

      IF(NROW.GT.9) GOTO 666
      IF(I.EQ.1) THEN
       WRITE(*,*) '*** Do you want to see the initial pressure? '
       WRITE(*,*) '*** 0/1 no/yes = '
       READ (*,*) ISEE
       IF(ISEE.EQ.0) GOTO 666
      ELSE
       GOTO 666
      ENDIF

      WRITE(*,*) '*** P2 ***'
      DO 55 IK = 1, NROW
55    WRITE(*,605) (P2((IK-1)*NCOL+J),J=1,NCOL)
605     FORMAT(9(1X,F7.3))
      WRITE(*,*) '*** 0/1 continue/stop = '
      READ (*,*) ISTOP
      IF(ISTOP.EQ.1) STOP

666  CONTINUE

      CALL SAT(IDT)

      IF(NROW.GT.9) GOTO 777
      IF(I.EQ.1) THEN
       WRITE(*,*) '*** Do you want to see the initial saturation? '
       WRITE(*,*) '*** 0/1 no/yes = '
       READ (*,*) ISEE
       IF(ISEE.EQ.0) GOTO 777
      ELSE
       GOTO 777
      ENDIF

      WRITE(*,*) '*** SP *** '
      DO 56 IK = 1, NROW
56    WRITE(*,605) (SW2((IK-1)*NCOL+J),J=1,NCOL)
      WRITE(*,*) '*** 0/1 continue/stop = '
```

```
        READ (*,*) ISTOP
        IF(ISTOP.EQ.1) STOP

777  CONTINUE

        IF(I.EQ.1) WRITE(*,*) '*** program is running, GOOD LUCK!! ***'

    CALL PVINJE(IPRINT)

C
C .... NBT means Break Through Node
C .... NBT1,NBT2 are input variables
C
        IF(ISWITCH.EQ.0) GOTO 102
        IF(SW2(NBT1).GT.0.999 .OR. SW2(NBT2).GT.0.999) THEN
         CALL PRINT
         WRITE(*,*)  '*** BREAKTHRU *** '
         WRITE(61,*)
         WRITE(61,*)
         WRITE(61,*) '*** BREAKTHRU *** '
         DO 61 J = 1, NODE
          CT1(J) = CTW1(J)*SW1(J)
61       CONTINUE
         ISWITCH = 0
         IPRINT = 0
         PVTP1 = PVINJ
         PVTP2 = PVINJ + 0.1
         DPV   = (PVTP2-PVTP1)/10.
         PVINJMAX = PVTP2
         PVPRINT = PVINJ+DPV
     WRITE(*,*) '*** printout,OUT96.DAT *** '
        ENDIF
102  CONTINUE

    IF(IPRINT.EQ.1) THEN
     CALL PRINT
     IPRINT = 0
     WRITE(*,*) '*** printout,OUT96.DAT *** '
    ENDIF

100  CONTINUE

    STOP
    END
***
    SUBROUTINE DATAIN
    INCLUDE 'INFRAC1.FOR'

    OPEN(51,FILE='DATAF1.DAT')
```

```
      OPEN(61,FILE='FRACOUT.DAT')

      READ(51,*) ICASE, ITMAX, ITRACER
           IF(ITRACER.EQ.1) THEN
            WRITE(61,*) '*** TRACER CASE *** '
            WRITE(*,*)  '*** TRACER CASE *** '
           ENDIF
      WRITE(*,*) '*** PLEASE ENTER CASE NO. *** '
      READ (*,*) ICASE
      READ(51,*) XKFWF, YKFWF, XPORO, XSWI
      READ(51,*) DT, DTMAX
      READ(51,*) PVPRINT, DPV
      READ(51,*)
      READ(51,*)
      READ(51,*) VISW, VISG
      READ(51,*) RESOL
      READ(51,*)
      READ(51,*) PINJ, PPRO
      READ(51,*) IINJ, IPRO
           READ(51,*) NBT1, NBT2
           READ(51,*) PVTRACER, PVTP1, PVTP2
           READ(51,*)
           READ(51,*)
           READ(51,*)

      READ(51,*)
      READ(51,*)
      READ(51,*)
      READ(51,*)
      READ(51,*)
      READ(51,*)
      READ(51,*)

      DO 5 I = 1, NODE
       READ(51,*) INODE, IYXM(I), DX(I), DY(I), KROW
5     CONTINUE

C
C .... convert field units to Darcy's units
C

       WFXFT = 5.03E-4*(XKFWF/30.48)**(1./3.)
       WFXCM = 30.48*WFXFT
       XKF   = XKFWF/WFXCM
       WFYFT = 5.03E-4*(YKFWF/30.48)**(1./3.)
       WFYCM = 30.48*WFYFT
       YKF   = YKFWF/WFYCM

           WRITE(*,*)
```

```
      WRITE(*,*) 'WKFWF (ft darcy) = ', XKFWF/30.48
      WRITE(*,*) 'XKF   (darcy)    = ', XKF
      WRITE(*,*) 'WKFWF (ft darcy) = ', YKFWF/30.48
      WRITE(*,*) 'YKF   (darcy)    = ', YKF
      WRITE(*,*)

      WRITE(61,*)
      WRITE(61,*) 'WKFWF (ft darcy) = ', XKFWF/30.48
      WRITE(61,*) 'XKF   (darcy)    = ', XKF
      WRITE(61,*) 'WKFWF (ft darcy) = ', YKFWF/30.48
      WRITE(61,*) 'YKF   (darcy)    = ', YKF
      WRITE(61,*)

      WRITE(*,*) ' 0/1 CONTINUE/STOP '
      READ (*,*) ISTOP
      IF(ISTOP.EQ.1) STOP

   DO 10 I = 1, NODE
    KX(I)  = XKF
    KY(I)  = YKF
    WFX(I) = WFXCM
    WFY(I) = WFYCM

    IF(IYXM(I).EQ.4) THEN
         KX(I) = 0.0
         KY(I) = 0.0
    ENDIF

    PORO(I) = XPORO
    SW1(I)  = XSWI
    SG1(I)  = 1 - SW1(I)
10  CONTINUE

   DO 20 I = 1, NODE

    IF(IYXM(I).EQ.4) THEN
         VOL(I) = (WFXCM*DX(I) + WFYCM*DY(I) - WFXCM*WFYCM)*DZ
    ELSEIF(IYXM(I).EQ.3) THEN
         VOL(I) = WFXCM*DX(I)*DZ
    ELSEIF(IYXM(I).EQ.2) THEN
         VOL(I) = WFYCM*DY(I)*DZ
    ELSEIF(IYXM(I).EQ.1) THEN
         VOL(I) = (WFXCM*DX(I) + WFYCM*DY(I) - WFXCM*WFYCM)*DZ
    ENDIF

    P1 (I) = PPRO + 25.

    IF(IYXM(I).EQ.4) P1(I) = 0.0
```

```
20  CONTINUE

    P1 (IINJ) = PINJ
    SW1(IINJ) = 1.0
    SG1(IINJ) = 0.0
    P1 (IPRO) = PPRO
    SW1(IPRO) = 0.0
    SG1(IPRO) = 1.0

        IF(ITRACER.EQ.1) THEN
         DO 30 I = 1, NODE
          CTW1(I) = 0.0
          CTW2(I) = 0.0
          CTG1(I) = 0.0
          CTG2(I) = 0.0
30   CONTINUE
          IF(I.EQ.IINJ) CTW1(IINJ) = 0.0
         ENDIF

         RETURN
         END


***
    SUBROUTINE WIP
    INCLUDE 'INFRAC1.FOR'

     CWIP = 0.0
    DO 10 I = 1, NODE
     IF(IYXM(I).EQ.4 .OR. I.EQ.IINJ .OR. I.EQ.IPRO) GOTO 10
     RHOW = RHOWI*EXP(CW*(P1(I)-P0))
     CWIP = CWIP + VOL(I)*PORO(I)*SW1(I)*RHOW
10   CONTINUE

    RETURN
    END
***
    SUBROUTINE GIP
    INCLUDE 'INFRAC1.FOR'

     CGIP = 0.0
    DO 10 I = 1, NODE
     IF(IYXM(I).EQ.4 .OR. I.EQ.IINJ .OR. I.EQ.IPRO) GOTO 10
     RHOG = RHOGI*EXP(CG*(P1(I)-P0))
     CGIP = CGIP + VOL(I)*PORO(I)*SG1(I)*RHOG
10   CONTINUE

         WRITE(*,*) ' *** PV tracer = ', PVTRACER
```

```
        PVDIR = 0
        DO 40 I = 1, NCOL
         PVDIR = PVDIR + VOL(I)*PORO(I)*SG1(I)*RHOG
40   CONTINUE
         PVTDIR = PVDIR/(CWIP+CGIP)
        WRITE(*,*) ' *** PV DIRECT = ', PVTDIR
        WRITE(*,*) ' *** enter 0/1 for continue/stop = '
        READ (*,*) ISTOP
        IF(ISTOP.EQ.1) STOP

    WRITE(61,*) ' *** PVTRACER  = ', PVTRACER
        WRITE(61,*) ' *** PV DIRECT = ', PVTDIR

    RETURN
    END
***
    SUBROUTINE PREXY
    INCLUDE 'INFRAC1.FOR'

C
C .... transmissibility of west
C
     INODE = 0
    DO 10 I = 1, NROW
     DO 10 J = 1, NCOL
      INODE = INODE + 1
      RHW = RHOWI*EXP(CW*(P1(INODE)-P0))
          RHG = RHOGI*EXP(CG*(P1(INODE)-P0))

          P1(0) = 0.0

          IF(J.EQ.1) THEN
                WTW(INODE) = 0.0
           GTW(INODE) = 0.0
           GOTO 10
          ENDIF

          INIM1 = INODE - 1
         IF(P1(INODE).GE.P1(INIM1)) THEN

       RHWUP = RHOWI*EXP(CW*(P1(INODE)-P0))
       XKRUP = SW1(INODE)**RESOL
       IF(RESOL.GT.4) THEN
        XKRUP = 0.0
        IF(SW1(INODE).GT.0.999) XKRUP = 1.0
       ENDIF
       RHGUP = RHOGI*EXP(CG*(P1(INODE)-P0))
```

```
      XKUP  = 2.*KX(INODE)*KX(INIM1)/(KX(INODE)+KX(INIM1))
           DIST  = (DX(INODE)+DX(INIM1))/2.

     ELSE
      RHWUP = RHOWI*EXP(CW*(P1(INIM1)-P0))
      XKRUP = SW1(INIM1)**RESOL
      IF(RESOL.GT.4) THEN
       XKRUP = 0.0
       IF(SW1(INIM1).GT.0.999) XKRUP = 1.0
      ENDIF
           RHGUP = RHOGI*EXP(CG*(P1(INIM1)-P0))

           XKUP  = 2.*KX(INODE)*KX(INIM1)/(KX(INODE)+KX(INIM1))
           DIST  = (DX(INODE)+DX(INIM1))/2.

     ENDIF

          XKRUPW = XKRUP
          XKRUPG = 1.-XKRUP
          WTW(INODE)= - RHWUP*XKRUPW*XKUP/VISW*WFX(INODE)*DZ/DIST*DT/RHW
     GTW(INODE)= - RHGUP*XKRUPG*XKUP/VISG*WFX(INODE)*DZ/DIST*DT/RHG

 10   CONTINUE

C
C .... transmissibility of east
C
       INODE = 0
     DO 20 I = 1, NROW
      DO 20 J = 1, NCOL
       INODE = INODE + 1
       RHW = RHOWI*EXP(CW*(P1(INODE)-P0))
           RHG = RHOGI*EXP(CG*(P1(INODE)-P0))

           P1(0) = 0.0

           IF(J.EQ.NCOL) THEN
                 WTE(INODE) = 0.0
            GTE(INODE) = 0.0
            GOTO 20
           ENDIF

           INIP1 = INODE + 1
          IF(P1(INODE).GE.P1(INIP1)) THEN

       RHWUP = RHOWI*EXP(CW*(P1(INODE)-P0))
       XKRUP = SW1(INODE)**RESOL
       IF(RESOL.GT.4) THEN
        XKRUP = 0.0
```

```
      IF(SW1(INODE).GT.0.999) XKRUP = 1.0
     ENDIF
     RHGUP = RHOGI*EXP(CG*(P1(INODE)-P0))

     XKUP  = 2.*KX(INODE)*KX(INIP1)/(KX(INODE)+KX(INIP1))
          DIST  = (DX(INODE)+DX(INIP1))/2.
   ELSE
     RHWUP = RHOWI*EXP(CW*(P1(INIP1)-P0))
     XKRUP = SW1(INIP1)**RESOL
     IF(RESOL.GT.4) THEN
      XKRUP = 0.0
      IF(SW1(INIP1).GT.0.999) XKRUP = 1.0
     ENDIF
          RHGUP = RHOGI*EXP(CG*(P1(INIP1)-P0))

          XKUP  = 2.*KX(INODE)*KX(INIP1)/(KX(INODE)+KX(INIP1))
          DIST  = (DX(INODE)+DX(INIP1))/2.
   ENDIF

        XKRUPW = XKRUP
        XKRUPG = 1.-XKRUP
        WTE(INODE)= - RHWUP*XKRUPW*XKUP/VISW*WFX(INODE)*DZ/DIST*DT/RHW
   GTE(INODE)= - RHGUP*XKRUPG*XKUP/VISG*WFX(INODE)*DZ/DIST*DT/RHG

20  CONTINUE

C
C .... transmissibility of south
C
     INODE = 0
    DO 30 I = 1, NROW
     DO 30 J = 1, NCOL
      INODE = INODE + 1
      RHW = RHOWI*EXP(CW*(P1(INODE)-P0))
          RHG = RHOGI*EXP(CG*(P1(INODE)-P0))

          P1(0) = 0.0

          IF(I.EQ.1) THEN
                WTS(INODE) = 0.0
           GTS(INODE) = 0.0
           GOTO 30
          ENDIF

          INJM1 = INODE - NCOL
         IF(P1(INODE).GE.P1(INJM1)) THEN

      RHWUP = RHOWI*EXP(CW*(P1(INODE)-P0))
      XKRUP = SW1(INODE)**RESOL
```

```
      IF(RESOL.GT.4) THEN
       XKRUP = 0.0
       IF(SW1(INODE).GT.0.999) XKRUP = 1.0
      ENDIF
      RHGUP = RHOGI*EXP(CG*(P1(INODE)-P0))

      XKUP  = 2.*KY(INODE)*KY(INJM1)/(KY(INODE)+KY(INJM1))
           DIST  = (DY(INODE)+DY(INJM1))/2.
    ELSE
      RHWUP = RHOWI*EXP(CW*(P1(INJM1)-P0))
      XKRUP = SW1(INJM1)**RESOL
      IF(RESOL.GT.4) THEN
       XKRUP = 0.0
       IF(SW1(INJM1).GT.0.999) XKRUP = 1.0
      ENDIF
           RHGUP = RHOGI*EXP(CG*(P1(INJM1)-P0))

           XKUP  = 2.*KY(INODE)*KY(INJM1)/(KY(INODE)+KY(INJM1))
           DIST  = (DY(INODE)+DY(INJM1))/2.
    ENDIF

         XKRUPW = XKRUP
         XKRUPG = 1.-XKRUP
         WTS(INODE)= - RHWUP*XKRUPW*XKUP/VISW*WFY(INODE)*DZ/DIST*DT/RHW
    GTS(INODE)= - RHGUP*XKRUPG*XKUP/VISG*WFY(INODE)*DZ/DIST*DT/RHG

 30   CONTINUE

C
C .... transmissibility of nouth
C
      INODE = 0
     DO 40 I = 1, NROW
      DO 40 J = 1, NCOL
       INODE = INODE + 1
       RHW = RHOWI*EXP(CW*(P1(INODE)-P0))
           RHG = RHOGI*EXP(CG*(P1(INODE)-P0))

           P1(0) = 0.0

           IF(I.EQ.NROW) THEN
                 WTN(INODE) = 0.0
            GTN(INODE) = 0.0
            GOTO 40
           ENDIF

           INJP1 = INODE + NCOL
          IF(P1(INODE).GE.P1(INJP1)) THEN
```

```
      RHWUP = RHOWI*EXP(CW*(P1(INODE)-P0))
      XKRUP = SW1(INODE)**RESOL
      IF(RESOL.GT.4) THEN
       XKRUP = 0.0
       IF(SW1(INODE).GT.0.999) XKRUP = 1.0
      ENDIF
      RHGUP = RHOGI*EXP(CG*(P1(INODE)-P0))

      XKUP  = 2.*KY(INODE)*KY(INJP1)/(KY(INODE)+KY(INJP1))
           DIST  = (DY(INODE)+DY(INJP1))/2.
    ELSE
      RHWUP = RHOWI*EXP(CW*(P1(INJP1)-P0))
      XKRUP = SW1(INJP1)**RESOL
      IF(RESOL.GT.4) THEN
       XKRUP = 0.0
       IF(SW1(INJP1).GT.0.999) XKRUP = 1.0
      ENDIF
           RHGUP = RHOGI*EXP(CG*(P1(INJP1)-P0))

           XKUP  = 2.*KY(INODE)*KY(INJP1)/(KY(INODE)+KY(INJP1))
           DIST  = (DY(INODE)+DY(INJP1))/2.
    ENDIF

         XKRUPW = XKRUP
         XKRUPG = 1.-XKRUP
         WTN(INODE)= - RHWUP*XKRUPW*XKUP/VISW*WFY(INODE)*DZ/DIST*DT/RHW
    GTN(INODE)= - RHGUP*XKRUPG*XKUP/VISG*WFY(INODE)*DZ/DIST*DT/RHG

 40  CONTINUE

    RETURN
    END
***
    SUBROUTINE SWEEP
    INCLUDE 'INFRAC1.FOR'
         PARAMETER(II=NCOL,JJ=NROW,KK=1,TOL=1.E-10)
         PARAMETER(IJKM=II*JJ*KK)
    DIMENSION AW(IJKM), AE(IJKM), AS(IJKM), AN(IJKM)
         DIMENSION AT(IJKM), AB(IJKM), E (IJKM), B (IJKM)
    DIMENSION AL3(IJKM),AL2(IJKM),AL1(IJKM),AD(IJKM)
    DIMENSION AU1(IJKM),AU2(IJKM),AU3(IJKM)
    DIMENSION QI(15,IJKM),AQI(15,IJKM),QN(IJKM),AQN(IJKM)
    DIMENSION RN(IJKM),DXN(IJKM),ADX(IJKM)

    DO 10 I = 1, NODE
     AW (I) = 0.0
     AE (I) = 0.0
     AS (I) = 0.0
     AN (I) = 0.0
```

```
        AT (I) = 0.0
        AB (I) = 0.0
        E       (I) = 0.0
        B       (I) = 0.0
10  CONTINUE

   DO 20 I = 1, NODE
    RHW   = RHOWI*EXP(CW*(P1(I)-P0))
    RHG   = RHOGI*EXP(CG*(P1(I)-P0))
    AW(I)  = - WTW(I) - GTW(I)
        AE(I)  = - WTE(I) - GTE(I)
        AS(I)  = - WTS(I) - GTS(I)
        AN(I)  = - WTN(I) - GTN(I)

    E (I)  = +WTW(I)+GTW(I)+WTE(I)+GTE(I)
   &         +WTS(I)+GTS(I)+WTN(I)+GTN(I)

    STOREW(I) = VOL(I)*PORO(I)*SW1(I)*CW*RHW/RHW
    STOREG(I) = VOL(I)*PORO(I)*SG1(I)*CG*RHG/RHG
    E (I)  = E(I) - STOREW(I) - STOREG(I)
    B (I)  = - STOREW(I)*P1(I) - STOREG(I)*P1(I)

       IF(I.EQ.IINJ .OR. I.EQ.IPRO .OR.IYXM(I).EQ.4) THEN
     AW(I) = 0.0
     AE(I) = 0.0
     AS(I) = 0.0
     AN(I) = 0.0
          E (I) = 1.0
          B (I) = P1(I)
          IF(IYXM(I).EQ.4) B(I) = 0.0
   ENDIF

20  CONTINUE

       ITMAX1 = 50

       CALL CMAT(AW,AE,AS,AN,AT,AB,E,B,TOL,II,JJ,KK,IJKM,ITMAX1
   &           ,QI,AQI,AL3,AL2,AL1,AD,AU1,AU2
   &           ,AU3,QN,AQN,RN,DXN,ADX,P2)

   DO 30 I = 1, NODE

        IF(I-1.EQ.0) THEN
              WFLUXW(I) = 0.0
          GFLUXW(I) = 0.0
        ELSE
              WFLUXW(I) = WTW(I)*(P2(I)-P2(I-1))
          GFLUXW(I) = GTW(I)*(P2(I)-P2(I-1))
              IF(ABS(P2(I)-P2(I-1)).LT.1.E-3) THEN
```

```
                WFLUXW(I) = 0.0
                GFLUXW(I) = 0.0
               ENDIF
      ENDIF

          IF(I+1.EQ.NODE+1) THEN
            WFLUXE(I) = 0.0
            GFLUXE(I) = 0.0
          ELSE
            WFLUXE(I) = WTE(I)*(P2(I+1)-P2(I))
          GFLUXE(I) = GTE(I)*(P2(I+1)-P2(I))
                IF(ABS(P2(I+1)-P2(I)).LT.1.E-3) THEN
                 WFLUXE(I) = 0.0
                 GFLUXE(I) = 0.0
                ENDIF
          ENDIF

      TERMXW(I) = WFLUXW(I) - WFLUXE(I)
      TERMXG(I) = GFLUXW(I) - GFLUXE(I)

          IF(I-NCOL.LE.0) THEN
            WFLUXS(I) = 0.0
            GFLUXS(I) = 0.0
          ELSE
            WFLUXS(I) = WTS(I)*(P2(I)-P2(I-NCOL))
                GFLUXS(I) = GTS(I)*(P2(I)-P2(I-NCOL))
                IF(ABS(P2(I)-P2(I-NCOL)).LT.1.E-3) THEN
                 WFLUXS(I) = 0.0
                 GFLUXS(I) = 0.0
                ENDIF
          ENDIF

          IF(I+NCOL.GE.NODE+1) THEN
            WFLUXN(I) = 0.0
                GFLUXN(I) = 0.0
          ELSE
         WFLUXN(I) = WTN(I)*(P2(I+NCOL)-P2(I))
            GFLUXN(I) = GTN(I)*(P2(I+NCOL)-P2(I))
                IF(ABS(P2(I+NCOL)-P2(I)).LT.1.E-3) THEN
                 WFLUXN(I) = 0.0
                 GFLUXN(I) = 0.0
                ENDIF
          ENDIF

          TERMYW(I) = WFLUXS(I) - WFLUXN(I)
          TERMYG(I) = GFLUXS(I) - GFLUXN(I)

C         WRITE(*,*) ' 0/1 CONTINUE/STOP '
C         READ (*,*) ISTOP
```

```
C       IF(ISTOP.EQ.1) STOP
C       ENDIF

 30  CONTINUE

     RETURN
     END
***
     SUBROUTINE SAT(IDT)
     INCLUDE 'INFRAC1.FOR'

         INODE = NODE

     DO 10 I = 1, INODE
      IF(I.EQ.IINJ) THEN
       SW2(I) = 1.0
       SG2(I) = 0.0
           IF(ITRACER.EQ.1 .AND. PVINJ.LT.PVTRACER) THEN
            CTW1(I) = 1.0
            CTW2(I) = 1.0
            CT1(I)  = 1.0
            CT2(I)  = 1.0
           ELSE
            CTW1(I) = 0.0
            CTW2(I) = 0.0
            CT1 (I) = 0.0
            CT2 (I) = 0.0
           ENDIF
      GOTO 10
     ENDIF
     IF(I.EQ.IPRO) THEN
      SW2(I) = 0.0
      SG2(I) = 1.0
           IF(ITRACER.EQ.1) CTW2(I)=0.0
           IF(ITRACER.EQ.1) CT2 (I)=0.0
      GOTO 10
     ENDIF

C         speed up procedure only if no tracer
          IF(ITRACER.EQ.1) GOTO 111
          IF(IYXM(I).EQ.1 .AND. SW1(I).GT.0.5) THEN
           SW2(I) = 1.0
           SG2(I) = 0.0
           GOTO 10
          ENDIF
 111      CONTINUE
C

C         WRITE(*,*) VOL(I), PORO(I)
```

```
      WLHS  = TERMXW(I) + TERMYW(I)
      WRHS2 = VOL(I)*PORO(I)*SW1(I)*CW*(P2(I)-P1(I))
      WRHS1 = WLHS - WRHS2

      SW2(I) = SW1(I) + WRHS1/VOL(I)/PORO(I)

      IF(SW2(I).GE.1.0) SW2(I)=1.0
      IF(SW2(I).LE.0.0) SW2(I)=0.0
C         the following statement is to speed up the program
C     assuming the interception's volume is neglegible
C         only for none tracer cases
          IF(ITRACER.EQ.1) GOTO 222
          IF(IYXM(I).EQ.1 .AND. SW2(I).GT.0.01) SW2(I)=1.0
 222  CONTINUE

          IF(ITRACER.EQ.0) GOTO 333

          RHW = RHOWI*EXP(CW*(P1(INODE)-P0))
          RHG = RHOGI*EXP(CG*(P1(INODE)-P0))


          IF(ISWITCH.EQ.0) GOTO 555

      IF(WFLUXW(I).GT.0.0) THEN
            CFLUXW = CTW1(I-1)*WFLUXW(I)*RHW
            IF(CTW1(I-1).GT.1.E-3) CFLUXW=1.0*WFLUXW(I)*RHW
          ELSE
            CFLUXW = CTW1(I)*WFLUXW(I)*RHW
            IF(CTW1(I).GT.1.E-3) CFLUXW=1.0*WFLUXW(I)*RHW
          ENDIF

C         WRITE(*,*) ' IN LOOP 3333, I = ', I

      IF(WFLUXE(I).GT.0.0) THEN
            CFLUXE = CTW1(I)*WFLUXE(I)*RHW
            IF(CTW1(I).GT.1.E-3) CFLUXE=1.0*WFLUXE(I)*RHW
          ELSE
            CFLUXE = CTW1(I+1)*WFLUXE(I)*RHW
            IF(CTW1(I+1).GT.1.E-3) CFLUXE=1.0*WFLUXE(I)*RHW
          ENDIF

C         WRITE(*,*) ' IN LOOP 3334, I = ', I

      IF(WFLUXS(I).GT.0.0) THEN
                CFLUXS = 0.0
            IF(I-NCOL.GT.0) THEN
                  CFLUXS = CTW1(I-NCOL)*WFLUXS(I)*RHW
             IF(CTW1(I-NCOL).GT.1.E-3) CFLUXS=1.0*WFLUXS(I)*RHW
            ENDIF
```

```
          ELSE
            CFLUXS = CTW1(I)*WFLUXS(I)*RHW
            IF(CTW1(I).GT.1.E-3) CFLUXS=1.0*WFLUXS(I)*RHW
          ENDIF
C         WRITE(*,*) ' IN LOOP 3335, I = ', I

      IF(WFLUXN(I).GT.0.0) THEN
            CFLUXN = CTW1(I)*WFLUXN(I)*RHW
            IF(CTW1(I).GT.1.E-3) CFLUXN=1.0*WFLUXN(I)*RHW
          ELSE
            CFLUXN = 0.0
            IF(I+NCOL.LT.NODE+1) THEN
                  CFLUXN = CTW1(I+NCOL)*WFLUXN(I)*RHW
             IF(CTW1(I+NCOL).GT.1.E-3) CFLUXN=1.0*WFLUXN(I)*RHW
            ENDIF
          ENDIF

       DSWW = SW2(I)
            IF(DSWW.LT.1.E-4) THEN
                  CTW2(I) = CTW1(I)
             GOTO 333
            ENDIF

            ACC    = CFLUXW-CFLUXE+CFLUXS-CFLUXN
       CT     = VOL(I)*SW1(I)*CTW1(I)*PORO(I)*RHW
            CTW2(I) = (ACC+CT)/VOL(I)/SW2(I)/PORO(I)/RHW

C         WRITE(*,*) ' IN LOOP 3334, ISWITCH = ', ISWITCH

 555  CONTINUE

          IF(ISWITCH.EQ.1) GOTO 666

      IF(WFLUXW(I)+GFLUXW(I).GT.0.0) THEN
            XXX   = (WFLUXW(I)*RHW+GFLUXW(I)*RHG)
            CFLUXW = CT1(I-1)*XXX
            IF(CT1(I-1).GT.1.E-3) CFLUXW=1.0*XXX
          ELSE
            XXX   = (WFLUXW(I)*RHW+GFLUXW(I)*RHG)
            CFLUXW = CT1(I)*XXX
            IF(CT1(I).GT.1.E-3) CFLUXW=1.0*XXX
          ENDIF

      IF(WFLUXE(I)+GFLUXE(I).GT.0.0) THEN
            XXX = (WFLUXE(I)*RHW+GFLUXE(I)*RHG)
            CFLUXE = CT1(I)*XXX
            IF(CT1(I).GT.1.E-3) CFLUXE=1.0*XXX
          ELSE
            XXX = (WFLUXE(I)*RHW+GFLUXE(I)*RHG)
```

```
          CFLUXE = CT1(I+1)*XXX
          IF(CT1(I+1).GT.1.E-3) CFLUXE=1.0*XXX
        ENDIF


    IF(WFLUXS(I)+GFLUXS(I).GT.0.0) THEN
              CFLUXS = 0.0
          IF(I-NCOL.GT.0) THEN
           XXX = (WFLUXS(I)*RHW+GFLUXS(I)*RHG)
                CFLUXS = CT1(I-NCOL)*XXX
           IF(CT1(I-NCOL).GT.1.E-3) CFLUXS=1.0*XXX
          ENDIF
        ELSE
          XXX = (WFLUXS(I)*RHW+GFLUXS(I)*RHG)
          CFLUXS = CT1(I)*XXX
          IF(CT1(I).GT.1.E-3) CFLUXS=1.0*XXX
        ENDIF

    IF(WFLUXN(I)+GFLUXN(I).GT.0.0) THEN
          XXX = (WFLUXN(I)*RHW+GFLUXN(I)*RHG)
          CFLUXN = CT1(I)*XXX
          IF(CT1(I).GT.1.E-3) CFLUXN=1.0*XXX
        ELSE
          CFLUXN = 0.0
          IF(I+NCOL.LT.NODE+1) THEN
           XXX = (WFLUXN(I)*RHW+GFLUXN(I)*RHG)
                CFLUXN = CT1(I+NCOL)*XXX
           IF(CT1(I+NCOL).GT.1.E-3) CFLUXN=1.0*XXX
          ENDIF
        ENDIF
         ACC   = CFLUXW-CFLUXE+CFLUXS-CFLUXN
     CT    = VOL(I)*(SW1(I)+SG1(I))*CT1(I)*PORO(I)*RHW
          CT2(I) = (ACC+CT)/VOL(I)/(SW1(I)+SG1(I))/PORO(I)/RHW

 666  CONTINUE

C        WRITE(*,*) ' AFTER 666, I = ', I


C          WRITE(*,*) 'BEFORE', I

        IF(CTW2(I).LT.0.0) CTW2(I) = 0.0
        IF(CTW2(I).GT.1.0) CTW2(I) = 1.0
        IF(CT2(I).LT.0.0) CT2(I) = 0.0
        IF(CT2(I).GT.1.0) CT2(I) = 1.0

 333  CONTINUE
C
     SG2(I) = 1.0 - SW2(I)
```

```
 10  CONTINUE

     IDT = 1

     DO 20 I = 1, NODE
      IF(I.EQ.IINJ .OR. I.EQ.IPRO) GOTO 20
      DP  = ABS(P2(I)-P1(I))
      DSW = ABS(SW2(I)-SW1(I))
           DC  = ABS(CTW2(I)-CTW1(I))
           IF(ISWITCH.EQ.0) DC = ABS(CT2(I)-CT1(I))
C          the following statement also to speed up the process
           IF(ITRACER.EQ.1) GOTO 444
           IF(IYXM(I).EQ.1) GOTO 20
 444  CONTINUE
C
     IF(DP.GT.0.1 .OR. DSW.GT.0.1 .OR. DC.GT.0.1) IDT = - 1
 20  CONTINUE

     XINJW = 0
     XPROW = 0
     XINJG = 0
     XPROG = 0
     DO 30 I = 1, NODE
     IF(I.EQ.IINJ) THEN
      XINJW = XINJW + TERMXW(I) + TERMYW(I)
      XINJG = XINJG + TERMXG(I) + TERMYG(I)
     ENDIF
     IF(I.EQ.IPRO) THEN
      XPROW = XPROW + TERMXW(I) + TERMYW(I)
      XPROG = XPROG + TERMXG(I) + TERMYG(I)
           COUT = CTW2(IPRO-1)*TERMXW(I)/(XPROW+XPROG)
           IF(ISWITCH.EQ.0) THEN
            COUT = CT2(IPRO-1)*(WFLUXW(I)+GFLUXW(I))/(XPROW+XPROG)
           ENDIF
     ENDIF
 30  CONTINUE

     XINJWT = XINJWT + XINJW
     XINJGT = XINJGT + XINJG
     XPROWT = XPROWT + XPROW
     XPROGT = XPROGT + XPROG

     DO 40 I = 1, NODE
     SW1(I) = SW2(I)
     SG1(I) = SG2(I)
     P1(I)  = P2(I)
           IF(ITRACER.EQ.1) THEN
            IF(CTW2(I).GT.1.0) CTW2(2) = 1.0
```

```
          IF(CTW2(I).LT.0.0) CTW2(2) = 0.0
          IF(CT2(I).GT.1.0) CT2(2)=1.0
          IF(CT2(I).LT.0.0) CT2(2)=0.0
          CTW1(I) = CTW2(I)
          CT1(I) = CT2(I)
         ENDIF

 40   CONTINUE

      RETURN
      END


***
      SUBROUTINE PVINJE(IPRINT)
      INCLUDE 'INFRAC1.FOR'

      XINJT = XINJWT + XINJGT
      PVINJ = ABS(XINJT/OWGIP)
      IF(PVINJ.GT.PVPRINT) THEN
       IPRINT  = 1
       PVPRINT = PVPRINT + DPV
      ELSE
       IPRINT  = 0
      ENDIF

      RETURN
      END
***

***
      SUBROUTINE PRINT
      INCLUDE 'INFRAC1.FOR'

          IF(ISWITCH.EQ.0) GOTO 111

      WRITE(61,*)
      WRITE(61,*)
      WRITE(61,*) ' *** CASE       = ', ICASE
      WRITE(61,*) ' *** PVINJ      = ', PVINJ
          WRITE(61,*) ' *** TIME(sec)  = ', TTOTAL

      XPROT = XPROW + XPROG

      WRITE(61,*) ' *** KfWf X(darcy cm) = ', XKFWF
      WRITE(61,*) ' *** KfWf Y(darcy cm) = ', YKFWF
      WRITE(61,*) ' *** VISW(cp)         = ', VISW
      WRITE(61,*) ' *** VISG(cp)         = ', VISG
      WRITE(61,*) ' *** RESOL(5=piston)  = ', RESOL
```

```
        if(ncol.gt.11) goto 111

   WRITE(61,*)
   WRITE(61,*) ' **** PRESSURE PROFILE (atm) **** '
   WRITE(61,*)

   INDEX=0
   DO 50 I = 1, NROW
    WRITE(61,601) (P2(INDEX+J),J=1,NCOL)
    INDEX=INDEX+NCOL
50  CONTINUE

601  FORMAT(11(1X,F7.2))

   WRITE(61,*)
   WRITE(61,*) ' **** Sp (-), p: injecting fluid **** '
   WRITE(61,*)

   INDEX=0
   DO 71 I = 1, NROW
    WRITE(61,602) (SW2(INDEX+J),J=1,NCOL)
    INDEX=INDEX+NCOL
71  CONTINUE

602  FORMAT(11(1X,F7.4))

        IF(ITRACER.EQ.0) GOTO 999

   WRITE(61,*)
   WRITE(61,*) ' **** C(TRACER) **** '
   WRITE(61,*)
        WRITE(61,*) ' **** COUT = ', COUT

   INDEX=0
   DO 72 I = 1, NROW
    WRITE(61,602) (CTW2(INDEX+J),J=1,NCOL)
    INDEX=INDEX+NCOL
72  CONTINUE

        IF(ISWITCH.EQ.1) GOTO 999

111     CONTINUE

   WRITE(61,*) ' *** PVINJ      = ', PVINJ
   WRITE(61,*) ' *** TIME(sec)  = ', TTOTAL
   WRITE(61,*) ' *** C(TRACER) *** '
        WRITE(61,*) ' *** COUT      = ', COUT
        WRITE(61,*) ' *** CTW2(NBT1) = ', CTW2(NBT1)
```

```
      WRITE(61,*) ' *** CT2(NBT1)  = ', CT2(NBT1)
      WRITE(61,*) ' *** SW2(NBT1)  = ', SW2(NBT1)

      if(ncol.gt.11) goto 999

   INDEX=0
   DO 73 I = 1, NROW
    WRITE(61,602) (CT2(INDEX+J),J=1,NCOL)
    INDEX=INDEX+NCOL
73  CONTINUE

999  CONTINUE

   RETURN
   END
***
   SUBROUTINE CMAT(AW,AE,AS,AN,AT,AB,E,B,TOL,II,JJ,KK,IJKM,ITMAX
  &           ,QI,AQI,AL3,AL2,AL1,AD,AU1,AU2
  &           ,AU3,QN,AQN,RN,DXN,ADX,P)
   DIMENSION AW(IJKM),AE(IJKM),AS(IJKM),AN(IJKM),AT(IJKM)
  &       ,AB(IJKM),E(IJKM),B(IJKM),P(IJKM)
   DIMENSION AL3(IJKM),AL2(IJKM),AL1(IJKM),AD(IJKM)
  &       ,AU1(IJKM),AU2(IJKM),AU3(IJKM)
   DIMENSION QI(15,IJKM),AQI(15,IJKM),QN(IJKM),AQN(IJKM)
   DIMENSION RN(IJKM),DXN(IJKM),ADX(IJKM)

C    Author: Eric Chang
C          Assistant Professor of Chemical Engineering
C          New Mexico Tech
C          Tel: 505-835-5564
C
C
C .... AW, west band,    X-Y
C    AE, east band,    X-Y
C    AS, south band,   X-Y
C    AN, north band,   X-Y
C    AT, top band,     Z
C    AB, bottom band,  Z
C    E,  diagonal band,
C    B,  RHS vector,
C    TOL  = 0.0001
C    IJKM  = II x JJ x KK = 20 x 20 x 20 = 8000
C    ITMAX = 50
C
C
C   ORTHOMIN SPARSE MATRIX SOLVER BASED ON PAPER BY P. K. W. VINSOME
C   FOUTH SYMPOSIUM ON RESERVOIR SIMULATION
C   LOS ANGELES, CALIFORNIA    FEBRUARY 19-20,1976
C
```

```
      INX = II
      INXY = II*JJ
      IB = 0
      DO 500 K = 1,KK
       DO 450 J = 1,JJ
        DO 400 I = 1,II
         IB = IB + 1
         FAC = 1.0/E(IB)
         IF(I .NE. 1) AL1(IB) = FAC*AW(IB)
         IF(I .NE. II) AU1(IB) = FAC*AE(IB)
         IF(J .NE. 1) AL2(IB) = FAC*AS(IB)
         IF(J .NE. JJ) AU2(IB) = FAC*AN(IB)
         IF(K .NE. 1) AL3(IB) = FAC*AT(IB)
         IF(K .NE. KK) AU3(IB) = FAC*AB(IB)
         RN(IB) = FAC*B(IB)
  400   CONTINUE
  450  CONTINUE
  500 CONTINUE
C
C     APPROXIMATE LDU FACTORIZATION
C

      AD(1) = 1.0
      DO 550 I = 2,INX
       TERM = 1.0 - AL1(I)*AD(I-1)*AU1(I-1)
       AD(I) = 1.0/TERM
  550 CONTINUE
      DO 600 I = INX+1,INXY
       TERM = 1.0 - AL1(I)*AD(I-1)*AU1(I-1)
     &          - AL2(I)*AD(I-INX)*AU2(I-INX)
       AD(I) = 1.0/TERM
  600 CONTINUE
      DO 650 I = INXY+1,IJKM
       TERM = 1.0 - AL1(I)*AD(I-1)*AU1(I-1)
     &          - AL2(I)*AD(I-INX)*AU2(I-INX)
     &          - AL3(I)*AD(I-INXY)*AU3(I-INXY)
       AD(I) = 1.0/TERM
  650 CONTINUE
      CALL ORTH(AL3,AL2,AL1,AD,AU1,AU2,AU3,TOL
     &       ,INX,INXY,IJKM,ITMAX
     &       ,RN,DXN,ADX,QI,AQI,QN,AQN,P)
      RETURN
      END


      SUBROUTINE MVEC(AL3,AL2,AL1,AU1,AU2,AU3,R
     &           ,INX,INXY,IJKM,C)
      DIMENSION AL3(IJKM),AL2(IJKM),AL1(IJKM)
     &       ,AU1(IJKM),AU2(IJKM),AU3(IJKM)
```

```
      DIMENSION R(IJKM), C(IJKM)
      DO 100 I = 1,IJKM
        C(I) = R(I)
  100 CONTINUE
      DO 200 I = 1,IJKM-1
        C(I) = C(I) + AU1(I)*R(I+1)
  200 CONTINUE
      DO 300 I = 1,IJKM-INX
        C(I) = C(I) + AU2(I)*R(I+INX)
  300 CONTINUE
      DO 400 I = 1,IJKM-INXY
        C(I) = C(I) + AU3(I)*R(I+INXY)
  400 CONTINUE
      DO 500 I = 2,IJKM
        C(I) = C(I) + AL1(I)*R(I-1)
  500 CONTINUE
      DO 600 I = INX+1,IJKM
        C(I) = C(I) + AL2(I)*R(I-INX)
  600 CONTINUE
      DO 700 I = INXY+1,IJKM
        C(I) = C(I) + AL3(I)*R(I-INXY)
  700 CONTINUE
      RETURN
      END


      SUBROUTINE ORTH(AL3,AL2,AL1,AD,AU1,AU2,AU3,TOL
     &              ,INX,INXY,IJKM,ITMAX
     &              ,RN,DXN,ADX,QI,AQI,QN,AQN,DP)
      DIMENSION AL3(IJKM),AL2(IJKM),AL1(IJKM),AD(IJKM)
     &         ,AU1(IJKM),AU2(IJKM),AU3(IJKM)
      DIMENSION DP(IJKM),RN(IJKM),DXN(IJKM),ADX(IJKM)
      DIMENSION AQIAQI(15),QI(15,IJKM),AQI(15,IJKM)
      DIMENSION QN(IJKM),AQN(IJKM)
      DATA NMAX/15/
      CONV1 = TOL*TOL
      IF(CONV1 .GT. 1.E-4) CONV1 = 1.E-4
      RSQ = 0.0
      DO 100 IB = 1,IJKM
        DP(IB) = 0.0
        RSQ = RSQ + RN(IB)*RN(IB)
  100 CONTINUE
      CONV = CONV1*RSQ
      N = 0
      DO 800 ITER = 1,ITMAX
        IT = ITER
        IF(N .EQ. NMAX) N = 0
        N = N + 1
        NM1 = N - 1
```

```
      CALL MSOLVE(AL3,AL2,AL1,AD,AU1,AU2,AU3,RN
     &           ,INX,INXY,IJKM,DXN)
      CALL MVEC(AL3,AL2,AL1,AU1,AU2,AU3,DXN
     &         ,INX,INXY,IJKM,ADX)
      IF(N .EQ. 1) THEN
       DO 200 IB = 1,IJKM
        QN(IB) = DXN(IB)
        AQN(IB) = ADX(IB)
        QI(1,IB) = QN(IB)
        AQI(1,IB) = AQN(IB)
200     CONTINUE
      ELSE
       DO 300 IB = 1,IJKM
        QN(IB) = DXN(IB)
300     CONTINUE
       DO 500 I = 1,NM1
        AQIADX = 0.0
        DO 350 IB = 1,IJKM
         AQIADX = AQIADX + AQI(I,IB)*ADX(IB)
350      CONTINUE
        AI = AQIADX/AQIAQI(I)
        DO 400 IB = 1,IJKM
         QN(IB) = QN(IB) - AI*QI(I,IB)
400      CONTINUE
500     CONTINUE
       CALL MVEC(AL3,AL2,AL1,AU1,AU2,AU3,QN
     &           ,INX,INXY,IJKM,AQN)
       DO 650 IB = 1,IJKM
        QI(N,IB) = QN(IB)
        AQI(N,IB) = AQN(IB)
650     CONTINUE
      ENDIF
      AQNAQN = 0.0
      AQNRN = 0.0
      DO 700 IB = 1,IJKM
       AQNAQN = AQNAQN + AQN(IB)*AQN(IB)
       AQNRN = AQNRN + AQN(IB)*RN(IB)
700   CONTINUE
      AQIAQI(N) = AQNAQN
      OMEGA = AQNRN/AQNAQN
      RSQ = 0.0
      DO 750 IB = 1,IJKM
       DP(IB) = DP(IB) + OMEGA*QN(IB)
       RN(IB) = RN(IB) - OMEGA*AQN(IB)
       RSQ = RSQ + RN(IB)*RN(IB)
750   CONTINUE
      IF(RSQ .LT. CONV) GOTO 900
800 CONTINUE
900 CONTINUE
```

```
C     WRITE(6,1900) IT
      RETURN
C 1900 FORMAT(5X,'ORTHOMIN CONVERGED AFTER ',I3,' ITERATIONS')
      END

      SUBROUTINE MSOLVE(AL3,AL2,AL1,AD,AU1,AU2,AU3,R
     &              ,INX,INXY,IJKM,XX)
      DIMENSION AL3(IJKM),AL2(IJKM),AL1(IJKM),AD(IJKM)
     &       ,AU1(IJKM),AU2(IJKM),AU3(IJKM)
      DIMENSION XX(IJKM),R(IJKM)
C
C     FORWARD ELIMINATION
C
      XX(1) = AD(1)*R(1)
      DO 100 I = 2,INX
        XX(I) = AD(I)*(R(I)-AL1(I)*XX(I-1))
  100 CONTINUE
      DO 200 I = INX+1,INXY
        XX(I) = AD(I)*(R(I)-AL1(I)*XX(I-1)-AL2(I)*XX(I-INX))
  200 CONTINUE
      DO 300 I = INXY+1,IJKM
        XX(I) = AD(I)*(R(I)-AL1(I)*XX(I-1)-AL2(I)*XX(I-INX)
     &       -AL3(I)*XX(I-INXY))
  300 CONTINUE
      DO 400 I = 1,IJKM
        XX(I) = XX(I)/AD(I)
  400 CONTINUE
C
C     BACK SUBSTITUTION
C
      DO 500 I = IJKM-1,IJKM-INX+1,-1
        XX(I) = AD(I)*(XX(I)-AU1(I)*XX(I+1))
  500 CONTINUE
      DO 600 I = IJKM-INX,IJKM-INXY+1,-1
        XX(I) = AD(I)*(XX(I)-AU1(I)*XX(I+1)-AU2(I)*XX(I+INX))
  600 CONTINUE
      DO 700 I = IJKM-INXY,1,-1
        XX(I) = AD(I)*(XX(I)-AU1(I)*XX(I+1)-AU2(I)*XX(I+INX)
     &       -AU3(I)*XX(I+INXY))
  700 CONTINUE
      RETURN
      END
```

The following is INFRAC1.FOR:

```
PARAMETER(NROW=41,NCOL=21)
      PARAMETER(NODE=NROW*NCOL)
      PARAMETER(DZ=100)
```

```
      PARAMETER(P0=1.0,RHOWI=1.0,RHOGI=1.0,CW=5.E-4,CG=5.E-4)

C         PARAMETER(II=NROW,JJ=NCOL,KK=1,TOL=1.E-4)
C         PARAMETER(IJKM=II*JJ*KK)
C     DIMENSION AW(IJKM), AE(IJKM), AS(IJKM), AN(IJKM)
C         DIMENSION AT(IJKM), AB(IJKM), E (IJKM), B (IJKM)
C     DIMENSION AL3(IJKM),AL2(IJKM),AL1(IJKM),AD(IJKM)
C     DIMENSION AU1(IJKM),AU2(IJKM),AU3(IJKM)
C     DIMENSION QI(15,IJKM),AQI(15,IJKM),QN(IJKM),AQN(IJKM)
C     DIMENSION RN(IJKM),DXN(IJKM),ADX(IJKM)

      REAL KX,KY

      COMMON /C1/ ICASE,ITMAX
      COMMON /C2/ DT,DTMAX,PVPRINT,DPV,PVINJ,TTOTAL
          COMMON /C3/ CWIP,CGIP,OWGIP
      COMMON /C4/ XINJW,XINJG,XPROW,XPROG,XINJWT,XINJGT,XPROWT,XPROGT
      COMMON /C5/ VISW,VISG,XKFWF,YKFWF
      COMMON /C6/ RESOL,PINJ,PPRO,
          COMMON /C7/ IINJ,IPRO,NBT1,NBT2,ITRACER,ISWITCH
      COMMON /C8/ PVTRACER,PVTP1,PVTP2,COUT

      COMMON /C001/ IYXM(NODE)
      COMMON /C002/ P1(NODE),P2(NODE)
      COMMON /C003/ SW1(NODE),SW2(NODE),SG1(NODE),SG2(NODE)
      COMMON /C004/ KX(NODE),KY(NODE),DX(NODE),DY(NODE)
      COMMON /C005/ WFX(NODE),WFY(NODE),PORO(NODE),VOL(NODE)
          COMMON /C006/ STOREW(NODE), STOREG(NODE)
      COMMON /C007/ WTW(NODE),WTE(NODE),WTS(NODE),WTN(NODE)
          COMMON /C008/ GTW(NODE),GTE(NODE),GTS(NODE),GTN(NODE)
      COMMON /C009/ TERMXW(NODE),TERMXG(NODE)
          COMMON /C010/ TERMYW(NODE),TERMYG(NODE)
          COMMON /C011/ CTW1(NODE),CTW2(NODE),CTG1(NODE),CTG2(NODE)
          COMMON /C012/ WFLUXW(NODE),WFLUXE(NODE)
          COMMON /C013/ WFLUXS(NODE),WFLUXN(NODE)
          COMMON /C014/ GFLUXW(NODE),GFLUXE(NODE)
          COMMON /C015/ GFLUXS(NODE),GFLUXN(NODE)
          COMMON /C016/ CT1(NODE),CT2(NODE)
```

APPENDIX E: Fortran Program for Finding Pressures, Flow Rates, and Front Positions During Displacement in a Simple Naturally Fractured Reservoir. Dispersion Included at Both the Front and Rear of the Tracer Bank.

```
PROGRAM FRAC1
    INCLUDE 'INFRAC1.FOR'

C .... authors: Robert Lee & Randy Seright

C .... it should be noted that, W: injection fluid


      WRITE(*,*)
      WRITE(*,*) '*** generate DATAN.DAT ?  ***'
      WRITE(*,*) '*** enter 0/1 for no/yes:'
      READ(*,*) IGO
      IF(IGO.EQ.1) THEN
       CALL NETWORK
       WRITE(*,*) '*** generated DATAN.DAT re-run ***'
       STOP
      ENDIF

      WRITE(*,*)
      WRITE(*,*) '*** Do you have consistent data in     *** '
      WRITE(*,*) '*** INFRAC1.FOR,DATAN.DAT,DATAF1.DAT ? *** '
      WRITE(*,*) '*** enter 0/1 to stop/go = '
      READ (*,*) IGO
      IF(IGO.EQ.0) STOP

     CALL DATAIN
     CALL WIP
     CALL GIP

      WRITE(*,*)
      WRITE(*,*) '*** enter 0/1 no/yes for Rheology = '
      READ(*,*) IPOLYMER

     OPEN(69,FILE='RANDY.OUT')
      WRITE(69,*) '*** Case No.          = ', ICASE
      WRITE(69,*) '*** PV tracer         = ', PVTRACER
      WRITE(69,*) '*** Rheology 0/1 no/yes = ', IPOLYMER
      WRITE(69,*) '*** time(sec), *** pvinj,  *** Cout '
      IF(IPOLYMER.EQ.1) DTMAX=100.*DTMAX

     OWGIP  = CWIP+CGIP
     IPRINT = 0
      ISWITCH = 1
     IDT    = 0
```

```
      INDEXP = 0
       TTOTAL = 0.0

       DO 10 I = 1, NODE
        VISWW(I) = VISW
        VISWE(I) = VISW
        VISWS(I) = VISW
        VISWN(I) = VISW
10     CONTINUE

       WRITE(*,*) '*** PVINJMAX = '
       READ (*,*) PVINJMAX

      DO 100 I = 1, ITMAX

      IF(IDT.EQ.1)   DT = 1.2*DT
      IF(IDT.EQ.-1)  DT = 0.8*DT
      IF(DT.GE.DTMAX) DT = DTMAX

      IDT = 0
      INDEXP = INDEXP+1
       TTOTAL = TTOTAL + DT

      IF(INDEXP.EQ.100) THEN
        WRITE(*,*) '*** I,DT,PVINJ   = ', I, DT, PVINJ
        WRITE(*,*) '*** ISWITCH (1/0)= ', ISWITCH
        WRITE(*,*) '*** PVINJMAX     = ', PVINJMAX
        IF(ISWITCH.EQ.1) THEN
         WRITE(*,*) '*** not breakthru yet *** '
        WRITE(*,*) 'CTW2(IINJ+1)  = ', CTW2(IINJ+1)
         WRITE(*,*) 'P1(IINJ+1)    = ', P1(IINJ+1)
         WRITE(*,*) 'P1(IINJ+2)    = ', P1(IINJ+2)
         WRITE(*,*) 'CTW2(NBT1)    = ', CTW2(NBT1)
         WRITE(*,*) 'SW2 (NBT1)    = ', SW2 (NBT1)
        ENDIF
        IF(ISWITCH.EQ.0) THEN
         WRITE(*,*) '*** breakthru *** '
        WRITE(*,*) 'CT2(IINJ+1) = ', CT2(IINJ+1)
         WRITE(*,*) 'CT2(NBT1)   = ', CT2(NBT1)
         WRITE(*,*) 'P1(NBT1)    = ', P1(NBT1)
         WRITE(*,*) 'SW2(NBT1)   = ', SW2(NBT1)
        ENDIF
       INDEXP = 0
      ENDIF

      IF(PVINJ.GT.PVINJMAX) THEN
        WRITE(*,*) '*** stop at PVINJMAX = ', PVINJMAX
        WRITE(*,*) '*** enter 1 to stop  = '
        READ (*,*) ISTOP
```

```
      IF(ISTOP.EQ.1) STOP
      ENDIF

    CALL PREXY

      IF(NROW.GT.9) GOTO 555
      IF(I.EQ.1) THEN
       WRITE(*,*) '*** Do you want to see the transmissibility? '
       WRITE(*,*) '*** 0/1 no/yes = '
       READ (*,*) ISEE
       IF(ISEE.EQ.0) GOTO 555
      ELSE
       GOTO 555
      ENDIF

      WRITE(*,*) '*** GTW+WTW ***'
      DO 51 IK = 1, NROW
51      WRITE(*,605)
     &  (GTW((IK-1)*NCOL+J)+WTW((IK-1)*NCOL+J),J=1,NCOL)
      WRITE(*,*) '*** 0/1 continue/stop = '
       READ (*,*) ISTOP
       IF(ISTOP.EQ.1) STOP

      WRITE(*,*) '*** GTE+WTE ***'
      DO 52 IK = 1, NROW
52      WRITE(*,605)
     &  (GTE((IK-1)*NCOL+J)+WTE((IK-1)*NCOL+J),J=1,NCOL)
      WRITE(*,*) '*** 0/1 continue/stop = '
       READ (*,*) ISTOP
       IF(ISTOP.EQ.1) STOP

      WRITE(*,*) '*** GTS+WTS ***'
      DO 53 IK = 1, NROW
53      WRITE(*,605)
     &  (GTS((IK-1)*NCOL+J)+WTS((IK-1)*NCOL+J),J=1,NCOL)
      WRITE(*,*) '*** 0/1 continue/stop = '
       READ (*,*) ISTOP
       IF(ISTOP.EQ.1) STOP

      WRITE(*,*) '*** GTN+WTN ***'
      DO 54 IK = 1, NROW
54      WRITE(*,605)
     &  (GTN((IK-1)*NCOL+J)+WTN((IK-1)*NCOL+J),J=1,NCOL)
      WRITE(*,*) '*** 0/1 continue/stop = '
       READ (*,*) ISTOP
       IF(ISTOP.EQ.1) STOP

555 CONTINUE
```

```
   CALL SWEEP

    IF(NROW.GT.9) GOTO 666
   IF(I.EQ.1) THEN
     WRITE(*,*) '*** Do you want to see the initial pressure? '
     WRITE(*,*) '*** 0/1 no/yes = '
     READ (*,*) ISEE
     IF(ISEE.EQ.0) GOTO 666
    ELSE
     GOTO 666
    ENDIF

    WRITE(*,*) '*** P2 ***'
    DO 55 IK = 1, NROW
55     WRITE(*,605) (P2((IK-1)*NCOL+J),J=1,NCOL)
605   FORMAT(9(1X,F7.3))
   WRITE(*,*) '*** 0/1 continue/stop = '
    READ (*,*) ISTOP
    IF(ISTOP.EQ.1) STOP

666  CONTINUE

   CALL SAT(IDT)

    IF(NROW.GT.9) GOTO 777
   IF(I.EQ.1) THEN
     WRITE(*,*) '*** Do you want to see the initial saturation? '
     WRITE(*,*) '*** 0/1 no/yes = '
     READ (*,*) ISEE
     IF(ISEE.EQ.0) GOTO 777
    ELSE
     GOTO 777
    ENDIF

    WRITE(*,*) '*** SP *** '
    DO 56 IK = 1, NROW
56     WRITE(*,605) (SW2((IK-1)*NCOL+J),J=1,NCOL)
   WRITE(*,*) '*** 0/1 continue/stop = '
    READ (*,*) ISTOP
    IF(ISTOP.EQ.1) STOP

777  CONTINUE

    IF(I.EQ.1) WRITE(*,*) '*** program is running, GOOD LUCK!! ***'

   CALL PVINJE(IPRINT)

C
C .... NBT means Break Through Node
```

```
C .... NBT1,NBT2 are input variables
C
      IF(ISWITCH.EQ.0) GOTO 102
      IF(SW2(NBT1).GT.0.999 .OR. SW2(NBT2).GT.0.999) THEN
       CALL PRINT
       WRITE(*,*)  '*** BREAKTHRU *** '
       WRITE(61,*)
       WRITE(61,*)
       WRITE(61,*) '*** BREAKTHRU *** '
       DO 61 J = 1, NODE
        CT1(J) = CTW1(J)*SW1(J)
 61    CONTINUE
       ISWITCH = 0
       IPRINT = 0
       PVTP1 = PVINJ
       PVTP2 = PVINJ + PVINJ*4
       DPV   = (PVTP2-PVTP1)/100.
       PVINJMAX = PVTP2
       PVPRINT = PVINJ+DPV
      WRITE(*,*) '*** printout,OUT96.DAT *** '
      ENDIF
 102  CONTINUE

     IF(IPRINT.EQ.1) THEN
      CALL PRINT
      IPRINT = 0
      WRITE(*,*) '*** printout,OUT96.DAT *** '
     ENDIF

      IF(IPOLYMER.EQ.1) THEN
       CALL RHEOLOGY
      ENDIF

 100  CONTINUE

     STOP
     END
***
      SUBROUTINE RHEOLOGY
      INCLUDE 'INFRAC1.FOR'

      DO 10 I = 1, NODE
       UW(I) = ABS(WFLUXW(I))/WFX(I)/DT/DZ
       UE(I) = ABS(WFLUXE(I))/WFX(I)/DT/DZ
       US(I) = ABS(WFLUXS(I))/WFY(I)/DT/DZ
       UN(I) = ABS(WFLUXN(I))/WFY(I)/DT/DZ
       IF(UW(I).LT.0.005) UW(I)=0.005
       IF(UE(I).LT.0.005) UE(I)=0.005
       IF(US(I).LT.0.005) US(I)=0.005
```

```
      IF(UN(I).LT.0.005) UN(I)=0.005
10    CONTINUE

      DO 20 I = 1, NODE

      IF(UW(I).GE.2.1872) THEN
       VISWW(I) = 20998.4*UW(I)**(-0.95)
      ELSEIF(UW(I).LE.2.1872.AND.UW(I).GE.0.2117) THEN
       VISWW(I) = 10000.
      ELSEIF(UW(I).LT.0.2117) THEN
       VISWW(I) = 2725.6*UW(I)**(-0.83)
      ENDIF

      IF(UE(I).GE.2.1872) THEN
       VISWE(I) = 20998.4*UE(I)**(-0.95)
      ELSEIF(UE(I).LE.2.1872.AND.UE(I).GE.0.2117) THEN
       VISWE(I) = 10000.
      ELSEIF(UE(I).LT.0.2117) THEN
       VISWE(I) = 2725.6*UE(I)**(-0.83)
      ENDIF

      IF(US(I).GE.2.1872) THEN
       VISWS(I) = 20998.4*US(I)**(-0.95)
      ELSEIF(US(I).LE.2.1872.AND.US(I).GE.0.2117) THEN
       VISWS(I) = 10000.
      ELSEIF(UW(I).LT.0.2117) THEN
       VISWS(I) = 2725.6*US(I)**(-0.83)
      ENDIF

      IF(UN(I).GE.2.1872) THEN
       VISWN(I) = 20998.4*UN(I)**(-0.95)
      ELSEIF(UN(I).LE.2.1872.AND.UN(I).GE.0.2117) THEN
       VISWN(I) = 10000.
      ELSEIF(UN(I).LT.0.2117) THEN
       VISWN(I) = 2725.6*UN(I)**(-0.83)
      ENDIF

20    CONTINUE

      RETURN
      END
***
     SUBROUTINE DATAIN
     INCLUDE 'INFRAC1.FOR'

     OPEN(51,FILE='DATAF1.DAT')
      OPEN(52,FILE='DATAN.DAT')
     OPEN(61,FILE='FRACOUT.DAT')
```

```
      READ(52,*)
      READ(52,*) NCOL1
      READ(52,*) NROW1
      READ(52,*) NODE1
      READ(52,*) NINJ1
      READ(52,*) NPRO1
      READ(52,*) NBT11

       IF(NCOL1.NE.NCOL .OR. NROW1.NE.NROW) THEN
        WRITE(*,*) '*** NCOL,NROW are not consistent in *** '
        WRITE(*,*) '*** DATAN.DAT and DATAF1.DAT       *** '
        STOP
       ENDIF

       WRITE(*,*) '*** read DATAN.DAT ***'

      DO 5 I = 1, NODE
       READ(52,*) INODE, IYXM(I), DX(I), DY(I), KROW
5     CONTINUE

      READ(51,*) ICASE, ITMAX, ITRACER
       IF(ITRACER.EQ.1) THEN
        WRITE(61,*) '*** TRACER CASE *** '
        WRITE(*,*)  '*** TRACER CASE *** '
       ENDIF
      WRITE(*,*) '*** PLEASE ENTER CASE NO. *** '
      READ (*,*) ICASE
      READ(51,*) XKFWF, YKFWF, XPORO, XSWI
      READ(51,*) DT, DTMAX
      READ(51,*) PVPRINT, DPV
      READ(51,*)
      READ(51,*)
      READ(51,*) VISW, VISG
      READ(51,*) RESOL
      READ(51,*)
      READ(51,*) PINJ, PPRO
      READ(51,*) IINJ, IPRO
       READ(51,*) NBT1, NBT2
       READ(51,*) PVTRACER

       IF(NINJ1.NE.IINJ .OR. NPRO1.NE.IPRO .OR. NBT11.NE.NBT1) THEN
        WRITE(*,*) '*** IINJ,IPRO,NBT1 are not consistent in *** '
        WRITE(*,*) '*** DATAN.DAT and DATAF1.DAT          *** '
        WRITE(*,*) '*** 0/1 no/yes stop/go = '
        READ(*,*) IGO
        IF(IGO.EQ.0) STOP
       ENDIF
```

```
C
C .... convert field units to Darcy's units
C

      WFXFT = 5.03E-4*(XKFWF/30.48)**(1./3.)
      WFXCM = 30.48*WFXFT
      XKF   = XKFWF/WFXCM
      WFYFT = 5.03E-4*(YKFWF/30.48)**(1./3.)
      WFYCM = 30.48*WFYFT
      YKF   = YKFWF/WFYCM

      WRITE(*,*)
      WRITE(*,*) 'WKFWF (ft darcy) = ', XKFWF/30.48
      WRITE(*,*) 'XKF   (darcy)    = ', XKF
      WRITE(*,*) 'WKFWF (ft darcy) = ', YKFWF/30.48
      WRITE(*,*) 'YKF   (darcy)    = ', YKF
      WRITE(*,*)

      WRITE(61,*)
      WRITE(61,*) 'WKFWF (ft darcy) = ', XKFWF/30.48
      WRITE(61,*) 'XKF   (darcy)    = ', XKF
      WRITE(61,*) 'WKFWF (ft darcy) = ', YKFWF/30.48
      WRITE(61,*) 'YKF   (darcy)    = ', YKF
      WRITE(61,*)

      WRITE(*,*) ' 0/1 CONTINUE/STOP '
      READ (*,*) ISTOP
      IF(ISTOP.EQ.1) STOP

     DO 10 I = 1, NODE
      KX(I)  = XKF
      KY(I)  = YKF
      WFX(I) = WFXCM
      WFY(I) = WFYCM

      IF(IYXM(I).EQ.4) THEN
        KX(I) = 0.0
        KY(I) = 0.0
      ENDIF

      PORO(I) = XPORO
      SW1(I)  = XSWI
      SG1(I)  = 1 - SW1(I)
10    CONTINUE

     DO 20 I = 1, NODE

      IF(IYXM(I).EQ.4) THEN
        VOL(I) = (WFXCM*DX(I) + WFYCM*DY(I) - WFXCM*WFYCM)*DZ
```

```
      ELSEIF(IYXM(I).EQ.3) THEN
        VOL(I) = WFXCM*DX(I)*DZ
      ELSEIF(IYXM(I).EQ.2) THEN
        VOL(I) = WFYCM*DY(I)*DZ
      ELSEIF(IYXM(I).EQ.1) THEN
        VOL(I) = (WFXCM*DX(I) + WFYCM*DY(I) - WFXCM*WFYCM)*DZ
      ENDIF

      P1 (I) = PPRO + 25.

      IF(IYXM(I).EQ.4) P1(I) = 0.0

 20   CONTINUE

      P1 (IINJ) = PINJ
      SW1(IINJ) = 1.0
      SG1(IINJ) = 0.0
      P1 (IPRO) = PPRO
      SW1(IPRO) = 0.0
      SG1(IPRO) = 1.0

      IF(ITRACER.EQ.1) THEN
       DO 30 I = 1, NODE
        CTW1(I) = 0.0
        CTW2(I) = 0.0
        CTG1(I) = 0.0
        CTG2(I) = 0.0
 30    CONTINUE
       IF(I.EQ.IINJ) CTW1(IINJ) = 0.0
      ENDIF

      RETURN
      END


***
     SUBROUTINE WIP
     INCLUDE 'INFRAC1.FOR'

      CWIP = 0.0
     DO 10 I = 1, NODE
      IF(IYXM(I).EQ.4 .OR. I.EQ.IINJ .OR. I.EQ.IPRO) GOTO 10
      RHOW = RHOWI*EXP(CW*(P1(I)-P0))
      CWIP = CWIP + VOL(I)*PORO(I)*SW1(I)*RHOW
 10   CONTINUE

     RETURN
     END
***
```

```
      SUBROUTINE GIP
      INCLUDE 'INFRAC1.FOR'

       CGIP = 0.0
      DO 10 I = 1, NODE
       IF(IYXM(I).EQ.4 .OR. I.EQ.IINJ .OR. I.EQ.IPRO) GOTO 10
       RHOG = RHOGI*EXP(CG*(P1(I)-P0))
       CGIP = CGIP + VOL(I)*PORO(I)*SG1(I)*RHOG
10    CONTINUE

       WRITE(*,*) ' *** PV tracer = ', PVTRACER


       PVDIR = 0
       DO 40 I = 1, NCOL
        PVDIR = PVDIR + VOL(I)*PORO(I)*SG1(I)*RHOG
40    CONTINUE
        PVTDIR = PVDIR/(CWIP+CGIP)
       WRITE(*,*) ' *** PV DIRECT = ', PVTDIR
       WRITE(*,*) ' *** enter 0/1 for continue/stop = '
       READ (*,*) ISTOP
       IF(ISTOP.EQ.1) STOP

      WRITE(61,*) ' *** PVTRACER  = ', PVTRACER
       WRITE(61,*) ' *** PV DIRECT = ', PVTDIR

      RETURN
      END
***
      SUBROUTINE PREXY
      INCLUDE 'INFRAC1.FOR'

C
C .... transmissibility of west
C
       INODE = 0
      DO 10 I = 1, NROW
       DO 10 J = 1, NCOL
        INODE = INODE + 1
        RHW = RHOWI*EXP(CW*(P1(INODE)-P0))
         RHG = RHOGI*EXP(CG*(P1(INODE)-P0))

         P1(0) = 0.0

         IF(J.EQ.1) THEN
            WTW(INODE) = 0.0
          GTW(INODE) = 0.0
          GOTO 10
         ENDIF
```

```
      INIM1 = INODE - 1
     IF(P1(INODE).GE.P1(INIM1)) THEN

      RHWUP = RHOWI*EXP(CW*(P1(INODE)-P0))
      XKRUP = SW1(INODE)**RESOL
      IF(RESOL.GT.4) THEN
       XKRUP = 0.0
       IF(SW1(INODE).GT.0.999) XKRUP = 1.0
      ENDIF
      RHGUP = RHOGI*EXP(CG*(P1(INODE)-P0))

      XKUP  = 2.*KX(INODE)*KX(INIM1)/(KX(INODE)+KX(INIM1))
       DIST  = (DX(INODE)+DX(INIM1))/2.

    ELSE
      RHWUP = RHOWI*EXP(CW*(P1(INIM1)-P0))
      XKRUP = SW1(INIM1)**RESOL
      IF(RESOL.GT.4) THEN
       XKRUP = 0.0
       IF(SW1(INIM1).GT.0.999) XKRUP = 1.0
      ENDIF
       RHGUP = RHOGI*EXP(CG*(P1(INIM1)-P0))

       XKUP  = 2.*KX(INODE)*KX(INIM1)/(KX(INODE)+KX(INIM1))
       DIST  = (DX(INODE)+DX(INIM1))/2.

    ENDIF

     XKRUPW = XKRUP
     XKRUPG = 1.-XKRUP
     WTW(INODE)= - RHWUP*XKRUPW*XKUP/VISWW(INODE)
     &           *WFX(INODE)*DZ/DIST*DT/RHW
    GTW(INODE)= - RHGUP*XKRUPG*XKUP/VISG*WFX(INODE)*DZ/DIST*DT/RHG

 10  CONTINUE

C
C .... transmissibility of east
C
      INODE = 0
     DO 20 I = 1, NROW
      DO 20 J = 1, NCOL
      INODE = INODE + 1
      RHW = RHOWI*EXP(CW*(P1(INODE)-P0))
       RHG = RHOGI*EXP(CG*(P1(INODE)-P0))

       P1(0) = 0.0
```

```
      IF(J.EQ.NCOL) THEN
          WTE(INODE) = 0.0
       GTE(INODE) = 0.0
       GOTO 20
      ENDIF

      INIP1 = INODE + 1
     IF(P1(INODE).GE.P1(INIP1)) THEN

      RHWUP = RHOWI*EXP(CW*(P1(INODE)-P0))
      XKRUP = SW1(INODE)**RESOL
      IF(RESOL.GT.4) THEN
       XKRUP = 0.0
       IF(SW1(INODE).GT.0.999) XKRUP = 1.0
      ENDIF
      RHGUP = RHOGI*EXP(CG*(P1(INODE)-P0))

      XKUP  = 2.*KX(INODE)*KX(INIP1)/(KX(INODE)+KX(INIP1))
       DIST  = (DX(INODE)+DX(INIP1))/2.
    ELSE
      RHWUP = RHOWI*EXP(CW*(P1(INIP1)-P0))
      XKRUP = SW1(INIP1)**RESOL
      IF(RESOL.GT.4) THEN
       XKRUP = 0.0
       IF(SW1(INIP1).GT.0.999) XKRUP = 1.0
      ENDIF
       RHGUP = RHOGI*EXP(CG*(P1(INIP1)-P0))

       XKUP  = 2.*KX(INODE)*KX(INIP1)/(KX(INODE)+KX(INIP1))
       DIST  = (DX(INODE)+DX(INIP1))/2.
    ENDIF

     XKRUPW = XKRUP
     XKRUPG = 1.-XKRUP
     WTE(INODE)= - RHWUP*XKRUPW*XKUP/VISWE(INODE)
     &           *WFX(INODE)*DZ/DIST*DT/RHW
    GTE(INODE)= - RHGUP*XKRUPG*XKUP/VISG*WFX(INODE)*DZ/DIST*DT/RHG

 20  CONTINUE

C
C .... transmissibility of south
C
      INODE = 0
     DO 30 I = 1, NROW
     DO 30 J = 1, NCOL
      INODE = INODE + 1
      RHW = RHOWI*EXP(CW*(P1(INODE)-P0))
       RHG = RHOGI*EXP(CG*(P1(INODE)-P0))
```

```
      P1(0) = 0.0

      IF(I.EQ.1) THEN
          WTS(INODE) = 0.0
        GTS(INODE) = 0.0
        GOTO 30
      ENDIF

      INJM1 = INODE - NCOL
     IF(P1(INODE).GE.P1(INJM1)) THEN

      RHWUP = RHOWI*EXP(CW*(P1(INODE)-P0))
      XKRUP = SW1(INODE)**RESOL
      IF(RESOL.GT.4) THEN
        XKRUP = 0.0
        IF(SW1(INODE).GT.0.999) XKRUP = 1.0
      ENDIF
      RHGUP = RHOGI*EXP(CG*(P1(INODE)-P0))

      XKUP  = 2.*KY(INODE)*KY(INJM1)/(KY(INODE)+KY(INJM1))
       DIST  = (DY(INODE)+DY(INJM1))/2.
    ELSE
      RHWUP = RHOWI*EXP(CW*(P1(INJM1)-P0))
      XKRUP = SW1(INJM1)**RESOL
      IF(RESOL.GT.4) THEN
        XKRUP = 0.0
        IF(SW1(INJM1).GT.0.999) XKRUP = 1.0
      ENDIF
       RHGUP = RHOGI*EXP(CG*(P1(INJM1)-P0))

       XKUP  = 2.*KY(INODE)*KY(INJM1)/(KY(INODE)+KY(INJM1))
       DIST  = (DY(INODE)+DY(INJM1))/2.
    ENDIF

     XKRUPW = XKRUP
     XKRUPG = 1.-XKRUP
     WTS(INODE)= - RHWUP*XKRUPW*XKUP/VISWS(INODE)
     &           *WFY(INODE)*DZ/DIST*DT/RHW
    GTS(INODE)= - RHGUP*XKRUPG*XKUP/VISG*WFY(INODE)*DZ/DIST*DT/RHG

 30   CONTINUE

C
C .... transmissibility of nouth
C
      INODE = 0
     DO 40 I = 1, NROW
      DO 40 J = 1, NCOL
```

```
      INODE = INODE + 1
      RHW = RHOWI*EXP(CW*(P1(INODE)-P0))
       RHG = RHOGI*EXP(CG*(P1(INODE)-P0))

       P1(0) = 0.0

       IF(I.EQ.NROW) THEN
           WTN(INODE) = 0.0
        GTN(INODE) = 0.0
        GOTO 40
       ENDIF

       INJP1 = INODE + NCOL
      IF(P1(INODE).GE.P1(INJP1)) THEN

       RHWUP = RHOWI*EXP(CW*(P1(INODE)-P0))
       XKRUP = SW1(INODE)**RESOL
       IF(RESOL.GT.4) THEN
        XKRUP = 0.0
        IF(SW1(INODE).GT.0.999) XKRUP = 1.0
       ENDIF
       RHGUP = RHOGI*EXP(CG*(P1(INODE)-P0))

       XKUP  = 2.*KY(INODE)*KY(INJP1)/(KY(INODE)+KY(INJP1))
        DIST  = (DY(INODE)+DY(INJP1))/2.
     ELSE
       RHWUP = RHOWI*EXP(CW*(P1(INJP1)-P0))
       XKRUP = SW1(INJP1)**RESOL
       IF(RESOL.GT.4) THEN
        XKRUP = 0.0
        IF(SW1(INJP1).GT.0.999) XKRUP = 1.0
       ENDIF
        RHGUP = RHOGI*EXP(CG*(P1(INJP1)-P0))

        XKUP  = 2.*KY(INODE)*KY(INJP1)/(KY(INODE)+KY(INJP1))
        DIST  = (DY(INODE)+DY(INJP1))/2.
     ENDIF

      XKRUPW = XKRUP
      XKRUPG = 1.-XKRUP
      WTN(INODE)= - RHWUP*XKRUPW*XKUP/VISWN(INODE)
      &           *WFY(INODE)*DZ/DIST*DT/RHW
     GTN(INODE)= - RHGUP*XKRUPG*XKUP/VISG*WFY(INODE)*DZ/DIST*DT/RHG

 40   CONTINUE

     RETURN
     END
***
```

```
      SUBROUTINE SWEEP
      INCLUDE 'INFRAC1.FOR'
       PARAMETER(II=NCOL,JJ=NROW,KK=1,TOL=1.E-10)
       PARAMETER(IJKM=II*JJ*KK)
      DIMENSION AW(IJKM), AE(IJKM), AS(IJKM), AN(IJKM)
       DIMENSION AT(IJKM), AB(IJKM), E (IJKM), B (IJKM)
      DIMENSION AL3(IJKM),AL2(IJKM),AL1(IJKM),AD(IJKM)
      DIMENSION AU1(IJKM),AU2(IJKM),AU3(IJKM)
      DIMENSION QI(15,IJKM),AQI(15,IJKM),QN(IJKM),AQN(IJKM)
      DIMENSION RN(IJKM),DXN(IJKM),ADX(IJKM)

      DO 10 I = 1, NODE
       AW (I) = 0.0
       AE (I) = 0.0
       AS (I) = 0.0
       AN (I) = 0.0
        AT (I) = 0.0
        AB (I) = 0.0
        E  (I) = 0.0
        B  (I) = 0.0
10    CONTINUE

      DO 20 I = 1, NODE
       RHW   = RHOWI*EXP(CW*(P1(I)-P0))
       RHG   = RHOGI*EXP(CG*(P1(I)-P0))
       AW(I)  = - WTW(I) - GTW(I)
        AE(I)  = - WTE(I) - GTE(I)
        AS(I)  = - WTS(I) - GTS(I)
        AN(I)  = - WTN(I) - GTN(I)

       E (I)  = +WTW(I)+GTW(I)+WTE(I)+GTE(I)
     &          +WTS(I)+GTS(I)+WTN(I)+GTN(I)

        STOREW(I) = VOL(I)*PORO(I)*SW1(I)*CW*RHW/RHW
        STOREG(I) = VOL(I)*PORO(I)*SG1(I)*CG*RHG/RHG
       E (I)  = E(I) - STOREW(I) - STOREG(I)
       B (I)  = - STOREW(I)*P1(I) - STOREG(I)*P1(I)

       IF(I.EQ.IINJ .OR. I.EQ.IPRO .OR.IYXM(I).EQ.4) THEN
        AW(I) = 0.0
        AE(I) = 0.0
        AS(I) = 0.0
        AN(I) = 0.0
         E (I) = 1.0
         B (I) = P1(I)
         IF(IYXM(I).EQ.4) B(I) = 0.0
      ENDIF

20    CONTINUE
```

```
 ITMAX1 = 50

 CALL CMAT(AW,AE,AS,AN,AT,AB,E,B,TOL,II,JJ,KK,IJKM,ITMAX1
&          ,QI,AQI,AL3,AL2,AL1,AD,AU1,AU2
&          ,AU3,QN,AQN,RN,DXN,ADX,P2)

DO 30 I = 1, NODE

 IF(I-1.EQ.0) THEN
      WFLUXW(I) = 0.0
   GFLUXW(I) = 0.0
 ELSE
      WFLUXW(I) = WTW(I)*(P2(I)-P2(I-1))
   GFLUXW(I) = GTW(I)*(P2(I)-P2(I-1))
      IF(ABS(P2(I)-P2(I-1)).LT.1.E-3) THEN
       WFLUXW(I) = 0.0
       GFLUXW(I) = 0.0
      ENDIF
ENDIF

 IF(I+1.EQ.NODE+1) THEN
   WFLUXE(I) = 0.0
   GFLUXE(I) = 0.0
 ELSE
   WFLUXE(I) = WTE(I)*(P2(I+1)-P2(I))
 GFLUXE(I) = GTE(I)*(P2(I+1)-P2(I))
      IF(ABS(P2(I+1)-P2(I)).LT.1.E-3) THEN
       WFLUXE(I) = 0.0
       GFLUXE(I) = 0.0
      ENDIF
 ENDIF

TERMXW(I) = WFLUXW(I) - WFLUXE(I)
TERMXG(I) = GFLUXW(I) - GFLUXE(I)

 IF(I-NCOL.LE.0) THEN
   WFLUXS(I) = 0.0
   GFLUXS(I) = 0.0
 ELSE
   WFLUXS(I) = WTS(I)*(P2(I)-P2(I-NCOL))
      GFLUXS(I) = GTS(I)*(P2(I)-P2(I-NCOL))
      IF(ABS(P2(I)-P2(I-NCOL)).LT.1.E-3) THEN
       WFLUXS(I) = 0.0
       GFLUXS(I) = 0.0
      ENDIF
 ENDIF

 IF(I+NCOL.GE.NODE+1) THEN
```

```
          WFLUXN(I) = 0.0
            GFLUXN(I) = 0.0
         ELSE
          WFLUXN(I) = WTN(I)*(P2(I+NCOL)-P2(I))
           GFLUXN(I) = GTN(I)*(P2(I+NCOL)-P2(I))
             IF(ABS(P2(I+NCOL)-P2(I)).LT.1.E-3) THEN
              WFLUXN(I) = 0.0
              GFLUXN(I) = 0.0
             ENDIF
         ENDIF

         TERMYW(I) = WFLUXS(I) - WFLUXN(I)
         TERMYG(I) = GFLUXS(I) - GFLUXN(I)

C    WRITE(*,*) ' 0/1 CONTINUE/STOP '
C    READ (*,*) ISTOP
C    IF(ISTOP.EQ.1) STOP
C    ENDIF

 30  CONTINUE

      RETURN
      END
***
      SUBROUTINE SAT(IDT)
      INCLUDE 'INFRAC1.FOR'

       INODE = NODE

      DO 10 I = 1, INODE
       IF(I.EQ.IINJ) THEN
        SW2(I) = 1.0
        SG2(I) = 0.0
         IF(ITRACER.EQ.1 .AND. PVINJ.LT.PVTRACER) THEN
          CTW1(I) = 1.0
          CTW2(I) = 1.0
          CT1(I)  = 1.0
          CT2(I)  = 1.0
         ELSE
          CTW1(I) = 0.0
          CTW2(I) = 0.0
          CT1 (I) = 0.0
          CT2 (I) = 0.0
         ENDIF
        GOTO 10
       ENDIF
       IF(I.EQ.IPRO) THEN
        SW2(I) = 0.0
        SG2(I) = 1.0
```

```
      IF(ITRACER.EQ.1) CTW2(I)=0.0
      IF(ITRACER.EQ.1) CT2 (I)=0.0
     GOTO 10
     ENDIF

C     speed up procedure only if no tracer
     IF(ITRACER.EQ.1) GOTO 111
     IF(IYXM(I).EQ.1 .AND. SW1(I).GT.0.5) THEN
      SW2(I) = 1.0
      SG2(I) = 0.0
      GOTO 10
     ENDIF
 111 CONTINUE
C

C     WRITE(*,*) VOL(I), PORO(I)
     WLHS  = TERMXW(I) + TERMYW(I)
     WRHS2 = VOL(I)*PORO(I)*SW1(I)*CW*(P2(I)-P1(I))
     WRHS1 = WLHS - WRHS2

     SW2(I) = SW1(I) + WRHS1/VOL(I)/PORO(I)

     IF(SW2(I).GE.1.0) SW2(I)=1.0
     IF(SW2(I).LE.0.0) SW2(I)=0.0
C     the following statement is to speed up the program
C     assuming the interception's volume is neglegible
C     only for none tracer cases
      IF(ITRACER.EQ.1) GOTO 222
      IF(IYXM(I).EQ.1 .AND. SW2(I).GT.0.01) SW2(I)=1.0
 222  CONTINUE

     IF(ITRACER.EQ.0) GOTO 333

     RHW = RHOWI*EXP(CW*(P1(INODE)-P0))
     RHG = RHOGI*EXP(CG*(P1(INODE)-P0))


     IF(ISWITCH.EQ.0) GOTO 555

     IF(WFLUXW(I).GT.0.0) THEN
        CFLUXW = CTW1(I-1)*WFLUXW(I)*RHW
        IF(CTW1(I-1).GT.1.E-3) CFLUXW=1.0*WFLUXW(I)*RHW
      ELSE
        CFLUXW = CTW1(I)*WFLUXW(I)*RHW
        IF(CTW1(I).GT.1.E-3) CFLUXW=1.0*WFLUXW(I)*RHW
      ENDIF

C     WRITE(*,*) ' IN LOOP 3333, I = ', I
```

```
      IF(WFLUXE(I).GT.0.0) THEN
        CFLUXE = CTW1(I)*WFLUXE(I)*RHW
        IF(CTW1(I).GT.1.E-3) CFLUXE=1.0*WFLUXE(I)*RHW
       ELSE
        CFLUXE = CTW1(I+1)*WFLUXE(I)*RHW
        IF(CTW1(I+1).GT.1.E-3) CFLUXE=1.0*WFLUXE(I)*RHW
       ENDIF

C     WRITE(*,*) ' IN LOOP 3334, I = ', I

      IF(WFLUXS(I).GT.0.0) THEN
           CFLUXS = 0.0
        IF(I-NCOL.GT.0) THEN
            CFLUXS = CTW1(I-NCOL)*WFLUXS(I)*RHW
         IF(CTW1(I-NCOL).GT.1.E-3) CFLUXS=1.0*WFLUXS(I)*RHW
        ENDIF
       ELSE
        CFLUXS = CTW1(I)*WFLUXS(I)*RHW
        IF(CTW1(I).GT.1.E-3) CFLUXS=1.0*WFLUXS(I)*RHW
       ENDIF
C     WRITE(*,*) ' IN LOOP 3335, I = ', I

      IF(WFLUXN(I).GT.0.0) THEN
        CFLUXN = CTW1(I)*WFLUXN(I)*RHW
        IF(CTW1(I).GT.1.E-3) CFLUXN=1.0*WFLUXN(I)*RHW
       ELSE
        CFLUXN = 0.0
        IF(I+NCOL.LT.NODE+1) THEN
           CFLUXN = CTW1(I+NCOL)*WFLUXN(I)*RHW
         IF(CTW1(I+NCOL).GT.1.E-3) CFLUXN=1.0*WFLUXN(I)*RHW
        ENDIF
       ENDIF

       DSWW = SW2(I)
        IF(DSWW.LT.1.E-4) THEN
           CTW2(I) = CTW1(I)
         GOTO 333
        ENDIF

        ACC    = CFLUXW-CFLUXE+CFLUXS-CFLUXN
       CT     = VOL(I)*SW1(I)*CTW1(I)*PORO(I)*RHW
        CTW2(I) = (ACC+CT)/VOL(I)/SW2(I)/PORO(I)/RHW

C     WRITE(*,*) ' IN LOOP 3334, ISWITCH = ', ISWITCH

 555  CONTINUE

      IF(ISWITCH.EQ.1) GOTO 666
```

```
      IF(WFLUXW(I)+GFLUXW(I).GT.0.0) THEN
         XXX   = (WFLUXW(I)*RHW+GFLUXW(I)*RHG)
         CFLUXW = CT1(I-1)*XXX
C        IF(CT1(I-1).GT.1.E-3) CFLUXW=1.0*XXX
       ELSE
         XXX   = (WFLUXW(I)*RHW+GFLUXW(I)*RHG)
         CFLUXW = CT1(I)*XXX
C        IF(CT1(I).GT.1.E-3) CFLUXW=1.0*XXX
       ENDIF

      IF(WFLUXE(I)+GFLUXE(I).GT.0.0) THEN
         XXX = (WFLUXE(I)*RHW+GFLUXE(I)*RHG)
         CFLUXE = CT1(I)*XXX
C        IF(CT1(I).GT.1.E-3) CFLUXE=1.0*XXX
       ELSE
         XXX = (WFLUXE(I)*RHW+GFLUXE(I)*RHG)
         CFLUXE = CT1(I+1)*XXX
C        IF(CT1(I+1).GT.1.E-3) CFLUXE=1.0*XXX
       ENDIF


      IF(WFLUXS(I)+GFLUXS(I).GT.0.0) THEN
           CFLUXS = 0.0
         IF(I-NCOL.GT.0) THEN
          XXX = (WFLUXS(I)*RHW+GFLUXS(I)*RHG)
            CFLUXS = CT1(I-NCOL)*XXX
C         IF(CT1(I-NCOL).GT.1.E-3) CFLUXS=1.0*XXX
         ENDIF
       ELSE
         XXX = (WFLUXS(I)*RHW+GFLUXS(I)*RHG)
         CFLUXS = CT1(I)*XXX
C        IF(CT1(I).GT.1.E-3) CFLUXS=1.0*XXX
       ENDIF

      IF(WFLUXN(I)+GFLUXN(I).GT.0.0) THEN
         XXX = (WFLUXN(I)*RHW+GFLUXN(I)*RHG)
         CFLUXN = CT1(I)*XXX
C        IF(CT1(I).GT.1.E-3) CFLUXN=1.0*XXX
       ELSE
         CFLUXN = 0.0
         IF(I+NCOL.LT.NODE+1) THEN
          XXX = (WFLUXN(I)*RHW+GFLUXN(I)*RHG)
            CFLUXN = CT1(I+NCOL)*XXX
C         IF(CT1(I+NCOL).GT.1.E-3) CFLUXN=1.0*XXX
         ENDIF
       ENDIF
        ACC   = CFLUXW-CFLUXE+CFLUXS-CFLUXN
       CT    = VOL(I)*(SW1(I)+SG1(I))*CT1(I)*PORO(I)*RHW
        CT2(I) = (ACC+CT)/VOL(I)/(SW1(I)+SG1(I))/PORO(I)/RHW
```

```
 666  CONTINUE

C     WRITE(*,*) ' AFTER 666, I = ', I


C       WRITE(*,*) 'BEFORE', I

      IF(CTW2(I).LT.0.0) CTW2(I) = 0.0
      IF(CTW2(I).GT.1.0) CTW2(I) = 1.0
      IF(CT2(I).LT.0.0) CT2(I) = 0.0
      IF(CT2(I).GT.1.0) CT2(I) = 1.0

 333  CONTINUE
C
     SG2(I) = 1.0 - SW2(I)

 10   CONTINUE

    IDT = 1

    DO 20 I = 1, NODE
     IF(I.EQ.IINJ .OR. I.EQ.IPRO) GOTO 20
     DP  = ABS(P2(I)-P1(I))
     DSW = ABS(SW2(I)-SW1(I))
      DC  = ABS(CTW2(I)-CTW1(I))
      IF(ISWITCH.EQ.0) DC = ABS(CT2(I)-CT1(I))
C     the following statement also to speed up the process
       IF(ITRACER.EQ.1) GOTO 444
       IF(IYXM(I).EQ.1) GOTO 20
 444  CONTINUE
C
     IF(DP.GT.0.1 .OR. DSW.GT.0.1 .OR. DC.GT.0.1) IDT = - 1
 20   CONTINUE

      XINJW = 0
      XPROW = 0
      XINJG = 0
      XPROG = 0
     DO 30 I = 1, NODE
      IF(I.EQ.IINJ) THEN
       XINJW = XINJW + TERMXW(I) + TERMYW(I)
       XINJG = XINJG + TERMXG(I) + TERMYG(I)
      ENDIF
      IF(I.EQ.IPRO) THEN
       XPROW = XPROW + TERMXW(I) + TERMYW(I)
       XPROG = XPROG + TERMXG(I) + TERMYG(I)
        COUT = CTW2(IPRO-1)*TERMXW(I)/(XPROW+XPROG)
        IF(ISWITCH.EQ.0) THEN
```

```
      COUT = CT2(IPRO-1)*(WFLUXW(I)+GFLUXW(I))/(XPROW+XPROG)
     ENDIF
    ENDIF
30  CONTINUE

    XINJWT = XINJWT + XINJW
    XINJGT = XINJGT + XINJG
    XPROWT = XPROWT + XPROW
    XPROGT = XPROGT + XPROG

   DO 40 I = 1, NODE
    SW1(I) = SW2(I)
    SG1(I) = SG2(I)
    P1(I)  = P2(I)
     IF(ITRACER.EQ.1) THEN
      IF(CTW2(I).GT.1.0) CTW2(2) = 1.0
      IF(CTW2(I).LT.0.0) CTW2(2) = 0.0
      IF(CT2(I).GT.1.0) CT2(2)=1.0
      IF(CT2(I).LT.0.0) CT2(2)=0.0
      CTW1(I) = CTW2(I)
      CT1(I) = CT2(I)
     ENDIF

40  CONTINUE

   RETURN
   END


***
   SUBROUTINE PVINJE(IPRINT)
   INCLUDE 'INFRAC1.FOR'

   XINJT = XINJWT + XINJGT
   PVINJ = ABS(XINJT/OWGIP)
   IF(PVINJ.GT.PVPRINT) THEN
    IPRINT  = 1
    PVPRINT = PVPRINT + DPV
   ELSE
    IPRINT  = 0
   ENDIF

   RETURN
   END
***

***
   SUBROUTINE PRINT
   INCLUDE 'INFRAC1.FOR'
```

```
      IF(ISWITCH.EQ.0) GOTO 111

      WRITE(61,*)
      WRITE(61,*)
      WRITE(61,*) ' *** CASE       = ', ICASE
      WRITE(61,*) ' *** PVINJ      = ', PVINJ
       WRITE(61,*) ' *** TIME(sec)  = ', TTOTAL

      XPROT = XPROW + XPROG

      WRITE(61,*) ' *** KfWf X(darcy cm) = ', XKFWF
      WRITE(61,*) ' *** KfWf Y(darcy cm) = ', YKFWF
      WRITE(61,*) ' *** VISW(cp)         = ', VISW
      WRITE(61,*) ' *** VISG(cp)         = ', VISG
      WRITE(61,*) ' *** RESOL(5=piston)  = ', RESOL

       if(ncol.gt.11) goto 111

      WRITE(61,*)
      WRITE(61,*) ' **** PRESSURE PROFILE (atm) **** '
      WRITE(61,*)

      INDEX=0
      DO 50 I = 1, NROW
       WRITE(61,601) (P2(INDEX+J),J=1,NCOL)
       INDEX=INDEX+NCOL
50    CONTINUE

601   FORMAT(11(1X,F7.2))

      WRITE(61,*)
      WRITE(61,*) ' **** Sp (-), p: injecting fluid **** '
      WRITE(61,*)

      INDEX=0
      DO 71 I = 1, NROW
       WRITE(61,602) (SW2(INDEX+J),J=1,NCOL)
       INDEX=INDEX+NCOL
71    CONTINUE

602   FORMAT(11(1X,F7.4))

       IF(ITRACER.EQ.0) GOTO 999

      WRITE(61,*)
      WRITE(61,*) ' **** C(TRACER) **** '
      WRITE(61,*)
       WRITE(61,*) ' **** COUT = ', COUT
```

```
C     INDEX=0
C     WRITE(61,*) '*** CTW2 ***'
C     DO 72 I = 1, NROW
C      WRITE(61,602) (CTW2(INDEX+J),J=1,NCOL)
C      INDEX=INDEX+NCOL
C 72   CONTINUE

      IF(ISWITCH.EQ.1) GOTO 999

 111 CONTINUE
      WRITE(61,*)
     WRITE(61,*) ' *** PVINJ      = ', PVINJ
     WRITE(61,*) ' *** TIME(sec)  = ', TTOTAL
     WRITE(61,*) ' *** C(TRACER) *** '
      WRITE(61,*) ' *** COUT      = ', COUT
      WRITE(61,*) ' *** CTW2(NBT1) = ', CTW2(NBT1)
      WRITE(61,*) ' *** CT2(NBT1)  = ', CT2(NBT1)
      WRITE(61,*) ' *** SW2(NBT1)  = ', SW2(NBT1)
      WRITE(69,*) TTOTAL, PVINJ, COUT

      if(ncol.gt.11) goto 999

C     INDEX=0
C     WRITE(61,*) '*** CT2 ***'
C     DO 73 I = 1, NROW
C     WRITE(61,602) (CT2(INDEX+J),J=1,NCOL)
C     INDEX=INDEX+NCOL
C 73   CONTINUE

 999  CONTINUE

     RETURN
     END
***
     SUBROUTINE CMAT(AW,AE,AS,AN,AT,AB,E,B,TOL,II,JJ,KK,IJKM,ITMAX
    &           ,QI,AQI,AL3,AL2,AL1,AD,AU1,AU2
    &           ,AU3,QN,AQN,RN,DXN,ADX,P)
     DIMENSION AW(IJKM),AE(IJKM),AS(IJKM),AN(IJKM),AT(IJKM)
    &       ,AB(IJKM),E(IJKM),B(IJKM),P(IJKM)
     DIMENSION AL3(IJKM),AL2(IJKM),AL1(IJKM),AD(IJKM)
    &       ,AU1(IJKM),AU2(IJKM),AU3(IJKM)
     DIMENSION QI(15,IJKM),AQI(15,IJKM),QN(IJKM),AQN(IJKM)
     DIMENSION RN(IJKM),DXN(IJKM),ADX(IJKM)

C     Author: Eric Chang
C           Assistant Professor of Chemical Engineering
C           New Mexico Tech
C           Tel: 505-835-5564
```

```
C
C
C .... AW, west band,    X-Y
C     AE, east band,    X-Y
C     AS, south band,   X-Y
C     AN, north band,   X-Y
C     AT, top band,     Z
C     AB, bottom band,  Z
C     E,  diagonal band,
C     B,  RHS vector,
C     TOL   = 0.0001
C     IJKM  = II x JJ x KK = 20 x 20 x 20 = 8000
C     ITMAX = 50
C
C
C    ORTHOMIN SPARSE MATRIX SOLVER BASED ON PAPER BY P. K. W. VINSOME
C    FOUTH SYMPOSIUM ON RESERVOIR SIMULATION
C    LOS ANGELES, CALIFORNIA    FEBRUARY 19-20,1976
C
     INX = II
     INXY = II*JJ
     IB = 0
     DO 500 K = 1,KK
      DO 450 J = 1,JJ
       DO 400 I = 1,II
        IB = IB + 1
        FAC = 1.0/E(IB)
        IF(I .NE. 1) AL1(IB) = FAC*AW(IB)
        IF(I .NE. II) AU1(IB) = FAC*AE(IB)
        IF(J .NE. 1) AL2(IB) = FAC*AS(IB)
        IF(J .NE. JJ) AU2(IB) = FAC*AN(IB)
        IF(K .NE. 1) AL3(IB) = FAC*AT(IB)
        IF(K .NE. KK) AU3(IB) = FAC*AB(IB)
        RN(IB) = FAC*B(IB)
  400   CONTINUE
  450  CONTINUE
  500 CONTINUE
C
C    APPROXIMATE LDU FACTORIZATION
C

     AD(1) = 1.0
     DO 550 I = 2,INX
      TERM = 1.0 - AL1(I)*AD(I-1)*AU1(I-1)
      AD(I) = 1.0/TERM
  550 CONTINUE
     DO 600 I = INX+1,INXY
      TERM = 1.0 - AL1(I)*AD(I-1)*AU1(I-1)
     &           - AL2(I)*AD(I-INX)*AU2(I-INX)
```

```
    AD(I) = 1.0/TERM
600 CONTINUE
   DO 650 I = INXY+1,IJKM
    TERM = 1.0 - AL1(I)*AD(I-1)*AU1(I-1)
  &          - AL2(I)*AD(I-INX)*AU2(I-INX)
  &          - AL3(I)*AD(I-INXY)*AU3(I-INXY)
    AD(I) = 1.0/TERM
650 CONTINUE
   CALL ORTH(AL3,AL2,AL1,AD,AU1,AU2,AU3,TOL
  &       ,INX,INXY,IJKM,ITMAX
  &       ,RN,DXN,ADX,QI,AQI,QN,AQN,P)
   RETURN
   END


   SUBROUTINE MVEC(AL3,AL2,AL1,AU1,AU2,AU3,R
  &           ,INX,INXY,IJKM,C)
   DIMENSION AL3(IJKM),AL2(IJKM),AL1(IJKM)
  &       ,AU1(IJKM),AU2(IJKM),AU3(IJKM)
   DIMENSION R(IJKM), C(IJKM)
   DO 100 I = 1,IJKM
    C(I) = R(I)
100 CONTINUE
   DO 200 I = 1,IJKM-1
    C(I) = C(I) + AU1(I)*R(I+1)
200 CONTINUE
   DO 300 I = 1,IJKM-INX
    C(I) = C(I) + AU2(I)*R(I+INX)
300 CONTINUE
   DO 400 I = 1,IJKM-INXY
    C(I) = C(I) + AU3(I)*R(I+INXY)
400 CONTINUE
   DO 500 I = 2,IJKM
    C(I) = C(I) + AL1(I)*R(I-1)
500 CONTINUE
   DO 600 I = INX+1,IJKM
    C(I) = C(I) + AL2(I)*R(I-INX)
600 CONTINUE
   DO 700 I = INXY+1,IJKM
    C(I) = C(I) + AL3(I)*R(I-INXY)
700 CONTINUE
   RETURN
   END


   SUBROUTINE ORTH(AL3,AL2,AL1,AD,AU1,AU2,AU3,TOL
  &           ,INX,INXY,IJKM,ITMAX
  &           ,RN,DXN,ADX,QI,AQI,QN,AQN,DP)
   DIMENSION AL3(IJKM),AL2(IJKM),AL1(IJKM),AD(IJKM)
```

```
     &       ,AU1(IJKM),AU2(IJKM),AU3(IJKM)
      DIMENSION DP(IJKM),RN(IJKM),DXN(IJKM),ADX(IJKM)
      DIMENSION AQIAQI(15),QI(15,IJKM),AQI(15,IJKM)
      DIMENSION QN(IJKM),AQN(IJKM)
      DATA NMAX/15/
      CONV1 = TOL*TOL
      IF(CONV1 .GT. 1.E-4) CONV1 = 1.E-4
      RSQ = 0.0
      DO 100 IB = 1,IJKM
       DP(IB) = 0.0
       RSQ = RSQ + RN(IB)*RN(IB)
  100 CONTINUE
      CONV = CONV1*RSQ
      N = 0
      DO 800 ITER = 1,ITMAX
       IT = ITER
       IF(N .EQ. NMAX) N = 0
       N = N + 1
       NM1 = N - 1
       CALL MSOLVE(AL3,AL2,AL1,AD,AU1,AU2,AU3,RN
     &           ,INX,INXY,IJKM,DXN)
       CALL MVEC(AL3,AL2,AL1,AU1,AU2,AU3,DXN
     &         ,INX,INXY,IJKM,ADX)
       IF(N .EQ. 1) THEN
        DO 200 IB = 1,IJKM
         QN(IB) = DXN(IB)
         AQN(IB) = ADX(IB)
         QI(1,IB) = QN(IB)
         AQI(1,IB) = AQN(IB)
  200    CONTINUE
       ELSE
        DO 300 IB = 1,IJKM
         QN(IB) = DXN(IB)
  300    CONTINUE
        DO 500 I = 1,NM1
         AQIADX = 0.0
         DO 350 IB = 1,IJKM
          AQIADX = AQIADX + AQI(I,IB)*ADX(IB)
  350     CONTINUE
         AI = AQIADX/AQIAQI(I)
         DO 400 IB = 1,IJKM
          QN(IB) = QN(IB) - AI*QI(I,IB)
  400     CONTINUE
  500    CONTINUE
        CALL MVEC(AL3,AL2,AL1,AU1,AU2,AU3,QN
     &           ,INX,INXY,IJKM,AQN)
        DO 650 IB = 1,IJKM
         QI(N,IB) = QN(IB)
         AQI(N,IB) = AQN(IB)
```

```
 650    CONTINUE
      ENDIF
      AQNAQN = 0.0
      AQNRN = 0.0
      DO 700 IB = 1,IJKM
        AQNAQN = AQNAQN + AQN(IB)*AQN(IB)
        AQNRN = AQNRN + AQN(IB)*RN(IB)
 700  CONTINUE
      AQIAQI(N) = AQNAQN
      OMEGA = AQNRN/AQNAQN
      RSQ = 0.0
      DO 750 IB = 1,IJKM
        DP(IB) = DP(IB) + OMEGA*QN(IB)
        RN(IB) = RN(IB) - OMEGA*AQN(IB)
        RSQ = RSQ + RN(IB)*RN(IB)
 750  CONTINUE
      IF(RSQ .LT. CONV) GOTO 900
 800 CONTINUE
 900 CONTINUE
C     WRITE(6,1900) IT
      RETURN
C 1900 FORMAT(5X,'ORTHOMIN CONVERGED AFTER ',I3,' ITERATIONS')
      END

      SUBROUTINE MSOLVE(AL3,AL2,AL1,AD,AU1,AU2,AU3,R
     &                 ,INX,INXY,IJKM,XX)
      DIMENSION AL3(IJKM),AL2(IJKM),AL1(IJKM),AD(IJKM)
     &         ,AU1(IJKM),AU2(IJKM),AU3(IJKM)
      DIMENSION XX(IJKM),R(IJKM)
C
C     FORWARD ELIMINATION
C
      XX(1) = AD(1)*R(1)
      DO 100 I = 2,INX
        XX(I) = AD(I)*(R(I)-AL1(I)*XX(I-1))
  100 CONTINUE
      DO 200 I = INX+1,INXY
        XX(I) = AD(I)*(R(I)-AL1(I)*XX(I-1)-AL2(I)*XX(I-INX))
  200 CONTINUE
      DO 300 I = INXY+1,IJKM
        XX(I) = AD(I)*(R(I)-AL1(I)*XX(I-1)-AL2(I)*XX(I-INX)
     &         -AL3(I)*XX(I-INXY))
  300 CONTINUE
      DO 400 I = 1,IJKM
        XX(I) = XX(I)/AD(I)
  400 CONTINUE
C
C     BACK SUBSTITUTION
C
```

```
      DO 500 I = IJKM-1,IJKM-INX+1,-1
        XX(I) = AD(I)*(XX(I)-AU1(I)*XX(I+1))
  500 CONTINUE
      DO 600 I = IJKM-INX,IJKM-INXY+1,-1
        XX(I) = AD(I)*(XX(I)-AU1(I)*XX(I+1)-AU2(I)*XX(I+INX))
  600 CONTINUE
      DO 700 I = IJKM-INXY,1,-1
        XX(I) = AD(I)*(XX(I)-AU1(I)*XX(I+1)-AU2(I)*XX(I+INX)
     &        -AU3(I)*XX(I+INXY))
  700 CONTINUE
      RETURN
      END
C
      SUBROUTINE NETWORK

       PARAMETER(NODET=5000)

       OPEN(52,FILE='DATAN.DAT')

       WRITE(*,*) ' *** what is the size of the network ?   *** '
       WRITE(*,*) ' *** if it is a 2 5x5, please enter 5.   *** '
       WRITE(*,*) ' *** size = '

       READ(*,*) NSIZE

       DLARGE = 40000/(NSIZE-1)
       DSMALL = DLARGE/1000

       NCOL = (NSIZE*2-1)
       NROW = (NSIZE*2-1)*2-1
       NODE = NCOL*NROW
       IINJ = NCOL*(NCOL-1)+1
       IPRO = NCOL*NCOL
       NBT1 = NCOL*(NCOL-1)+(NCOL+1)/2

       WRITE(52,*) NODET, ' ! *** NODET '
       WRITE(52,*) NCOL,  ' ! *** NCOL  '
       WRITE(52,*) NROW,  ' ! *** NROW  '
       WRITE(52,*) NODE,  ' ! *** NODE  '
       WRITE(52,*) IINJ,  ' ! *** IINJ  '
       WRITE(52,*) IPRO,  ' ! *** IPRO  '
       WRITE(52,*) NBT1,  ' ! *** NBT1  '
       WRITE(*,*) NODET, '! *** NODET '
       WRITE(*,*) NCOL,  '! *** NCOL  '
       WRITE(*,*) NROW,  '! *** NROW  '
       WRITE(*,*) NODE,  '! *** NODE  '
       WRITE(*,*) IINJ,  '! *** IINJ  '
       WRITE(*,*) IPRO,  '! *** IPRO  '
       WRITE(*,*) NBT1,  '! *** NBT1  '
```

```
      IF(NODE.GT.NODET) THEN
       WRITE(*,*) ' *** NODET too small ***'
       STOP
      ENDIF

      INODE = 1
      IROW  = 1

111   CONTINUE

      IYXM = 1
      DO 10 I = 1, NCOL
       IF(IYXM.EQ.1) THEN
        DX = DSMALL
        DY = DSMALL
       ELSE
        DX = DLARGE
        DY = DSMALL
       ENDIF
       WRITE(52,*) INODE, IYXM, DX, DY, IROW
       INODE = INODE + 1
       IF(IYXM.EQ.1) THEN
        IYXM = 3
       ELSE
        IYXM = 1
       ENDIF
10    CONTINUE
      IROW = IROW+1
      IF(IROW.EQ.NROW+1) GOTO 222

      IYXM = 2
      DO 20 I = 1, NCOL
       IF(IYXM.EQ.2) THEN
        DX = DSMALL
        DY = DLARGE
       ELSE
        DX = DLARGE
        DY = DLARGE
       ENDIF
       WRITE(52,*) INODE, IYXM, DX, DY, IROW
       INODE = INODE + 1
       IF(IYXM.EQ.2) THEN
        IYXM = 4
       ELSE
        IYXM = 2
       ENDIF
20    CONTINUE
```

```
      IROW = IROW+1
      IF(IROW.EQ.NROW+1) GOTO 222

     GOTO 111

222  CONTINUE

      IF(NCOL.GT.20) GOTO 333
      WRITE(52,*)
      DO 25 I = 1, NROW
       IJ = (I-1)*NCOL
       WRITE(52,601) (IJ+K,K=1,NCOL)
25    CONTINUE
601   FORMAT(25I5)
      WRITE(52,*)
      GOTO 999

333   CONTINUE
      NHALF = NCOL/2
      WRITE(52,*) '*** LEFT '
      DO 26 I = 1, NROW
       IJ = (I-1)*NCOL
       WRITE(52,601) (IJ+K,K=1,NHALF)
26    CONTINUE
     WRITE(52,*)   '*** RIGHT '
      DO 27 I = 1, NROW
       IJ = (I-1)*NCOL
       WRITE(52,601) (IJ+K,K=NHALF+1,NCOL)
27    CONTINUE

999   CONTINUE

      RETURN
      END
```

APPENDIX F: Derivation of Eq. 55 in Chapter 5

In the Bingham rheological model,[50] the fluid will not move until a minimum shear stress, τ_o, is exceeded. Above this minimum shear stress, flow is basically Newtonian. The following equations describe the Bingham model:

$$\tau_{xy} = -\mu_o \frac{dv_y}{dx} + \tau_o \qquad \text{if } |\tau_{xy}| > \tau_o \tag{F1}$$

$$\frac{dv_y}{dx} = 0 \qquad \text{if } |\tau_{xy}| < \tau_o \tag{F2}$$

In these equations, μ_o is the fluid viscosity, and v_y is the y-direction component of fluid velocity. Consider flow of this fluid through a fracture, as illustrated in Fig. F1. Fluid injection is in the y-direction.

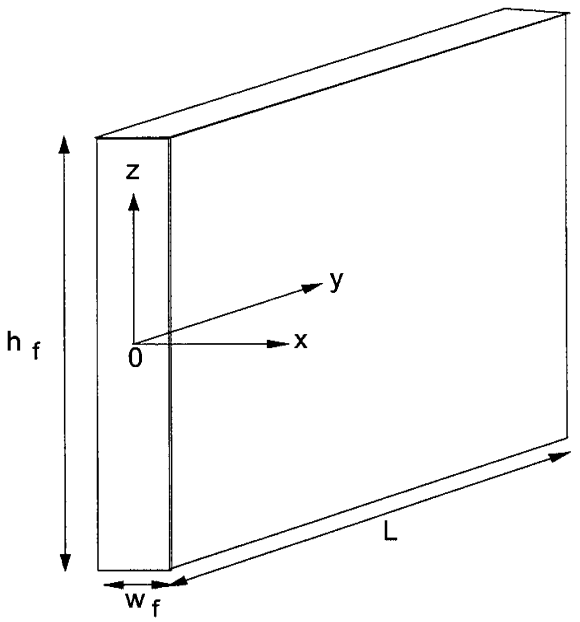

Fig. F1. Schematic illustrating coordinate system for flow in a fracture.

If a pressure drop, Δp, is applied over the length of the fracture, L, a momentum balance[50] yields Eq. F3.

$$\tau_o - \mu_o \frac{dv_y}{dx} = \frac{x\Delta p}{L} \tag{F3}$$

Separation of variables leads to Eq. F4.

$$dv_y = \left[\frac{\tau_o}{\mu_o} - \frac{x\Delta p}{\mu_o L}\right] dx \tag{F4}$$

Integrating Eq. F4 gives Eq. F5.

$$v_y = \frac{\tau_o x}{\mu_o} - \frac{x^2 \Delta p}{2\mu_o L} + C \tag{F5}$$

In moving from the center of the fracture toward the fracture wall (i.e., in the x-direction), the shear stress will be less than τ_0 and the velocity gradient, dv_y/dx, will be zero until some distance, x_o, is reached. This is the region of plug flow for our gel.

Let us first consider the region between x_o and the fracture wall. At the fracture wall ($x=w_f/2$), $v_y=0$, so Eq. F5 leads to Eq. F6.

$$0 = \frac{\tau_o w_f}{2\mu_o} - \frac{w_f^2 \Delta p}{8\mu_o L} + C \tag{F6}$$

So, the constant of integration, C, is given by Eq. F7.

$$C = \frac{w_f^2 \Delta p}{8\mu_o L} - \frac{\tau_o w_f}{2\mu_o} \tag{F7}$$

Thus, when $x_o < x < w_f/2$, Eq. F8 applies.

$$v_y = \frac{\tau_o x}{\mu_o} - \frac{x^2 \Delta p}{2\mu_o L} + \frac{w_f^2 \Delta p}{8\mu_o L} - \frac{\tau_o w_f}{2\mu_o} \tag{F8}$$

Eq. F8 can be rearranged to form Eq. F9.

$$v_y = \frac{w_f^2 \Delta p}{8\mu_o L}\left[1 - \frac{4x^2}{w_f^2}\right] - \frac{\tau_o w_f}{2\mu_o}\left[1 - \frac{2x}{w_f}\right] \tag{F9}$$

Now, let's consider the case when $x \le x_o$. From our definition of x_o, Eq. F10 follows.[50]

$$\tau_o = \frac{x_o \Delta p}{L} \tag{F10}$$

Next, we substitute Eq. F10 into Eq. F9 and let $x=x_o$.

$$v_y = \frac{w_f^2 \Delta p}{8\mu_o L}\left[1 - \frac{4x_o^2}{w_f^2}\right] - \frac{\Delta p w_f x_o}{2\mu_o L}\left[1 - \frac{2x_o}{w_f}\right] \tag{F11}$$

Eq. F11 simplifies to Eq. F12.

$$v_y = \frac{w_f^2 \Delta p}{8\mu_o L}\left[1 - \frac{2x_o}{w_f}\right]^2 \tag{F12}$$

So, Eq. F9 applies when $x \ge x_o$, Eq. F12 applies when $x \le x_o$.

Now, let's determine the total volumetric flow rate through the fracture.

$$q = 2h_f \int_0^{w_f/2} v_y dx = 2h_f \int_0^{x_o} v_y dx + 2h_f \int_{x_o}^{w_f/2} v_y dx \tag{F13}$$

Substituting Eq. F12 into one of the above integrals gives Eq. F14.

$$\int_o^{x_o} v_y dx = \frac{w_f^2 \Delta p}{8\mu_o L}\left[1 - \frac{2x_o}{w_f}\right]^2 x_o \tag{F14}$$

Substituting Eq. F9 into the other integral in Eq. F13 gives Eq. F15.

$$\int_{x_o}^{w_f/2} v_y dx = \int_{x_o}^{w_f/2} \frac{w_f^2 \Delta p}{8\mu_o L}\left[1-\frac{4x^2}{w_f^2}\right]-\frac{\tau_o w_f}{2\mu_o}\left[1-\frac{2x}{w_f}\right]dx \tag{F15}$$

Integration gives Eq. F16.

$$\int_{x_o}^{w_f/2} v_y dx = \frac{w_f^2 \Delta p}{8\mu_o L}\left[\left(\frac{w_f}{2}-x_o\right)-\frac{4}{3w_f^2}\left(\frac{w_f^3}{8}-x_o^3\right)\right]-\frac{\tau_o w_f}{2\mu_o}\left[\left(\frac{w_f}{2}-x_o\right)-\frac{2}{w_f}\left(\frac{w_f^2}{8}-\frac{x_o^2}{2}\right)\right] \tag{F16}$$

Substituting Eq. F10 into Eq. F16 gives Eq. F17.

$$\int_{x_o}^{w_f/2} v_y dx = \frac{w_f^3 \Delta p}{8\mu_o L}\left[\left(\frac{1}{2}-\frac{x_o}{w_f}\right)-\frac{4}{3}\left(\frac{1}{8}-\frac{x_o^3}{w_f^3}\right)\right]-\frac{w_f^2 \Delta p x_o}{2\mu_o L}\left[\left(\frac{1}{2}-\frac{x_o}{w_f}\right)-\left(\frac{1}{4}-\frac{x_o^2}{w_f^2}\right)\right] \tag{F17}$$

Simplifying Eq. F17 gives Eq. F18.

$$\int_{x_o}^{w_f/2} v_y dx = \frac{w_f^3 \Delta p}{8\mu_o L}\left[\left(\frac{1}{3}-\frac{x_o}{w_f}\right)+\left(\frac{4}{3}\frac{x_o^3}{w_f^3}\right)\right]-\frac{w_f^2 \Delta p x_o}{8\mu_o L}\left[\left(1+\frac{4x_o^2}{w_f^2}-\frac{4x_o}{w_f}\right)\right] \tag{F18}$$

Substituting Eqs. F18 and F14 into Eq. F13 gives Eq. F19.

$$q = \frac{h_f w_f^3 \Delta p}{4\mu_o L}\left[\left(\frac{1}{3}-\frac{x_o}{w_f}\right)+\left(\frac{4}{3}\frac{x_o^3}{w_f^3}\right)\right]-\frac{h_f w_f^2 \Delta p x_o}{4\mu_o L}\left[\left(1+\frac{4x_o^2}{w_f^2}-\frac{4x_o}{w_f}-1+\frac{4x_o}{w_f}-\frac{4x_o^2}{w_f^2}\right)\right] \tag{F19}$$

This equation simplifies to Eq. F20.

$$q = \frac{h_f w_f^3 \Delta p}{12\mu_o L}\left[1-\frac{3x_o}{w_f}+\frac{4x_o^3}{w_f^3}\right] \tag{F20}$$

When τ_o=0, x_o=0, and Eq. F20 reduces to the standard equation for laminar flow of a Newtonian fluid through a slit.[50]

$$q = \frac{h_f w_f^3 \Delta p}{12\mu_o L} \tag{F21}$$

The resistance factor, F_r, can be found by solving for μ_o in Eqs. F20 and F21, and then dividing the expression for viscosity from Eq. F21 by Eq. F20. Eq. F22 gives the result.

$$F_r = \left[1-\frac{3x_o}{w_f}+\frac{4x_o^3}{w_f^3}\right]^{-1} \tag{F22}$$

Eq. F22 is identical to Eq. 55 in Chapter 5.

Eq. F22 can be rearranged to form Eq. F23.

$$\frac{x_o}{w_f} = \frac{1}{3}\left[1+4\left(\frac{x_o}{w_f}\right)^3-\frac{1}{F_r}\right] \tag{F23}$$

Consideration of Eq. F23 reveals that as F_r increases, x_o/w_f rapidly approaches a value of 0.5.

The width of the lubricating layer, w_l, relative to the fracture width is given by Eq. F24.

$$\frac{w_l}{w_f} = \frac{(w_f / 2) - x_o}{w_f} = \frac{1}{2} - \frac{1}{3}\left[1 + 4\left(\frac{x_o}{w_f}\right)^3 - \frac{1}{F_r}\right] \tag{F24}$$

For moderate to large resistance factors, Eq. F24 reduces to Eq. F25.

$$\frac{w_l}{w_f} = \frac{1}{3F_r} \tag{F25}$$

APPENDIX G: Data Supplement for Chapter 6

Table G.1a. Summary of Water and Oil Mobilities Before Gel Treatment
(Core SSH-137, High-permeability Berea sandstone, 41°C)

$(k/\mu)_w$, md/cp @ S_w=1.0	$(k/\mu)_o$, md/cp @ S_{wr}=0.28	$(k/\mu)_w$, md/cp @ S_{or}=0.25
1,052	536	362

Table G.1b. Summary of Water and Oil Mobilities Before Gel Treatment
(Core SSH-138, High-permeability Berea sandstone, 41°C)

$(k/\mu)_w$, md/cp @ S_w=1.0	$(k/\mu)_o$, md/cp @ S_{wr}=0.23	$(k/\mu)_w$, md/cp @ S_{or}=0.22
1,100	571	365

Table G.1c. Summary of Water and Oil Mobilities Before Gel Treatment
(Core SSH-145, High-permeability Berea sandstone, 41°C)

$(k/\mu)_w$, md/cp @ S_w=1.0	$(k/\mu)_o$, md/cp @ S_{wr}=0.28	$(k/\mu)_w$, md/cp @ S_{or}=0.23
1,080	632	365

Table G.1d. Summary of Water and Oil Mobilities Before Gel Treatment
(Core SSH-151, High-permeability Berea sandstone, 41°C)

$(k/\mu)_w$, md/cp @ S_w=1.0	$(k/\mu)_o$, md/cp @ S_{wr}=0.29	$(k/\mu)_w$, md/cp @ S_{or}=0.31
978	617	326

Table G.1e. Summary of Water and Oil Mobilities Before Gel Treatment
(Core SSH-152, High-permeability Berea sandstone, 41°C)

$(k/\mu)_w$, md/cp @ S_w=1.0	$(k/\mu)_o$, md/cp @ S_{wr}=0.27	$(k/\mu)_w$, md/cp @ S_{or}=0.25	$(k/\mu)_o$, md/cp @ S_{wr}=0.26
1,061	604	287	403

Table G.1f. Summary of Water and Oil Mobilities Before Gel Treatment
(Core SSH-154, High-permeability Berea sandstone, 41°C)

$(k/\mu)_w$, md/cp @ S_w=1.0
1,116

Table G.1g. Summary of Water and Oil Mobilities Before Gel Treatment
(Core SSH-155, High-permeability Berea sandstone, 41°C)

$(k/\mu)_w$, md/cp @ S_w=1.0	$(k/\mu)_o$, md/cp @ S_{wr}=0.29	$(k/\mu)_w$, md/cp @ S_{or}=0.26
971	563	278

Table G.1h. Summary of Water and Oil Mobilities Before Gel Treatment
(Core SSH-156, High-permeability Berea sandstone, 41°C, μ_w=0.67 cp, μ_o=1.05 cp)

	$(k/\mu)_w$, md/cp @ S_w=1.0	$(k/\mu)_o$, md/cp @ S_{wr}=0.30	$(k/\mu)_w$, md/cp @ S_{or}=0.23
Short section	860	825	260
Internal section 1	1,520	850	326
Internal section 2	1,545	805	315
Internal section 3	1,565	778	328

Table G.1i. Summary of Water and Oil Mobilities Before Gel Treatment
(Core SSH-160, High-permeability Berea sandstone, 41°C)

$(k/\mu)_w$, md/cp @ S_w=1.0	$(k/\mu)_o$, md/cp @ S_{wr}=0.27	$(k/\mu)_w$, md/cp @ S_{or}=0.26	$(k/\mu)_o$, md/cp @ S_{wr}=0.26
1,170	705	353	443

Table G.1j. Summary of Water and Oil Mobilities Before Gel Treatment
(Core SSH-164, High-permeability Berea sandstone, 41°C)

$(k/\mu)_w$, md/cp @ S_w=1.0	$(k/\mu)_o$, md/cp @ S_{wr}=0.30	$(k/\mu)_w$, md/cp @ S_{or}=0.23	$(k/\mu)_o$, md/cp @ S_{wr}=0.26
1,237	677	333	412

Table G.1k. Summary of Water and Oil Mobilities Before Gel Treatment
(Core SSH-168, High-permeability Berea sandstone, 41°C)

$(k/\mu)_w$, md/cp @ S_w=1.0	$(k/\mu)_o$, md/cp @ S_{wr}=0.25	$(k/\mu)_w$, md/cp @ S_{or}=0.24
1,156	665	361

Table G.1l. Summary of Water and Oil Mobilities Before Gel Treatment
(Core SSH-169, High-permeability Berea sandstone, 41°C)

$(k/\mu)_w$, md/cp @ S_w=1.0	$(k/\mu)_o$, md/cp @ S_{wr}=0.28	$(k/\mu)_w$, md/cp @ S_{or}=0.25
1,100	632	291

Table G.1m. Summary of Water and Oil Mobilities Before Gel Treatment
(Core SSH-170, High-permeability Berea sandstone, 41°C)

$(k/\mu)_w$, md/cp @ S_w=1.0	$(k/\mu)_o$, md/cp @ S_{wr}=0.26	$(k/\mu)_w$, md/cp @ S_{or}=0.24
1,087	667	322

Table G.1n. Summary of Water and Oil Mobilities Before Gel Treatment
(Core SSH-171, High-permeability Berea sandstone, 41°C)

$(k/\mu)_w$, md/cp @ S_w=1.0	$(k/\mu)_o$, md/cp @ S_{wr}=0.28	$(k/\mu)_w$, md/cp @ S_{or}=0.23
1,175	657	350

Table G.2a. Summary of Residual Resistance Factors-Core SSH-137
Core: 705-md Berea sandstone
Gel: 0.5% HPAM, 0.0417% Cr(III)-acetate, 1% NaCl

1st Waterflood		
Pressure gradient, psi/ft	F_{rrw} (1st short core segment)	F_{rrw} (center core segment)
90	4,910	10,085
1st Oilflood		
Pressure gradient, psi/ft	F_{rro} (1st short core segment)	F_{rro} (center core segment)
90	12	20
2nd Waterflood		
Pressure gradient, psi/ft	F_{rrw} (1st short core segment)	F_{rrw} (center core segment)
90	36	140
2nd Oilflood		
Pressure gradient, psi/ft	F_{rro} (1st short core segment)	F_{rro} (center core segment)
90	2	10
3rd Waterflood		
Pressure gradient, psi/ft	F_{rrw} (1st short core segment)	F_{rrw} (center core segment)
90	3	13

Table G.2b. Summary of Residual Resistance Factors-Core SSH-138
Core: 737-md Berea sandstone
Gel: 0.5% HPAM, 0.0417% Cr(III)-acetate, 1% NaCl

1st Oilflood		
Pressure gradient, psi/ft	F_{rro} (1st short core segment)	F_{rro} (center core segment)
90	1	14
1st Waterflood		
Pressure gradient, psi/ft	F_{rrw} (1st short core segment)	F_{rrw} (center core segment)
90	15	321
2nd Oilflood		
Pressure gradient, psi/ft	F_{rro} (1st short core segment)	F_{rro} (center core segment)
90	1	11
2nd Waterflood		
Pressure gradient, psi/ft	F_{rrw} (1st short core segment)	F_{rrw} (center core segment)
90 (9.213 ft/d)	1	23
45 (3.937 ft/d)	1	27
22 (1.661 ft/d)	1	30
11 (0.63 ft/d)	1	39
5.6 (0.248 ft/d)	1	52
2.6 (0.076 ft/d)	1	79
F_{rrw} (center segment) = 37.4 $u^{-0.26}$, r=0.9860		
3rd Oilflood		
Pressure gradient, psi/ft	F_{rro} (1st short core segment)	F_{rro} (center core segment)
90 (46.85 ft/d)	1	7
45 (26.535 ft/d)	1	6
22.4 (14.331 ft/d)	1	6
11.4 (7.087 ft/d)	1	6
5.5 (4.197 ft/d)	1	5
Avg. F_{rro} (center segment) = 6		

Table G.2c. Summary of Residual Resistance Factors-Core SSH-151
Core: 655-md Berea sandstone
Gel: 0.5% HPAM, 0.0417% Cr(III)-acetate, 1% NaCl, 0.1% $CaCl_2$
Gelant/Oil volume ratio during placement: 95/5

1st Oilflood		
Flux, ft/d	F_{rro} (1st short core segment)	F_{rro} (center core segment)
0.197	150	390
1st Waterflood		
Flux, ft/d	F_{rrw} (1st short core segment)	F_{rrw} (center core segment)
0.025	6,400	11,100
2nd Oilflood		
Flux, ft/d	F_{rro} (1st short core segment)	F_{rro} (center core segment)
0.197	330	500
3rd Waterflood		
Flux, ft/d	F_{rrw} (1st short core segment)	F_{rrw} (center core segment)
0.025	5,020	11,450

Table G.2d. Summary of Residual Resistance Factors-Core SSH-152
Core: 711-md Berea sandstone
Gel: 0.5% HPAM, 0.0417% Cr(III)-acetate, 1% NaCl, 0.1% $CaCl_2$
Gelant/Oil volume ratio during placement: 95/5 (1 ml/hr continuous oil during gelation)

1st Oilflood		
Flux, ft/d	F_{rro} (1st short core segment)	F_{rro} (center core segment)
3.15	1	23
1st Waterflood		
Flux, ft/d	F_{rrw} (1st short core segment)	F_{rrw} (center core segment)
0.025	71	2,380
2nd Oilflood		
Flux, ft/d	F_{rro} (1st short core segment)	F_{rro} (center core segment)
3.15	6	28
3.15 (core faces cleaned)	3	33
2nd Waterflood		
Flux, ft/d	F_{rrw} (1st short core segment)	F_{rrw} (center core segment)
0.025	36	3,020
3rd Oilflood		
Flux, ft/d	F_{rro} (1st short core segment)	F_{rro} (center core segment)
3.15	6	30
1.575	6	28
Avg. F_{rro} (center segment)= 29		
3rd Waterflood		
Flux, ft/d	F_{rrw} (1st short core segment)	F_{rrw} (center core segment)
0.025	58	2,800
0.050	75	1,985
0.025	149	2,775
0.101	70	1,351
0.050	91	1,850
0.025	120	2,340
0.202	59	830
0.101	73	1,200
0.050	100	1,650
0.025	148	2,170
0.202	69	850
F_{rrw} (center segment) = 375.4 $u^{-0.26}$, r=0.9796		

Table G.2e. Summary of Residual Resistance Factors-Core SSH-156
Core: 2-ft,1034-md Berea sandstone
Gel: 0.5% HPAM, 0.0417% Cr(III)-acetate, 1% NaCl, 0.1% $CaCl_2$

1st Oilflood				
Flux, ft/d	F_{rro} (short section)	F_{rro} (Internal section 1)	F_{rro} (Internal section 2)	F_{rro} (Internal section 3)
1.211	11	39	46	58
1st Waterflood				
Flux, ft/d	F_{rrw} (short section)	F_{rrw} (Internal section 1)	F_{rrw} (Internal section 2)	F_{rrw} (Internal section 3)
0.019	4,300	9,000	7,800	9,000
2nd Oilflood				
Flux, ft/d	F_{rro} (short section)	F_{rro} (Internal section 1)	F_{rro} (Internal section 2)	F_{rro} (Internal section 3)
1.211	39	83	107	134
2nd Waterflood				
Flux, ft/d	F_{rrw} (short section)	F_{rrw} (Internal section 1)	F_{rrw} (Internal section 2)	F_{rrw} (Internal section 3)
0.019	3,920	8,430	7,640	8,920
0.039	2,910	5,870	5,270	6,180
0.019	3,650	7,630	7,490	9,000
0.078	1,890	3,800	3,340	3,880
0.039	2,320	5,100	4,820	5,760
0.019	2,830	6,600	6,470	7,900
0.155	1,115	2,220	1,980	2,165
0.078	1,370	2,975	2,910	3,215
0.039	1,730	4,020	4,130	5,050
0.019	2,150	5,200	5,420	6,800
	$F_{rrw}=618u^{-0.315}$ r=0.9997	$F_{rrw}=1{,}047u^{-0.41}$ r=0.9991	$F_{rrw}=831u^{-0.48}$ r=0.9962	$F_{rrw}=783u^{-0.56}$ r=0.9962
3rd Oilflood				
Flux, ft/d	F_{rro} (short section)	F_{rro} (Internal section 1)	F_{rro} (Internal section 2)	F_{rro} (Internal section 3)
19.382	8	23	27	33
9.691	8	27	35	45
4.846	8	29	43	60
2.423	8	29	49	76
	Avg. $F_{rro}=8$	Avg. $F_{rro}=27$	Avg. $F_{rro}=39$	Avg. $F_{rro}=54$

Table G.2f. Summary of Residual Resistance Factors-Core SSH-160
Core: 784-md Berea sandstone
Gel: 0.5% HPAM, 0.0417% Cr(III)-acetate, 1% NaCl, 0.1% $CaCl_2$
Gelant/Oil volume ratio during placement: 50/50
(102 psi/ft continuous oil during gelation)

1st Oilflood		
Flux, ft/d	F_{rro} (1st short core segment)	F_{rro} (center core segment)
6.229	17	22
1st Waterflood		
Flux, ft/d	F_{rrw} (1st short core segment)	F_{rrw} (center core segment)
0.202	250	465
2nd Oilflood		
Flux, ft/d	F_{rro} (1st short core segment)	F_{rro} (center core segment)
1.575	29	59
2nd Waterflood		
Flux, ft/d	F_{rrw} (1st short core segment)	F_{rrw} (center core segment)
0.394	152	298
3rd Oilflood		
Flux, ft/d	F_{rro} (1st short core segment)	F_{rro} (center core segment)
6.3	26	53
3rd Waterflood		
Flux, ft/d	F_{rrw} (1st short core segment)	F_{rrw} (center core segment)
0.787	103	319
4th Oilflood		
Flux, ft/d	F_{rro} (1st short core segment)	F_{rro} (center core segment)
6.3	25	52
4th Waterflood		
Flux, ft/d	F_{rro} (1st short core segment)	F_{rro} (center core segment)
0.787	123	307

Table G.2g. Summary of Residual Resistance Factors-Core SSH-164
Core: 829-md Berea sandstone
Gel: 0.5% HPAM, 0.0417% Cr(III)-acetate, 1% NaCl, 0.1% $CaCl_2$
Gelant/Oil volume ratio during placement: 95/5 (1 ml/hr continuous oil during gelation)

1st Oilflood		
Flux, ft/d	F_{rro} (1st short core segment)	F_{rro} (center core segment)
25.2	3	6
1st Waterflood		
Flux, ft/d	F_{rrw} (1st short core segment)	F_{rrw} (center core segment)
0.101	34	850
2nd Oilflood		
Flux, ft/d	F_{rro} (1st short core segment)	F_{rro} (center core segment)
25.2	2	6
25.2 (core faces cleaned)	2	6
2nd Waterflood		
Flux, ft/d	F_{rrw} (1st short core segment)	F_{rrw} (center core segment)
0.787	13	92
3rd Oilflood		
Flux, ft/d	F_{rro} (1st short core segment)	F_{rro} (center core segment)
25.2	2	5
100.8	2	3
50.4	2	3
25.2	2	3
12.6	2	3
Avg. F_{rro} (center segment)= 3 (last four readings)		

Table G.2g (cont'd). Summary of Residual Resistance Factors-Core SSH-164
Core: 829-md Berea sandstone
Gel: 0.5% HPAM, 0.0417% Cr(III)-acetate, 1% NaCl, 0.1% $CaCl_2$
Gelant/Oil volume ratio during placement: 95/5 (1 ml/hr continuous oil during gelation)

3rd Waterflood		
Flux, ft/d	F_{rrw} (1st short core segment)	F_{rrw} (center core segment)
0.787	11	83
1.575	12	46
0.787	15	54
3.15	11	29
1.575	13	31
0.787	13	33
6.3	10	20
3.15	12	22
1.575	13	23
0.787	12	27
12.6	8	14
6.3	9	15
3.15	10	15
1.575	9	15
0.787	9	18
12.6	8	14
Avg. F_{rrw} (center segment)= 15 (last six readings)		

Table G.2h. Summary of Residual Resistance Factors-Core SSH-168
Core: 705-md Berea sandstone
Gel: 0.5% HPAM, 0.0417% Cr(III)-acetate, 1% NaCl, 0.1% $CaCl_2$

1st Waterflood		
Pressure gradient, psi/ft	F_{rrw} (1st short core segment)	F_{rrw} (center core segment)
180	7	9
1st Oilflood		
Pressure gradient, psi/ft	F_{rro} (1st short core segment)	F_{rro} (center core segment)
180	2	2
2nd Waterflood		
Pressure gradient, psi/ft	F_{rrw} (1st short core segment)	F_{rrw} (center core segment)
180	5	7
2nd Oilflood		
Pressure gradient, psi/ft	F_{rro} (1st short core segment)	F_{rro} (center core segment)
180	2	2
3rd Waterflood		
Pressure gradient, psi/ft	F_{rrw} (1st short core segment)	F_{rrw} (center core segment)
180	4	5

Table G.2i. Summary of Residual Resistance Factors-Core SSH-169
Core: 737-md Berea sandstone
Gel: 0.5% HPAM, 0.0417% Cr(III)-acetate, 1% NaCl, 0.1% $CaCl_2$

1st Oilflood		
Pressure gradient, psi/ft	F_{rro} (1st short core segment)	F_{rro} (center core segment)
180	3	5
1st Waterflood		
Pressure gradient, psi/ft	F_{rrw} (1st short core segment)	F_{rrw} (center core segment)
180	15	49
2nd Oilflood		
Pressure gradient, psi/ft	F_{rro} (1st short core segment)	F_{rro} (center core segment)
180	2	5
2nd Waterflood		
Pressure gradient, psi/ft	F_{rrw} (1st short core segment)	F_{rrw} (center core segment)
180	7	30
3rd Oilflood		
Pressure gradient, psi/ft	F_{rro} (1st short core segment)	F_{rro} (center core segment)
180	2	4

Table G.2j. Summary of Residual Resistance Factors-Core SSH-170
Core: 728-md Berea sandstone
Gel: 0.5% HPAM, 0.0417% Cr(III)-acetate, 1% NaCl, 0.1% $CaCl_2$

1st Waterflood		
Pressure gradient, psi/ft	F_{rrw} (1st short core segment)	F_{rrw} (center core segment)
135	1,360	4,510
1st Oilflood		
Pressure gradient, psi/ft	F_{rro} (1st short core segment)	F_{rro} (center core segment)
135	3	12
2nd Waterflood		
Pressure gradient, psi/ft	F_{rrw} (1st short core segment)	F_{rrw} (center core segment)
135	20	151
2nd Oilflood		
Pressure gradient, psi/ft	F_{rro} (1st short core segment)	F_{rro} (center core segment)
135	2	10
3rd Waterflood		
Pressure gradient, psi/ft	F_{rrw} (1st short core segment)	F_{rrw} (center core segment)
135	17	98

Table G.2k. Summary of Residual Resistance Factors-Core SSH-171
Core: 787-md Berea sandstone
Gel: 0.5% HPAM, 0.0417% Cr(III)-acetate, 1% NaCl, 0.1% $CaCl_2$

1st Oilflood		
Pressure gradient, psi/ft	F_{rro} (1st short core segment)	F_{rro} (center core segment)
135	5	16
1st Waterflood		
Pressure gradient, psi/ft	F_{rrw} (1st short core segment)	F_{rrw} (center core segment)
135	89	4,500
2nd Oilflood		
Pressure gradient, psi/ft	F_{rro} (1st short core segment)	F_{rro} (center core segment)
135	3	16
2nd Waterflood		
Pressure gradient, psi/ft	F_{rrw} (1st short core segment)	F_{rrw} (center core segment)
135	36	441
3rd Oilflood		
Pressure gradient, psi/ft	F_{rro} (1st short core segment)	F_{rro} (center core segment)
135	2	14

APPENDIX H: Technology Transfer

On October 8, 1997, we presented SPE paper 38835 and the talk, "Sizing Gelant Treatments in Hydraulically Fractured Production Wells," at the 1997 SPE Annual Technical Conference and Exhibition in San Antonio, Texas.

On August 6, 1997, we presented the talk, "The Importance of Reducing Water Permeability More than Oil Permeability Through the Use of Gels," at the 3rd International Conference on Reservoir Conformance, Profile Control, and Water and Gas Shutoff in Houston, Texas.

On June 19, 1997, we presented an overview of our project at the DOE's Contractor Review Meeting in Houston, Texas.

On May 20, 1997, we presented the talk, "A Strategy for Diagnosing and Attacking Water Shutoff Problems," at the SPE Applied Technology Workshop in Dunkeld, Scotland.

On April 29 and 30, 1997, we held a project review in Socorro, NM. The review was attended by 28 people (not including New Mexico Tech personnel) representing 16 different organizations.

On February 18, 1997, we presented SPE paper 37249 and the talk, "Further Investigations of Why Gels Reduce k_w More Than k_o," at the 1997 SPE International Symposium on Oilfield Chemistry in Houston, Texas.

On September 24, 1996, we presented the talk, "Issues Involved with Sizing Gel Treatments," at the 2nd Annual Subsurface Fluid Control Symposium and Exhibition that was held in Houston, Texas.

On August 19, 1996, we presented the paper, "What Gels Can and Cannot Do," at the 2nd International Conference on Reservoir Conformance, Profile Control, and Water and Gas Shutoff in Houston, Texas.

On June 4 and 5, 1996, we held a project review in Socorro, NM. The review was attended by 27 people (not including New Mexico Tech personnel) representing 18 different organizations.

Recent Publications. Our recent publications include:

Liang, J-T. and Seright, R.S.: "Further Investigations of Why Gels Reduce k_w More Than k_o," *SPE Production & Facilities* (Nov. 1997).

Seright, R.S., Seldal, M., and Liang, J.: "Sizing Gelant Treatments in Hydraulically Fractured Production Wells," paper SPE 38835 presented at the 1997 SPE Annual Technical Conference and Exhibition, San Antonio, TX , Oct. 5-8.

Taber, J.J., Martin, FD., and Seright, R.S.: "EOR Screening Criteria Revisited—Part 1: Introduction to Screening Criteria and Enhanced Recovery Field Projects," *SPE Reservoir Engineering* (Aug. 1997) 189-198.

Taber, J.J., Martin, FD., and Seright, R.S.: "EOR Screening Criteria Revisited—Part 2: Applications and Impact of Oil Prices," *SPE Reservoir Engineering* (Aug. 1997) 199-205.

Seright, R.S.: "Improved Methods for Water Shutoff," DOE/PC/91008-1, Contract No. DE-AC22-94PC91008, BDM-Oklahoma Subcontract No. G4S60330 (Aug. 1997).

Seright, R.S.: "Use of Preformed Gels for Conformance Control in Fractured Systems," *SPE Production & Facilities* (Feb. 1997) 59-65.